



Microbiome-Targeted Interventions for Colitis-Associated Bacteria

Citation

Rooks, Michelle Gabrielle. 2016. Microbiome-Targeted Interventions for Colitis-Associated Bacteria. Doctoral dissertation, Harvard University, Graduate School of Arts & Sciences.

Permanent link

<http://nrs.harvard.edu/urn-3:HUL.InstRepos:33493456>

Terms of Use

This article was downloaded from Harvard University's DASH repository, and is made available under the terms and conditions applicable to Other Posted Material, as set forth at <http://nrs.harvard.edu/urn-3:HUL.InstRepos:dash.current.terms-of-use#LAA>

Share Your Story

The Harvard community has made this article openly available.
Please share how this access benefits you. [Submit a story](#).

[Accessibility](#)

Microbiome-targeted interventions for colitis-associated bacteria

A dissertation presented

by

Michelle Gabrielle Rooks

to

The Committee on Higher Degrees in Biological Sciences in Public Health

in partial fulfillment of the requirements

for the degree of

Doctor of Philosophy

in the subject of

Biological Sciences in Public Health

Harvard University

Cambridge, Massachusetts

April 2016

© 2016 *Michelle Gabrielle Rooks*

All rights reserved.

Microbiome-targeted interventions for colitis-associated bacteria

ABSTRACT

Complex interactions between mammalian hosts and their gut microbes have evolved over many millennia and have established a sophisticated communication system that is essential for symbiosis and mutualism. Perturbations to host-microbiota homeostasis in the context of a genetically susceptible host are central to the development of inflammatory bowel disease (IBD). In-depth understanding of the underlying mechanisms that control homeostasis and dysbiosis are essential for determining how to reliably modulate the host-microbiota continuum to prevent and treat disease. However, deciphering whether alterations in the microbiota are a cause or consequence of IBD remains a considerable challenge, as is defining the role of specific microbes in the pathogenesis of disease. This thesis explores the gut microbiome in mouse models of experimental colitis and evaluates the contribution of specific microbial clades and pathways in potentiating mucosal inflammation with the goal of identifying novel microbiome-targeted interventions for disease management.

To improve our understanding of microbial dysbiosis and dysfunction in IBD, we use the TRUC (*T-bet*^{-/-}*RAG2*^{-/-} ulcerative colitis) mouse model to profile the gut microbiome in active disease versus treatment-induced remission. 16S ribosomal RNA gene surveys of stool from mice treated with antibiotics, immunodulatory therapies, or a fermented-milk dietary intervention reveal microbial features modified among health and disease states. Discriminatory biomarkers of active disease included increased *Enterobacteriaceae* and shifts from carbohydrate and energy metabolism to pathways favoring bacterial pathogenesis, specifically cell motility and two-

component systems. An unexpected observation is a significant enrichment in genes for microbial benzoate degradation in active colitis. Intermediates of benzoate metabolism – catechols – share the same backbone as host catecholamines, which can signal through two-component systems to promote virulence in pathogenic *Enterobacteriaceae*. Based on expansions in *Enterobacteriaceae* and increased gene abundances for benzoate degradation, two-component systems, and bacterial motility proteins, we identify a potential signaling axis linking host adrenergic stress with enhanced bacterial virulence in a preclinical model of colitis.

Enterobacteriaceae sense and respond to microbiota-generated signals and host-derived catecholamines through the QseBC two-component quorum sensing system. QseC is a membrane-bound sensor kinase that surveys the external milieu and, upon signal detection, activates its cognate response regulator, QseB, to induce expression of virulence genes. To investigate whether blocking QseC signaling could reduce disease severity, we test the effects of a QseC inhibitor (LED209) in the TRUC, *Il-10*^{-/-}, and dextran sodium-sulfate models of experimental colitis. LED209 attenuates disease across all three models, with the most striking protective effect in TRUC and dextran sodium sulfate-treated mice. LED209 also prevents the expansion of *Enterobacteriaceae* in *Il-10*^{-/-} and dextran sodium-sulfate-exposed mice, but not in TRUC mice, indicating a potential difference in microbiota responses based on genetic context. Moreover, measuring catecholamines in cecal content and stool show that LED209 does not significantly affect the luminal catecholamine pool and thus, may not disrupt host or microbial catecholamine metabolism. Collectively, these data show that QseC inhibition can ameliorate disease in distinct models of experimental colitis and suggest a role for QseC-mediated bacterial virulence in the pathogenesis of IBD.

Although a single pathogen has not been identified as a causative agent, several bacteria continue to be implicated in the initiation and progression of IBD, including adherent-invasive

Escherichia coli (AIEC). As a proof-of-principle, we genetically inactivate *qseC* in the Crohn's disease-associated AIEC strain LF82. We show that absence of *qseC* leads to downregulated virulence gene expression and defects in flagellar assembly and motility *in vitro* and reduced colonization efficiency *in vivo*. Overall, these studies provide evidence that QseC may be an upstream virulence node utilized by colitogenic bacteria to survey their host and potentiate disease and may be a useful target for microbiota-directed therapies in IBD.

TABLE OF CONTENTS

Abstract	iii
Table of Contents	vi
Acknowledgements	viii
Dedication	x
List of Figures	xi
List of Tables	xiii
Chapter 1: Introduction	1
Background	2
Microbiome Tools and Technologies	3
IBD Pathogenesis: A Role for Microbial Dysbiosis	11
Current Treatment Approaches for IBD	20
Thesis Overview	25
References	26
Chapter 2: Gut microbiome composition and function in experimental colitis during active disease and treatment-induced remission	33
Abstract	34
Introduction	34
Results	36
Discussion	54
Materials and Methods	56
Acknowledgments	64
References	64
Chapter 3: Testing the efficacy of LED209, an inhibitor of the bacterial quorum-sensing receptor and virulence regulator QseC, in experimental colitis	69
Background	70
Results	72
Discussion	77
Materials and Methods	80
References	84

<u>Chapter 4: Genetic inactivation of QseC in the IBD-associated AIEC strain LF82</u>	86
Background	87
Results	89
Discussion	101
Materials and Methods	107
References	115
<u>Chapter 5: Conclusion</u>	119
Summary of Findings	120
New Perspectives	123
References	124
<u>Appendix A: Supplementary Materials</u>	126
Supplementary Figures	127
Supplementary Tables	150
<u>Appendix B: Supplementary Methods</u>	155
DNA/RNA co-isolation from bacterial cultures and stool	156
<u>Appendix C: Additional Data</u>	162
Characterizing host colonic catecholamine metabolism	163

ACKNOWLEDGMENTS

I would like to express my gratitude and appreciation for the people who have supported and encouraged me throughout my scientific journey. First, I would like to thank my advisor, Professor Wendy Garrett, who has been instrumental in teaching me how to strategize an actionable work plan and effectively communicate my science to others. I have appreciated her passion for science, her critical and always rapid feedback, her incredible memory and foresight, and her unexpected humor in even the most unsuspected circumstances. Although my start in the lab required me to sharpen my culinary skills for a project that involved cooking and feeding red meat to mice, it culminated in me developing a much larger arsenal of valuable skills. Joining Wendy's Lab has truly made me a more proficient and intuitive scientist.

I would like to thank members of my Preliminary Qualifying Examination, Dissertation Advisory, and Dissertation Defense committees for their time, direction, and support. Listed alphabetically: Drs. Isaac Chiu, Dirk Gevers, Les Kobzik, Chih-Hao Lee, Brendan Manning, James Mitchell, Eric Rubin, and Zhi-Min Yuan. I would also like to specifically acknowledge Dirk Gevers as well as Curtis Huttenhower and his group members for their assistance in facilitating and fostering my computational skills and patience fielding any and all of my questions.

My Ph.D. experience was greatly enhanced by the intellectual, technical, and emotional support of Garrett Lab members – past and present. I have delighted in fruitful scientific discussions equally as much as less fruitful non-scientific discussions over the years. Carey Gallini and Monia Michaud, thank you for allowing the lab to run like a well-oiled machine. First-generation Garrett Lab members – Eunyoung Chun, Sonia Ballal, Leslie Wardwell-Scott, Patrick Smith, Michael Howitt, and Sydney Lavoie – thank you for establishing a dynamic and fun work environment. Interim Garrett Lab members, Patrick Veiga and Jason Kim, thank you for being refreshing additions to the lab. I have also enjoyed working with and getting to know the second

wave of Garrett Lab members: Caitlin Brennan, Nora Ou, Kathrin Fenn, Lior Lobel, and Diogo Fonseca Pereira.

It is impossible not to thank my previous scientific mentors – Dr. David Louis at Massachusetts General Hospital and Dr. Gregory Hannon previously at Cold Spring Harbor Laboratory. I gained valuable technical skills during my tenure in their labs, which I continued to build on during my graduate studies. A special thank you to Dr. Emily Hodges, a former post-doctoral fellow in the Hannon Lab who encouraged me to think critically, work independently, and not shy away from a technical challenge – even one that involved handling precious Neandertal DNA. My experiences working with her were a significant factor in my decision to pursue a Ph.D.

Lastly, I would like to thank my family and friends for keeping me grounded and encouraging balance. My parents, Aldwyn and Gloria, have supported all my academic pursuits and have been role models for me by demonstrating the benefits of hard work, integrity, and commitment. My sister, Janelle, and her husband, Michael, although I do not see them often, I always sense their support from afar. My classmates – Allison Demas, Eylul Harputlugil, Caeul Lim, Alex Sakatos, and Peter Wagner (and honorary classmate Lear Brace) – have been an important social outlet over the years. Thank you for enforcing mandatory fun. Many other friends both near and far, most who are not in science or academia, you have all been tremendous motivating forces. Finally, I would like to thank my boyfriend, Justin Gordon, for entering my life at a critical juncture and offering patience, support, lots of laughter, and much needed perspective. While my culinary adventures petered out in lab, our shared love for food has allowed us to enjoy many homemade creations and meals from restaurants all over the world.

DEDICATION

For my grandmothers Sheila Chapman and Danica Legovic

and my parents Aldwyn and Gloria Rooks

LIST OF FIGURES

Figure 1.1. Functions of the gut microbiota and its importance to host physiology	3
Figure 1.2. Global prevalence of IBD in 2015	12
Figure 1.3. Protective and pathogenic role of the gut microbiota in IBD	16
Figure 2.1. Experimental design and influence of interventions on the gut microbiome	38
Figure 2.2. Antibiotic-driven microbial community shifts may be influenced by early-life exposures and are associated with specific clade responses	40
Figure 2.3. Immunomodulators influence low abundance gut microbial community members and drive distinct microbial responses	44
Figure 2.4. A fermented milk product influences the microbial communities of the gut and MLNs	47
Figure 2.5. Gut microbiome composition in active colitis and treatment-induced remission with <i>in vivo</i> functional validation of proinflammatory activity in gnotobiotic TRUC mice	50
Figure 2.6. Inferred gut microbiome functions associated with active colitis and treatment-induced remission	52
Figure 3.1. LED209 intervention study design and effects of bacterial QseC inhibition in three mouse models of experimental colitis	73
Figure 3.2. Shifts in <i>Enterobacteriaceae</i> relative abundance following an LED209 intervention in mouse models of experimental colitis	75
Figure 3.3. CA levels in cecal content and stool following an LED209 intervention in mouse models of experimental colitis	76
Figure 4.1. Effects of <i>qseC</i> inactivation on the expression of LF82 virulence genes	90
Figure 4.2. Representative TEM images of WT and mutant LF82 strains	91
Figure 4.3. Plate-based motility assays of LF82 strains grown in LB or NE-supplemented LB	92
Figure 4.4. 16S rRNA gene surveys of microbial communities of LF82-colonized ex-ASF mice	96
Figure 4.5. Effects of DSS-induced inflammation on the host and on LF82 and <i>Enterobacteriaceae</i> levels in mice harboring microbiotas of differing complexity	99
Figure 4.6. Comparing LF82 growth curves under aerobic and anaerobic conditions	101
Supplementary Figure 2.1. 16S rRNA analysis pipeline for investigating the influence of perturbations on gut-associated microbial communities	127
Supplementary Figure 2.2. PCoA of weighted Unifrac distances of gut microbial communities	128
Supplementary Figure 2.3. 16S rRNA gene surveys of gut microbiome diversity following treatment exposure	129
Supplementary Figure 2.4. PCoA and LEfSe analyses to assess the influence of early-life exposures on antibiotic-driven microbial clade responses	130
Supplementary Figure 2.5. LEfSe rank plots of differentially abundant microbial clades in gut microbiomes associated with active colitis versus remission following antibiotic treatment	131
Supplementary Figure 2.6. LEfSe rank plots of differentially abundant microbial clades in gut microbiomes exposed to immunomodulators	132
Supplementary Figure 2.7. LEfSe rank plots of differentially abundant microbial clades in gut microbiomes following a daily dietary intervention	133

Supplementary Figure 2.8. PCoA of weighted Unifrac distances of stool and MLN microbial communities of mice administered a daily dietary intervention	134
Supplementary Figure 2.9. LEfSe rank plot of differentially abundant microbial clades between stool and MLN microbial communities of mice receiving a daily dietary intervention	135
Supplementary Figure 2.10. LEfSe rank plot of differentially abundant microbial clades between MLN microbial communities of mice receiving a daily dietary intervention	136
Supplementary Figure 2.11. LEfSe rank plot of differentially abundant microbial clades in gut microbiomes associated with active colitis and treatment-induced remission	137
Supplementary Figure 2.12. LEfSe rank plot of differentially abundant microbial genes in gut microbiomes associated with active colitis and treatment-induced remission	138
Supplementary Figure 2.13. Model summarizing the effects of treatment interventions in the TRUC model of experimental colitis	139
Supplementary Figure 3.1. Microbial benzoate metabolism, host CA biosynthesis, and bacterial QseC-mediated CA sensing and virulence inhibition	140
Supplementary Figure 3.2. Changes in baseline body weight and post-intervention colon lengths for an LED209 intervention in three mouse models of experimental colitis	141
Supplementary Figure 3.3. Gender differences in disease severity in <i>Il-10</i> ^{-/-} mice following an LED209 intervention	142
Supplementary Figure 3.4. Shifts in <i>Enterobacteriaceae</i> abundance in gut microbiomes of TRUC mice following treatment with antibiotics, immunomodulators, or a dietary intervention	143
Supplementary Figure 4.1. Confirmation of <i>qseC</i> deletion and replacement in the LF82 genome	144
Supplementary Figure 4.2. Gibson plasmid for <i>qseC</i> complementation	145
Supplementary Figure 4.3. Effects of <i>qseC</i> inactivation on NE-induced expression of LF82 virulence genes	146
Supplementary Figure 4.4. Culturable counts of LF82 in stool from LF82-inoculated ex-ASF mice	147
Supplementary Figure 4.5. Biogeography experiments to determine LF82 niche-specificity in the intestinal tract	148
Supplementary Figure 4.6. Changes in baseline body weight and post-intervention colon lengths for DSS-exposed mice	149
Appendix Figure C.1. Catecholamine metabolic enzyme expression in colons	164
Appendix Figure C.2. Catecholamine biosynthetic gene expression of colonic cell subsets	165
Appendix Figure C.3. TH expression analysis of colons and brains of GFP reporter mice	167

LIST OF TABLES

Table 1.1. Common experimental models of IBD	14
Table 1.2. Medical treatments for IBD	21
Supplementary Table 2.1. Summary of pyrosequenced samples	150
Supplementary Table 2.2. Summary of PICRUSt analysis of post-intervention samples	151
Supplementary Table 4.1. Bacterial strains and plasmids used in this study	152
Supplementary Table 4.2. Primers used in this study	153

CHAPTER 1

Introduction

Portions of this Chapter were adapted from:

Michelle G. Rooks¹ and Wendy S. Garrett¹⁻⁴. Gut microbiota, metabolites, and host immunity. *Nat. Rev. Immunol.* (accepted).

¹Harvard T.H. Chan School of Public Health, Boston, MA, USA

²Harvard Medical School, Boston, MA, USA

³Broad Institute of MIT and Harvard, Cambridge, MA, USA

⁴Dana-Farber Cancer Institute, Boston, MA USA

Author Contributions:

M.G.R. researched and wrote manuscript. W.S.G. provided critical editorial input.

BACKGROUND

Mammals harbor widely diverse and immensely active microbial communities. The gastrointestinal tract alone is home to trillions of microorganisms whose collective genomes (the gut microbiome) influence host metabolic, nervous, and immune system development and, thus, have profound effects on host health and disease (**Figure 1.1**). Through an enduring mutualistic partnership, the host has evolved to coordinate and integrate conserved metabolic signaling, microbial sensing, and immune response pathways to ensure its survival in a microbially-dominated world. This dynamic crosstalk between the host and its microbiota are important for achieving and maintaining homeostasis. If or when this dialogue goes awry – via perturbations to the microbiota or the host, ranging from environmental exposures to diet, antibiotics, pathogens, and stress – dysbiosis (microbial imbalance) can ensue. Myriad studies continue to establish the role of an altered microbiome in an ever-increasing number of human disorders and diseases.

Recent advances in characterizing the composition and function of individual microbial species and complex microbial communities have expanded our understanding of host-microbiota mutualism. These discoveries prompt questions regarding the mechanisms by which microbes and microbial functions shape host physiology and influence resistance and susceptibility to disease. In the first half of this Chapter, technologies for profiling the microbiome and investigating its role in regulating host immunity are reviewed, with a dominant focus on the gut microbiota and intestinal immune homeostasis. In the second half, microbial dysbiosis in the context of inflammatory bowel disease (IBD) is discussed, with a specific focus on understanding the dialogue between the host and its microbes in order to develop microbiota-targeted interventions to prevent and treat disease.

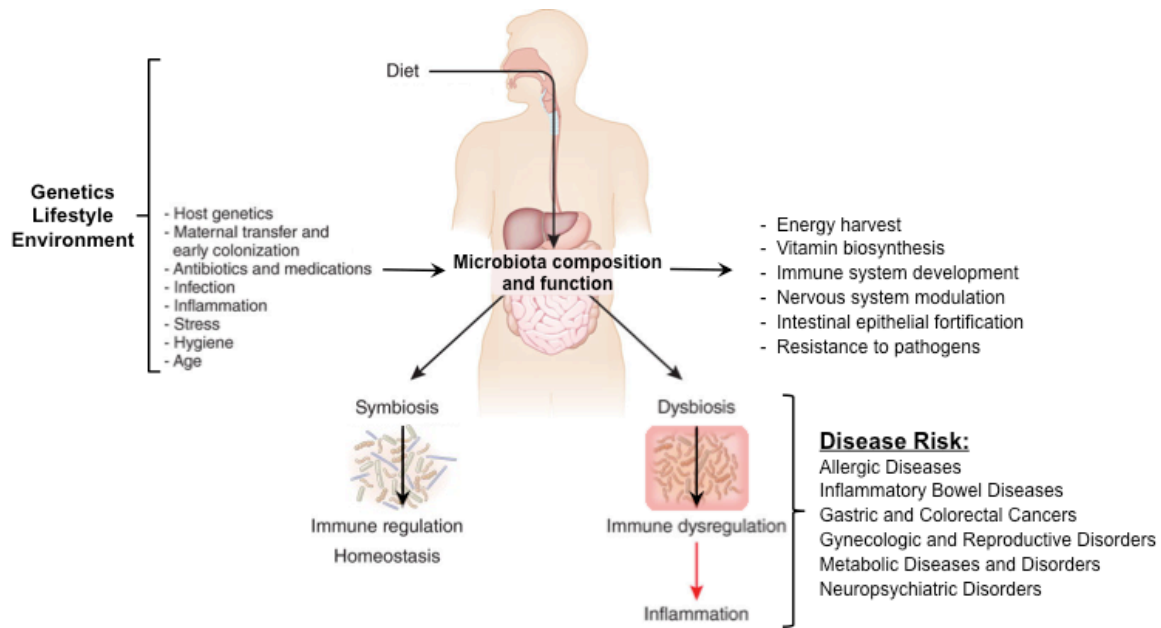


Figure 1.1. Functions of the gut microbiota and its importance to host physiology. The human body harbors trillions of microbes, with the vast majority residing in the gut. These microbes (the gut microbiota) and their collective genomes (the gut microbiome) are influenced by many genetic and environmental factors and play pivotal roles in human health and disease. In healthy individuals, the gut microbiota is in a state of symbiosis with its host, which helps regulate immune responses and maintain intestinal homeostasis. Perturbations to the gut microbiota or abnormal interactions between host cells and microbes can lead to dysbiosis, which often results in dysregulated immune responses leaving the host susceptible to inflammation. Adapted from: Maslowski, K. M. & Mackey, C. R. *Nat. Immunol.* **12**, (2011).

MICROBIOME TOOLS AND TECHNOLOGIES

Characterizing microbiome composition

Until the 1990s, analyzing the composition of microbial communities of the human gut and other mucosal surfaces relied on classic microbiological techniques and the ability to cultivate pure isolates, which limited detection to culturable microbes¹. The advent of high-throughput DNA sequencing technology – initially clustering reads based on bacterial and archaeal 16S ribosomal RNA (rRNA) amplicon sequences and now by aligning whole genomes to all domains of life extending to fungi, protozoa, and viruses – allows the direct classification of samples without the need for culturing². These technological advances provide a robust method for profiling complex microbial communities from diverse environments and for analyzing

changes in community structure over time. Accompanying the surge in sequencing throughput are computational challenges that have necessitated and driven the development of novel tools for high-complexity data analysis, such as Quantitative Insights Into Microbial Ecology (QIIME), mothur, the BioBakery of analysis tools, and other software packages for analyzing microbial communities, which have expanded the possibility for more sophisticated hypotheses and lines of investigation.

Large-scale sequencing efforts, including those of the Human Microbiome Project (HMP) and the metagenomics of the human intestinal tract (MetaHIT), revealed that microbiome composition is not constant; rather our collection of microbes is dynamic and highly influenced by temporal and spatial factors^{3,4}. Evidence for this is found in studies examining changes in microbiome composition and structure throughout the lifespan. Remarkably, while the mammalian fetal gut is sterile, colonization is initiated immediately after birth and is affected by mode of delivery, diet, genetics, hygiene, and antibiotic use⁵⁻⁷. By the first few years of life, gut microbial diversity increases and eventually converges toward a distinct and stable microbiome signature comparable to that found in adults⁶⁻⁹. Although microbiome composition differs between individuals and at times fluctuates markedly within individuals, core features exist in the microbial communities populating the human body¹⁰. Each body habitat is spatially distinct and differentially dominated by specific phyla. Different collections of Actinobacteria, Bacteroidetes, Cyanobacteria, Deferribacteres, Firmicutes, Fusobacteria, Proteobacteria, and Verrucomicrobia are found on the skin, in the oral cavity, and in the tracts of the respiratory, gastrointestinal, and urogenital systems³. These niche-specific microbiomes are present in varying abundance and distribution across anatomical sites. In the gut, the quantity and diversity of microbial species increase longitudinally from the stomach to the colon¹¹, with the colon being home to the most dense and metabolically active community (comprising more than 10^{13} individual microbial

cells)¹². An appreciation of the magnitude of microbial diversity within and across individuals is affecting how the microbiome is studied, changing from descriptive studies of members of the microbial communities to more mechanistic studies of the functional contribution of the microbiota to human health and disease.

Investigating microbiome function

Whole metagenomic (DNA) and metatranscriptomic (cDNA) sequencing endeavors are defining the functional potential and real-time activity of microbiomes and revealing interactions between microbes, microbial metabolic products, and host development. With a dominant lens on the gut microbiome and in particular fecal material given its abundant microbial biomass, the development of tools to identify and reconstruct genes into broader biological pathways have allowed functional features of the microbiome to be divided into distinct but related categories that are essential to host health¹³. A primary function of the gut microbiome is its ability to aid in energy extraction and nutrient absorption. Through a collection of specialized enzymes, gut microbes metabolize dietary components that are indigestible or only partially digested by the host and synthesize essential vitamins and cofactors¹⁴. By competing for available nutrients and releasing antimicrobial peptides (AMPs), the gut microbiota also protects the host from colonization by non-resident microbes and pathogens¹⁵. In addition to supporting host metabolism and offering colonization resistance, the gut microbiota regulates the development of the enteric nervous system (ENS) and multi-directional signaling between intestinal epithelial cells (IECs), the immune system, and the central nervous system (CNS)¹⁶, which has major implications for inflammatory responses and host defense.

The single layer of epithelial cells that make up the mucosal surface represents a critical interface between host and microbe. Such an intimate spatial arrangement allows microbes and

microbial components and metabolites to gain access to and interact with host cells, and thus influence immune responses and disease risk. A significant and constant challenge for the host is determining whether the microbes or microbial antigens it encounters are a threat and deciding if, when, and what kind and extent of an immune response to elicit. As a first line of defense, the intestinal mucus layer provides a barrier that physically segregates the gut microbiota from the intestinal epithelium. To protect host cells from coming in direct contact with microbial cells, members of the gut microbiota stimulate host production of mucins and antibodies (mainly secretory IgA; sIgA) that limit microbial migration toward and translocation across the IEC barrier¹⁷. The gut microbiome also stimulates the development of gut-associated lymphoid tissue, which serves as a self-contained immune system that restricts immune responses to the gut rather than allowing them to spread system-wide¹⁸. Sampling of microbial components by specialized epithelial cells (M-cells and goblet cells) and antigen-presenting cells (APCs) – via interaction of microbe-associated molecular patterns (MAMPs) with host pattern-recognition receptors (PRRs) – primes local immune responses toward either a regulatory or inflammatory direction, which promotes tolerance to the microbiota and responsiveness to invading pathogens¹⁹. Thus, microbial genes and pathways are essential for coordinating host metabolic, nervous, and immune system development and function and have profound effects on host health and disease.

The ability to profile the regulation and dynamics of microbiome and host gene expression patterns is revealing how microbial community functions can influence the host²⁰ and, conversely, how host genetics shape the composition and function of the microbiome. Mining of the HMP dataset for host reads and subsequent genome-wide analysis to correlate host genetic variation and microbiome composition across sampled body sites, identified significant associations between host genes and microbiome composition²¹. Notably, enriched host genes were strongly associated with immune-related pathways, including chemokine signaling and PRR recognition,

and several complex diseases including obesity and IBD²¹. Simultaneous sequencing of the metagenomes and metatranscriptomes of the host and microbiome is providing insight into mechanisms involved of host-microbiota mutualism and the differences between healthy and diseased individuals.

Attributing causality and directionality

Gnotobiotic animal models are highly valuable systems for elucidating microbiome function in health and disease. Gnotobiotic animals are generated by colonizing germ-free (GF) animals with a defined microbial community or consortia of bacteria from a mammalian host. In addition to controlling the influence of host genetics and environmental factors, similar to other conventional animal models, GF animals also provide opportunities to investigate the contribution of microbes to host development and disease pathogenesis.

GF animals have a distinct metabolic phenotype, including the tendency to consume more calories, excrete more lipids, and weigh significantly less than their conventional counterparts²². Microbial colonization of GF mice corrects the defects in metabolic function and leads to more efficient energy extraction from the diet²³. GF animals also show alterations in their behavior and stress responses, which is attributed to reduced levels of neurotransmitters, such as dopamine, norepinephrine, and serotonin, which are important for ENS development and signaling by the hypothalamic-pituitary-adrenal axis²⁴. This evidence suggests that the microbiota contributes to brain development and that colonization during critical neurodevelopmental windows may have implications for CNS disorders and mental health outcomes.

GF animals also have severe immune defects and a higher susceptibility to infection. These defects are most pronounced in the gut, where there is underdevelopment of gut-associated lymphoid tissue, including smaller and fewer Peyer's patches and mesenteric lymph nodes

(MLNs), altered crypt morphology, and reduced mucus thickness^{25,26}. At a cellular level, GF mice have less abundant B cell production of sIgA²⁷. In addition, the balance between splenic CD4⁺ T helper (T_H) cell subsets is skewed towards a T_{H2} cell phenotype in GF mice, which corresponds to fewer T_{H1} cells and a heightened allergic response²⁸. GF mice also have decreased peripheral CD4⁺ T cells, including T_{H17} cells²⁹ and regulatory T cells (T_{Regs})³⁰, which are potent mediators of mucosal immunity via pro-inflammatory interleukin-17 (IL-17) and anti-inflammatory IL-10 cytokine production, respectively. Colonization of GF mice rescues the T_{H1}-T_{H2} cell imbalance and results in rapid increases in peripheral CD4⁺ T cell numbers to levels seen in conventional mice³¹, demonstrating that the microbiota is necessary for the maintenance of systemic and mucosal T cell populations.

Indeed, use of gnotobiotic animals has led to key insights into the role of the gut microbiome in intra- and extra-intestinal immune-mediated. Notably, GF status confers complete protection from the spontaneous development of IBD in genetically susceptible mice³²⁻³⁷. Furthermore, it is now possible to reconstitute a functional human immune system in these models by transplanting human liver and thymus tissue and injecting human hematopoietic stem cells into immunodeficient mouse hosts³⁸. Bone marrow, liver, thymus (BLT) humanized mice develop gut-associated lymphoid tissue-like structures that contain all the human hematopoietic lineages, and thus, provide an *in vivo* system to more accurately investigate human immune responses at the mucosal interface and the development of inflammatory and autoimmune diseases³⁹. Considerable efforts have also extended to the development and utilization of standardized defined microbial communities across gnotobiotic studies, such as the Altered Shadler Flora (ASF). The ASF is comprised of 8 mouse-derived bacterial strains that can partially restore the mucosal immune system of GF mice, including increasing the numbers of mucosal T_{Regs}⁴⁰ and production of sIgA⁴¹. However, the ASF, similar to other simplified, minimal microbial

communities, does not completely rescue all of the metabolic and immune defects of GF animals⁴². With all 8 strains having near complete genome sequences as well as being culturable and quantifiable *in vitro*⁴³, the ASF microbiota remains a useful and tractable model community. As with all animal model systems, there are limitations to how well they recapitulate the developmental complexity of human disease, especially when considering the heterogeneity of the gut microbiome⁴⁴. However, both gnotobiotic and humanized mouse models will continue to be important systems for understanding host-microbiome communication in the context of disease initiation and progression and for evaluating therapeutic strategies that manipulate the microbiome to prevent and treat disease.

Profiling biochemical activity and structure

Chromatography- and mass spectrometry-based techniques have been available for over a century; however, they have only recently been applied to host-microbiome studies⁴⁵⁻⁴⁷. Metabolite profiles of biofluid and tissue samples have been gathered using separation techniques, such as high-resolution nuclear magnetic resonance spectroscopy, gas chromatography, and high-performance liquid chromatography (HPLC), often in combination with mass spectrometry. Individual sample components can then be identified and quantified by comparing generated profiles to reference databases. Both targeted and untargeted metabolomic and metaproteomic strategies hold promise for uncovering the chemical diversity and full biochemical capacity of synthetic/engineered and natural microbial communities. However, there remain many experimental challenges related to the extraction and processing of samples, especially fecal material, for these techniques^{48,49}. As technical hurdles are overcome, data will continue to expand our knowledge of the widespread influences of the microbiome on host

physiology and provide opportunities for developing and testing diagnostics and therapeutic approaches to mitigate disease.

Targeting the microbiome's most wanted

Given the abundance and diversity of microbial communities, it is important to analyze the individual species and strains within these communities and their associated functions, especially for uncultured or low-abundance microorganisms. These can be achieved by using tools that assign strain specificity and assemble individual genomes from whole metagenomic sequencing data^{50,51} or by using hybrid capture and single-cell approaches that involve the isolation and sequencing of rare species or single microbial cells.

Hybridization methods that selectively enrich for genomic targets of interest have been applied to diverse studies and have been used successfully to capture rare, ancient, and difficult to obtain DNAs and cDNAs⁵²⁻⁵⁵. This technology involves array- or solution-based capture of target homologous DNA fragments from a next generation sequence library using synthesized oligonucleotide probes or PCR products with DNA sequences of interest as bait. Library fragments with homology to the bait sequences are selected and can then be sequenced and analyzed. Although this technique improves the recovery of whole genomes and transcriptomes from rare species, it is still limited by the need for *a priori* knowledge of target sequences⁵⁶.

Characterization and quantification of individual microbial cells can be achieved using flow cytometry and mass spectroscopy to measure metabolic activity⁵⁷. However, while single-cell strategies enable the analysis of cell-to-cell functional variation and the discovery of novel regulatory mechanisms, it remains difficult to sort individual cells from a heterogeneous community and sample at enough depth to retrieve biologically meaningful data⁵⁸. Despite these limitations, targeted enrichment sequencing can minimize host sequence contamination, reduce

the difficulty of assembling genes and individual genomes, and decrease amplification bias⁵⁹, which often burdens the analysis of more diverse microbial communities. The promise of these approaches has led to a push for improved microfluidics platforms and software applications⁶⁰ that can more accurately capture and analyze microbiome diversity and provide an enhanced understanding of the genetic variation and functional contribution of individual members.

Summary

While much knowledge has been gleaned about the complex assemblage of microbes inhabiting the human body, there is still room for new and improved technologies and animal models that tackle the challenge of relating the microbiota to host health and disease. Expanding our understanding of microbiome diversity, dynamics, and function is essential for realizing the potential for modulating features of the microbiota to promote human health.

IBD PATHOGENESIS: A ROLE FOR MICROBIAL DYSBIOSIS

Clinical presentation and epidemiology

IBD is an idiopathic, chronic and relapsing inflammatory disorder of the gastrointestinal tract. It has two main clinical phenotypes, Crohn's disease (CD) and ulcerative colitis (UC). Pathologically, CD differs from UC both in location and extent of mucosal inflammation. In CD, inflammation can extend through all the layers of the intestines, affect any part of the gastrointestinal tract (most commonly the terminal ileum or proximal colon), and occur in a discontinuous fashion⁶¹. Conversely, UC is characterized by superficial inflammation that is limited to the mucosal lining of the colon, beginning in the rectum and expanding proximally in a continuous fashion⁶². Clinically, IBD is associated with intermittent symptoms of persistent and bloody diarrhea, abdominal pain, cramping, weight loss, and fatigue. These clinical

manifestations present in early adulthood, with a diagnosis often occurring before age 30, and persist in a remitting and relapsing manner throughout life⁶³. In addition, IBD patients are prone to extra-intestinal chronic inflammatory conditions⁶⁴ and an elevated risk of developing colorectal cancer later in life⁶⁵.

The incidence and prevalence of IBD is increasing worldwide, with the highest rates reported in North America and northern Europe⁶³ (**Figure 1.3**). In the United States, IBD affects approximately 1.5 million individuals, with the number of new cases rising each year. An increase in incidence is also reported in Asia, where IBD has previously been rare. Indeed, epidemiological evidence has undoubtedly mirrored shifts towards a more western, industrialized lifestyle and suggested a role for environmental factors in IBD risk and disease pathogenesis.

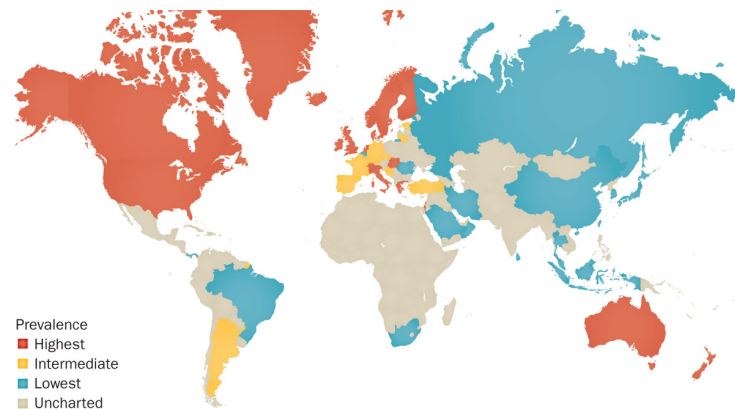


Figure 1.2. Global prevalence of IBD in 2015. Reported rates of IBD prevalence are highest in North America, northern Europe, and Australia. However, rates are increasing worldwide and are mirroring shifts towards a more western, industrialized lifestyle. Reproduced from: Kaplan, G.G. *Nat Rev Gastroenterol Hepatol.* **12**, (2015).

Host genetics in IBD

IBD was initially considered a genetic disease based on the increased risk of disease development in specific ethnic populations and between relatives, especially monozygotic twins. To gain insight into the genetic factors that contribute to IBD pathogenesis, large-scale sequencing efforts were conducted. Rare variant analysis found that distinct homozygous loss-of-

function mutations in the IL-10 receptor were associated with an aggressive, early-onset colitis⁶⁶. Genome-wide association studies between healthy and diseased individuals identified an additional 160 susceptible loci associated with IBD⁶⁷⁻⁶⁹, with many risk alleles located in genes that influence host-microbiota interactions and mucosal immune homeostasis.

For CD, polymorphisms were observed in genes involved in bacterial recognition (nucleotide-binding oligomerization domain-containing protein 2 [NOD2]) and autophagy-mediated bacterial killing (autophagy-related 16-like 1 protein [ATG16L1], immunity-related GTPase M proteins [IRGM])⁷⁰. NOD2 is an intracellular PRR that senses bacterial peptidoglycan and is expressed by diverse cell types, including APCs, endothelial cells, epithelial cells, and Paneth cells. Similar to other PRRs, activation of NOD2 leads to the production of pro-inflammatory cytokines and AMPs, which are important for bacterial clearance and maintaining intestinal homeostasis. Autophagy is a conserved mechanism for degrading intracellular components, such as apoptotic bodies, microbes, and organelles, that involves the coordinated interaction of many proteins, including ATG16L1 and IRGM⁷¹. Low ATG16L1 expression in mice is associated with abnormal Paneth cell morphology and function, including reduced secretion of AMPs and increased expression of pro-inflammatory effector molecules⁷². T-cell tolerance is also regulated by autophagy and defects may augment intestinal inflammation^{73,74}. For both CD and UC, polymorphisms were observed in genes in the IL-23-T_H17 immune response pathway, a signaling pathway implicated in multiple immune-mediated diseases⁷⁵.

How and to what extent these and other risk alleles increase susceptibility to IBD has been speculated but remains elusive. Moreover, the predicted disease heritability of these susceptibility loci is less than 30%⁶⁹, indicating that genetic risk alone is not sufficient to cause disease. Thus, extensive analysis of genome-wide association studies across multiple, large cohort populations confirms the complexity of IBD pathogenesis and the importance of considering the interaction of

host genetics with other factors, including microbial and environmental factors, in the development of disease.

Microbial dysbiosis in IBD

The involvement of bacteria in the pathogenesis of IBD has been substantiated by data generated from preclinical models. In chemically-induced and genetically-engineered mouse models of IBD, disease pathology is often attenuated or absent when mice are maintained under GF conditions^{32-37,76} (Table 1.1). Remarkably, in some genetically-engineered models, transferring the microbiota from IBD donor mice to wild-type recipients can induce disease^{37,77}. Indeed, these observations suggest that the gut microbiota can trigger and/or potentiate chronic intestinal inflammation and support the possibility that gut microbiome disease phenotypes may be transmissible.

Table 1.1. Common experimental models of IBD. Chemically-induced and genetically-engineered mouse models of IBD have been extensively used and characterized in great detail. Listed here are several models, including the nature and kinetics of their response and their disease status when maintained under GF conditions.

Model	Nature of Model	Nature of Response ^a	Kinetics of Response	Disease Status when GF	Ref.
DSS	Chemically-induced	Epithelial damage and bacterial translocation	Acute or Chronic	Absent	78
<i>Il-10</i> ^{-/-}	Spontaneous	Macrophage dysfunction and loss of immunoregulation	Chronic	Absent	34
<i>T-bet</i> ^{-/-} <i>RAG2</i> ^{-/-} (TRUC)	Spontaneous	Defects in innate and adaptive immunity including dysregulated TNF- α production by dendritic cells	Chronic	Absent	37
Adoptive transfer of naïve CD4 ⁺ T cells	Spontaneous	Deficiency in FOXP3 ⁺ T _{Regs} and loss of immunoregulation	Chronic	Absent	30

^a TNF- α , tumor necrosis factor-alpha. FOXP3, forkhead box P3.

Advances in microbiome tools and technologies have enabled an in-depth characterization of the gut microbiota and dysbiosis in IBD. Gut microbiomes of healthy individuals are taxonomically diverse and comprised of approximately 90% Firmicutes and Bacteroidetes and 10% Actinobacteria and Proteobacteria³. A shared feature of IBD-associated gut microbiomes is reduced microbial density and biodiversity, both in terms of clades and gene abundances, which is often more prominent in CD than UC⁷⁹⁻⁸¹. At the phylum-level, compared to healthy controls, IBD patients exhibit reductions in Firmicutes and Bacteroidetes and expansions in Proteobacteria^{82,83}. Most of the known pathogens associated with intra- and extra-intestinal inflammatory disorders in humans are Gram-negative facultative anaerobes that belong to the phylum Proteobacteria⁸³. Many within the diverse *Enterobacteriaceae* family, including *Escherichia*, *Klebsiella*, and *Proteus*, are considered opportunistic pathogens because they are normally low-abundance members of the microbiota but have the potential to bloom and cause disease^{37,84,85}. Shifts toward more Proteobacteria in IBD suggest that members of this microbial lineage may play a role in the initiation and progression of chronic inflammation.

Accompanying gains in colitogenic bacteria are often reciprocal losses in protective symbionts⁸⁶. Bacteria with beneficial immunomodulatory properties are typically less prevalent in IBD-associated gut microbiomes, including species of *Bacteroides*^{87,88}, *Clostridium*^{89,90}, *Feacalibacterium*^{88,91}, and *Bifidobacterium*⁹². How perturbations to gut microbial community diversity and composition influence the host and contribute to disease pathogenesis remains unclear; however, novel computational approaches have begun to provide new insights into the molecular and metabolic functions of the microbiome in IBD. Mapping differences in gut microbiota composition and function between IBD patients and healthy controls revealed more changes in community-wide (metagenome) function than community membership⁹³. IBD-associated microbiomes favored pathways for bacterial survival and pathogenesis in favor of

pathways for energy biosynthesis and metabolism⁹³, further implicating a shift from a symbiotic protective microbiota to one with greater pathogenic potential in IBD (**Figure 1.4**). Pioneering studies, like this one, underscore the importance of interrogating microbiome dysfunctions in IBD and elucidating the functional consequences of microbial dysbiosis for the host.

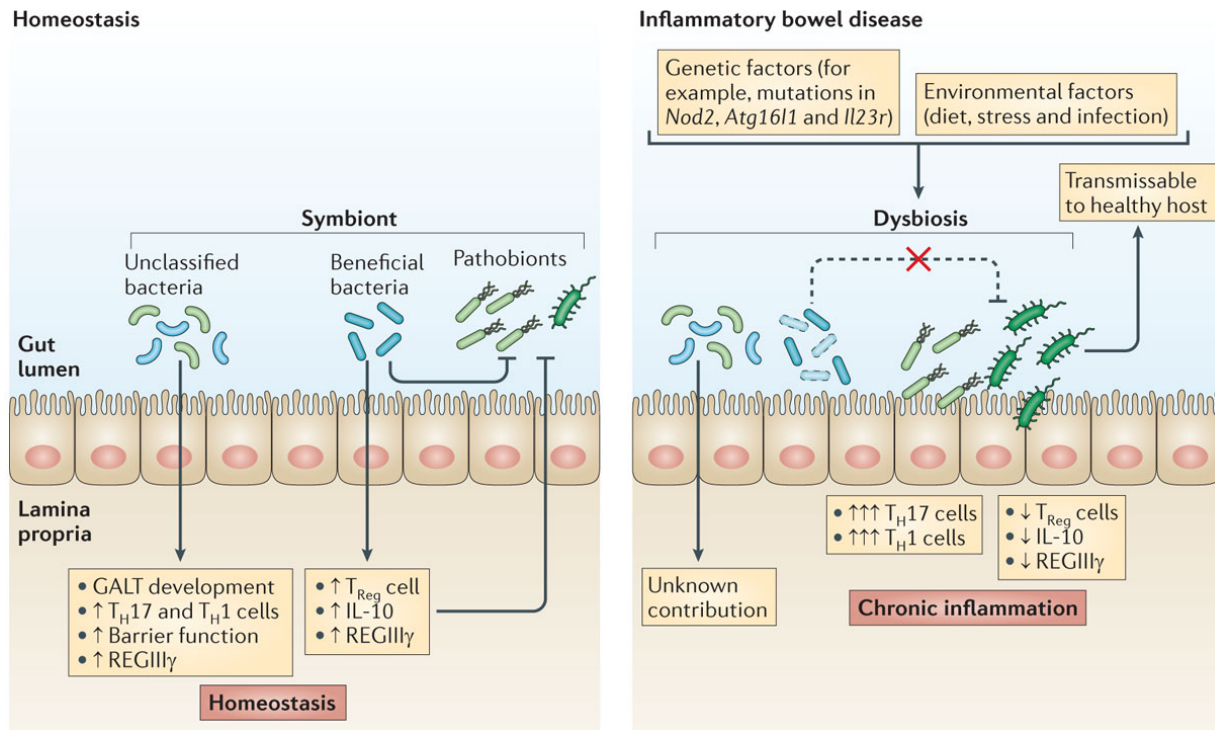


Figure 1.3. Protective and pathogenic role of the gut microbiota in IBD. A ‘healthy’ microbiome provides crucial molecular cues – through microbial surface components and metabolites – that are essential for priming the mucosal immune system and maintaining intestinal homeostasis. Left panel: During homeostasis, protective (i.e. beneficial) symbionts with anti-inflammatory properties can suppress colitogenic bacteria partly through the induction of regulatory responses, involving the expansion of T_{Reg}s and the production of IL-10 and AMPs (REGIIIγ). Right panel: A combination of genetic and environmental factors can promote dysbiosis and trigger the loss of protective symbionts and/or the accumulation of colitogenic bacteria. This shift in the gut microbiota can fuel chronic inflammation via enhanced inflammatory responses, involving T_H1 and T_H17 cells, and reduced regulatory responses. REGIIIγ, regenerating islet-derived protein 3γ. Reproduced from: Kamada, N. *et al. Nat Rev. Immunol.* **13**, (2013).

Protective symbionts and their beneficial components or metabolites

The single layer of epithelial cells that make up the mucosal interface between host and microbiota allows microbial components and metabolic products to gain access to and interact with host cells and thus influence immune responses and disease risk. *Bacteroides fragilis* is an

obligate anaerobe found in the outer mucus layer of the colon. Its structural component, polysaccharide A, can suppress inflammation in preclinical models of colitis by inducing IL-10 production and enhancing the frequency and function of T_{Regs}^{87,94}. Short-chain fatty acids (SCFAs: acetate, butyrate, propionate) have also emerged as important regulators of host mucosal immune responses and bacteria that produce SCFAs are reduced in IBD⁸⁹. SCFAs are metabolites generated from bacterial fermentation of undigested dietary fibers and their effects are mediated, in part, by inhibition of histone deacetylases and by signaling through G protein-coupled receptors. SCFA-induced histone deacetylase inhibition can inactivate nuclear factor-kappa B and down-regulate the production of pro-inflammatory cytokines^{95,96} as well as regulate the number and function of colonic T_{Regs}^{90,97,98}. Providing mice high-fiber or SCFA-supplemented diets can suppresses colonic inflammation through the increased suppressive activity of T_{Regs}^{89,98-100}. SCFAs also enhance IEC barrier function. Inoculating GF mice with SCFA-producing bacteria can induce goblet cell differentiation and mucus production, as was observed with *Bacteroides thetaiotaomicron* and *Feacalibacterium prausnitzii*⁸⁸ and can protect against enteropathogenic *E. coli* O157:H7 infection, as was observed with *Bifidobacterium longum*⁹². These observations illuminate the role of microbial components and metabolites in modulating host immunity and how the loss of immunomodulatory functions can disrupt host-microbial immune homeostasis.

Pathogens and opportunistic pathogens with the ability to fuel host inflammation

The innate immune system encounters an abundant and diverse number of microbial antigens and is equipped with PRRs to monitor, coordinate and respond to changes in the microbial landscape. PRRs initiate conserved signaling cascades that drive effector responses, including the production of AMPs, cytokines, chemokines and apoptotic factors¹⁰¹, that are crucial for host defense. A shared characteristic of many pathogens is the ability to evade or disrupt host

innate immune responses and incite inflammation. Many enteric pathogens, including species of *Campylobacter*, *Escherichia*, *Helicobacter*, *Mycobacterium*, *Salmonella*, are enriched in some IBD patients and are speculated to contribute to disease pathogenesis⁸³. Despite these associations, no single pathogen has been proven to cause disease¹⁰². However, evidence suggests that some pathogens and opportunistic bacteria can employ divisive mechanisms to exploit the host to initiate or exacerbate disease¹⁰³.

Several pathogens associated with acute intestinal inflammation, including *Salmonella enterica* serovar Typhimurium and enterohemorrhagic *Escherichia coli* (EHEC), have evolved strategies to both subvert host immune defenses and to outcompete endogenous bacteria in the gut. *S. Typhimurium*'s virulence is mediated by its ability to invade the epithelium and survive within macrophages. As a result of infection, a neutrophil-induced inflammatory oxidative burst facilitates the conversion of thiosulfate into tetrathionate, which is an exclusive terminal electron acceptor for anaerobic respiration in *S. Typhimurium*⁸⁵. By invading the IEC barrier, triggering inflammation, and promoting tetrathionate production, *S. Typhimurium* in turn acquires a unique growth advantage. Similarly, nitrogen sources released into the epithelium during IEC turnover, such as ethanolamine, contribute selectively to *S. Typhimurium* and EHEC growth and not other gut microbiota symbionts¹⁰⁴. EHEC's virulence, in particular, is mediated by its ability to attach and localize to the epithelium where there is less competition for nutrients or direct competition with other bacteria¹⁰⁵. These subtle changes in the mode of respiration, from anaerobic fermentation to anaerobic respiration, are fundamental mechanism employed by pathogens to overcome competition and to gain a survival advantage and provide key insights into the biomolecular cues involved in pathogen-host interactions.

Other opportunistic bacteria have developed mechanisms that have allowed them to adapt to and co-exist with the host¹⁰⁶, which holds true for certain *E. coli* species implicated in the

pathogenesis of IBD given their abnormal abundance in mucosal lesions of CD patients and their pathogenic properties *in vitro* and *in vivo*¹⁰⁷. The prototype AIEC strain LF82 is capable of adhering to and invading IECs through the induction of virulence genes for flagellar and type-1 pili proteins¹⁰⁸. Moreover, LF82 can evade host defenses by invading and surviving within macrophages and by perturbing host signaling pathways to enable intracellular replication without inducing macrophage cell death^{109,110}. Identifying genetic susceptibility loci associated with CD risk has strengthened LF82's clinical relevance. Many loci are located in genes that mediate innate immunity, influencing aspects of bacterial recognition, handling of intracellular pathogens, and immune regulation^{68,69}. Distinctive virulence mechanisms utilized by AIEC in the context of a genetically predisposed host have warranted additional studies to understand their role IBD pathogenesis.

Summary

While accumulating data support a link between perturbations to the gut microbiome and loss of host-microbiota homeostasis in IBD, many of these observations are descriptive and correlative in nature. They do not inform on whether dysbiosis is a cause or consequence of IBD or whether the dynamics of dysregulated host-microbe interactions are constant or evolve throughout the course of disease¹¹¹. While the focus of this Chapter is on changes in bacterial populations, there is also evidence for alterations in other microbiota constituents, such as archaea, fungi, protozoa, and viruses in IBD; however, their role in disease pathogenesis is less well understood. Thus, further research is needed to unravel the consequences of gut microbiota shifts in IBD in order to explore the potential of manipulating the microbiome to restore homeostasis, and ultimately, prevent and treat disease.

CURRENT TREATMENT APPROACHES FOR IBD

Host-directed therapies

As there is no cure for IBD, medical treatments that target host inflammation are the first therapeutic option for managing disease. The goal of every treatment is to either induce clinical remission (defined by the absence of symptoms) or to maintain remission. Treatments are tailored based on disease activity (mild, moderate, severe), extent of gastrointestinal involvement, patient disease history, and previous responses to treatment. Current host-directed therapies for IBD include: anti-inflammatories, corticosteroids, immunomodulators, biologics, and, if required or recommended due to complications, surgery (**Table 1.2**).

Biologic therapies have been an important advancement in management of IBD. Unlike corticosteroids, which suppress the body's entire immune system and often cause major side effects, biologics act selectively by targeting specific proteins with abnormal expression or activity in IBD patients and are useful for both inducing and maintaining remission. The first IBD biologic to reach the clinic was an antibody that neutralizes the activity of the pro-inflammatory cytokine TNF- α . Although successful in some IBD patients, up to one-third do not have an effective response or are unable to tolerate treatment^{112,113}. Additional biologic therapies have emerged that inhibit a different target protein, integrins. This family of receptor proteins are expressed on the surface of immune cells and are involved in the recruitment of circulating immune cells to sites of inflammation¹¹². A potential benefit of one of these integrin inhibitors, Vedolizumab, is that it specifically blocks the interaction of integrins with gut-specific adhesins and thus, may not affect immune cell trafficking to other body sites, like its earlier counterpart Natalizumab¹¹². Other biologic agents that are still in Phase III trials have also shown promising results. This includes Ustekinumab, an antibody to IL-12/23 that has been successful in psoriasis, another IL-23-mediated autoimmune disease^{114,115}. It also includes Tofacitinib, a Janus kinase (JAK) inhibitor that

interferes with the function of several cytokine receptors, which has been successful in rheumatoid arthritis¹⁶. Whether these next-generation biologics will eventually reach the clinic and how they will fit into the current treatment paradigm remains to be determined.

Table 1.2 Medical treatments for IBD. Treatments for IBD are often provided using a step-up approach – starting with anti-inflammatories and progressing toward anti-TNF- α biologics. A sequential therapy is recommended or introduced if there was failure at the prior step. However, this treatment paradigm is shifting with the advent of newer biologics. Surgery is indicated for patients with complications or disease that is unresponsive to standard treatments. Antibiotics are provided in certain circumstances.

Treatment	Mode of Action	Examples ^a	Indication ^b	Use	Notes
Anti-inflammatories (5-ASA)	Decrease mucosal inflammation	Mesalamine Olsalazine Sulfasalazine	For mild-to moderate disease or maintaining remission	Mostly UC	Well tolerated; More effective in UC than CD
Corticosteroids	Block the initiation and/or maintenance of inflammation	Budesonide Prednisolone Prednisone	For short-term control of flare-ups	CD or UC	Not recommended for long-term use or maintenance due to increased risk of toxicity and infection
Immunomodulators	Weaken or modulate immune activity	Azathioprine 6-MP Methotrexate	For maintaining remission in high-risk patients	CD or UC	Not always tolerated; Increased risk of certain cancers
Biologics	Target the pro-inflammatory cytokine TNF- α	Adalimumab Certolizumab Golimumab Infliximab	For moderate-to-severe disease in high-risk patients	CD or UC	Need for alternate therapy among initial responders due to a loss of response or intolerance; Not effective in 1/3 of patients; Increased risk of infection
	Target integrins involved in immune cell trafficking	Natalizumab Vedolizumab	For moderate-to-severe disease in high-risk patients refractory to anti-TNF- α therapy	CD only	For Natalizumab, reports of rare brain infection, liver damage, and allergic reactions
Surgery	Remove areas with severe complications or areas unresponsive to treatment	Proctocolectomy (removal of colon and rectum)	For severe disease	CD or UC	Approximately 30% of UC and 75% of CD patients eventually require surgery
Antibiotics	Target subsets of the microbiota	Ciprofloxacin Metronidazole	For blocking translocation of bacterial toxins and treating infections	Mostly CD	Used sparingly

^a 5-ASA, 5-aminosalicylic acid; 6-MP, 6-mercaptopurine.

^b high-risk patient, patient with disease refractory to standard treatment.

Microbiome-directed therapies

Antibiotics

Antibiotics were initially thought to be useful for IBD management based on the assumption that reducing concentrations of intestinal bacteria could in turn suppress aberrant intestinal immune responses and promote remission. Antibiotics have been evaluated in both CD and UC patient cohorts but the results have been conflicting¹¹⁷. Currently, antibiotics are used prophylactically in IBD when there is concern for translocation of bacterial toxins into systemic circulation, such as toxic megacolon in UC or fistulas or recurrent abscesses in CD¹¹⁸. A small subset of CD patients, whose active disease is effectively treated with antibiotics, have benefited from long-term antibiotic maintenance therapy¹¹⁷. The two most common antibiotics used clinically are the broad-spectrum antibiotics Ciprofloxacin and Metronidazole, which target Gram-negative bacteria and obligate anaerobic bacteria, respectively¹¹⁹. These antibiotics have been successful in treating complications of IBD and maintaining remission in some CD patients, but have also been associated with adverse side effects, including increased risk of *Clostridium difficile* infection, and overgrowth of antibiotic resistant bacteria. Given their ability to alter gut microbial populations through broad and potentially specific ways and to modulate IBD activity, antibiotics will likely continue to be a useful option in select cases.

Probiotics and Prebiotics

Probiotics refer to live bacteria that, when administered in adequate amounts, confer a health benefit to the host. Probiotics impart their protective effect through several proposed mechanisms including: competitive interactions with other gut microbes, production of AMPs, and providing enzymes or metabolites that modulate host responses¹²⁰. Sustained exposure to probiotics has been demonstrated to promote enhanced IEC function and less volatile innate and

adaptive immune responses¹²⁰. Moreover, specific probiotic bacteria are able to antagonize pathogenic bacteria and block their ability to adhere and translocate across the intestinal epithelium, including *Bifidobacterium* and *Lactobacillus* species¹²¹. The well-studied probiotic *E. coli* Nissle 1917, in some cases, can promote maintenance of remission in UC and its product VSL#3 in active UC¹²². Much of our understanding of the functional potential of probiotics has been drawn from experimental colitis models. There is still no definitive evidence from human studies supporting the use of probiotics in IBD¹¹² and in some cases probiotics may have detrimental effects^{112,122}.

Prebiotics refer to fermentable dietary substrates that can promote the selective growth or activity of protective bacteria in the gut. These substrates are usually non-digestible carbohydrates, such as inulin, oligofructose, and galacto-oligosaccharide, that stimulate the growth of bifidobacteria and lactobacilli in the colon and potentially contribute to IEC barrier function and enhanced immune regulation through production and function of SCFAs^{123,124}. Similar to probiotics, reports on their benefit in IBD are inconclusive or contradictory and have been mostly limited to patients with active CD¹¹². Thus, probiotics and prebiotics have the potential to improve IBD by modulating the gut microbiota and host immune function, but require more stringent analysis to discern predictive outcomes in IBD and possible side effects.

Fecal microbiota transplant (FMT)

Fecal bacteriotherapy or FMT involves the infusion or engraftment of a homogenized fecal suspension from a healthy donor into the intestinal tract of a recipient and is implemented with the expectation of restoring intestinal microbial homeostasis. Clinical effectiveness has been shown for refractory and recurrent *C. difficile* infection¹²⁵, but evidence for efficacy of FMT in IBD is less convincing¹²⁶. While *C. difficile* infection is associated with acute disruption of gut

microbiome homeostasis by a single pathogen, IBD is linked to a chronic microbial imbalance, which may explain why FMT trials have been less successful in IBD patients. From both a regulatory and ethical standpoint, more rigorous studies in animal models and clinical cohorts are required to resolve how to screen and select appropriate donors and uniformly process and administer samples as well as address long-term safety concerns. Efforts toward developing synthetic microbial communities with defined composition and predictive function may circumvent some of the current drawbacks of FMT and are a promising new area of therapeutic research for IBD.

Summary

Despite the importance of the gut microbiota to IBD pathogenesis, current medical therapies primarily focus on suppressing the host immune system rather than removing the putative agent responsible for the underlying aberrant response. However, discordant responses among patients receiving the same treatment regimens are a shared setback across host- and microbiota-directed therapies. While knowledge of the genetic and environmental factors contributing to IBD pathogenesis is incomplete, even less is known about the factors driving differences between patients and their responses to treatment. Thus, the search for definitive microbiome alterations in IBD and whether and how these features vary depending on disease phenotype is ongoing. Only through well-controlled studies incorporating multifaceted approaches to understanding treatment effects on the host and the gut microbiome can more precise ways of manipulating the microbiome be realized.

THESIS OVERVIEW

This thesis reports on the characterization of the gut microbiome in experimental colitis and describes the consequences of biochemically inhibiting and genetically inactivating a microbial virulence pathway implicated in IBD pathogenesis. In **Chapter 2**, we introduce a computational toolkit for analyzing the gut microbiome that takes 16S rRNA gene sequences as input and generates taxonomic and inferred functional abundance data as output. Using this computational pipeline, we evaluated the effects of treatment interventions in the *T-bet*^{-/-}*RAG2*^{-/-} ulcerative colitis (TRUC) model and identified features of the gut microbiome that were modulated in active disease versus treatment-induced remission. From this analysis, we observed enrichments in *Enterobacteriaceae* and pathways linking host adrenergic stress with enhanced *Enterobacteriaceae* growth and virulence in active colitis. In **Chapter 3**, we investigate whether the antivirulence drug LED209, an inhibitor of the bacterial adrenergic receptor QseC, could influence disease outcomes in three mouse models of experimental colitis. We found that LED209 reduced disease severity and differentially modified *Enterobacteriaceae* levels in these models. Given enrichments in adherent-invasive *E. coli* in IBD, in **Chapter 4**, we genetically inactivate *qseC* in the IBD-associated AIEC strain LF82 to assess its virulence potential *in vitro* and *in vivo*. We observed that the LF82- Δ *qseC* mutant had decreased expression of virulence genes, defects in motility, and reduced colonization efficiency *in vivo*. In **Chapter 5**, we end with a brief summary of findings, new perspectives, and concluding remarks.

REFERENCES

1. Eckburg, P. B. *et al.* Diversity of the human intestinal microbial flora. *Science* **308**, 1635–1638 (2005).
2. Weinstock, G. M. Genomic approaches to studying the human microbiota. *Nature* **489**, 250–256 (2012).
3. Human Microbiome Project Consortium. Structure, function and diversity of the healthy human microbiome. *Nature* **486**, 207–214 (2012).
4. Qin, J. *et al.* A human gut microbial gene catalogue established by metagenomic sequencing. *Nature* **464**, 59–65 (2010).
5. Dominguez-Bello, M. G. *et al.* Delivery mode shapes the acquisition and structure of the initial microbiota across multiple body habitats in newborns. *Proc. Natl. Acad. Sci. U.S.A.* **107**, 11971–11975 (2010).
6. Koenig, J. E. *et al.* Succession of microbial consortia in the developing infant gut microbiome. *Proc. Natl. Acad. Sci. U.S.A.* **108 Suppl 1**, 4578–4585 (2011).
7. Koren, O. *et al.* Host remodeling of the gut microbiome and metabolic changes during pregnancy. *Cell* **150**, 470–480 (2012).
8. Palmer, C., Bik, E. M., DiGiulio, D. B., Relman, D. A. & Brown, P. O. Development of the human infant intestinal microbiota. *PLoS Biol.* **5**, e177 (2007).
9. Bäckhed, F. *et al.* Dynamics and stabilization of the human gut microbiome during the first year of life. *Cell Host and Microbe* **17**, 690–703 (2015).
10. Ding, T. & Schloss, P. D. Dynamics and associations of microbial community types across the human body. *Nature* **509**, 357–360 (2014).
11. Donaldson, G. P., Lee, S. M. & Mazmanian, S. K. Gut biogeography of the bacterial microbiota. *Nat. Rev. Microbiol.* **14**, 20–32 (2016).
12. Sender, R., Fuchs, S. & Milo, R. Are we really vastly outnumbered? Revisiting the ratio of bacterial to host cells in humans. *Cell* **164**, 337–340 (2016).
13. Morgan, X. C. & Huttenhower, C. Meta'omic analytic techniques for studying the intestinal microbiome. *Gastroenterology* **146**, 1437–1448.e1 (2014).
14. Hooper, L. V., Midtvedt, T. & Gordon, J. I. How host-microbial interactions shape the nutrient environment of the mammalian intestine. *Annu. Rev. Nutr.* **22**, 283–307 (2002).
15. Ostaff, M. J., Stange, E. F. & Wehkamp, J. Antimicrobial peptides and gut microbiota in homeostasis and pathology. *EMBO Mol Med* **5**, 1465–1483 (2013).
16. Costes, L. M. M., Boeckxstaens, G. E., de Jonge, W. J. & Cailotto, C. Neural networks in intestinal immunoregulation. *Organogenesis* **9**, 216–223 (2013).
17. Peterson, L. W. & Artis, D. Intestinal epithelial cells: regulators of barrier function and immune homeostasis. *Nat. Rev. Immunol.* **14**, 141–153 (2014).
18. Hooper, L. V., Littman, D. R. & Macpherson, A. J. Interactions between the microbiota and the immune system. *Science* **336**, 1268–1273 (2012).

19. Littman, D. R. & Pamer, E. G. Role of the commensal microbiota in normal and pathogenic host immune responses. *Cell Host and Microbe* **10**, 311–323 (2011).
20. Franzosa, E. A. *et al.* Sequencing and beyond: integrating molecular ‘omics’ for microbial community profiling. *Nat. Rev. Microbiol.* **13**, 360–372 (2015).
21. Blekhman, R. *et al.* Host genetic variation impacts microbiome composition across human body sites. *Genome Biol.* **16**, 191 (2015).
22. Wostmann, B. S., Larkin, C., Moriarty, A. & Bruckner-Kardoss, E. Dietary intake, energy metabolism, and excretory losses of adult male germfree Wistar rats. *Lab. Anim. Sci.* **33**, 46–50 (1983).
23. Rosenbaum, M., Knight, R. & Leibel, R. L. The gut microbiota in human energy homeostasis and obesity. *Trends Endocrinol. Metab.* **26**, 493–501 (2015).
24. Borre, Y. E. *et al.* Microbiota and neurodevelopmental windows: implications for brain disorders. *Trends Mol Med* **20**, 509–518 (2014).
25. Deplancke, B. & Gaskins, H. R. Microbial modulation of innate defense: goblet cells and the intestinal mucus layer. *Am. J. Clin. Nutr.* **73**, 1131S–1141S (2001).
26. Smith, K., McCoy, K. D. & Macpherson, A. J. Use of axenic animals in studying the adaptation of mammals to their commensal intestinal microbiota. *Semin. Immunol.* **19**, 59–69 (2007).
27. Pabst, O. New concepts in the generation and functions of IgA. *Nat. Rev. Immunol.* **12**, 821–832 (2012).
28. Mazmanian, S. K., Liu, C. H., Tzianabos, A. O. & Kasper, D. L. An immunomodulatory molecule of symbiotic bacteria directs maturation of the host immune system. *Cell* **122**, 107–118 (2005).
29. Ivanov, I. I. *et al.* Specific microbiota direct the differentiation of IL-17-producing T-helper cells in the mucosa of the small intestine. *Cell Host and Microbe* **4**, 337–349 (2008).
30. Strauch, U. G. *et al.* Influence of intestinal bacteria on induction of regulatory T cells: lessons from a transfer model of colitis. *Gut* **54**, 1546–1552 (2005).
31. Belkaid, Y. & Naik, S. Compartmentalized and systemic control of tissue immunity by commensals. *Nat. Immunol.* **14**, 646–653 (2013).
32. Rath, H. C. *et al.* Normal luminal bacteria, especially *Bacteroides* species, mediate chronic colitis, gastritis, and arthritis in HLA-B27/human beta2 microglobulin transgenic rats. *J. Clin. Invest.* **98**, 945–953 (1996).
33. Dianda, L. *et al.* T cell receptor-alpha beta-deficient mice fail to develop colitis in the absence of a microbial environment. **150**, 91–97 (1997).
34. Sellon, R. K. *et al.* Resident enteric bacteria are necessary for development of spontaneous colitis and immune system activation in interleukin-10-deficient mice. *Infect. Immun.* **66**, 5224–5231 (1998).
35. Bohn, E. *et al.* Host gene expression in the colon of gnotobiotic interleukin-2-deficient mice colonized with commensal colitogenic or noncolitogenic bacterial strains: common patterns and bacteria strain specific signatures. *Inflamm. Bowel Dis.* **12**, 853–862 (2006).
36. Stěpánková, R. *et al.* Segmented filamentous bacteria in a defined bacterial cocktail induce intestinal inflammation in SCID mice reconstituted with CD45RBhigh CD4+ T cells. *Inflamm. Bowel Dis.* **13**, 1202–1211 (2007).

37. Garrett, W. S. *et al.* Enterobacteriaceae act in concert with the gut microbiota to induce spontaneous and maternally transmitted colitis. *Cell Host and Microbe* **8**, 292–300 (2010).
38. Melkus, M. W. *et al.* Humanized mice mount specific adaptive and innate immune responses to EBV and TSST-1. *Nat. Med.* **12**, 1316–1322 (2006).
39. Nochi, T., Denton, P. W., Wahl, A. & Garcia, J. V. Cryptopatches are essential for the development of human GALT. *Cell Rep* **3**, 1874–1884 (2013).
40. Geuking, M. B. *et al.* Intestinal bacterial colonization induces mutualistic regulatory T cell responses. *Immunity* **34**, 794–806 (2011).
41. Hapfelmeier, S. *et al.* Reversible microbial colonization of germ-free mice reveals the dynamics of IgA immune responses. *Science* **328**, 1705–1709 (2010).
42. Stecher, B., Berry, D. & Loy, A. Colonization resistance and microbial ecophysiology: using gnotobiotic mouse models and single-cell technology to explore the intestinal jungle. *FEMS Microbiol. Rev.* **37**, 793–829 (2013).
43. Wannemuehler, M. J., Overstreet, A.-M., Ward, D. V. & Phillips, G. J. Draft genome sequences of the altered schaedler flora, a defined bacterial community from gnotobiotic mice. *Genome Announc* **2**, e00287–14–e00287–14 (2014).
44. Laukens, D., Brinkman, B. M., Raes, J., De Vos, M. & Vandenaabeele, P. Heterogeneity of the gut microbiome in mice: guidelines for optimizing experimental design. *FEMS Microbiol. Rev.* **40**, 117–132 (2016).
45. Lichtman, J. S., Marcobal, A., Sonnenburg, J. L. & Elias, J. E. Host-centric proteomics of stool: a novel strategy focused on intestinal responses to the gut microbiota. *Mol. Cell Proteomics* **12**, 3310–3318 (2013).
46. Marcobal, A. *et al.* A metabolomic view of how the human gut microbiota impacts the host metabolome using humanized and gnotobiotic mice. *ISME J* **7**, 1933–1943 (2013).
47. Sridharan, G. V. *et al.* Prediction and quantification of bioactive microbiota metabolites in the mouse gut. *Nat Commun* **5**, 5492 (2014).
48. Kolmeder, C. A. & de Vos, W. M. Metaproteomics of our microbiome - developing insight in function and activity in man and model systems. *J Proteomics* **97**, 3–16 (2014).
49. Xiong, W., Abraham, P. E., Li, Z., Pan, C. & Hettich, R. L. Microbial metaproteomics for characterizing the range of metabolic functions and activities of human gut microbiota. *Proteomics* **15**, 3424–3438 (2015).
50. Cleary, B. *et al.* Detection of low-abundance bacterial strains in metagenomic datasets by eigengene partitioning. *Nature Biotechnology* **33**, 1053–1060 (2015).
51. Luo, C. *et al.* ConStrains identifies microbial strains in metagenomic datasets. *Nature Biotechnology* **33**, 1045–1052 (2015).
52. Maricic, T., Whitten, M. & Pääbo, S. Multiplexed DNA sequence capture of mitochondrial genomes using PCR products. *PLoS ONE* **5**, e14004 (2010).
53. Burbano, H. A. *et al.* Targeted investigation of the Neandertal genome by array-based sequence capture. *Science* **328**, 723–725 (2010).

54. Duncavage, E. J. *et al.* Hybrid capture and next-generation sequencing identify viral integration sites from formalin-fixed, paraffin-embedded tissue. *J Mol Diagn* **13**, 325–333 (2011).
55. Cabanski, C. R. *et al.* cDNA hybrid capture improves transcriptome analysis on low-input and archived samples. *J Mol Diagn* **16**, 440–451 (2014).
56. Lim, S. W., Tran, T. M. & Abate, A. R. PCR-activated cell sorting for cultivation-free enrichment and sequencing of rare microbes. *PLoS ONE* **10**, e0113549 (2015).
57. Maurice, C. F. & Turnbaugh, P. J. Quantifying the metabolic activities of human-associated microbial communities across multiple ecological scales. *FEMS Microbiol. Rev.* **37**, 830–848 (2013).
58. Lasken, R. S. & McLean, J. S. Recent advances in genomic DNA sequencing of microbial species from single cells. *Nat. Rev. Genet.* **15**, 577–584 (2014).
59. Segata, N. *et al.* Computational meta'omics for microbial community studies. *Mol. Syst. Biol.* **9**, 666 (2013).
60. Ufarté, L., Potocki-Veronese, G. & Laville, É. Discovery of new protein families and functions: new challenges in functional metagenomics for biotechnologies and microbial ecology. *Front Microbiol* **6**, 563 (2015).
61. Baumgart, D. C. & Sandborn, W. J. Crohn's disease. *Lancet* **380**, 1590–1605 (2012).
62. Ordás, I., Eckmann, L., Talamini, M., Baumgart, D. C. & Sandborn, W. J. Ulcerative colitis. *Lancet* **380**, 1606–1619 (2012).
63. Ananthakrishnan, A. N. Epidemiology and risk factors for IBD. *Nat Rev Gastroenterol Hepatol* **12**, 205–217 (2015).
64. Larsen, S., Bendtzen, K. & Nielsen, O. H. Extraintestinal manifestations of inflammatory bowel disease: epidemiology, diagnosis, and management. *Ann. Med.* **42**, 97–114 (2010).
65. Herszényi, L., Barabás, L., Miheller, P. & Tulassay, Z. Colorectal cancer in patients with inflammatory bowel disease: the true impact of the risk. *Dig Dis* **33**, 52–57 (2015).
66. Glocker, E.-O. *et al.* Inflammatory bowel disease and mutations affecting the interleukin-10 receptor. *N. Engl. J. Med.* **361**, 2033–2045 (2009).
67. Abraham, C. & Cho, J. H. Inflammatory bowel disease. *N. Engl. J. Med.* **361**, 2066–2078 (2009).
68. Khor, B., Gardet, A. & Xavier, R. J. Genetics and pathogenesis of inflammatory bowel disease. *Nature* **474**, 307–317 (2011).
69. Jostins, L. *et al.* Host-microbe interactions have shaped the genetic architecture of inflammatory bowel disease. *Nature* **491**, 119–124 (2012).
70. Abraham, C. & Cho, J. H. Functional consequences of NOD2 (CARD15) mutations. *Inflamm. Bowel Dis.* **12**, 641–650 (2006).
71. Levine, B. & Deretic, V. Unveiling the roles of autophagy in innate and adaptive immunity. *Nat. Rev. Immunol.* **7**, 767–777 (2007).
72. Cadwell, K. *et al.* A key role for autophagy and the autophagy gene Atg16l1 in mouse and human intestinal Paneth cells. *Nature* **456**, 259–263 (2008).

73. Nedjic, J., Aichinger, M., Emmerich, J., Mizushima, N. & Klein, L. Autophagy in thymic epithelium shapes the T-cell repertoire and is essential for tolerance. *Nature* **455**, 396–400 (2008).
74. McGeachy, M. J. & Cua, D. J. Th17 cell differentiation: the long and winding road. *Immunity* **28**, 445–453 (2008).
75. Fujino, S. *et al.* Increased expression of interleukin 17 in inflammatory bowel disease. *Gut* **52**, 65–70 (2003).
76. Kamada, N., Seo, S.-U., Chen, G. Y. & Nuñez, G. Role of the gut microbiota in immunity and inflammatory disease. *Nat. Rev. Immunol.* **13**, 321–335 (2013).
77. Garrett, W. S. *et al.* Communicable ulcerative colitis induced by T-bet deficiency in the innate immune system. *Cell* **131**, 33–45 (2007).
78. Pils, M. C. *et al.* Commensal gut flora reduces susceptibility to experimentally induced colitis via T-cell-derived interleukin-10. *Inflamm. Bowel Dis.* **17**, 2038–2046 (2011).
79. Ott, S. J. *et al.* Reduction in diversity of the colonic mucosa associated bacterial microflora in patients with active inflammatory bowel disease. *Gut* **53**, 685–693 (2004).
80. Manichanh, C. *et al.* Reshaping the gut microbiome with bacterial transplantation and antibiotic intake. *Genome Res.* **20**, 1411–1419 (2010).
81. Erickson, A. R. *et al.* Integrated metagenomics/metaproteomics reveals human host-microbiota signatures of Crohn's disease. *PLoS ONE* **7**, e49138 (2012).
82. Frank, D. N. *et al.* Disease phenotype and genotype are associated with shifts in intestinal-associated microbiota in inflammatory bowel diseases. *Inflamm. Bowel Dis.* **17**, 179–184 (2011).
83. Mukhopadhyay, I., Hansen, R., El-Omar, E. M. & Hold, G. L. IBD-what role do Proteobacteria play? *Nat Rev Gastroenterol Hepatol* **9**, 219–230 (2012).
84. Lupp, C. *et al.* Host-mediated inflammation disrupts the intestinal microbiota and promotes the overgrowth of Enterobacteriaceae. *Cell Host and Microbe* **2**, 119–129 (2007).
85. Winter, S. E. *et al.* Gut inflammation provides a respiratory electron acceptor for Salmonella. *Nature* **467**, 426–429 (2010).
86. Kamada, N., Chen, G. Y., Inohara, N. & Nuñez, G. Control of pathogens and pathobionts by the gut microbiota. *Nat. Immunol.* **14**, 685–690 (2013).
87. Round, J. L. *et al.* The Toll-like receptor 2 pathway establishes colonization by a commensal of the human microbiota. *Science* **332**, 974–977 (2011).
88. Wrzosek, L. *et al.* Bacteroides thetaiotaomicron and Faecalibacterium prausnitzii influence the production of mucus glycans and the development of goblet cells in the colonic epithelium of a gnotobiotic model rodent. *BMC Biol.* **11**, 61 (2013).
89. Atarashi, K. *et al.* Induction of colonic regulatory T cells by indigenous Clostridium species. *Science* **331**, 337–341 (2011).
90. Furusawa, Y. *et al.* Commensal microbe-derived butyrate induces the differentiation of colonic regulatory T cells. *Nature* **504**, 446–450 (2013).
91. Sokol, H. *et al.* Faecalibacterium prausnitzii is an anti-inflammatory commensal bacterium identified

- by gut microbiota analysis of Crohn disease patients. *Proc. Natl. Acad. Sci. U.S.A.* **105**, 16731–16736 (2008).
92. Fukuda, S. *et al.* Bifidobacteria can protect from enteropathogenic infection through production of acetate. *Nature* **469**, 543–547 (2011).
 93. Morgan, X. C. *et al.* Dysfunction of the intestinal microbiome in inflammatory bowel disease and treatment. *Genome Biol.* **13**, R79 (2012).
 94. Mazmanian, S. K., Round, J. L. & Kasper, D. L. A microbial symbiosis factor prevents intestinal inflammatory disease. *Nature* **453**, 620–625 (2008).
 95. Usami, M. *et al.* Butyrate and trichostatin A attenuate nuclear factor kappaB activation and tumor necrosis factor alpha secretion and increase prostaglandin E2 secretion in human peripheral blood mononuclear cells. *Nutr Res* **28**, 321–328 (2008).
 96. Vinolo, M. A. R. *et al.* Suppressive effect of short-chain fatty acids on production of proinflammatory mediators by neutrophils. *J. Nutr. Biochem.* **22**, 849–855 (2011).
 97. Arpaia, N. *et al.* Metabolites produced by commensal bacteria promote peripheral regulatory T-cell generation. *Nature* **504**, 451–455 (2013).
 98. Smith, P. M. *et al.* The microbial metabolites, short-chain fatty acids, regulate colonic Treg cell homeostasis. *Science* **341**, 569–573 (2013).
 99. Maslowski, K. M. *et al.* Regulation of inflammatory responses by gut microbiota and chemoattractant receptor GPR43. *Nature* **461**, 1282–1286 (2009).
 100. Thorburn, A. N., Macia, L. & Mackay, C. R. Diet, metabolites, and ‘western-lifestyle’ inflammatory diseases. *Immunity* **40**, 833–842 (2014).
 101. Sellge, G. & Kufer, T. A. PRR-signaling pathways: Learning from microbial tactics. *Semin. Immunol.* **27**, 75–84 (2015).
 102. Packey, C. D. & Sartor, R. B. Commensal bacteria, traditional and opportunistic pathogens, dysbiosis and bacterial killing in inflammatory bowel diseases. *Curr. Opin. Infect. Dis.* **22**, 292–301 (2009).
 103. Porter, C. K., Tribble, D. R., Aliaga, P. A., Halvorson, H. A. & Riddle, M. S. Infectious gastroenteritis and risk of developing inflammatory bowel disease. *Gastroenterology* **135**, 781–786 (2008).
 104. Thiennimitr, P. *et al.* Intestinal inflammation allows Salmonella to use ethanolamine to compete with the microbiota. *Proc. Natl. Acad. Sci. U.S.A.* **108**, 17480–17485 (2011).
 105. Kamada, N. *et al.* Regulated virulence controls the ability of a pathogen to compete with the gut microbiota. *Science* **336**, 1325–1329 (2012).
 106. Tomkovich, S. & Jobin, C. Microbiota and host immune responses: a love-hate relationship. *Immunology* **147**, 1–10 (2016).
 107. Rolhion, N. & Darfeuille-Michaud, A. Adherent-invasive Escherichia coli in inflammatory bowel disease. *Inflamm. Bowel Dis.* **13**, 1277–1283 (2007).
 108. Barnich, N., Boudeau, J., Claret, L. & Darfeuille-Michaud, A. Regulatory and functional co-operation of flagella and type 1 pili in adhesive and invasive abilities of AIEC strain LF82 isolated from a patient with Crohn’s disease. *Mol. Microbiol.* **48**, 781–794 (2003).

109. Boudeau, J., Barnich, N. & Darfeuille-Michaud, A. Type 1 pili-mediated adherence of *Escherichia coli* strain LF82 isolated from Crohn's disease is involved in bacterial invasion of intestinal epithelial cells. *Mol. Microbiol.* **39**, 1272–1284 (2001).
110. Glasser, A. L. *et al.* Adherent invasive *Escherichia coli* strains from patients with Crohn's disease survive and replicate within macrophages without inducing host cell death. *Infect. Immun.* **69**, 5529–5537 (2001).
111. Dalal, S. R. & Chang, E. B. The microbial basis of inflammatory bowel diseases. *J. Clin. Invest.* **124**, 4190–4196 (2014).
112. Bernstein, C. N. Treatment of IBD: where we are and where we are going. *Am J Gastroenterol* **110**, 114–126 (2015).
113. DeFilippis, E. M., Longman, R., Harbus, M., Dannenberg, K. & Scherl, E. J. Crohn's Disease: Evolution, Epigenetics, and the Emerging Role of Microbiome-Targeted Therapies. *Curr Gastroenterol Rep* **18**, 13–9 (2016).
114. Feagan, B. G. *et al.* Vedolizumab as induction and maintenance therapy for ulcerative colitis. *N. Engl. J. Med.* **369**, 699–710 (2013).
115. Sandborn, W. J. *et al.* Vedolizumab as induction and maintenance therapy for Crohn's disease. *N. Engl. J. Med.* **369**, 711–721 (2013).
116. Sandborn, W. J. *et al.* Ustekinumab induction and maintenance therapy in refractory Crohn's disease. *N. Engl. J. Med.* **367**, 1519–1528 (2012).
117. Khan, K. J. *et al.* Antibiotic therapy in inflammatory bowel disease: a systematic review and meta-analysis. *Am J Gastroenterol* **106**, 661–673 (2011).
118. Sandborn, W. J. *et al.* Tofacitinib, an oral Janus kinase inhibitor, in active ulcerative colitis. *N. Engl. J. Med.* **367**, 616–624 (2012).
119. Kociolek, L. K. & Gerding, D. N. Breakthroughs in the treatment and prevention of *Clostridium difficile* infection. *Nat Rev Gastroenterol Hepatol* **13**, 150–160 (2016).
120. Ng, S. C., Hart, A. L., Kamm, M. A., Stagg, A. J. & Knight, S. C. Mechanisms of action of probiotics: recent advances. *Inflamm. Bowel Dis.* **15**, 300–310 (2009).
121. Servin, A. L. Antagonistic activities of lactobacilli and bifidobacteria against microbial pathogens. *FEMS Microbiol. Rev.* **28**, 405–440 (2004).
122. Jonkers, D., Penders, J., Masclee, A. & Pierik, M. Probiotics in the management of inflammatory bowel disease: a systematic review of intervention studies in adult patients. *Drugs* **72**, 803–823 (2012).
123. Marchesi, J. R. *et al.* The gut microbiota and host health: a new clinical frontier. *Gut* **65**, 330–339 (2016).
124. Sartor, R. B. Therapeutic manipulation of the enteric microflora in inflammatory bowel diseases: antibiotics, probiotics, and prebiotics. *Gastroenterology* **126**, 1620–1633 (2004).
125. Surawicz, C. M. & Alexander, J. Treatment of refractory and recurrent *Clostridium difficile* infection. *Nat Rev Gastroenterol Hepatol* **8**, 330–339 (2011).
126. Smits, L. P., Bouter, K. E. C., de Vos, W. M., Borody, T. J. & Nieuwdorp, M. Therapeutic potential of fecal microbiota transplantation. *Gastroenterology* **145**, 946–953 (2013).

CHAPTER 2

Gut microbiome composition and function in experimental colitis during active disease and treatment-induced remission

This Chapter is a reproduction of a published manuscript with minor modifications:

Michelle G. Rooks¹, Patrick Veiga^{1,2}, Leslie H. Wardwell-Scott^{1,3}, Timothy Tickle¹, Nicola Segata¹, Monia Michaud¹, Carey Ann Gallini¹, Chloé Beal², Johan E.T. van Hylckama-Vlieg², Sonia A. Ballal⁴, Xochitl C. Morgan¹, Jonathan N. Glickman³, Dirk Gevers⁵, Curtis Huttenhower^{1,5}, and Wendy S. Garrett. Gut microbiome composition and function in experimental colitis during active disease and treatment-induced remission. *ISME J.* **8**, 1403-1417 (2014).

¹Harvard T.H. Chan School of Public Health, Boston, MA, USA

²Danone Research, Palaiseau, France

³Harvard Medical School, Boston, MA, USA

⁴Children's Hospital, Boston, MA, USA

⁵Broad Institute of MIT and Harvard, Cambridge, MA, USA

⁶Dana-Farber Cancer Institute, Boston, MA USA

Author Contributions:

M.G.R. organized the computational pipeline implemented in this study and performed all sequence analysis. M.G.R. and W.S.G. conceptualized the study design and wrote the manuscript. C.A.G., W.S.G., and L.H.W. conducted conventional and gnotobiotic experiments. M.M. and C.B. helped carry out validation experiments. T.T., N.S., D.G., and C.H. assisted with computational analyses. J.N.G. performed blinded histological assessment. P.V., J.E.V., S.A.B., and X.C.M. offered insight into the interpretation and visualization of data.

ABSTRACT

Dysregulated immune responses to gut microbes are central to inflammatory bowel disease, and gut microbial activity can fuel chronic inflammation. Examining how IBD-directed therapies influence gut microbiomes may identify microbial community features integral to mitigating disease and maintaining health. However, IBD patients often receive multiple treatments during disease flares, confounding such analyses. Preclinical models of IBD with well-defined disease courses and opportunities for controlled treatment exposures provide a valuable solution. Here, we surveyed the gut microbiome of the TRUC (*T-bet*^{-/-}*RAG2*^{-/-} ulcerative colitis) mouse model during active disease and treatment-induced remission. Microbial features modified among these conditions included altered potential for carbohydrate and energy metabolism and bacterial pathogenesis, specifically cell motility and signal transduction pathways. We also observed an increased capacity for xenobiotics metabolism, including benzoate degradation, a pathway linking host adrenergic stress with enhanced bacterial virulence, and found decreased levels of fecal dopamine in active colitis. When transferred to gnotobiotic mice, gut microbiomes from mice with active disease versus treatment-induced remission elicited varying degrees of colitis. Thus, our study provides insight into specific microbial clades and pathways associated with health, active disease and treatment interventions in a mouse model of colitis.

INTRODUCTION

Inflammatory bowel disease (IBD) is linked to alterations in gut microbial communities and dysregulated mucosal immune responses¹⁻⁷. Management of IBD has relied on nonspecific immunosuppressive therapies, agents targeting pro-inflammatory pathways, antibiotics and more recently, probiotics⁸⁻¹⁴. However, many IBD-directed therapies are not effective in all patients and some carry a high risk of complications and side effects. How these therapies perturb the

aggregate ecology and biomolecular environment of the gut microbiome is poorly understood. Thus, determining what aspects of the gut microbiome structurally and functionally change in active colitis and treatment-induced remission may provide improved therapeutic targets.

Mouse models of IBD provide an opportunity to identify microbes and microbial pathways involved in IBD and host-microbiota responses to therapies, which can be difficult to discern in humans given their genetic diversity and variability in environmental and treatment exposures. Deciphering which gut microbial community members and functions are similarly or differentially modulated by therapeutic interventions has important implications for IBD management and may facilitate customization of existing and future therapies.

TRUC mice develop an early onset, spontaneous UC due to genetic defects in innate and adaptive immunity¹⁵. TRUC pathogenesis is driven, in part, by tumor necrosis factor-alpha (TNF- α)¹⁵ and is dependent on the gut microbiome, as germ-free (GF) TRUC mice do not develop disease¹⁶. In the presence of an endogenous microbiota, specific gut microbes have been shown to trigger TRUC colitis, including *Klebsiella pneumoniae* and *Proteus mirabilis*¹⁶ – and more recently, *Helicobacter typhlonius*¹⁷. Like human IBD, TRUC colitis is responsive to immunomodulators that dampen pro-inflammatory responses to gut microbes¹⁵ and to oral antibiotics¹⁶. Daily consumption of a fermented milk product (FMP) has also been shown to mitigate TRUC colitis¹⁸. Provided that antibiotics, immunomodulators and dietary interventions mechanistically act on different aspects of the host-microbiota interface to ameliorate TRUC colitis, they likely differentially modify the gut microbiome. Thus, TRUC mice offer a tractable model for evaluating gut microbiome contributions to colonic inflammatory pathogenesis and for characterizing gut microbiome responses to therapeutic interventions.

Here, we investigated the effects of diverse treatment interventions on host disease status and on gut microbiome structure and function in TRUC mice. Using 16S ribosomal RNA (rRNA) gene surveys, we analyzed gut microbial communities following treatment with: oral antibiotics (gentamicin, metronidazole or vancomycin), immunomodulators (TNF- α neutralizing antibodies [anti-TNF- α] or infusion of T-regulatory cells [T_{Regs}]) and dietary interventions (FMP or non-fermented milk control [MC]). In addition to examining taxonomic shifts associated with treatment exposure, we used gnotobiotic TRUC mice to test the inflammatory phenotypes of gut microbiomes from treatment groups *in vivo*. To functionally interrogate the metabolic potential of gut microbiomes associated with active colitis versus treatment-induced remission, we performed *in silico* analysis of 16S rRNA gene sequences coupled with reference genomes to infer microbial community function. We found that TRUC gut microbiomes with active colitis had a reduced potential for both carbohydrate and energy metabolism and an enhanced potential for flagellar assembly, tetrathionate respiration and benzoate degradation. Collectively, our study identified microbes and microbial functions underlying colitis-associated dysbiosis that were similarly or differentially modulated by host- and microbiota-targeted therapies, illustrating the potential for therapeutic manipulation of the gut microbiome in colitis.

RESULTS

Assessing gut microbiome structure during active disease and treatment-induced remission with 16S rRNA gene surveys

TRUC mice manifest signs of colitis prior to 3 weeks of age, which increase in severity over time¹⁵. At 3 weeks of age, mice were randomized to the following groups: antibiotics (gentamicin, metronidazole or vancomycin), immunomodulators (anti-TNF- α or T_{Regs}), dietary interventions (FMP or MC), or untreated (sham) control, and began treatment 1 week later. Stool samples were

collected from mice at 4 weeks of age (baseline/pre-intervention) and directly upon completion of the intervention at 8 weeks of age (post-intervention). The study design and histology-based colitis scores to relate gut microbiome changes to host disease status are shown (**Figure 2.1a-b**).

In total, 1,014,181 quality-filtered 16S rRNA gene sequences were obtained from 152 stool samples ($6,672 \pm 335$ reads/sample; **Supplementary Table 2.1**). Reads were binned *de novo* into approximately species-level operational taxonomic units (OTUs) at $\geq 97\%$ sequence similarity (586 ± 30 OTUs/sample; **Supplementary Table 2.1**). Microbiome analysis tools included: QIIME (Quantitative Insights Into Microbial Ecology) for sequence processing¹⁹, PICRUSt (Phylogenetic Investigation of Communities by Reconstruction of Unobserved States) for metagenome inference²⁰, HUMAnN (HMP Unified Metabolic Analysis Network) for functional profiling²¹, and LEfSe (Linear Discriminate Analysis with Effect Size) for univariate contrasts²² (**Supplementary Figure 2.1**).

Effects of treatment interventions on gut microbiome composition

Principal coordinate analysis (PCoA) of the unweighted UniFrac distances²³ revealed that baseline (pre-intervention) communities clustered together (**Figure 2.1c**, far left panel). Comparing post-treatment stool, samples tended to separate by type of intervention, with distinct clusters observed for gut microbiomes exposed to antibiotics, immunomodulators and dietary interventions (**Figure 2.1c**, middle right panel). PCoA of the weighted UniFrac distances demonstrated similar trends (**Supplementary Figure 2.2**), as did a single-dimensional UPGMA (unweighted pair group method with arithmetic mean) hierarchical clustering of these samples (**Figure 2.1d**).

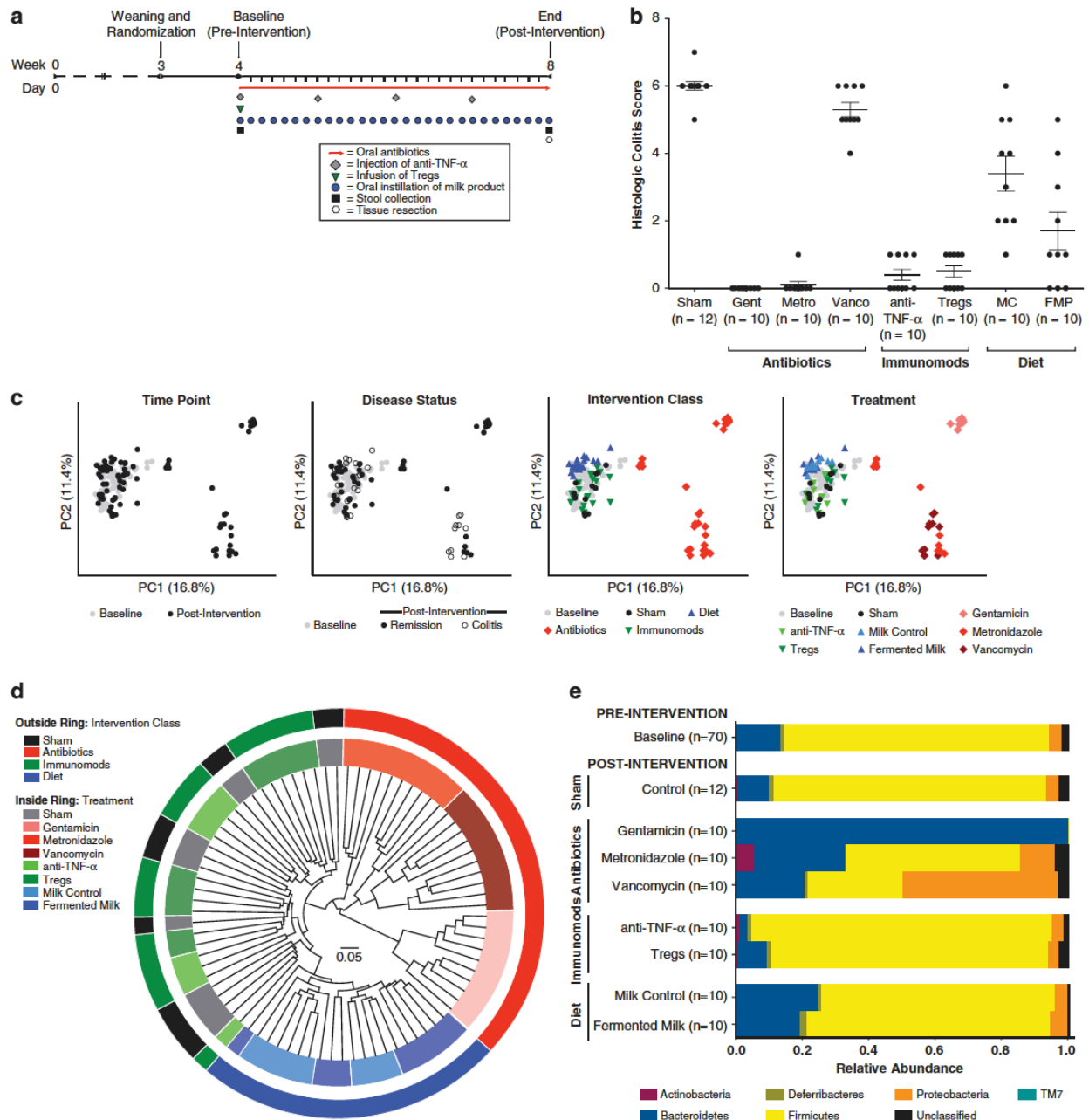


Figure 2.1. Experimental design and influence of interventions on the gut microbiome. (a) Study experimental schema. (b) Histologic colitis scores. Symbols represent individual mice. Error bars indicate mean \pm SEM. Colitis scores >2 indicate active colitis and scores ≤ 2 remission. Sham, untreated, handling control; Gent, gentamicin; Metro, metronidazole; Vanco, vancomycin; Immunomods, anti-TNF- α or T_{Reg}s; MC, non-fermented milk control; FMP, fermented milk product; Diet, dietary intervention with FMP or MC in addition to *ad libitum* chow. (c) PCoA using unweighted UniFrac distances of gut microbial communities obtained from stool samples collected at baseline (pre-intervention) and upon treatment completion (post-intervention). The first two principal coordinates (PC) from the PCoA are plotted. Symbols represent data from individual mice, color-coded by the indicated metadata. (d) Gut microbiomes were clustered by similarity using the UPGMA clustering algorithm on the unweighted UniFrac distances. Samples from individual mice were clustered by the indicated intervention class (outside ring) or by the specific treatment (inside ring). (e) Phylum-level phylogenetic classification of 16S rRNA gene sequences. Bars represent mean relative abundances for each pre- or post-intervention group.

The 16S rRNA gene survey data revealed the greatest variation in gut microbial community composition with antibiotic exposure, particularly for gentamicin and vancomycin (**Figure 2.1c**, far right panel; **Supplementary Figure 2.3**). In contrast, immunomodulators and dietary interventions (**Figure 2.1c**) induced changes of smaller effect size. Shifts in phylum-level relative abundances of samples collected at baseline and upon intervention completion also confirmed these high taxonomic level gut microbial response patterns (**Figure 2.1e**). Both in terms of microbial presence/absence and in overall clade abundances, immunomodulators, dietary interventions and individual antibiotics each perturbed the gut microbiome in distinctive ways and to varying extents, with antibiotics having the most substantial effect on microbial community structure.

Antibiotic-driven microbial community shifts may be influenced by early-life exposures and are associated with specific clade responses

Despite mitigating some IBD flares²⁴, antibiotics disrupt gut microbial community structure and diversity, pushing the microbiome to an alternate state and potentially prolonging susceptibility to pathogens^{8,11,12,14,25}. We investigated the extent to which three oral antibiotics perturb the gut microbiomes of TRUC mice: metronidazole, gentamicin and vancomycin. Gentamicin and metronidazole (the latter used clinically to treat IBD and *Clostridium difficile* colitis) both ameliorated TRUC colitis (**Figure 2.1b**). However, vancomycin, also employed clinically to treat *C. difficile* colitis, did not attenuate TRUC colitis (**Figure 2.1b**). Given that gentamicin, metronidazole and vancomycin have disparate modes of action and effects on TRUC colitis, we characterized shifts in community composition and diversity following treatment exposure and identified which members of the gut microbiome were similarly or differentially modulated by each antibiotic.

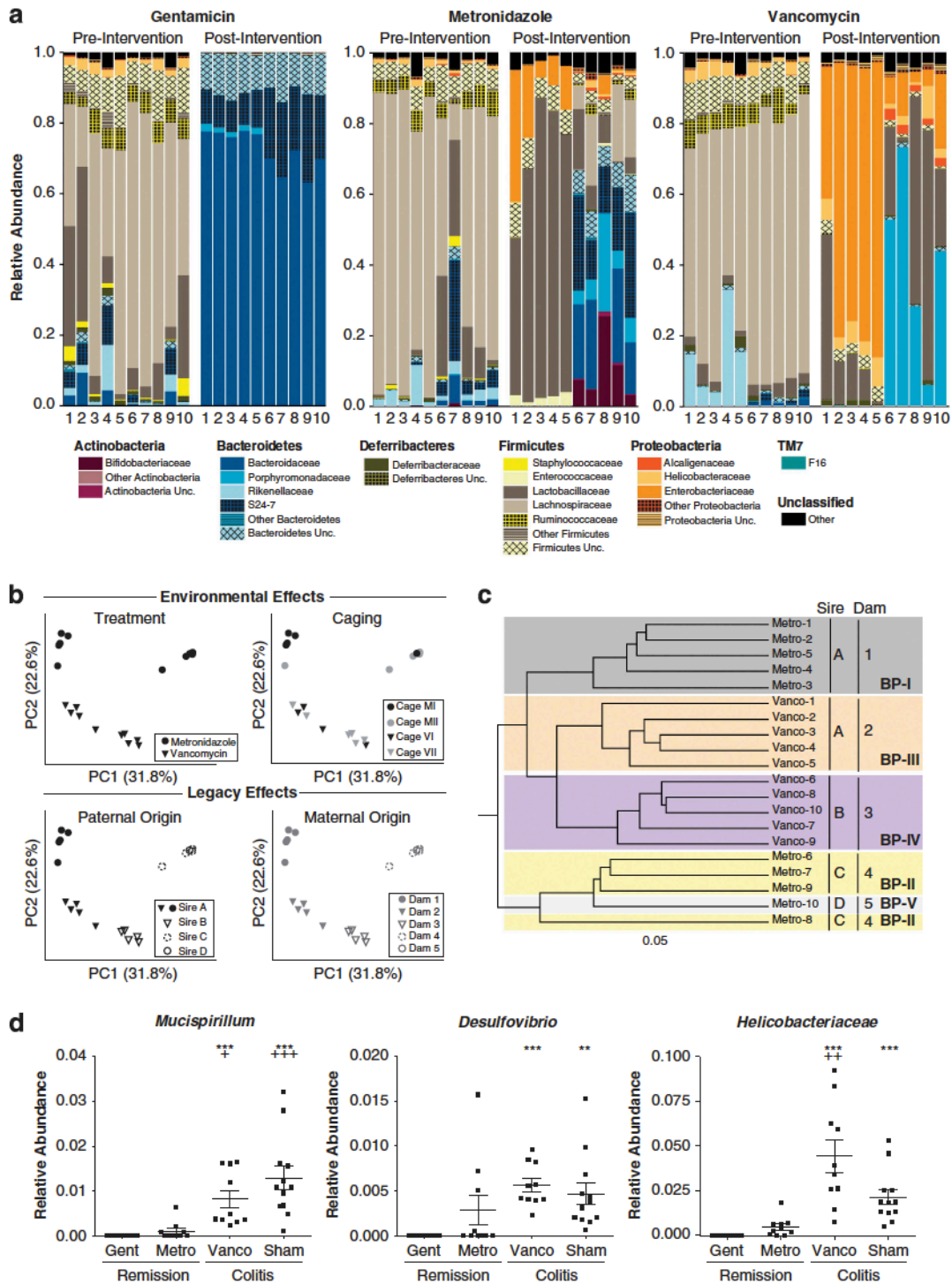


Figure 2.2. Antibiotic-driven microbial community shifts may be influenced by early-life exposures and are associated with specific clade responses. (a) Family-level phylogenetic classification of 16S rRNA gene sequences from stool samples collected pre- and post-intervention. Bars represent relative abundances of samples from individual mice. Labels indicate families with average relative abundances $\geq 1\%$ in at least one pre- or post-intervention group. Remaining families and reads assigned to higher level taxonomies were binned together in their associated phylum as ‘other’ or ‘unclassified’ (unc.), respectively.

Figure 2.2. (Continued). (b) PCoA plots of the unweighted UniFrac distances of post-intervention stool from metronidazole- and vancomycin-treated mice ($n = 10/\text{group}$). The first two PCs from the PCoA are plotted. Symbols represent data from individual mice, color-coded by the indicated metadata. For caging, M, metronidazole-treated; V, vancomycin-treated. (c) UPGMA clustering algorithm on the unweighted UniFrac distances of samples, color-coded by breeding pair (BP). The letter and number assigned to the sire and dam, respectively, correspond to the PCoA plots in **b**. (d) Differentially abundant microbial clades in stool from mice with active colitis ($n = 20$) versus remission ($n = 22$). Symbols represent data from individual mice from three independent experiments. Error bars indicate mean \pm SEM. Kruskal-Wallis test with Dunn's multiple comparison test: * or ⁺ $P < 0.05$, ** or ⁺⁺ $P < 0.01$, and *** or ⁺⁺⁺ $P < 0.001$.

In contrast to baseline microbial communities, which consisted mostly of Firmicutes followed in decreasing order of relative abundance by Bacteroidetes, Proteobacteria, Actinobacteria, Deferribacteres, and TM7, each antibiotic had marked effects on gut microbiome composition (**Figure 2.2a**). Gentamicin exposure led to a dominance of Bacteroidetes ($99.6 \pm 0.1\%$, relative abundance), particularly *Bacteroidaceae*, whereas vancomycin promoted an expansion of Proteobacteria – levels increased from $3.4 \pm 1.8\%$ to $47.0 \pm 10.8\%$. Responses within the metronidazole and vancomycin treatment groups were distinct in terms of overall community composition (**Figure 2.1c**) and by relative abundance analysis (**Figure 2.2a**). To address if host or environmental factors affect gut microbiome responses to these antibiotics, we evaluated whether treatment, caging or legacy effects (influence of parental transmission on microbial composition) corresponded to the greatest degree of microbial variation. The greatest source of variation was not cage effects – observed in some mouse gut microbiome studies and attributed to cohabitation and coprophagia²⁶. Rather, microbial communities segregated first by parental origin and second by the antibiotic administered (metronidazole versus vancomycin) (**Figure 2.2b-c**; **Supplementary Figure 2.4a**), suggesting that community structure may be influenced by early-life exposures and by post-weaning interactions with other environmental exposures, respectively.

To identify gut microbiome responses associated with antibiotics and legacy effects, we determined pre- and post-treatment microbial clade differences in progeny of breeding pairs using LEfSe. Mice enriched in Actinobacteria and *Bacteroides* (BP-II) (**Supplementary Figure**

2.4b) at baseline became further enriched in these microbial clades with metronidazole treatment (**Figure 2.2a**, Metro-6-8,10). Because metronidazole selectively targets anaerobic bacteria, it may enable aerotolerant members of the Actinobacteria and Bacteroidetes phyla to bloom. Mice enriched in *δ-proteobacteria* (BP-III) (**Supplementary Figure 2.4c**) at baseline became further enriched in Proteobacteria with vancomycin treatment (**Figure 2.2a**, Vanco-1-5). This vancomycin-induced expansion of Proteobacteria has been observed previously^{14,27}. Thus, identifying microbial clades enriched at baseline may predict gut microbial responses to antibiotics and may be useful for tailoring antibiotic treatment.

Alterations of gut microbial communities following gentamicin, metronidazole and vancomycin treatment coupled with their disparate effects on colitis provided an opportunity to identify which gut microbiome members are preferentially targeted by a given antibiotic and probe for members that are consistently associated with disease pathogenesis. Using LEfSe, we performed an all-against-all multi-class comparison of gut microbiome samples from antibiotic-treated mice to identify clades specifically modulated by each antibiotic. Although gentamicin-treated communities were completely dominated by Bacteroidetes, the remaining Firmicutes were enriched in *Erysipelotrichi* (**Supplementary Figure 2.5a**). Metronidazole treatment was associated with enrichments in Firmicutes and unclassified bacteria (**Supplementary Figure 2.5a**). In contrast with gentamicin and metronidazole, vancomycin treatment led to a significant expansion of *γ-proteobacteria* and *ε-proteobacteria*, including *Escherichia* and *Helicobacter* (**Supplementary Figure 2.5a**), which have been associated with intestinal inflammatory pathogenesis²⁸.

To explore microbial biomarkers of active colitis, we looked for clades consistently reduced in gentamicin- and metronidazole-treated communities but augmented in vancomycin and sham communities. There were significant enrichments across three microbial lineages in

colitogenic gut microbiomes: *Mucispirillum*, *Desulfovibrio* and *Helicobacteraceae* (**Figure 2.2d**; **Supplementary Figure 2.5b**), all of which discriminated between active colitis versus remission. Other studies have pointed to their opportunistic nature given their putative capacity to degrade mucin (*Mucispirillum*)^{29,30}, and during active inflammation to produce high levels of hydrogen sulfide (*Desulfovibrio*)³¹ and ammonia (*Helicobacteraceae*)³², which may further fuel inflammation.

Immunomodulators alter low abundance communities of the gut microbiome and drive distinct clade responses

Use of immunomodulators in IBD has increased given their longer disease-remission periods and fewer side effects as compared with corticosteroids^{13,33}. However, knowledge of the effects of specific immunomodulators on gut microbiomes is limited⁹. Because TRUC colitis is driven, in part, by dysregulated colonic TNF- α production, which can be ameliorated with TNF- α neutralizing antibodies or infusion of immunosuppressive T_{Reg}¹⁵, we utilized TRUC mice to unravel the effects of TNF- α -directed therapies on a colitogenic gut microbiome.

To determine the extent to which gut microbiomes are affected by immunomodulators, we inspected exclusive and shared species-level phylotypes (OTUs) among anti-TNF- α injected, T_{Reg} infused, and untreated mice. In all, 1,611 out of 4,420 total OTUs (36.5%) identified in immunomodulatory-treated and untreated mice were shared (**Figure 2.3a**, left panel). Shared OTUs were mostly more abundant species – 240,306 out of 265,344 (90.6%) of all the sequences present across samples – whereas OTUs unique to each group were mostly low abundance species (**Figure 2.3a**, right panel). T_{Reg}-infused mice had the largest number of unique species (17.3%) compared to anti-TNF- α treated (10.3%) and untreated (10.4%) mice (**Figure 2.3a**, left panel), suggesting that immunomodulators, particularly T_{Reg}s, modulate low abundance gut

microbiome members as compared to antibiotics, in agreement with the smaller effect size of shifts in community structure (Figure 2.1c, right panels).

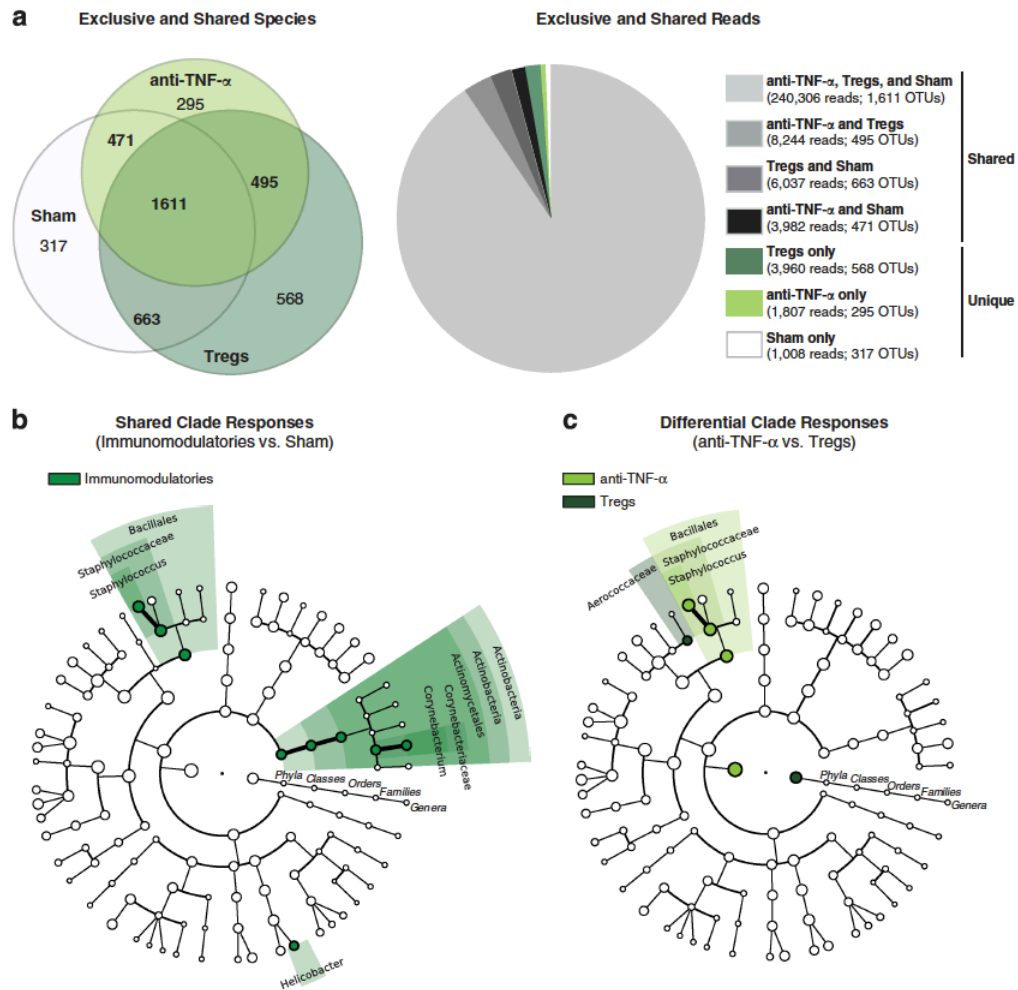


Figure 2.3. Immunomodulatories influence low abundance gut microbial community members and drive distinct microbial responses. (a) Left panel: Venn diagram of exclusive and shared species-level phylotypes (non-singleton OTUs, at $\geq 97\%$ sequence identity) in anti-TNF- α injected ($n = 10$), T_{Reg} infused ($n = 10$) or sham (untreated; $n = 12$) mice. In total, 4,420 OTUs were present across samples. Right panel: number of 16S rRNA gene sequences in each of the indicated segments of the Venn diagram. In total, 265,344 sequences were present across samples. (b) Differentially abundant microbial clades in stool from immunomodulatory-treated (anti-TNF- α or T_{Reg}s; $n = 20$) versus sham ($n = 12$) mice. (c) Differentially abundant microbial clades in stool from anti-TNF- α - versus T_{Reg}-treated mice ($n = 10$ /group). For cladograms, white circles represent non-significant microbial clades.

FMP consumption has subtle but distinct effects on the gut microbiome

Lactic acid-producing bacteria (LAB) within FMPs can improve gut homeostasis by providing microbes with beneficial functions to the host^{36,37}. LAB have shown promise in IBD

management, given their ability to promote anti-inflammatory immune responses without inducing severe side effects in IBD patients³⁷. However, little is known of how LAB modify the gut microbiome in IBD in relation to other therapies³⁸. Previous studies in TRUC mice have shown that colitis can be ameliorated with daily consumption of a LAB-containing FMP consisting of *Bifidobacterium animalis* subsp. *lactis* (CNCM I-2494), *Streptococcus thermophilus* (CNCM I-1630), two strains of *Lactobacillus delbrueckii* subsp. *bulgaricus* (CNCM I-1519 and CNCM I-1632) and *Lactococcus lactis* subsp. *cremoris* (CNCM I-1631)¹⁸. In contrast, MC administration was less effective in attenuating colitis¹⁸. To determine the differential effects of the FMP and MC on the gut microbiome, we orally instilled either product daily for 4 weeks (**Figure 2.1a-b**).

Bifidobacteriaceae and *Coriobacteriaceae* have been associated with human colonic health and IBD remission^{6,39}, and were enriched with FMP treatment (**Figure 2.4a; Supplementary Figure 2.7a**). The observed increase in *Bifidobacteriaceae* may reflect its presence in the FMP or an FMP-mediated expansion of endogenous bifidobacteria. Similar to earlier studies, we found an increase in lactate-consuming bacteria with FMP, such as *Desulfovibrionaceae*, that may be associated with elevated levels of the electron donor lactate produced by the dietary LAB in the FMP¹⁸. Differential clade responses between FMP- and MC-fed mice included enrichments of *Lactobacillus* and *Streptococcus* in the MC group, which may have been secondary to the presence of lactose and absence of LAB in the MC product (**Figure 2.4b; Supplementary Figure 2.7b-c**). Proteobacteria were enriched with FMP – this finding reflects the presence of *Helicobacter* spp., specifically *H. ganmani*, as was observed with immunomodulators (**Figure 2.3b and 4b, Supplementary Figure 2.7c**). These results point to administration of FMP having subtle but distinctive effects on the gut microbiome, which facilitate gut microbial community changes that directly or indirectly ameliorate colitis.

FMP administration influences the mucosal immune system by modulating microbial communities trafficked to the MLNs

Given the subtle clade differences in stool observed with the FMP, we questioned whether there were greater changes in other gut-associated microbial communities, like the MLNs. MLNs function as a 'firewall' that prevents live gut microbes from reaching the systemic immune system^{40,41}. Microbial DNA was sequenced from pooled MLNs ($n = 5$ MLNs/mouse) of individual FMP- and MC-fed mice. In total, 288,500 quality-filtered 16S rRNA gene sequences were obtained with an average of $7,797 \pm 5,728$ reads/sample. Comparing stool and MLN microbial communities, we observed that the major variation is explained by sampling site (biogeography) (**Figure 2.4c; Supplementary Figure 2.8**).

To identify which microbes are preferentially sampled by the host mucosal immune system or otherwise trafficked through the lymphatics to the MLNs, we examined taxonomic differences between microbiomes from stool and MLNs. We observed greater differences between MLN microbial communities than between stool communities with administration of FMP versus MC, particularly for the ratio of Firmicutes to Bacteroidetes and the proportion of total Proteobacteria (**Figure 2.4d**). This suggests that FMP exposure might affect which gut microbes reach the MLNs and consequently shape host immune responses. Microbial communities of MLNs were highly enriched in aerobes and facultative anaerobes (**Figure 2.4e**). TRUC MLNs compositionally resembled deep colonic crypt communities⁴², with both being enriched in aerotolerant clades that are rare in stool (**Figure 2.4e; Supplementary Figure 2.9**). Based on evidence for a dominant presence of aerotolerant genera at the oxygen-rich mucosal surfaces of intestinal epithelial cells^{9,13,43}, our findings suggest that aerotolerant microbes may have greater access to the MLNs.

Figure 2.4. (Continued). (a) Differentially abundant microbial clades in stool collected before and after FMP ($n = 10$). (b) Differentially abundant microbial clades in stool after FMP versus MC ($n = 10$ /group). (c) PCoA plots of the unweighted UniFrac distances of post-intervention stool samples (FMP, $n = 10$; MC, $n = 10$) and MLNs (FMP, $n = 21$; MC, $n = 16$; 5 MLNs/mouse). The first two PCs from the PCoA are plotted. Symbols represent data from individual mice, color-coded by the indicated metadata. (d) Phylum-level phylogenetic classification of 16S rRNA gene sequences from pre-intervention ($n = 20$) and post-intervention stool samples (FMP, $n = 10$; MC, $n = 10$) and post-intervention MLNs (FMP, $n = 21$; MC, $n = 16$; 5 MLNs/mouse). Pie charts represent the mean relative abundances of phyla across mice from each group. (e) Differentially abundant microbial clades in post-intervention samples from stool (FMP, $n = 10$; MC, $n = 10$) versus MLNs (FMP, $n = 21$; MC, $n = 16$; 5 MLNs/mouse). (f) Differentially abundant microbial clades in post-intervention MLNs of FMP- versus MC-fed mice ($n = 21$ and 16, respectively). *, aerotolerant genera; +, genera shared between MLNs and deep colonic crypt communities [Pédron, T. *et al. MBio* 3, (2012)]. For cladograms, white circles represent non-significant microbial clades.

MLNs of MC-fed mice, which tended to have more severe colitis compared with FMP-fed mice (**Figure 2.1b**), were highly enriched in Proteobacteria, including an increased relative abundance of *Enterobacteriaceae*. Gut microbiome studies of IBD patients have demonstrated expansions of Proteobacteria, particularly *Enterobacteriaceae*^{16,28}. We observed increased levels of *Klebsiella* in the MLNs of MC-fed mice (**Figure 2.4f; Supplementary Figure 2.10**), which have been implicated as opportunistic drivers of inflammation in TRUC mice¹⁶. In contrast, MLNs of FMP-fed mice were enriched in Firmicutes – including *Lactobacillales*, *Clostridiales* and *Coriobacteriales* (**Figure 2.4f; Supplementary Figure 2.10**). Gut microbiome status (homeostasis versus dysbiosis) can influence transport of commensal and pathogenic bacterial antigens from the lumen to the MLNs⁴⁴. Our analyses of stool and MLN microbial communities support these findings. Furthermore, increased Proteobacteria in stool and MLNs of mice with active colitis aligns with the association between Proteobacteria and IBD-associated dysbiosis.

Microbial community perturbations in active disease versus treatment-induced remission and their functional validation in gnotobiotic mice

Discriminatory microbial lineages for active colitis included the Deferribacteres, *Mucispirillum*; *Anaerotruncas*; and Proteobacteria, particularly *Enterobacteriaceae*, *Desulfovibrio*,

Helicobacteraceae, and *Sutterella* (**Figure 2.5a**; **Supplementary Figure 2.11**). In contrast, clades associated with remission included Actinobacteria; the Bacteroidetes, *S24-7*; and the Firmicutes, *Staphylococcaceae* and *Erysipelotrichales* (**Figure 2.5a**; **Supplementary Figure 2.11**).

Gnotobiotic mice represent a tractable system for testing the function or inflammatory capacity of gut microbiomes⁴⁵. Disease phenotypes, for example, diabetes and obesity, can be transferred to gnotobiotic mice by inoculating them with gut microbiomes of afflicted mice or human donors^{46,47}. To assess the inflammatory potential of gut microbiomes exposed to antibiotics, immunomodulators or FMP compared with an untreated (sham) control, we performed fecal transfers from treated or untreated specified pathogen-free (SPF) TRUC donors to germ-free (GF) TRUC recipients (**Figure 2.5b**, experimental schema). Pro-inflammatory input communities from untreated donors, on average, induced colitis over the duration of an 8-week association, whereas anti-inflammatory input communities from gentamicin and anti-TNF- α -treated donors did not induce colitis (**Figure 2.5c**). Despite FMP ameliorating colitis in SPF donors, gnotobiotic recipients tended to develop mild to moderate colitis (**Figure 2.5c**). To follow up on this finding, we measured levels of two FMP bacterial strains, *B. lactis* and *L. lactis*, in donor and recipient stool samples using real-time quantitative PCR (RT-qPCR). FMP strains were detected in donor but not recipient stool (**Figure 2.5d**). These findings suggest inefficient intestinal colonization of FMP strains from the donor stool samples and support studies showing that maintaining the benefits of FMPs requires routine administration^{18,48}. In contrast with antibiotics and immunomodulators, these experiments suggest a transient protective effect of FMP on the gut microbiome. Together, these experiments demonstrate that inflammatory phenotypes of gut microbiomes are capable of being transmitted and tested *in vivo*. Moreover, our results point to differences in the durability of gut microbiomes and their associated disease phenotypes with treatment.

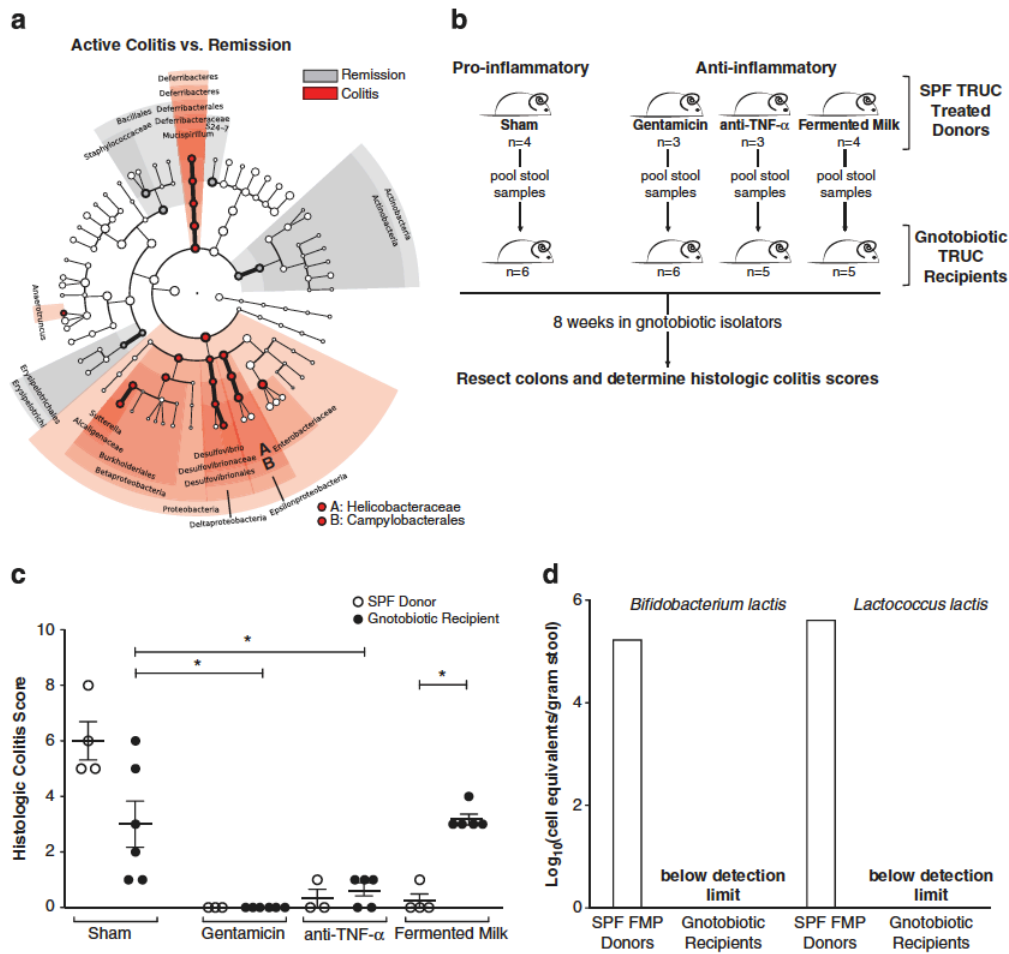


Figure 2.5. Gut microbiome composition in active colitis and treatment-induced remission with *in vivo* functional validation of proinflammatory activity in gnotobiotic TRUC mice. (a) Differentially abundant microbial clades in stool from mice with active colitis ($n = 31$) versus remission ($n = 51$) upon intervention completion. For cladogram, white circles represent non-significant microbial clades. (b) Experimental schema of 8-week gnotobiotic TRUC association with conventionally-raised, SPF TRUC donor stool. SPF donors were treated for 4 weeks prior to stool collection. Stool from the indicated number of donors was pooled and transplanted into gnotobiotic TRUC recipients. (c) Histologic colitis scores of donors and recipients. Symbols represent data from individual mice. Error bars indicate mean \pm SEM. Mann-Whitney test: * $P < 0.05$. (d) *B. lactis* and *L. lactis* levels quantified by RT-qPCR in stool from FMP-treated donors (pooled; $n = 4$) and their corresponding GF recipients ($n = 5$).

Microbial metabolic functions associated with active colitis versus treatment-induced remission

To investigate the gut microbiome functions associated with active colitis versus remission in TRUC mice following treatment, we used PICRUST to infer putative metagenomes from our 16S rRNA gene profiles²⁰. Reads were binned into OTUs at $\geq 97\%$ sequence identity using

a closed reference-based strategy that searches against the available collection of Greengenes reference OTUs. PICRUSt transformed counts of reference-based OTUs into metagenome prediction counts of functional genes on a per-sample basis and evaluated prediction accuracy by calculating the extent to which microbes in a sample are related to sequenced reference genomes using the weighted Nearest Sequenced Taxon Index (NSTI) (**Supplementary Table 2.2**).

Identified microbial gene families (specified by Kyoto Encyclopedia of Genes and Genomes [KEGG] Orthology groups [KOs]) were grouped into metabolic pathways and broader functional categories based on the BRITE hierarchy. We used LEfSe to identify significant, differentially abundant microbially relevant functions associated with active colitis versus remission following treatment (**Supplementary Figure 2.12**). Categories associated with remission included carbohydrate metabolism and energy metabolism, as well as the biosynthesis of secondary metabolites. In contrast, gut microbiomes with active colitis were enriched in categories associated with cell motility, signal transduction and xenobiotics biodegradation and metabolism, as well as lipid metabolism (**Figure 2.6a**). Thus, gut microbiomes associated with active colitis may have a reduced capacity for energy harvest and dysregulated microbial signaling and cellular processing pathways.

Within the cell motility category, we observed an increased capacity for bacterial motility proteins, including genes for flagellar assembly (**Figure 2.6b**). Flagellar bacterial antigens have been implicated as disease drivers in both mouse models of colitis and human IBD⁴⁹. Within the signal transduction category, we detected the most significant gene abundances within two-component regulatory systems (**Figure 2.6c**). Data suggest that opportunistic microbes have an ability to utilize substrates generated under inflammatory conditions. We examined whether there were differential gene abundances for tetrathionate respiration, a metabolic pathway underlying the fitness advantage of *Salmonella enterica* serovar Typhimurium in an inflamed

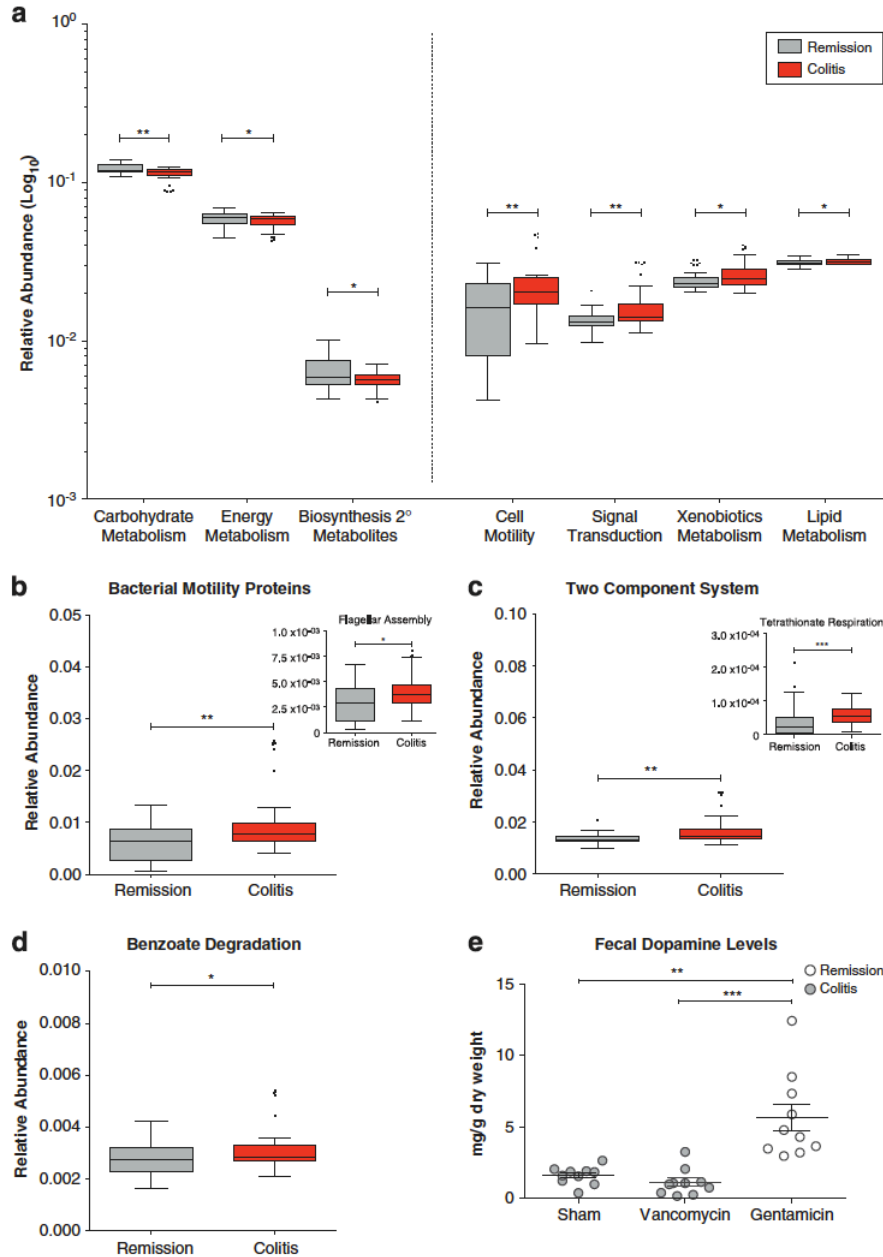


Figure 2.6. Inferred gut microbiome functions associated with active colitis and treatment-induced remission. Relative abundances of KO gene families grouped into BRITE functional hierarchies, as inferred by PICRUSt from 16S rRNA gene sequences. Differentially abundant microbial functions associated with active colitis ($n = 31$) versus remission ($n = 51$) upon intervention completion organized by KEGG BRITE categories (**a**) and pathways (**b–d**). Boxplots denote top quartile, median and bottom quartile. Whiskers and outliers are plotted by the Tukey method. (**e**) ELISA-based determinations of fecal dopamine levels. Symbols represent data from individual mice from three independent experiments. Mann-Whitney test: * $P < 0.05$, ** $P < 0.01$, and *** $P < 0.001$.

gut⁵⁰, and observed enhanced potential for tetrathionate respiration with active disease in TRUC mice (Kos: 08357, 08358, 08359, 13040, 13041; **Figure 2.6c**, inset). Within the xenobiotics biodegradation and metabolism category, we found an enhanced potential for benzoate degradation (**Figure 2.6d**). Catechols (1,2-dihydroxybenzene) – intermediaries of benzoate metabolism – have the ability to promote *Enterobacteriaceae* growth and virulence^{51,52}. Catecholamines, which are host-derived catechols with a side-chain amine, are detectable in the gut lumen⁵³. *K. pneumoniae* has been implicated in TRUC pathogenesis¹⁶ and members of the *Klebsiella* genus are one of the few *Enterobacteriaceae* with the genomic potential to fully metabolize catecholamines (see benzoate degradation pathway kpn00362). Thus, active colitis, with its *Enterobacteriaceae* enrichment, may result in decreased levels of fecal catecholamines. To test this hypothesis, we measured dopamine, the most abundant catecholamine in the colonic lumen⁵³, in stool collected from mice with active colitis and treatment-induced remission. We examined samples from mice treated with vancomycin and gentamicin, which increases or decreases *Enterobacteriaceae*, respectively. Dopamine levels were significantly decreased in stool of sham- and vancomycin-treated mice with active colitis as compared with gentamicin-treated mice in remission. In addition, there was a trend, although not statistically significant, toward lower levels of dopamine in mice treated with vancomycin versus sham (**Figure 2.6e**).

To validate the inferred functions determined by PICRUSt, we performed whole-metagenome shotgun (WMS) sequencing – the conventional means of assessing microbiome functional potential – on a subset of banked stool samples from anti-TNF- α -treated mice ($n = 6$). A total of 419,659,443 quality-filtered shotgun sequences were obtained with an average of $69,943,241 \pm 31,774,397$ reads/sample. Microbial gene abundances estimated from WMS and 16S rRNA gene sequence data were correlated (Spearman correlation, $r = 0.6835$). This was consistent with correlations in WMS and 16S rRNA functional data for human stool samples⁶.

DISCUSSION

A goal of microbiome research is defining the structure and function of the gut microbiome in health and active disease states⁵⁴. Our study identified shifts in microbial clades and inferred functions associated with active colitis and remission following treatment with antibiotics, immunomodulators or a fermented milk-dietary intervention in an experimental colitis mouse model (see **Supplementary Figure 2.13** for a 'Model summarizing the effects of treatment interventions in the TRUC model of experimental colitis'). Using gnotobiotic fecal transplant experiments, we found that treatments' effect on the durability of gut microbiome inflammatory phenotypes varies. Collectively, we identified microbial biomarkers (both clades and functions) that may have clinical relevance for tracking disease when it is asymptomatic and utility as therapeutic targets for managing IBD.

An emerging concept in dysbiosis and bacterial pathogenesis is that certain bacteria have the ability to utilize host substrates to gain a fitness advantage during inflammation^{50,55,56}. The ability to respire tetrathionate and nitrate is central to the fitness of several *Enterobacteriaceae*⁵⁰, as these metabolites are readily available in an inflamed gut and can be used as electron acceptors to generate ATP. We observed that tetrathionate utilization was associated with active colitis, which supports a link between enhanced oxidative stress and *Enterobacteriaceae*-mediated dysbiosis previously described in the TRUC model¹⁶. Dampening the redox stress associated with intestinal inflammation may reduce the abundance of these electron acceptors and eliminate the fitness advantage of colitogenic bacteria, thus restoring intestinal homeostasis.

Enrichment of genes for microbial benzoate degradation in active colitis was unexpected. Catecholamines have garnered interest as communication molecules between host and microbes⁵². *Enterobacteriaceae* can degrade catecholamines and catecholamines can promote *Enterobacteriaceae* growth and expression of bacterial virulence factors⁵⁷. The histidine sensor

kinase QseC (quorum-sensing *E. coli* regulator C) is necessary for bacterial responses to host catecholamines and a compound that inhibits QseC, LED209, has been shown to inhibit pathogen virulence *in vivo* and *in vitro*⁵⁸. Given that LED209 selectively interferes with bacterial virulence and colonization without affecting bacterial growth, typical antibiotic resistance patterns that plague traditional antimicrobials are unlikely to develop⁵⁹. Our observations on tetrathionate respiration and benzoate degradation highlight how gut microbiome studies in mouse models of disease are useful for identifying novel microbial therapeutic targets.

Fecal transplantation represents a long-standing treatment with the potential to address IBD dysbioses and its practice is resurging⁵⁶. However, its use requires substantial consideration from a safety and regulatory perspective. We observed that the health status of a host and its gut microbiome could be transient in some cases. Despite a host being in a state of health, as confirmed by histology, transferring its gut microbiome to a GF recipient resulted in colonic inflammation. As applications for fecal transplantation develop for humans, gnotobiotic mouse models may prove useful for evaluating whether microbiomes selected for transplant will confer the intended health outcomes for the recipient.

In summary, our analyses point to features of microbiome dysbiosis and dysfunction in experimental colitis. Improvements in animal model systems and opportunities for translational medical research warrant future studies that incorporate 16S rRNA gene surveys with other 'omic' approaches to recognize the gut microbiome's full potential and ultimately guide therapeutic strategies for manipulating the microbiome to manage disease.

MATERIALS AND METHODS

Animal husbandry

SPF BALB/c TRUC mice were weaned at 3 weeks of age and randomized into experimental cages, as previously described¹⁵. Mice were fed irradiated standard mouse chow (PicoLab Mouse Diet 20 [5058]; LabDiet) and housed in a barrier facility at the Harvard School of Public Health. Animal experiments were approved and conducted in accordance with Harvard Medical School Standing Committee on Animals and National Institutes of Health guidelines.

Treatment interventions

Antibiotics. Mice were treated with antibiotics dissolved in their drinking water: gentamicin (2 g/L; Cellgro), metronidazole (1 g/L; Sigma), vancomycin (500 mg/L; Sigma)¹⁶.

Anti-TNF- α injections. Mice were injected (15 mg/kg) with a hamster anti-mouse TNF- α neutralizing antibody (clone TN4-19.12) (Bio X Cell) weekly starting at 4 weeks of age¹⁵.

T_{Reg} cell infusion. Fluorescent-activated cell sorted (FACS) peripheral lymph node CD4⁺CD62L^{hi}CD25⁺ cells (75,000 cells/mouse) were intravenously injected at 4 weeks of age¹⁵.

Dietary interventions. The test product was a fermented milk containing the following bacterial strains: *B. lactis* [strain I-2494 in the French National Collection of Cultures of Microorganisms (CNCM)], *S. thermophilus* (CNCM I-1630), *L. bulgaricus* (CNCM I-1519), *L. bulgaricus* (CNCM I-1632), and *L. lactis* (CNCM I-1631). The test product contained 10⁸ colony-forming units (CFUs) *B. lactis*/g and 10⁷ CFUs *S. thermophiles*/g, *L. bulgaricus*/g, and *L. lactis*/g. The control product was a milk-based non-fermented product with 1.6% lactose/serving. The control product was acidified to mimic the effects of bacterial milk fermentation so that it resembled the test product in taste and consistency. The test and control products were 6.0-7.2 kcal/g and the pH values were 4.3-4.5 and 4.1-4.3, respectively. A 100 mg quantity was orally

instilled daily and approximately 100 mg/mouse was provided for *ad libitum* consumption in each cage¹⁸.

Histology

Upon sacrifice, colons were resected, fixed in 4% paraformaldehyde (Sigma) and embedded in paraffin. Sections were H&E-stained and evaluated in a blinded fashion for epithelial hyperplasia (0–3), epithelial injury (0–3), polymorphonuclear infiltration (0–3) and mononuclear infiltration (0–3), these indices were summed to generate the histologic colitis score¹⁵.

Microbial DNA preparation from stool and MLNs

Stool collection and processing. Stool was collected and homogenized in *RNAlater* (Ambion), held at 4°C overnight, and stored at -80°C before processing. DNA was extracted using a phenol-chloroform bead-beating procedure. Briefly, samples were thawed on ice and centrifuged to remove the *RNAlater* supernatant. Samples were washed with 1 ml of PBS (Cellgro) and resuspended in a solution containing: 500 µl of Tris-EDTA (TE)-saturated phenol (Sigma), 300 µl of TE-SDS buffer pH 8.0 [200 mM Tris-HCl, 80 mM EDTA, 10% SDS (all Sigma)], and 0.3 g of 0.1 mm-diameter zirconia/silica beads (BioSpec Products). Microbial cells were lysed by mechanical disruption with a FastPrep FP120 homogenizer (MP Biomedicals) set at power level 5.0 for 30 sec at 4°C. The homogenate was centrifuged and 400 µl of supernatant was transferred to a new micro tube containing 400 µl of phenol:chloroform:isoamyl alcohol (Sigma). Samples underwent a second round of lysis using the FastPrep FP120 homogenizer set at power level 4.0 for 45 sec at 4°C. The homogenate was centrifuged and 250 µl of supernatant was precipitated in 25 µl 3M sodium acetate pH 5.2 (Ambion) and 300 µl isopropanol (Sigma). DNA pellets were washed with 500 µl 70% ethanol, resuspended in TE (Ambion), and stored at -20°C.

MLN collection and processing. MLNs were collected from mice receiving the dietary interventions – either the fermented milk or milk control product. Upon sacrifice, MLNs (5 MLNs/mouse) were resected and collected in RNA*later*, held at 4°C overnight, and stored at -80°C. DNA was extracted from MLNs and processed using the same method described for stool.

16S rRNA gene survey analysis of gut microbial communities

16S rRNA gene amplification and 454 pyrosequencing. Extracted DNA underwent partial 16S rRNA gene amplification by PCR using a forward primer containing the Titanium A adaptor sequence, a 5-10 base pair (bp) barcode identifier sequence, and a template-specific primer sequence. The reverse primer contained the Titanium B adaptor sequence and a template-specific primer sequence. The template-specific primer sequences (5'-AGGATTAGATACCCTGGTA-3' and 5'-CRRACGAGCTGACGAC-3') allowed targeting of the V5-V6 hypervariable bacterial 16S rRNA regions⁶⁰. Each reaction mixture of 100 µl contained: 1x KAPA HiFi Buffer, 2U of KAPA HiFi Hotstart DNA polymerase, 0.3 mM of each dNTP (Kapa Biosystems), 300 nM of each primer, and 60 ng of template DNA. Thermocycling was performed with an initial denaturation step at 95°C for 5 min, followed by 25 cycles of denaturation of 98°C for 20 sec, annealing at 56°C for 40 sec, and extension at 72°C for 20 sec, with a final extension of 5 min at 72°C. Specificity and amplicon size were verified by gel electrophoresis, and amplicons were purified using a Gel and PCR Clean-up System (Promega). Amplicons were quantitated using a Quant-iT PicoGreen dsDNA assay kit (Life Technologies) and combined in equimolar concentrations for multiplexing. The final pool of DNA was purified using an Agencourt AMPure XP system (Agencourt Bioscience) and resuspended in 100 µl of TE buffer. Pyrosequencing was performed at DNAVision using Primer A on the Roche 454 Life Sciences Genome Sequencer FLX instrument with Titanium chemistry.

16S rRNA gene sequence processing and OTU selection. Reads were de-multiplexed and pre-processed using the automated Roche GS Run Processor pipeline to remove adapter sequences and low quality reads. Reads were further quality filtered and analyzed with QIIME software package v1.5¹⁹. QIIME pre-processing involved removing reads with greater than 2 mismatches in the forward or reverse primer sequences, and then truncating primer sequences from the reads. Additional reads were filtered out if: 1) ambiguous bases were detected, 2) homopolymer runs were greater than 6 bp, 3) lengths were outside the bounds of 200-350 bp, and/or 4) average quality scores over a sliding window of 50 bp dropped below 25. Reads were then processed by the USEARCH quality-filtering pipeline⁶¹, which removed noise and chimeras prior to performing *de novo* clustering into OTUs at 97% sequence identity.

Microbial composition and community structure analysis. A representative sequence was selected for each OTU and classified with the RDP (Ribosomal Database Project) classifier v2.2⁶² using the Greengenes (GG) reference set (Dec. 2012 release)⁶³. The taxonomic assignment of each sequence was truncated at the most specific taxonomic level with a confidence score of at least 80%. Classified reads were then binned by taxonomy and normalized to generate a relative abundance table. The OTU representative sequence set was also aligned to the GG core set using PyNAST⁶⁴ with a minimum alignment length of 150 bp and minimum identity of 75%. The PH Lane mask was applied to the alignment to retain the conserved regions of the 16S rRNA gene and omit the hypervariable regions for phylogenetic inference. Based on the alignment of OTU representative sequences, a phylogenetic tree was constructed using FastTree⁶⁵ prior to performing diversity analysis. Microbial diversity was evaluated within samples (alpha-diversity) and between samples (beta-diversity) with QIIME. All alpha-diversity measures were performed on OTU tables rarefied to 1,750 sequences/sample with 10 iterations each to account for variations in sequencing depth. Beta-diversity was analyzed using UniFrac, a phylogenetic distance metric

that measures community similarity based on the degree to which pairs of communities share branch length in a common phylogenetic tree²³. Unweighted and weighted UniFrac distances and sample metadata comprised the data matrices used as inputs for PCoA. Unweighted UniFrac distances compare microbial communities based on presence/absence of members (community membership), while weighted UniFrac also incorporates relative abundance information (community structure). PCoA was employed to assess the amount of variation in microbial community composition between samples and to visualize potential clustering of samples by metadata. Distances between samples on a PCoA plot reflect the corresponding dissimilarities in their community membership or structure. Samples were also hierarchically clustered based on their inter-sample UniFrac distances using UPGMA. All beta-diversity measures were performed on OTU tables rarefied to 1,750 sequences/sample for stool and 1,320 sequences/sample for MLNs to account for variations in sequencing depth.

Metagenome inference and metabolic pathway reconstruction. To construct a gene catalog (or metagenome) for each sample, the gene content of available IMG (Integrated Microbial Genomes and Metagenomes) reference genomes was used to infer the approximate gene content of detected phylotypes (OTUs) using PICRUSt v0.9.0²⁰. The FastTree GG phylogeny annotated with these organisms' genomes was used to pick closed reference OTUs from the de-multiplexed and USEARCH quality-filtered reads at 97% identity. Each genus-level OTU was assigned to the GG clade containing the most genomes from that genus and fewest from other genera. Higher-level clades continued with this same assignment pattern. The gene contents were then reconstructed across the GG tree and assigned KEGG Orthology copy numbers⁶⁶. Metagenome prediction accuracy was calculated using the weighted NSTI (**Supplementary Table 2.2**). NSTI scores represent the average branch length that separates each OTU in a sample from a referenced bacterial genome, weighted by the abundance of that OTU in the sample. Low

NSTI scores reflect a shorter branch length and higher prediction accuracy. For example, an NSTI score of 0.03 indicates that the average OTU in a given sample can be predicted using a relative from the same (97%) species. The relative abundance of each gene (KO) was then estimated for each sample. Inferred relative gene abundances were subsequently binned into pathways and functional categories defined by the BRITe hierarchy. Non-microbial categories, for example 'Organismal Systems' and 'Human Diseases', were excluded from further analysis.

Microbial biomarker discovery and visualization. Candidate microbes and microbial functions associated with specific interventions or host disease status were identified by LEfSe²². LEfSe couples robust tests for measuring statistical significance (Kruskal-Wallis test) with quantitative tests for biological consistency (Wilcoxon-rank sum test). The differentially abundant and biologically relevant features (clades, genes, pathways, functional categories) are ranked by effect size after undergoing linear discriminant analysis. All *P*-values were corrected for multiple hypothesis testing using Benjamini and Hochberg's false discovery rate (FDR) correction (*q*-value)⁶⁷. A *q*-value of 0.25 and an effect size threshold of 2 (on a log₁₀ scale) were used for all biomarkers discussed. In some cases, organismal biomarkers are graphically represented on hierarchical trees reflecting the RDP taxonomy for 16S rRNA gene data.

WMS sequence analysis

Illumina shotgun sequencing. Extracted DNA from mice treated with anti-TNF- α underwent multiplexed paired-end library preparation and shotgun sequencing. WMS sequencing was performed by DNAnvision on the Illumina HiSeq 2000 platform, which generated 100 bp reads.

Shotgun sequence processing. WMS reads were de-multiplexed and pre-processed by DNAnvision to remove adapter sequences and low quality reads. The FastX Toolkit (Hannon Lab, CSHL) was used to filter out additional reads with: 1) average quality scores less than 10, 2) lengths

less than 60 bp, and/or 3) ambiguous bases. Filtered sequences that mapped to the host reference genome were also excluded [based on default BWA (Burrows-Wheeler Aligner) alignments⁶⁸ to the full mouse mm9 genome].

Microbial gene and pathway abundance analysis. Metabolic gene and pathway frequencies were analyzed with HUMAnN²¹. Quality-filtered shotgun reads were filtered further for duplicates prior to undergoing an accelerated translated nucleotide BLAST against the KEGG protein database⁶⁶. HUMAnN calculated gene, module, and pathway relative abundances for all metagenomes present in the sequenced stool samples.

Dopamine ELISA

Mice in the sham, vancomycin, and gentamicin treatment groups had stool collected and immediately flash frozen in liquid nitrogen upon completion of the 4-week intervention. After thawing on ice, samples from each mouse were weighed and either incubated overnight at 37°C for fecal dry weight determination or processed using the DOP Research ELISA kit (Labor Diagnostika) according to the manufacturer's instructions with the following modifications. Samples were first resuspended in 1 ml of buffer [0.01 N HCl, 1mM EDTA, and 4mM sodium metabisulfite (all Sigma)] and 0.3 g of 0.1 mm-diameter glass beads (BioSpec Products) prior to undergoing homogenization in a mini-bead beater (Biospec Products) at maximum power for 90 sec at 4°C. Dopamine levels were normalized based on the calculated fecal dry weights of respective samples.

Gnotobiotic mouse experiments

GF BALB/c TRUC mice were weaned at 3 weeks of age and randomized into experimental cages. At 4 weeks of age, frozen stool from conventionally-raised, SPF TRUC donors were

separately pooled, resuspended in PBS, and transplanted into GF TRUC recipients. Mice were colonized by orally gavaging and spreading the stool slurries on their fur and anus using sterile plastic transfer pipets (Samco Scientific Corporation). Mice were associated for 8 weeks in flexible film gnotobiotic isolators. Upon sacrifice, stool was collected in RNA_{later} and colons were resected for histologic analysis to assess colitis activity, as described above. All animal experiments were approved and conducted in accordance with Harvard Medical School Standing Committee on Animals and National Institutes of Health guidelines.

RT-qPCR for FMP strains

To facilitate comparison with other bacterial quantification methods, the number of detected RNA molecules was converted to cell equivalents. Bacterial cultures of 2 lactic acid bacterial reference strains in the fermented milk product – *B. lactis* (CNCM I-2494) and *L. lactis* (CNCM I-1631) grown in the appropriate media and collected at stationary phase – were used to generate a standard curve relating cycling threshold to bacterial cell number (determined microscopically with DAPI staining from a dilution series of the reference strains). For detection of the target bacteria, 10-fold serial dilutions of extracted RNA from TRUC donor and recipient stool samples underwent RT-qPCR. Quantification of *B. lactis* involved the primers Blact-F (5'-CCCTTTCCACGGGTCCC-3') and Blact-R (5'-AAGGGAAACCGTGTCTCCAC-3') with an annealing temp of 60°C⁶⁹. Quantification of *L. lactis* involved the primers Llac-05 (5'-AGCAGTAGGGAATCTTCG GCA-3') and Llac-02 (5'-GGGTAGTTACCGTCACTTGATGAG-3') with an annealing temp of 60°C⁷⁰. Using cycle threshold values in the linear range of the assay, bacterial equivalents were interpolated from a standard curve generated in the same experiment and then weight corrected to yield a value in bacterial cell equivalents/g stool¹⁸.

Statistical analysis

Significant *P*-values associated with microbial clades and functions identified by LEfSe were corrected for multiple hypothesis testing using the Benjamini and Hochberg's FDR correction⁶⁷. Other statistical tests for significance were performed in Prism v5.0b for Mac OS X (GraphPad Software). All averages are mean \pm standard error of the mean (SEM).

Accession Number

Sequences have been deposited on MG-RAST under project ID 6698.

ACKNOWLEDGEMENTS

We thank members of the Garrett and Huttenhower Labs for discussion. The following grants supported this study: to MGR, NIAID 5T32AI007638; to CH, NIH R01HG005969, NSF DBI-1053486 and ARO W911NF-11-1-0473; to WSG, NIH (R01CA154426, K08AI078942), Burroughs Wellcome CAMS, Searle Scholars, Cancer Research Institute and Danone Research Awards.

REFERENCES

1. Ott, S. J. *et al.* Reduction in diversity of the colonic mucosa associated bacterial microflora in patients with active inflammatory bowel disease. *Gut* **53**, 685–693 (2004).
2. Sokol, H., Lay, C., Seksik, P. & Tannock, G. W. Analysis of bacterial bowel communities of IBD patients: what has it revealed? *Inflamm. Bowel Dis.* **14**, 858–867 (2008).
3. Packey, C. D. & Sartor, R. B. Commensal bacteria, traditional and opportunistic pathogens, dysbiosis and bacterial killing in inflammatory bowel diseases. *Curr. Opin. Infect. Dis.* **22**, 292–301 (2009).
4. Frank, D. N. *et al.* Disease phenotype and genotype are associated with shifts in intestinal-associated microbiota in inflammatory bowel diseases. *Inflamm. Bowel Dis.* **17**, 179–184 (2011).
5. Erickson, A. R. *et al.* Integrated metagenomics/metaproteomics reveals human host-microbiota signatures of Crohn's disease. *PLoS ONE* **7**, e49138 (2012).
6. Morgan, X. C. *et al.* Dysfunction of the intestinal microbiome in inflammatory bowel disease and treatment. *Genome Biol.* **13**, R79 (2012).

7. Presley, L. L. *et al.* Host-microbe relationships in inflammatory bowel disease detected by bacterial and metaproteomic analysis of the mucosal-luminal interface. *Inflamm. Bowel Dis.* **18**, 409–417 (2012).
8. Dethlefsen, L., Huse, S., Sogin, M. L. & Relman, D. A. The pervasive effects of an antibiotic on the human gut microbiota, as revealed by deep 16S rRNA sequencing. *PLoS Biol.* **6**, e280 (2008).
9. Engel, M. A. & Neurath, M. F. New pathophysiological insights and modern treatment of IBD. *J. Gastroenterol.* **45**, 571–583 (2010).
10. Hill, D. A. & Artis, D. Intestinal bacteria and the regulation of immune cell homeostasis. *Annu. Rev. Immunol.* **28**, 623–667 (2010).
11. Jakobsson, H. E. *et al.* Short-term antibiotic treatment has differing long-term impacts on the human throat and gut microbiome. *PLoS ONE* **5**, e9836 (2010).
12. Manichanh, C. *et al.* Reshaping the gut microbiome with bacterial transplantation and antibiotic intake. *Genome Res.* **20**, 1411–1419 (2010).
13. Pineton de Chambrun, G. P. & Sandborn, W. J. IBD in 2011: advances in IBD management--towards a tailored approach. *Nat Rev Gastroenterol Hepatol* **9**, 70–72 (2012).
14. Ubeda, C. & Pamer, E. G. Antibiotics, microbiota, and immune defense. *Trends Immunol.* **33**, 459–466 (2012).
15. Garrett, W. S. *et al.* Communicable ulcerative colitis induced by T-bet deficiency in the innate immune system. *Cell* **131**, 33–45 (2007).
16. Garrett, W. S. *et al.* Enterobacteriaceae act in concert with the gut microbiota to induce spontaneous and maternally transmitted colitis. *Cell Host and Microbe* **8**, 292–300 (2010).
17. Powell, N. *et al.* The transcription factor T-bet regulates intestinal inflammation mediated by interleukin-7 receptor+ innate lymphoid cells. *Immunity* **37**, 674–684 (2012).
18. Veiga, P. *et al.* Bifidobacterium animalis subsp. lactis fermented milk product reduces inflammation by altering a niche for colitogenic microbes. *Proc. Natl. Acad. Sci. U.S.A.* **107**, 18132–18137 (2010).
19. Caporaso, J. G. *et al.* QIIME allows analysis of high-throughput community sequencing data. *Nat. Methods* **7**, 335–336 (2010).
20. Langille, M. G. I. *et al.* Predictive functional profiling of microbial communities using 16S rRNA marker gene sequences. *Nature Biotechnology* **31**, 814–821 (2013).
21. Abubucker, S. *et al.* Metabolic reconstruction for metagenomic data and its application to the human microbiome. *PLoS Comput. Biol.* **8**, e1002358 (2012).
22. Segata, N. *et al.* Metagenomic biomarker discovery and explanation. *Genome Biol.* **12**, R60 (2011).
23. Lozupone, C., Lladser, M. E., Knights, D., Stombaugh, J. & Knight, R. UniFrac: an effective distance metric for microbial community comparison. *ISME J* **5**, 169–172 (2011).
24. Wang, S.-L., Wang, Z.-R. & Yang, C.-Q. Meta-analysis of broad-spectrum antibiotic therapy in patients with active inflammatory bowel disease. *Exp Ther Med* **4**, 1051–1056 (2012).
25. Hill, D. A. *et al.* Metagenomic analyses reveal antibiotic-induced temporal and spatial changes in intestinal microbiota with associated alterations in immune cell homeostasis. *Mucosal Immunol* **3**, 148–158 (2010).

26. Hildebrand, F. *et al.* Inflammation-associated enterotypes, host genotype, cage and inter-individual effects drive gut microbiota variation in common laboratory mice. *Genome Biol.* **14**, R4 (2013).
27. Carvalho, F. A. *et al.* Transient inability to manage proteobacteria promotes chronic gut inflammation in TLR5-deficient mice. *Cell Host and Microbe* **12**, 139–152 (2012).
28. Mukhopadhyaya, I., Hansen, R., El-Omar, E. M. & Hold, G. L. IBD-what role do Proteobacteria play? *Nat Rev Gastroenterol Hepatol* **9**, 219–230 (2012).
29. Robertson, D. J. *et al.* Fat, fiber, meat and the risk of colorectal adenomas. *Am J Gastroenterol* **100**, 2789–2795 (2005).
30. Berry, D. *et al.* Phylotype-level 16S rRNA analysis reveals new bacterial indicators of health state in acute murine colitis. *ISME J* **6**, 2091–2106 (2012).
31. Carbonero, F., Benefiel, A. C. & Gaskins, H. R. Contributions of the microbial hydrogen economy to colonic homeostasis. *Nat Rev Gastroenterol Hepatol* **9**, 504–518 (2012).
32. Hansen, R., Thomson, J. M., Fox, J. G., El-Omar, E. M. & Hold, G. L. Could Helicobacter organisms cause inflammatory bowel disease? *FEMS Immunol. Med. Microbiol.* **61**, 1–14 (2011).
33. Yanai, H. & Hanauer, S. B. Assessing response and loss of response to biological therapies in IBD. *Am J Gastroenterol* **106**, 685–698 (2011).
34. Robertson, B. R., O'Rourke, J. L., Vandamme, P., On, S. L. & Lee, A. Helicobacter ganmani sp. nov., a urease-negative anaerobe isolated from the intestines of laboratory mice. *Int. J. Syst. Evol. Microbiol.* **51**, 1881–1889 (2001).
35. Tolia, V. *et al.* Detection of Helicobacter ganmani-like 16S rDNA in pediatric liver tissue. *Helicobacter* **9**, 460–468 (2004).
36. Nanau, R. M. & Neuman, M. G. Nutritional and probiotic supplementation in colitis models. *Dig. Dis. Sci.* **57**, 2786–2810 (2012).
37. Veerappan, G. R., Betteridge, J. & Young, P. E. Probiotics for the treatment of inflammatory bowel disease. *Curr Gastroenterol Rep* **14**, 324–333 (2012).
38. Rijkers, G. T. *et al.* Guidance for substantiating the evidence for beneficial effects of probiotics: current status and recommendations for future research. *J. Nutr.* **140**, 671S–6S (2010).
39. Papa, E. *et al.* Non-invasive mapping of the gastrointestinal microbiota identifies children with inflammatory bowel disease. *PLoS ONE* **7**, e39242 (2012).
40. Macpherson, A. J. & Smith, K. Mesenteric lymph nodes at the center of immune anatomy. *J. Exp. Med.* **203**, 497–500 (2006).
41. Eberl, G. & Lochner, M. The development of intestinal lymphoid tissues at the interface of self and microbiota. *Mucosal Immunol* **2**, 478–485 (2009).
42. Pédrón, T. *et al.* A crypt-specific core microbiota resides in the mouse colon. *MBio* **3**, (2012).
43. Marteyn, B. *et al.* Modulation of Shigella virulence in response to available oxygen in vivo. *Nature* **465**, 355–358 (2010).
44. Diehl, G. E. *et al.* Microbiota restricts trafficking of bacteria to mesenteric lymph nodes by CX(3)CR1(hi) cells. *Nature* **494**, 116–120 (2013).

45. Tremaroli, V. & Bäckhed, F. Functional interactions between the gut microbiota and host metabolism. *Nature* **489**, 242–249 (2012).
46. Turnbaugh, P. J. *et al.* An obesity-associated gut microbiome with increased capacity for energy harvest. *Nature* **444**, 1027–1031 (2006).
47. Wen, L. *et al.* Innate immunity and intestinal microbiota in the development of type 1 diabetes. *Nature* **455**, 1109–1113 (2008).
48. Sanders, M. E. Impact of probiotics on colonizing microbiota of the gut. *J. Clin. Gastroenterol.* **45 Suppl**, S115–9 (2011).
49. Steiner, T. S. How flagellin and toll-like receptor 5 contribute to enteric infection. *Infect. Immun.* **75**, 545–552 (2007).
50. Winter, S. E. *et al.* Host-derived nitrate boosts growth of *E. coli* in the inflamed gut. *Science* **339**, 708–711 (2013).
51. Freestone, P. P. E., Walton, N. J., Haigh, R. D. & Lyte, M. Influence of dietary catechols on the growth of enteropathogenic bacteria. *Int. J. Food Microbiol.* **119**, 159–169 (2007).
52. Lyte, M., Vulchanova, L. & Brown, D. R. Stress at the intestinal surface: catecholamines and mucosa-bacteria interactions. *Cell Tissue Res.* **343**, 23–32 (2011).
53. Asano, Y. *et al.* Critical role of gut microbiota in the production of biologically active, free catecholamines in the gut lumen of mice. *Am. J. Physiol. Gastrointest. Liver Physiol.* **303**, G1288–95 (2012).
54. Lemon, K. P., Armitage, G. C., Relman, D. A. & Fischbach, M. A. Microbiota-targeted therapies: an ecological perspective. *Sci Transl Med* **4**, 137rv5 (2012).
55. Fleckenstein, J. M. *et al.* Molecular mechanisms of enterotoxigenic *Escherichia coli* infection. *Microbes Infect.* **12**, 89–98 (2010).
56. Buffie, C. G. & Pamer, E. G. Microbiota-mediated colonization resistance against intestinal pathogens. *Nat. Rev. Immunol.* **13**, 790–801 (2013).
57. Eloie-Fadrosh, E. A. & Rasko, D. A. The human microbiome: from symbiosis to pathogenesis. *Annu. Rev. Med.* **64**, 145–163 (2013).
58. Rasko, D. A. *et al.* Targeting QseC signaling and virulence for antibiotic development. *Science* **321**, 1078–1080 (2008).
59. Rasko, D. A. & Sperandio, V. Anti-virulence strategies to combat bacteria-mediated disease. *Nat Rev Drug Discov* **9**, 117–128 (2010).
60. Andersson, A. F. *et al.* Comparative analysis of human gut microbiota by barcoded pyrosequencing. *PLoS ONE* **3**, e2836 (2008).
61. Edgar, R. C. Search and clustering orders of magnitude faster than BLAST. *Bioinformatics* **26**, 2460–2461 (2010).
62. Cole, J. R. *et al.* The Ribosomal Database Project: improved alignments and new tools for rRNA analysis. *Nucleic Acids Res.* **37**, D141–5 (2009).
63. McDonald, D. *et al.* An improved Greengenes taxonomy with explicit ranks for ecological and

evolutionary analyses of bacteria and archaea. *ISME J* **6**, 610–618 (2012).

64. Caporaso, J. G. *et al.* PyNAST: a flexible tool for aligning sequences to a template alignment. *Bioinformatics* **26**, 266–267 (2010).
65. Price, M. N., Dehal, P. S. & Arkin, A. P. FastTree: computing large minimum evolution trees with profiles instead of a distance matrix. *Mol. Biol. Evol.* **26**, 1641–1650 (2009).
66. Kanehisa, M., Goto, S., Sato, Y., Furumichi, M. & Tanabe, M. KEGG for integration and interpretation of large-scale molecular data sets. *Nucleic Acids Res.* **40**, D109–14 (2012).
67. Benjamini, Y. & Hochberg, Y. Controlling the False Discovery Rate: A Practical and Powerful Approach to Multiple Testing on JSTOR. *Journal of the Royal Statistical Society Series B ...* (1995). doi:10.2307/2346101
68. Li, H. & Durbin, R. Fast and accurate long-read alignment with Burrows-Wheeler transform. *Bioinformatics* **26**, 589–595 (2010).
69. Bartosch, B. *et al.* An interplay between hypervariable region 1 of the hepatitis C virus E2 glycoprotein, the scavenger receptor BI, and high-density lipoprotein promotes both enhancement of infection and protection against neutralizing antibodies. *J. Virol.* **79**, 8217–8229 (2005).
70. Firmesse, O., Rabot, S., Bermúdez-Humarán, L. G., Corthier, G. & Furet, J.-P. Consumption of Camembert cheese stimulates commensal enterococci in healthy human intestinal microbiota. *FEMS Microbiol. Lett.* **276**, 189–192 (2007).

CHAPTER 3

Testing the efficacy of LED209, an inhibitor of the bacterial quorum-sensing receptor and virulence regulator QseC, in experimental colitis

Michelle G. Rooks¹, Patrick Veiga², Yasunari Asano³, Kazufumi Yoshihara³, Monia Michaud¹, Carey Ann Gallini¹, Jonathan N. Glickman⁴, Nobuyuki Sudo³, and Wendy S. Garrett^{1,4-6}.

¹Harvard T.H. Chan School of Public Health, Boston, MA, USA

²Danone Research, Palaiseau, France

³Kyushu University, Fukuoka, Japan

⁴Harvard Medical School, Boston, MA, USA

⁵Broad Institute of MIT and Harvard, Cambridge, MA, USA

⁶Dana-Farber Cancer Institute, Boston, MA USA

Author Contributions:

M.G.R., P.V., and W.S.G. conceived and designed the study. All experiments were performed by M.G.R., with the following exceptions. Y.A., K.Y., and N.S. measured catecholamines by HPLC. M.M. offered technical assistance and advice on protocols. C.A.G. helped with animal husbandry. J.N.G. performed blinded histological assessment.

BACKGROUND

16S ribosomal RNA (rRNA) gene amplicon surveys of TRUC mice following diverse treatment interventions revealed that gut microbiomes with persistent colitis had enrichments in *Enterobacteriaceae* and an enhanced capacity for bacterial pathogenesis, including pathways involved in flagellar assembly, two-component systems, and benzoate degradation¹ (Chapter 2). Catechols are intermediates of microbial benzoate degradation and catecholamines (CAs) are host-derived catechols with a side-chain amine (see **Supplementary Figure 3.1a-b** for ‘Microbial benzoate metabolism’ and ‘Host CA biosynthesis’). Evidence suggests that CAs – dopamine (DOP), norepinephrine (NE), and epinephrine (EPI) – are detectable in the intestinal lumen and that levels are gut microbiota-dependent². Typically known for their role as “fight-or-flight” stress hormones produced by the CNS and adrenal glands, CAs are also produced by the ENS and are important for regulating intestinal motility, electrolyte transport, and immune homeostasis³. Moreover, CAs have garnered interest as communication molecules between host and microbes, as these host stress signals may influence microbial dysbiosis and increase susceptibility to infection by altering the growth and virulence potential of pathogens and colitogenic bacteria, including species of *Enterobacteriaceae*^{4,5}.

CAs have the ability to promote *Enterobacteriaceae* virulence by signaling through quorum-sensing two-component systems (TCSs)^{6,7}. Unlike mammalian cells, which sense CAs through G-protein coupled receptors, *Enterobacteriaceae* sense and respond to CAs through the membrane-bound histidine sensor kinase QseC, which is part of the QseBC TCS. QseC detection of microbiota-derived autodinducer-3 and/or host-derived CAs (NE or EPI) initiates a signaling cascade that leads to the activation of its cognate response regulator, QseB, and induction of virulence genes⁸ (see **Supplementary Figure 3.1c** for ‘Bacterial QseC-mediated CA sensing and virulence inhibition’). Similar to other bacterial TCSs, activation is concentration-dependent.

Small diffusible hormone-like molecules synthesized and secreted by bacteria, such as autoinducer-3, are used to count and monitor the local bacterial population density. Once a certain concentration threshold is reached and recognized, bacteria can then synchronize gene expression and coordinate shifts in community-wide behaviors, including virulence. However, bacteria have evolved ways to use their QseBC machinery to also sense and respond to host stress signals⁹. This function allows bacteria to monitor host signaling and in doing so, regulate the expression of metabolically expensive virulence factors to ensure a survival advantage¹⁰.

A synthetic compound that blocks QseC signaling, LED209, inhibits the virulence of clinically-relevant Gram-negative pathogens *in vitro* and *in vivo*¹¹⁻¹⁴. This small molecule inhibitor was discovered in a high-throughput screen of 150,000 compounds¹¹ (see **Supplementary Figure 3.1d** for 'LED209 chemical structure'). Follow-up structure-activity relationship studies revealed that LED209 is a potent prodrug that is highly selective for QseC and its metabolism is restricted to bacterial cells¹². Bacterial-specific hydrolysis of LED209 exposes a reactive chemical isothiocyanate group that covalently modifies lysines in QseC¹², thereby impairing its function and preventing the activation of QseC-mediated virulence. LED209 selectively blocks the virulence of a range of human pathogens both *in vitro* and in animal infection models, including enterohemorrhagic *Escherichia coli* (EHEC), *Salmonella enterica* Typhimurium, and *Francisella tularensis*¹¹. QseC signaling in these pathogens activates diverse virulence programs with many of them regulating genes involved in attachment or invasion of host cells, biofilm formation, chemotaxis, motility, and/or toxin production, the result of which promotes their infectivity and survival in mammalian hosts. The ability of LED209 to impede virulence and attenuate infections aligns with genetic inactivation studies of *qseC* in these pathogens, confirming both its specificity and usefulness as a broad-spectrum approach for targeting virulent Gram-negative bacteria.

A major benefit of antivirulence approaches that target TCSs is the potential to intercept microbe-microbe and host-microbe signaling and to block virulence mechanisms without placing selective pressure on bacteria to develop drug resistance, as is common with traditional antimicrobials (antibiotics)¹⁵. Given that microbial pathways involved in CA-related metabolism are enriched in experimental colitis and human IBD¹⁶ and that QseC may mediate CA-induced virulence in colitogenic bacteria, we investigated whether QseC-blockade could be an effective microbiota-targeted approach for disease management. Here, we performed LED209 interventions in three distinct mouse models of experimental colitis to evaluate the effects of inhibiting QseC-mediated bacterial virulence on host disease status.

RESULTS

A bacterial adrenergic receptor antagonist can attenuate experimental colitis

Based on LED209's ability to inhibit QseC and to reduce the virulence of *Enterobacteriaceae* pathogens *in vivo*^{11,12}, we examined the effects of QseC blockade on host disease status in three distinct mouse models of experimental colitis. LED209 was orally administered daily to TRUC, *Il-10*^{-/-}, and dextran sodium sulfate (DSS)-treated WT mice. The LED209 study design and histology-based colitis scores (**Figure 3.1**) and other parameters of disease are shown (**Supplementary Figure 3.2**).

Treatment with LED209 conferred almost complete protection from colitis in TRUC mice and significantly reduced disease severity in DSS-exposed mice (**Figure 3.1c and e**). In *Il-10*^{-/-} mice, a greater proportion of LED209-treated mice (9/13; 69.2%) showed no signs of mucosal inflammation or injury compared to sham (7/11; 63.6%) and vehicle-treated (6/11; 54.5%) controls (**Figure 3.1d**). *Il-10*^{-/-} mice often show gender differences in disease activity, with males tending to have more severe disease than females, which was also observed with LED209 treatment

(Supplementary Figure 3.3). Our histopathology data indicates that LED209 can attenuate disease severity in genetic and chemically-induced models of experimental colitis.

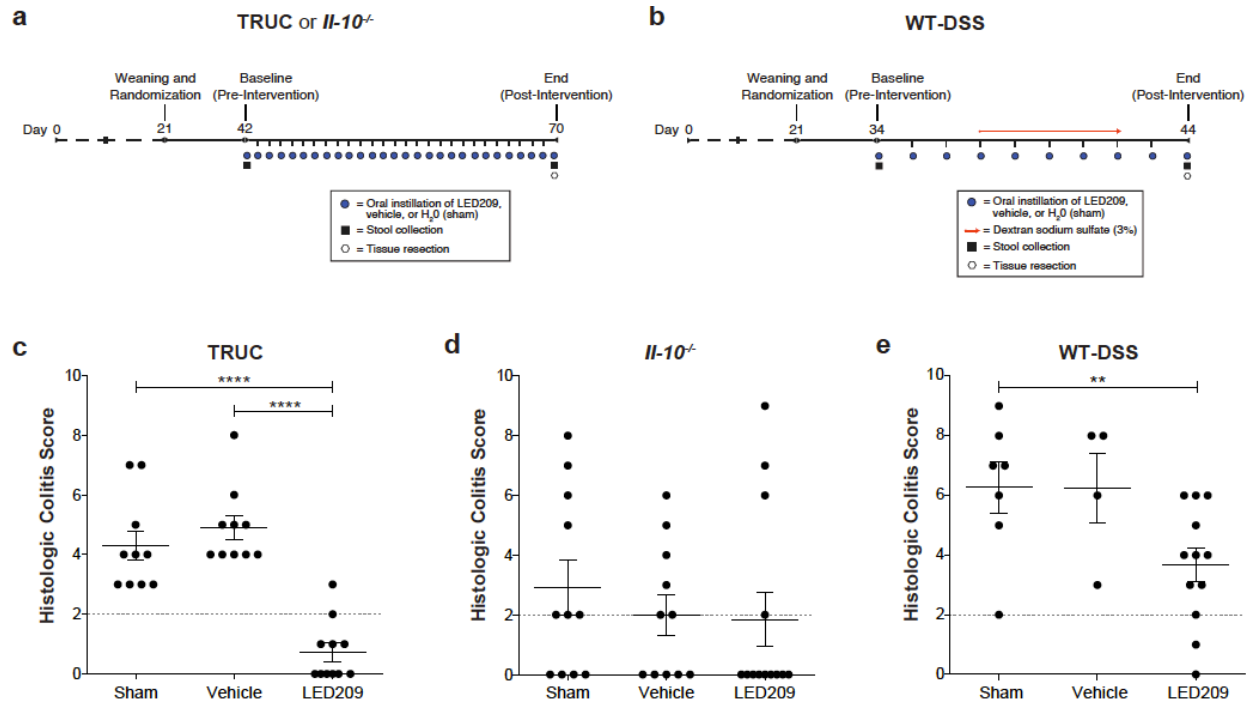


Figure 3.1. LED209 intervention study design and effects of bacterial QseC inhibition in three mouse models of experimental colitis. (a-b) Experimental schema in: TRUC ($n = 31$), *Il-10*^{-/-} ($n = 35$), and WT dextran sodium sulfate (DSS)-exposed ($n = 23$; excluding 1 mouse in the vehicle-control group that died on intervention day 9) mice. Mice were orally administered LED209 (0.4 mg/mouse), vehicle, or water (sham) daily. Colonic inflammation was chemically-induced in WT mice by adding 3% (wt/vol) DSS to the drinking water. (c-e) Post-intervention histologic colitis scores. Symbols represent data from individual mice from 2-3 independent experiments. Error bars indicate mean \pm SEM. Colitis scores >2 indicate active disease and scores ≤ 2 remission. One-way analysis of variance (ANOVA) with Tukey's multiple comparison test: ** $P < 0.01$ and **** $P < 0.0001$.

LED209 differentially perturbs *Enterobacteriaceae* levels in experimental colitis models

Accumulating evidence suggests that *Enterobacteriaceae* can become more colitogenic under inflammatory conditions and may participate in initiating and potentiating inflammation in IBD^{17,18}. LED209 studies measuring pathogen growth and survival *in vitro* and in animal models of infection suggest that antivirulence approaches can reduce pathogenicity without affecting

bacterial growth¹¹. Thus, we measured shifts in *Enterobacteriaceae* levels from baseline to assess whether we could relate abundance to treatment response in these models of experimental colitis. Using DNA from stool collected at baseline and upon treatment completion, we performed quantitative PCR using primers specific to the *Enterobacteriaceae* 23S ribosomal RNA (rRNA) gene and normalized to total bacterial 16S rRNA. In *Il-10^{-/-}* and WT-DSS mice, LED209 blocked the expansion of *Enterobacteriaceae* as compared to vehicle controls, which had a >5.5-fold increase from baseline (**Figure 3.2b-c**). Conversely, TRUC mice displayed an inverse trend, where levels remained stable in vehicle controls and increased 2.4-fold in LED209-treated mice (**Figure 3.2a**). Segregating *Enterobacteriaceae* relative abundance in LED209 treatment groups based on active disease versus remission for each model revealed comparable levels between disease states in TRUC and WT-DSS mice (**Figure 3.2d**). However, *Il-10^{-/-}* mice with active disease had marked variations in *Enterobacteriaceae* levels that were, on average, significantly higher than mice in remission (**Figure 3.2d**). Thus, LED209 has differential effects on *Enterobacteriaceae* levels that are distinct between models and between disease states of treated mice.

LED209 treatment does not alter the luminal catecholamine pool of the cecum or colon

Since QseC is important for *Enterobacteriaceae* virulence and since QseC senses host NE and EPI, we evaluated the effects of QseC inhibition on the luminal CA pool of the cecum and colon. A recent report characterized luminal CA levels in mice and described a detailed method for measuring them by HPLC². Using the same technique, we analyzed CAs in stool collected pre- and post-intervention and cecal content removed upon sacrifice. Luminal CA levels matched what had previously been described both in terms of the expected range of values for each compound and the absolute values increasing 2-fold from the cecum to the colon². Levels of CAs in cecal

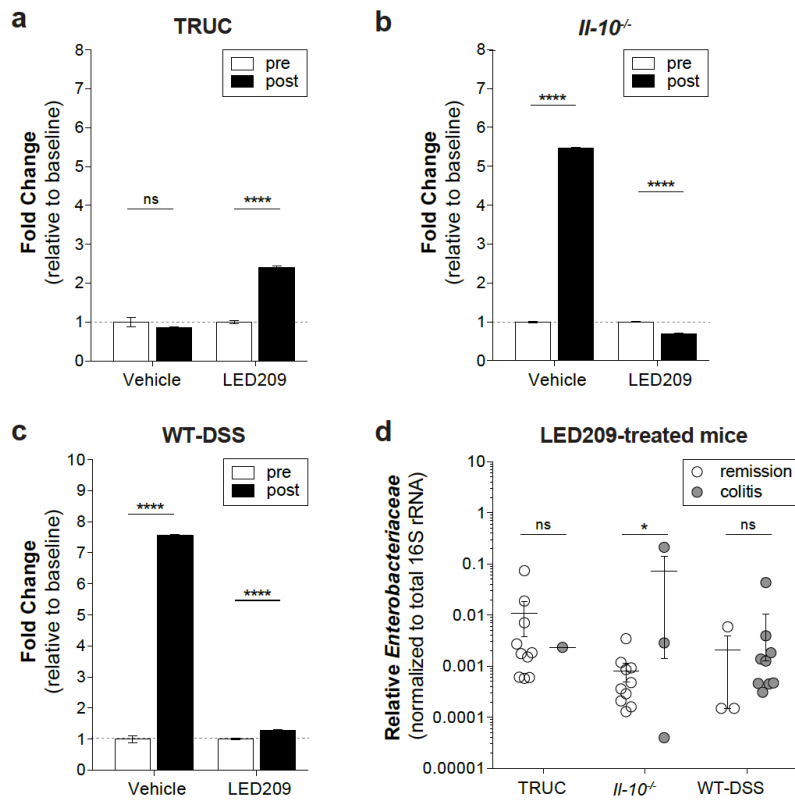


Figure 3.2. Shifts in *Enterobacteriaceae* relative abundance following an LED209 intervention in mouse models of experimental colitis. *Enterobacteriaceae* 23S rRNA levels measured by qPCR using microbial DNA from pre- and post-intervention stool: (a) TRUC ($n = 10$, vehicle; $n = 11$, LED209), (b) *Il-10*^{-/-} ($n = 11$, vehicle; $n = 13$, LED209), and (c) WT DSS-exposed ($n = 4$, vehicle; $n = 13$, LED209) mice. *Enterobacteriaceae* levels were normalized to total 16S rRNA and fold change was calculated relative to baseline for each treatment group using the $2^{-\Delta\Delta Ct}$ method. Error bars indicate mean \pm fractional SD. Two-way ANOVA with Sidak's multiple comparison test to compare pre- and post-intervention levels within each treatment group: **** $P < 0.0001$; ns, not significant. (d) Differentially abundant *Enterobacteriaceae* levels in stool from LED209-treated mice with active disease versus remission for each experimental model. Log₁₀ scale. Symbols represent individual mice, color-coded by the indicated metadata. Error bars indicate mean \pm SEM. Two-way ANOVA with Sidak's multiple comparison test to compare levels in mice with active disease versus remission for each model: * $P < 0.05$; ns, not significant.

content samples were comparable between treatment groups and across models; significant differences in cecal NE and EPI were only observed for WT-DSS mice, but this effect was driven by a single sample (Figure 3.3a). Fold change in CA levels from baseline for stool samples also did not show any significant differences or trends between treatment groups or across models

(Figure 3.3b). Despite differences in disease activity and differential shifts in *Enterobacteriaceae* abundance between treatment groups in these experimental models of colitis, we did not observe major perturbations to the CA economy of the intestinal lumen. These observations suggest that LED209 may alter bacterial virulence and intestinal inflammation without dramatically shifting luminal CAs.

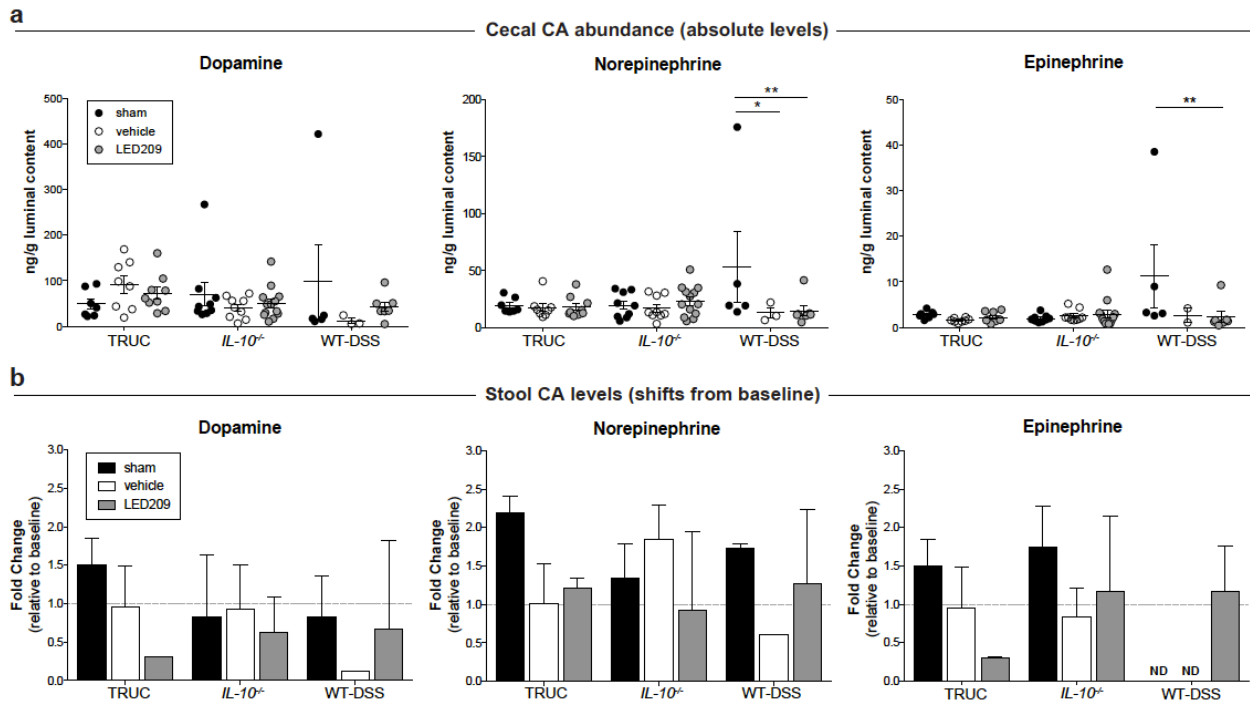


Figure 3.3. CA levels in cecal content and stool following an LED209 intervention in mouse models of experimental colitis. Cecal contents were collected upon sacrifice and stool was collected pre- and post-intervention. Samples were flash-frozen immediately after collection. For each treatment group, samples were combined into >100 mg pools to meet the limit of detection and underwent CA extraction and measurement by HPLC. Quantities were weight corrected to ng/g stool based on the pooled sample wet weights. **(a)** CA abundance in post-intervention cecal content samples. Symbols represent pooled samples for each treatment group, color-coded by indicated metadata. Error bars indicate mean \pm SEM. Two-way ANOVA with Tukey's multiple comparison test to compare treatment groups in each model: * $P < 0.05$ and ** $P < 0.01$. Number of mice and associated number of cecal pools: TRUC (sham, $n = 10$ [7 pools]; vehicle, $n = 10$ [8 pools]; LED209, $n = 11$ [9 pools]), *IL-10^{-/-}* (sham, $n = 11$ [9 pools]; vehicle, $n = 11$ [9 pools]; LED209, $n = 13$ [13 pools]), and WT-DSS (sham, $n = 7$ [5 pools]; vehicle, $n = 4$ [3 pools]; LED209, $n = 13$ [7 pools]). **(b)** Post-intervention CA fold change calculated relative to baseline for each treatment group for each experimental model. Error bars indicate mean \pm fractional SD. No significant differences observed by two-way ANOVA. ND, outside of lower limit of detection by HPLC. Number of mice and associated number of stool pools: TRUC (sham, $n = 6$ [2 pre/2 post]; vehicle, $n = 6$ [2 pre/2 post]; LED209, $n = 7$ [2 pools/2 post]), *IL-10^{-/-}* (sham, $n = 11$ [4 pre/5 post]; vehicle, $n = 10$ [7 pre/5 post]; LED209, $n = 13$ [9 pre/9 post]), and WT-DSS (sham, $n = 6$ [2 pre/3 post]; vehicle, $n = 4$ [2 pre/1 post]; LED209, $n = 13$ [4 pre/4 post]).

DISCUSSION

Core features of IBD are microbial dysbiosis and dysregulated host-microbiota interactions in a genetically susceptible host. Microbial dysbiosis in IBD is often linked to gut microbiome dysfunction characterized by increases in colitogenic bacteria coupled with shifts in microbial metabolism favoring pathways involved in bacterial pathogenesis¹⁹. In-depth profiling of the TRUC gut microbiome in active disease versus treatment-induced remission led to the discovery that host stress molecules may be associated with increased *Enterobacteriaceae* growth and virulence in experimental colitis¹ (Chapter 2). A connection between microbial CA metabolism and active disease was further supported by gut microbiome studies in IBD patients¹⁶.

Physiological stress has long been correlated with susceptibility to inflammation and microbial infection, particularly in the gut^{5,20}. One explanation for this phenomenon is the ability of pathogens and opportunistic bacteria, including *Enterobacteriaceae*, to sense and respond to host stress signals and to induce virulence by triggering the bacterial quorum sensor QseC⁸. Quorum sensing through TCSs is considered an adaptive and auxiliary function of bacteria; one that is critical for virulence, infection, and enhanced fitness, but not essential for growth and survival¹⁰. This has been strengthened by studies demonstrating that quorum sensing inhibitors, like LED209, can reduce bacterial virulence without affecting growth¹¹. Thus, we tested whether inhibition of QseC could reduce disease severity in three preclinical models of colitis. In addition to the TRUC model, which has defects in both innate and adaptive immunity, we also used the genetically-engineered *Il-10*^{-/-} model, where mice develop spontaneous colitis from loss of regulatory immune function, and the DSS-induced acute colonic injury model that recapitulates features of human ulcerative colitis. Employing three distinct models of experimental colitis allowed us to assess the applicability of QseC inhibition in different genetic contexts.

We demonstrated that LED209 can attenuate disease across all three experimental colitis models, with the most striking protective effect in TRUC and WT-DSS mice (**Figure 3.1**). Examining the effects of treatment on *Enterobacteriaceae* levels revealed that LED209 can prevent the expansion of *Enterobacteriaceae* in *Il-10^{-/-}* and WT-DSS mice, but not TRUC mice (**Figure 3.2**). Furthermore, measuring CAs in cecal contents and stool showed that LED209 does not significantly affect the luminal CA pool and may not disrupt host or microbial CA metabolism, as levels were comparable between controls and LED209-treated mice (**Figure 3.3**).

Several unexpected observations were made that warrant further investigation. LED209 treatment was less effective in the *Il-10^{-/-}* model. Intriguingly, histology-based colitis scores and levels of *Enterobacteriaceae* were more varied in LED209-treated *Il-10^{-/-}* mice compared to LED209-treated mice in the other models examined. Closer analysis of cohort metadata and comparing LED209 responders to non-responders suggest that differences in disease severity in *Il-10^{-/-}* mice may be related to sex-dependent susceptibility and to *Enterobacteriaceae* burden. Disentangling if and to what extent these factors influence disease severity could be achieved by testing LED209 in a larger cohort of male and female mice and by working in a gnotobiotic setting, where levels of *Enterobacteriaceae* can be more rigorously monitored and controlled.

Unlike the *Il-10^{-/-}* and WT-DSS models, where LED209 blocked the expansion of *Enterobacteriaceae*, especially for mice in remission, levels of *Enterobacteriaceae* were 2.4-fold higher than baseline in LED209-treated TRUC mice. Based on previous studies in the TRUC model, specific *Enterobacteriaceae* species, including *Klebsiella pneumoniae* and *Proteus mirabilis* in the presence of an endogenous microbiota, can trigger colitis²¹. Interventions that target various aspects of the host-microbiota interface, including antibiotics, immunomodulators, and a fermented-milk product (FMP), can ameliorate colitis and differentially modify the TRUC gut microbiome¹ (Chapter 2). Antibiotics induce massive changes in microbiota composition whereas,

immunomodulators and FMP produce more subtle shifts. Consistent among treatments that do not ameliorate disease are increased *Enterobacteriaceae*, further supporting a role for these opportunistic bacteria in promoting microbial dysbiosis and disease pathogenesis. Conversely, treatments that attenuate disease have variable effects on *Enterobacteriaceae* abundance (**Supplementary Figure 3.4**), with metronidazole allowing *Enterobacteriaceae* to bloom, immunomodulators maintaining relatively constant *Enterobacteriaceae* levels, and gentamicin and FMP completely depleting *Enterobacteriaceae*. Exploring this data in more depth reveals that remission can be associated with an *Enterobacteriaceae* continuum. The implications of this observation are manifold. First, it suggests that LED209 may function more like a host-directed therapy than a traditional broad-spectrum antibiotic, as it targets a very specific subset of bacteria and their auxiliary functions versus wiping out an entire segment of the microbiota by inhibiting their essential functions. Confirming this would require 16S rRNA or whole metagenome sequencing to capture LED209's effect on the gut microbiome as a whole. Second, it suggests that *Enterobacteriaceae* may be more useful as a diagnostic rather than as a prognostic biomarker for IBD, based on its elevated abundance in active disease but variable abundance in remission. Third, it justifies developing clinical assays for measuring microbiome expression and activity over microbiome composition, as markers for microbiome dysfunction may be a more appropriate indicator of colitogenic potential.

A notable facet of LED209 function described in the original study of EHEC in a rabbit model of infection was that despite reducing its virulence, LED209 failed to reduce EHEC colonization¹¹. Activation of QseC in EHEC induces expression of proteins that cause attaching-effacing lesions and mediates expression of Shiga toxin²². They attributed the inability of LED209 to reduce EHEC colonization to the rapid absorption of LED209 from the gastrointestinal tract and suggested that non-invasive pathogens, such as EHEC, may be less susceptible to its

inhibitory effects¹¹. That data suggests that LED209 may differentially target *Enterobacteriaceae* clades based on their invasive capacity and ability to survive in host cells and thus, escape the activity of LED209. Whether this can explain differences in LED209 treatment effects in experimental colitis remains to be determined. Understanding LED209's specificity for invasive versus non-invasive bacteria and evaluating whether oral formulas are reaching the epithelium at adequate enough concentrations will necessitate more *in vitro* and *in vivo* analysis as well as incorporating measurements of mucosa-associated bacteria. Moreover, although studies with LED209 in animal models of infection did not result in host toxicity or off-target effects^{11,12}, experiments examining whether LED209 has microbiota-independent effects in IBD-susceptible hosts is also required.

While several mechanisms have been suggested for how antivirulence drugs inhibit exogenous pathogens, including preventing the colonization of pathogens during passage through the gastrointestinal tract or enabling pathogens to be more easily eliminated by the host immune system¹⁵, whether these mechanisms hold true for colitogenic bacteria, which are already a part of the endogenous microbiota, merits further investigation. In summary, we show that LED209 can ameliorate disease in mouse models of experimental colitis and provide insight into QseC as a feasible microbiota-targeted approach for the treatment of IBD.

MATERIALS AND METHODS

Animal husbandry

Specified pathogen-free (SPF) BALB/c TRUC, *Il-10*^{-/-}, and WT mice were weaned and randomized into experimental cages between postnatal days (p) 21 and 25. Mice were housed in a barrier facility at the Harvard T.H. Chan School of Public Health. Animal experiments were

approved and conducted in accordance with Harvard Medical School Standing Committee on Animals and National Institutes of Health guidelines.

LED209 interventions

LED209 [*N*-phenyl-4-(3-phenylthioureido)benzenesulfonamide] (Cayman Chemical) was dissolved in vehicle containing 70% sodium bicarbonate pH 9, 23% polyethylene glycol [PEG], 5% dimethyl sulfoxide [DMSO], and 2% Tween-80 (all Sigma). For all experimental models, mice were orally administered an equal volume of LED209 (0.4 mg/mouse), vehicle, or water (sham). TRUC and *Il-10*^{-/-} mice underwent a 28-day intervention from p42 ± 4 until p70 ± 4. WT mice underwent a 10-day intervention from p34 ± 2 until p44 ± 2, with 3% (wt/vol) DSS (Affymetrix) added to the drinking water from experimental day 3 through 7. Body weight, body condition, and stool consistency were measured frequently throughout the intervention to monitor disease activity. All mice were sacrificed on the final day of feeding.

Histology

Upon sacrifice, colons were resected, fixed in 4% paraformaldehyde (Sigma), and embedded in paraffin. Sections were H&E-stained and evaluated in a blinded fashion for epithelial hyperplasia (0–3), epithelial injury (0–3), polymorphonuclear infiltration (0–3), and mononuclear infiltration (0–3), these indices were summed to generate the histologic colitis score²³.

Stool collection and processing for qPCR analysis

DNA/RNA co-isolation. Stool was collected and homogenized in *RNAlater* (Ambion), held at 4°C overnight, and stored at -80°C before processing. Nucleic acids were extracted using a phenol-chloroform bead-beating procedure followed by DNA/RNA separation and purification using the

Qiagen AllPrep DNA/RNA mini kit (Qiagen). DNase treatments were performed on RNA samples using both on-column (Qiagen) and solution-based (Ambion) kits. DNA was quantified using a NanoPhotometer Pearl (Denville). RNA was quantified using the Quant-iT RNA HS assay kit (Life Technologies) and quality assessed via assignment of an RNA integrity number (RIN) using an Agilent 2100 Bioanalyzer (Agilent). DNA was stored at -20°C prior to qPCR. RNA was divided into 30 µg aliquots and stored at -80°C. See **Supplementary Methods** for the extended protocol.

Lithium chloride extraction of stool DNA from DSS-treated mice. *In vivo* DSS treatment can completely inhibit the activity of polymerases and therefore affect qPCR amplification and analysis of extracted DNA from exposed tissues²⁴. To remove residual DSS, extracted post-intervention stool DNA from WT-DSS exposed mice was purified using a lithium chloride (LiCl)-based method published for RNA²⁴ prior to undergoing DNase treatment. DNA was incubated with 0.1 volume of 8M LiCl (Cellgro) diluted in RNase-free water (Ambion) at -20°C for 30 min and then centrifuged at 14,000 *g* for 30 min at 4°C. DNA pellets were resuspended in 200 µl of water. The 30-min incubation with LiCl, the centrifugation, and the pellet resuspension were repeated for a second round. DNA was precipitated at -20°C for 30 min in 200 µl 3M sodium acetate pH 5.2 (Ambion) and 400 µl 100% ethanol. DNA was centrifuged for 30 min at 4°C. DNA pellets were washed with 500 µl 70% ethanol, centrifuged for 10 min at 4°C, resuspended in water, and stored at -20°C.

qPCR for changes in relative Enterobacteriaceae abundance. Quantification of *Enterobacteriaceae* involved the 23S rRNA-targeted primers En-Isu3-F (5'-TGCCGTAACCTTCGGGA GAAGGCA-3') and En-Isu3-R (5'-TCAAGGCTCAATGTTCAGTGTC-3') (200 nM each) with an annealing temp of 60°C²⁵. Quantification of total bacteria involved the 16S rRNA-targeted primers, NadK-F (5'-TCCTACGGGAGGCAGCAGT-3') and NadK-R (5'-GGACTACCAGGGTATCTAATCCTGTT-3'), and the probe NadK-P (5'-[6-FAM]-CGTATTACCGCGGCTGCTGGCAC-[BHQ1]-3') (200 nM each)

with an annealing temp of 60°C²⁶. qPCR with *Enterobacteriaceae* (23S rRNA) primer and total bacteria (16S rRNA) primer-probe sets were performed using the KAPA SYBR FAST Universal and KAPA PROBE FAST ROX Low qPCR kits, respectively (Kapa Biosystems). Each reaction contained 15 ng of extracted stool DNA. All reactions were performed in duplicate. Fold change was analyzed using the $2^{-\Delta\Delta C_t}$ method²⁷, $\Delta\Delta C_t = (C_{t, \text{Enterobacteriaceae 23S rRNA}} - C_{t, \text{Total 16S rRNA}})_{\text{post-intervention}} - (C_{t, \text{Enterobacteriaceae 23S rRNA}} - C_{t, \text{Total 16S rRNA}})_{\text{baseline}}$. Error is calculated as the fractional standard deviation (SD), fractional SD = (standard deviation)/(mean value) for samples from each treatment group.

Luminal CA measurements by HPLC

Stool and cecal content were collected and immediately flash-frozen in liquid nitrogen. For the 3 experimental models, samples from each treatment group (sham, vehicle, or LED209) were weighed, combined into at least 100 mg pools, and stored at -80°C. Pooling was required to reach the assays limit of detection. CAs – DOP, NE, EPI – were extracted and measured by post-column HPLC (HLC-8030, Tosoh) using diphenylethylene-diamine as a fluorogenic reagent². Samples were homogenized by vigorous pipetting and vortexing in 1 ml of 0.01 M PBS. The supernatants were collected by centrifugation for 15 min at 13,000 *g* at 4°C and then mixed with 1 ml of 0.2 M perchloric acid (Sigma) for deproteinization. The solutions were centrifuged at 13,000 *g* for 15 min and the deproteinized supernatant was processed for catecholamine analysis by HPLC. Quantities were weight corrected to ng/g stool based on the initial pooled sample wet weights.

Statistical analysis

All statistical tests for significance were performed in Prism v6.0h for Mac OS X (GraphPad Software). All averages are mean ± standard error of the mean (SEM) except for fold change calculations where averages are mean ± fractional standard deviation (SD).

REFERENCES

1. Rooks, M. G. *et al.* Gut microbiome composition and function in experimental colitis during active disease and treatment-induced remission. *ISME J* **8**, 1403–1417 (2014).
2. Asano, Y. *et al.* Critical role of gut microbiota in the production of biologically active, free catecholamines in the gut lumen of mice. *Am. J. Physiol. Gastrointest. Liver Physiol.* **303**, G1288–95 (2012).
3. Lomax, A. E., Sharkey, K. A. & Furness, J. B. The participation of the sympathetic innervation of the gastrointestinal tract in disease states. *Neurogastroenterol. Motil.* **22**, 7–18 (2010).
4. Rasko, D. A. & Sperandio, V. Anti-virulence strategies to combat bacteria-mediated disease. *Nat Rev Drug Discov* **9**, 117–128 (2010).
5. Sandrini, S., Aldriwesh, M., Alruways, M. & Freestone, P. Microbial endocrinology: host-bacteria communication within the gut microbiome. *J. Endocrinol.* **225**, R21–34 (2015).
6. Freestone, P. P. E., Walton, N. J., Haigh, R. D. & Lyte, M. Influence of dietary catechols on the growth of enteropathogenic bacteria. *Int. J. Food Microbiol.* **119**, 159–169 (2007).
7. Lyte, M., Vulchanova, L. & Brown, D. R. Stress at the intestinal surface: catecholamines and mucosa-bacteria interactions. *Cell Tissue Res.* **343**, 23–32 (2011).
8. Sperandio, V., Torres, A. G., Jarvis, B., Nataro, J. P. & Kaper, J. B. Bacteria-host communication: the language of hormones. *Proceedings of the National Academy of Sciences* **100**, 8951–8956 (2003).
9. Sperandio, V., Torres, A. G., Jarvis, B., Nataro, J. P. & Kaper, J. B. Bacteria-host communication: the language of hormones. *Proceedings of the National Academy of Sciences* **100**, 8951–8956 (2003).
10. Karavolos, M. H., Winzer, K., Williams, P. & Khan, C. M. A. Pathogen espionage: multiple bacterial adrenergic sensors eavesdrop on host communication systems. *Mol. Microbiol.* **87**, 455–465 (2013).
11. Rasko, D. A. *et al.* Targeting QseC signaling and virulence for antibiotic development. *Science* **321**, 1078–1080 (2008).
12. Curtis, M. M. *et al.* QseC inhibitors as an antivirulence approach for Gram-negative pathogens. *MBio* **5**, e02165 (2014).
13. Yang, Q., Anh, N. D. Q., Bossier, P. & Defoirdt, T. Norepinephrine and dopamine increase motility, biofilm formation, and virulence of *Vibrio harveyi*. *Front Microbiol* **5**, 584 (2014).
14. Harrison, C. F. *et al.* Adrenergic antagonists restrict replication of *Legionella*. *Microbiology* **161**, 1392–1406 (2015).
15. Eloë-Fadrosh, E. A. & Rasko, D. A. The human microbiome: from symbiosis to pathogenesis. *Annu. Rev. Med.* **64**, 145–163 (2013).
16. Gevers, D. *et al.* The treatment-naive microbiome in new-onset Crohn's disease. *Cell Host and Microbe* **15**, 382–392 (2014).
17. Kamada, N., Chen, G. Y., Inohara, N. & Nuñez, G. Control of pathogens and pathobionts by the gut microbiota. *Nat. Immunol.* **14**, 685–690 (2013).

18. Mukhopadhyay, I., Hansen, R., El-Omar, E. M. & Hold, G. L. IBD-what role do Proteobacteria play? *Nat Rev Gastroenterol Hepatol* **9**, 219–230 (2012).
19. Morgan, X. C. *et al.* Dysfunction of the intestinal microbiome in inflammatory bowel disease and treatment. *Genome Biol.* **13**, R79 (2012).
20. Freestone, P. P. E., Sandrini, S. M., Haigh, R. D. & Lyte, M. Microbial endocrinology: how stress influences susceptibility to infection. *Trends Microbiol.* **16**, 55–64 (2008).
21. Garrett, W. S. *et al.* Enterobacteriaceae act in concert with the gut microbiota to induce spontaneous and maternally transmitted colitis. *Cell Host and Microbe* **8**, 292–300 (2010).
22. Clements, A., Young, J. C., Constantinou, N. & Frankel, G. Infection strategies of enteric pathogenic *Escherichia coli*. *Gut Microbes* **3**, 71–87 (2012).
23. Garrett, W. S. *et al.* Communicable ulcerative colitis induced by T-bet deficiency in the innate immune system. *Cell* **131**, 33–45 (2007).
24. Viennois, E., Chen, F., Laroui, H., Baker, M. T. & Merlin, D. Dextran sodium sulfate inhibits the activities of both polymerase and reverse transcriptase: lithium chloride purification, a rapid and efficient technique to purify RNA. *BMC Res Notes* **6**, 360 (2013).
25. Veiga, P. *et al.* *Bifidobacterium animalis* subsp. *lactis* fermented milk product reduces inflammation by altering a niche for colitogenic microbes. *Proc. Natl. Acad. Sci. U.S.A.* **107**, 18132–18137 (2010).
26. Nadkarni, M. A., Martin, F. E., Jacques, N. A. & Hunter, N. Determination of bacterial load by real-time PCR using a broad-range (universal) probe and primers set. *Microbiology (Reading, Engl.)* **148**, 257–266 (2002).
27. Livak, K. J. & Schmittgen, T. D. Analysis of relative gene expression data using real-time quantitative PCR and the $2^{-\Delta\Delta C(T)}$ Method. *Methods* **25**, 402–408 (2001).

CHAPTER 4

Genetic inactivation of QseC in the IBD-associated AIEC strain LF82

Michelle G. Rooks¹, Analise Z. Reeves^{2,3}, Koji Yasuda^{1,3}, Leslie H. Wardwell-Scott³, Carey Ann Gallini¹, Monia Michaud¹, Jonathan N. Glickman³, Cammie F. Lesser^{2,3,4}, Curtis Huttenhower^{1,5}, Patrick Veiga⁶, and Wendy S. Garrett^{1,3,5,7}.

¹Harvard T.H. Chan School of Public Health, Boston, MA, USA

²Massachusetts General Hospital, Boston, MA, USA

³Harvard Medical School, Boston, MA, USA

⁴Harvard Stem Cell Institute, Cambridge, MA, USA

⁵Broad Institute of MIT and Harvard, Cambridge, MA, USA

⁶Danone Research, Palaiseau, France

⁷Dana-Farber Cancer Institute, Boston, MA USA

Author Contributions:

M.G.R. and W.S.G. conceived and designed the study. All experiments and analysis were performed by M.G.R., with the following exceptions. A.Z.W. and C.F.L. provided plasmids and protocols for λ -Red recombination. K.Y. and C.H. facilitated 16S rRNA gene library generation, sequencing, and analysis. C.A.G. and L.H.W. helped with conventional and gnotobiotic animal husbandry, respectively. M.M. and P.V. offered technical advice on bacterial protocols and P.V. provided LF82. J.N.G. performed blinded histological assessment.

BACKGROUND

Escherichia coli species are the predominant Gram-negative aerobes of the mammalian gut microbiota¹, where they contribute to microbial community stability and the maintenance of intestinal homeostasis. Compared to their symbiotic counterparts, pathogenic *E. coli* strains have acquired novel or modified sets of virulence factors, many of which are involved in host cell attachment, invasion, and production of toxins². Gut microbiota alterations, including a higher abundance of *E. coli* in mucosal biopsies and stool, are consistently observed in inflammatory bowel disease (IBD)^{3,4}. Presence of mucosal-associated *E. coli* has been estimated to be upwards of 10-fold higher in IBD patients than controls⁵ and *E. coli* strains isolated from patients with active disease often display pathogenic properties, such as adhesion to and invasion of host cells⁶. Moreover, a central role for adherent-invasive *E. coli* (AIEC) in the pathogenesis of IBD is substantiated by whole metagenome sequencing data from human cohorts⁷.

E. coli LF82 is the AIEC reference strain originally isolated from a mucosal lesion of a Crohn's disease (CD) patient⁸. LF82's virulence potential, including its ability to adhere to and invade intestinal epithelial cells (IECs) and to survive and replicate within macrophages, is well established^{9,10}. Two mechanisms driving LF82's virulence are the production of flagellar and type-1 pili proteins for motility and adhesion. Inactivating the flagellar protein FliC blocks LF82 invasion and reduces its adhesion to cultured IECs¹¹. In the setting of induced colonic injury and inflammation, LF82 can exacerbate colitis and flagellar proteins – via direct signaling through toll-like receptor 5 (TLR5) on IECs – are the virulence factors responsible for potentiating the observed inflammatory mucosal immune response¹².

A hallmark feature of IECs of CD patients is abnormal expression of the glycoprotein CEACAM6 (carcinoembryonic antigen-related cell adhesion molecule) and CEACAM6 is a canonical receptor for LF82¹³. Remarkably, the overexpression of CEACAM6 promotes AIEC

colonization and AIEC infection in turn upregulates CEACAM6 by inducing pro-inflammatory cytokines interferon- γ and tumor necrosis factor- α ¹³, creating a positive feedback loop that fuels chronic intestinal inflammation. Given the interest in CEACAM6 in human IBD and that mice lack analogous genes for human CEACAM6, transgenic CEABAC10 mice were generated that harbor a 187-kb human bacterial artificial chromosome containing part of the human CEA family gene cluster, including complete human CEACAM6¹⁴. Although CEACAM6 expression is restricted to the colon of mice, this model enables a more accurate *in vivo* setting for elucidating LF82-host interactions. Indeed, perturbing the gut microbiota of transgenic CEABAC10 mice and orally challenging them with LF82 leads to persistent LF82 colonization that is dependent on type-1 pili expression¹⁵. Similarly, in this model, inducing mucosal inflammation in the presence of LF82 can augment disease severity¹³. Taken together, these observations undoubtedly support a role for AIEC virulence in the pathogenesis of IBD.

Quorum-sensing *E. coli* regulator C (QseC) is a master regulator of virulence in many clinically-relevant *E. coli* strains^{16,17}. Activation of QseC directly activates flagellar and type-1 pili expression, which are crucial for LF82 colonization and virulence. QseC is part of the QseBC quorum-sensing two-component system (TCS) that is activated upon detection of microbiota-generated autoinducer-3 or host stress signals, specifically the catecholamines norepinephrine (NE) and epinephrine (EPI)¹⁸. Both NE and EPI have been shown to induce QseC-mediated virulence *in vitro* and blocking QseC signaling with the inhibitor LED209 can reduce the virulence of pathogens *in vivo*¹⁹⁻²¹. From a gut microbiome survey of a mouse model of experimental colitis, we revealed that microbial genes and pathways involved in CA-related metabolism, TCS signaling, and motility were enriched in active colitis (Chapter 2) and demonstrated that disease could be attenuated with LED209 (Chapter 3). Given the essential function of flagellar proteins in LF82 virulence, we hypothesized that targeting QseC, an upstream node involved in the activation of

flagellar gene expression, may reduce its virulence potential. Besides its clinical relevance, the LF82 genome is sequenced and annotated²² making this IBD-associated strain a particularly useful and tractable tool for understanding the role of QseC in mediating AIEC virulence. Here, we generated isogenic LF82- $\Delta qseC$ deletion and LF82- $\Delta qseC::qseC$ complementation mutants to assess the effects of *qseC* inactivation on LF82 virulence *in vitro* and *in vivo*.

RESULTS

Generating LF82 *qseC* deletion and complementation mutants using the λ -Red system

To determine whether QseC plays an essential role in mediating LF82 virulence, using the LF82 parent strain, we generated an isogenic deletion mutant LF82- $\Delta qseC$ and complementation mutant LF82- $\Delta qseC::qseC$ using λ -Red recombination. See Materials and Methods.

Absence of *qseC* downregulates expression of LF82 virulence genes

To investigate whether *qseC* regulates the expression of virulence genes in LF82, we selected primers targeting candidate QseC-regulated genes, including CA-mediated quorum-sensing genes and their downstream transcriptional targets involved in flagellar assembly and motility. Total RNA was extracted from bacterial cultures of wild-type (WT) LF82 and mutant LF82 strains and analyzed by real-time quantitative PCR (RT-qPCR). No *qseC* transcripts were detected in LF82- $\Delta qseC$, as expected, and expression was significantly reduced in LF82- $\Delta qseC$ compared to LF82-WT and LF82- $\Delta qseC::qseC$ for all genes examined (**Figure 4.1**). Notably, *qseB* expression in LF82- $\Delta qseC$ was >90-fold higher than the WT and complemented strains (**Figure 4.1**). This observation aligns with evidence of QseC functioning as a phosphatase that autoregulates QseBC TCS activation and of QseC deficiency resulting in compensatory upregulation of QseB²³. QseE is another histidine sensor kinase that detects NE and EPI and is

part of the QseEF TCS²⁴. Both QseC and QseE activate the response regulator QseF that induces genes involved in the formation of attaching-effacing (A/E) lesions. However, these virulence genes are encoded within a chromosomal pathogenicity island found only in enterohemorrhagic *E. coli* (EHEC) and enteropathogenic *E. coli* (EPEC) and not in AIEC²⁵. Previous reports demonstrated that transcription of *qseEF* is activated by QseC and that QseC acts upstream of QseF²⁴; this directional TCS crosstalk may also hold true for LF82. Importantly, genes in the flagellar regulon (*flhDC*) and genes involved in flagellar assembly (*fliA*, *fliC*) and motility (*motB*) are all significantly lower in LF82- Δ *qseC* compared to LF82-WT and LF82- Δ *qseC*::*qseC* (Figure 4.1). This expression data substantiates that QseC regulates LF82 virulence by inducing genes involved in flagellar assembly and motility.

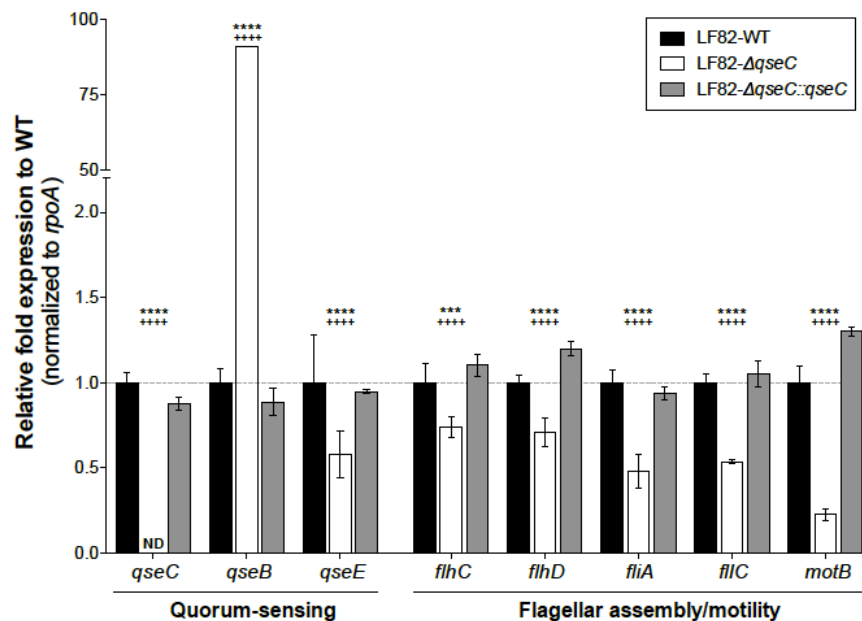


Figure 4.1. Effects of *qseC* inactivation on the expression of LF82 virulence genes. RT-qPCR analysis of putative QseC-regulated virulence genes in WT and mutant LF82 strains. Cultures were grown in Luria Bertani (LB) broth overnight at 37°C without agitation, back diluted to an OD₆₀₀ of 0.02, and grown for 6 hrs at 37°C without agitation. Total RNA was extracted from bacterial pellets and underwent rigorous DNase treatments and cDNA synthesis prior to RT-qPCR. Genes were normalized to *rpoA* and fold change was calculated relative to WT using the $2^{-\Delta\Delta C_t}$ method. Bars represent data from 2 independent experiments. Error bars indicate mean \pm fractional SD. Two-way analysis of variance (ANOVA) with Tukey's multiple comparison test to compare expression between strains for each primer set: *** or +++ $P < 0.001$, **** or ++++ $P < 0.0001$. * and + indicate a significant difference in relation to LF82-WT and LF82- Δ *qseC*::*qseC*, respectively. ND, transcripts not detected by RT-qPCR.

Morphological analysis confirms *qseC*-dependent defects in flagellar protein production

To visualize morphological differences between LF82 strains and to corroborate our expression data obtained by RT-qPCR, transmission electron microscopy (TEM) was performed on WT and mutant LF82 strains. Images revealed a massive reduction or complete absence of flagella on LF82- $\Delta qseC$ compared to LF82-WT and LF82- $\Delta qseC::qseC$ strains, further indicating that QseC regulates flagellar protein production (**Figure 4.2**). Thus, TEM analysis supports that QseC mediates virulence in LF82 by inducing flagellar protein production.

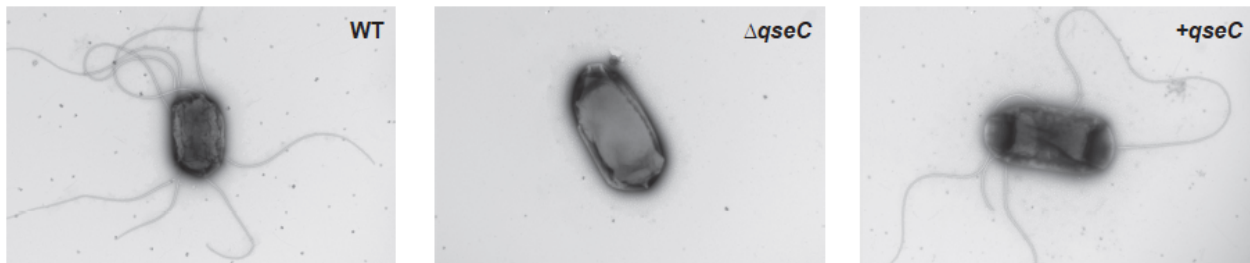


Figure 4.2. Representative TEM images of WT and mutant LF82 strains. LF82 strains were grown in LB broth overnight at 37°C without agitation. Transmission electron microscopy (TEM) was performed via negative staining with uranyl formate (pH 4) on carbon-formvar gold grids. Magnification, 12,000x.

QseC regulates LF82 swimming motility and mediates NE-induced motility

Recognizing that flagella proteins are required for LF82 virulence¹² and observing that *qseC* inactivation in LF82 abrogates expression of flagellar genes and proteins, we next assessed flagella function using plate-based motility assays. With this method, swimming motility is measured as the diameter of the circular halo formed by the growing motile bacterial cells away from the point of inoculation. LF82- $\Delta qseC$ had defects in motility based on a smaller swim diameter compared to LF82-WT and this mutant phenotype was rescued by complementation (**Figure 4.3a**).

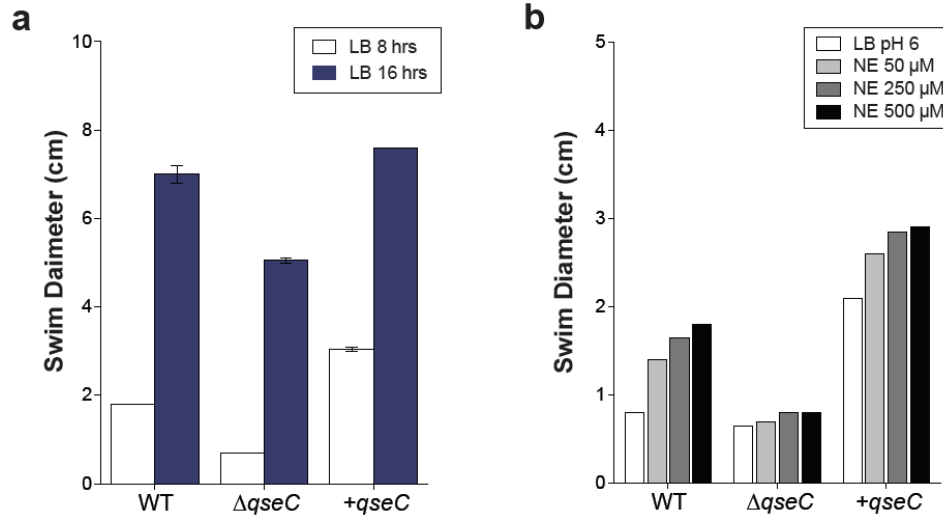


Figure 4.3. Plate-based motility assays of LF82 strains grown in LB or NE-supplemented LB. Swimming motility assay on 0.3% LB agar plates using overnight cultures (adjusted to an OD_{600} of 1.0, 3 μ l spotted/plate) of indicated strains. (a) Bacteria were spotted into separate plates and incubated at 37°C. Swim diameter was measured at 8 and 16 hrs post-inoculation. (b) LB agar was supplemented with NE and pH-matched to pH 6. Each LF82 strain was spotted into the same plate equidistant from the center and incubated at 37°C. Swim diameter was measured at 8 hrs post-inoculation. All plates were performed in duplicate. Motility was assessed by measuring the swim diameter (cm) of growing motile bacterial cells away from the point of inoculation. WT, parent LF82; $\Delta qseC$, LF82- $\Delta qseC$ deletion mutant; +*qseC*, LF82- $\Delta qseC::qseC$ complementation mutant.

As an adrenergic receptor, QseC can sense host stress molecules (NE or EPI) and directly activate a signaling cascading that induces expression of virulence genes, including flagellar proteins²⁶. Thus, we evaluated the effects of *qseC* inactivation on NE-induced motility in LF82 using agar plates supplemented with NE. As it is the more abundant catecholamine in the intestinal lumen, we selected NE over EPI²⁷. To dissolve and maintain the stability of NE, we used acidified water and subsequently pH-matched the LB control (to pH 6). NE enhanced the motility of LF82-WT and LF82- $\Delta qseC::qseC$ strains in a dose-dependent manner, but did not induce motility in LF82- $\Delta qseC$ (Figure 4.3b). When agar was supplemented with acidified LB alone, WT and LF82- $\Delta qseC$ had similar swim diameters (Figure 4.3b), with levels matching the diameter of LF82- $\Delta qseC$ in neutral LB (Figure 4.3a), which was unexpected. Modest differences in pH can influence *E. coli* motility^{28,29}, which may explain this observed phenomenon. Intriguingly, LF82-

$\Delta qseC::qseC$ showed enhanced motility compared to LF82-WT and LF82- $\Delta qseC$ (Figure 4.3b). This may be a consequence of the residual scar sequence from λ -Red recombination potentially disrupting regulatory elements surrounding the native target gene³⁰. Based on these results from the swim motility assays, we further investigated the effects of NE on the expression of flagellar motility genes in LF82-WT and LF82- $\Delta qseC$. NE significantly upregulated the expression of quorum-sensing and flagellar genes in LF82-WT, but not LF82- $\Delta qseC$, which further confirmed the QseC-dependent stimulatory effect of NE on flagellar motility (Supplementary Figure 4.3). Collectively, these observations confirm that QseC mediates NE-induced motility in LF82.

Establishing an *in vivo* system for monitoring the effects of *qseC* on LF82 colonization and virulence

In specified pathogen-free (SPF) WT mice, colonization by LF82 does not alter bacterial load or microbiota composition and is not sufficient to induce intestinal inflammation³¹, suggesting that AIEC colonization is only transient and does not activate innate immune responses in a healthy host. Thus, we hypothesized that gnotobiotic mice harboring a defined, minimal microbial community devoid of Proteobacteria (Altered Schaedler Flora [ASF]³²) could provide a unique niche for LF82 and be an alternative *in vivo* system to assess whether absence of *qseC* affects LF82 colonization efficiency and virulence potential. This approach has been successful for other Gram negative-pathogens, including *Salmonella enterica*, *Campylobacter jejuni*, other pathogenic *E. coli*, that are typically unable to stably colonize mice under SPF conditions³³. Thus, we transferred 6-week old gnotobiotic-ASF mice from germ-free isolators to our SPF animal facility (hereafter referred to as 'ex-ASF mice'). Cages of ex-ASF mice were handled separately to minimize microbial transfer from other mouse lines in our colony and to thus maintain a low-complexity microbiota. Ex-ASF mice were inoculated with 10^8 colony-forming units (CFUs) of LF82-WT or LF82- $\Delta qseC$. LF82 persistence was monitored by plating stool serial

dilutions on selective and differential agar for *Enterobacteriaceae* (MacConkey agar) and enumerating ampicillin-erythromycin resistant colonies. This antibiotic combination is specific for LF82¹⁵ and allows differentiation of LF82 from other *Enterobacteriaceae* in our SPF mouse facility. Both LF82-WT and LF82- $\Delta qseC$ strains were able to colonize ex-ASF mice when maintained in an SPF setting (**Supplementary Figure 4.4**), confirming the usefulness of this approach for assessing differences between WT and mutant LF82 strains *in vivo*.

QseC influences LF82's persistence in a low-complexity microbiota

Patients with IBD tend to harbor a low complexity microbiota, which is characterized by a loss in biodiversity or species richness³⁴. To mirror features of a low complexity microbiota *in vivo* and evaluate LF82's ability to colonize and persist in a host, we took advantage of the ASF standardized microbial community. The ASF consortia is comprised of 8 bacterial strains originating from the gut of a healthy mouse³². Despite its low complexity, it can effectively colonize mice and endow them with proper immunological development and physiology, making it a useful tool for studying host-microbe interactions in a defined setting. To determine whether QseC promotes LF82 persistence in a host with a low-complexity microbiota, we used 16S ribosomal RNA (rRNA) gene surveys to analyze the gut microbial communities of gnotobiotic-ASF and ex-ASF mice inoculated with LF82-WT or LF82- $\Delta qseC$. Microbial DNA was isolated from the cecum of a gnotobiotic-ASF mouse (ASF input community) and stool pooled from LF82-colonized ex-ASF breeding pairs and their corresponding litters. Samples underwent 16S rRNA gene amplification and sequencing on an Illumina HiSeq platform. Reads were binned into approximately species-level operational taxonomic units (OTUs; $\geq 97\%$ sequence similarity) and were analyzed for within- and between-sample diversity using QIIME³⁵.

Examining the phylum-level relative abundance data, only reads aligning to the 8 strains of the ASF community were present in the gnotobiotic-ASF cecal sample (**Figure 4.4a**). We also observed that ex-ASF-LF82-WT mice had greater Proteobacteria enrichments compared to ex-ASF-LF82- $\Delta qseC$ mice (**Figure 4.4a**). While 16S rRNA gene sequencing approaches only reach species-level resolution, >98% of the sequences for Proteobacteria belonged to the family *Enterobacteriaceae*, with ex-ASF-LF82-WT mice having an average 6-fold higher abundance than ex-ASF-LF82- $\Delta qseC$ mice (**Figure 4.4b**). Thus, loss of *qseC* may hinder LF82's ability to colonize and persist in a host even when there is minimal niche competition.

Although stool is often a sufficient proxy for estimating mucosal and luminal bacterial levels³⁶, a major caveat in LF82 research in animal models is that studies are typically limited to the colon where colonic injury and inflammation is more straightforward to induce. However, based on reports that AIEC are found in one-third of ileal biopsy samples from CD patients compared to 6% in healthy controls and <5% in colons of either IBD patients or controls, suggests that LF82's preferred niche in humans is the ileum⁶. This prompted us to characterize the niche-specificity of LF82 along the intestinal tract of LF82-associated ex-ASF mice and to relate observed CFUs to relative abundance data from 16S rRNA gene surveys of stool. We performed biogeography experiments by partitioning the intestines into 4 sections: distal small intestine, cecum, proximal colon, and distal colon. For each section, luminal contents and adjacent mucosal tissue were collected, homogenized, and serially diluted onto MacConkey agar with and without antibiotics. CFUs of LF82 versus total *Enterobacteriaceae* were enumerated for mucosal-luminal matched samples. Both LF82 and total *Enterobacteriaceae* were higher in ex-ASF-LF82-WT mice than ex-ASF-LF82- $\Delta qseC$ mice and levels correlated between mucosal and luminal samples (**Supplementary Figure 4.5a-b**). We also observed that the cecum was a particularly rich reservoir for LF82 and that LF82 could be detected in the distal small intestine (**Supplementary**

Figure 4.5a). This analysis revealed that stool LF82 and *Enterobacteriaceae* abundances correlate with luminal levels throughout the intestinal tract and further supports that LF82-WT is more proficient at colonizing and persisting *in vivo*.

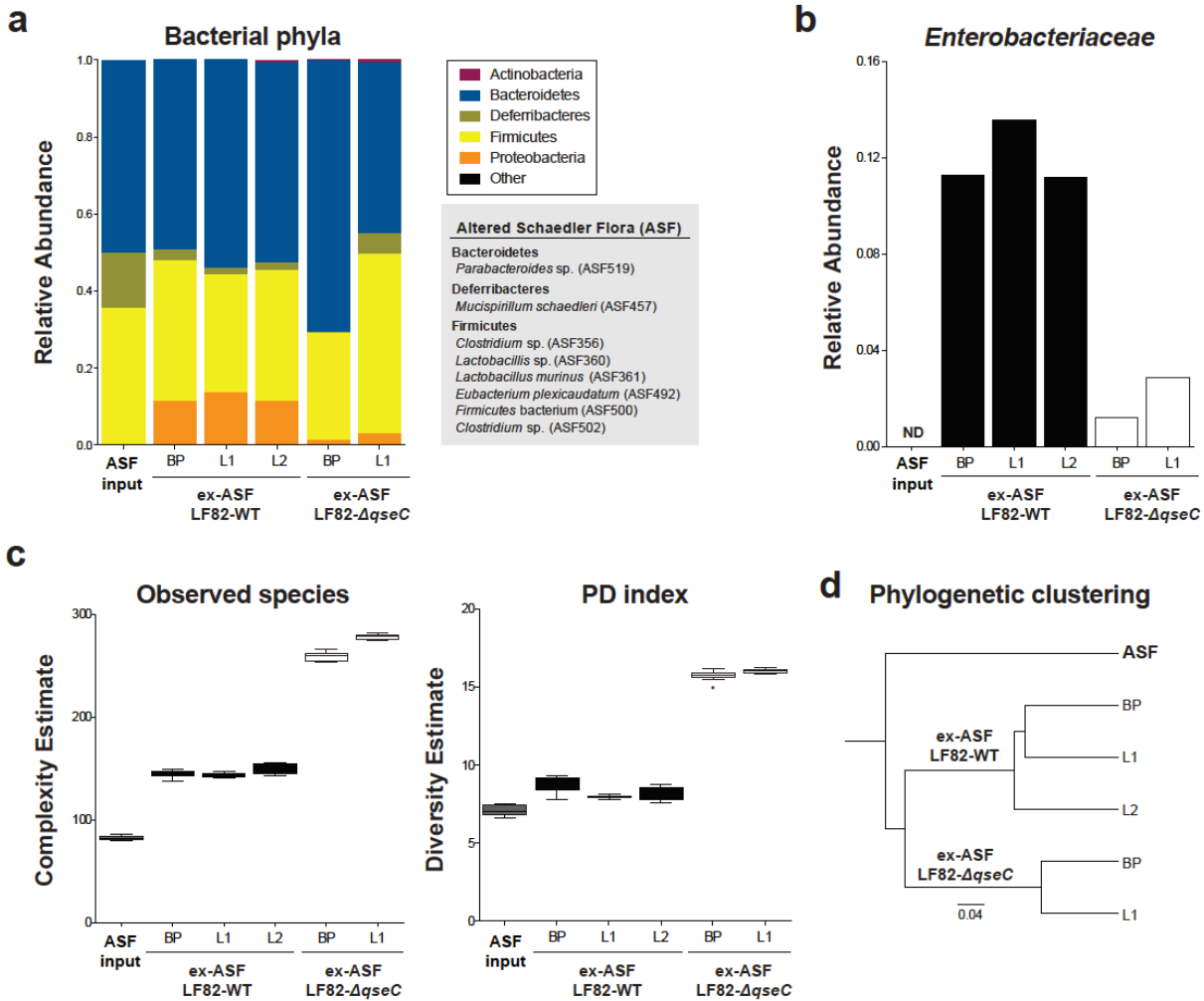


Figure 4.4. 16S rRNA gene surveys of microbial communities of LF82-colonized ex-ASF mice. Microbial community analysis of 16S rRNA gene sequences of microbial DNA isolated from the cecal content of a gnotobiotic mouse associated with Altered Schaedler Flora (ASF input) and stool from LF82-inoculated ex-ASF breeding pairs (BP) and their corresponding litters (L). Number of samples pooled: ex-ASF-LF82-WT (BP, n = 2; L1, n = 3; L2, n = 5) or ex-ASF-LF82-ΔqseC (BP, n = 2; L1, n = 9). (a) Phylum-level relative abundance data from 16S rRNA gene sequences classified by QIIME (Quantitative Insights Into Microbial Ecology). The 8 strains of the ASF community are listed. (b) *Enterobacteriaceae* relative abundance data. ND, sequences were not detected. (c) Metrics for measuring within-sample diversity. OTU table was sampled 10x at a depth of 40,000 reads/sample. Observed species metric estimates complexity and represents the total number of species-level OTUs/sample. Phylogenetic diversity (PD) index metric estimates diversity and represents the evolutionary relatedness of within-sample OTUs based on phylogenetic tree distances. Boxplots denote top quartile, median, and bottom quartile. Whiskers and outliers are plotted by the Tukey method. (d) Hierarchical clustering by similarity using the UPGMA clustering algorithm on the un-weighted UniFrac distance matrix to assess between-sample diversity.

Next, we analyzed the diversity of sequenced microbial communities to characterize differences in community structure in the presence of LF82-WT and LF82- $\Delta qseC$. Within-sample diversity of LF82-WT samples deviated less from the original ASF community compared to LF82- $\Delta qseC$ samples (**Figure 4.4c**). This observation suggests that LF82-WT may be more adept at colonizing and persisting in a low-complexity microbiota and may even facilitate the maintenance of a state of reduced diversity, as seen in human and experimental IBD³¹. Between-sample diversity and hierarchical clustering by similarity demonstrated that microbial communities segregated according to ASF input alone or presence of LF82-WT or LF82- $\Delta qseC$, indicating that these LF82 strains induce distinct microbiota changes (**Figure 4.4d**). Moreover, these data provide evidence that LF82-associated microbiota phenotypes may be transmissible to offspring, as breeding pairs and their corresponding litters had similar community composition, structure, and diversity (**Figure 4.4a-d**). These studies substantiate LF82's ability to sustain and thrive in a microbiota with reduced diversity.

QseC mediates LF82's ability to exacerbate colonic inflammation in a DSS-injury model

Prior studies in the dextran sodium sulfate (DSS) chemically-induced model of experimental colitis demonstrated that WT LF82 can exacerbate colonic injury compared to a non-pathogenic *fliC* mutant¹². This prompted us to examine whether the presence of QseC can affect the virulence of LF82 *in vivo* in the context of DSS-induced inflammation. To incorporate standard models with varying levels of microbiota complexity but lacking LF82 as a comparison, we performed parallel DSS experiments in SPF mice from Jackson Laboratories (JAX) and mice bred in-house (BIH) in the Harvard T.H. Chan School of Public Health barrier facility, which have low and high complexity gut microbiotas, respectively^{37,38}. Upon arrival, JAX mice were handled and maintained using the prudent husbandry practices described for ex-ASF mice to preserve

their original microbiota complexity. Age-matched JAX, BIH, ex-ASF-LF82-WT, and ex-ASF-LF82- $\Delta qseC$ mice underwent a 7-day intervention where 3% DSS (wt/vol) was provided in the drinking water from day 0 to day 5. Post-intervention histology-based colitis scores and other parameters of disease are provided (**Figure 4.5a** and **Supplementary Figure 4.6**). As has been observed previously, JAX mice exhibited less severe DSS-induced inflammation than BIH mice ($P = 0.0618$), with some mice not displaying any signs of mucosal injury or inflammation (**Figure 4.5a**). The colonic injury in ex-ASF-LF82- $\Delta qseC$ mice was comparable to the mild colitis observed in JAX mice (**Figure 4.5a**). Conversely, ex-ASF-LF82-WT mice exhibited significantly more severe colitis compared to JAX and ex-ASF-LF82- $\Delta qseC$ mice ($P < 0.0001$) that more closely resembled disease activity in BIH mice (**Figure 4.5a**). These findings support that QseC may mediate virulence and exacerbate colitis in the acute DSS-injury model.

To determine whether disease severity was related to changes in LF82 abundance within the larger *Enterobacteriaceae* population, we enumerated the number of CFUs in stool collected throughout the DSS intervention. Aligning with published data on the gut microbiome of JAX mice³⁷, we observed that JAX mice harbored significantly less *Enterobacteriaceae* than BIH mice (**Figure 4.5b**). Differential responses to DSS between JAX and BIH mice may, in part, be due to differences in *Enterobacteriaceae* burden (**Figure 4.5a-b**), further implicating this bacterial clade as a potentiator of intestinal inflammation³⁹. Interestingly, stool from JAX and BIH mice had less *Enterobacteriaceae* than ex-ASF mice inoculated with WT or mutant LF82 (**Figure 4.5b**). ASF, as a minimal microbial community devoid of Proteobacteria, may have provided an unoccupied, optimal niche for LF82 and other *Enterobacteriaceae* to expand and persist.

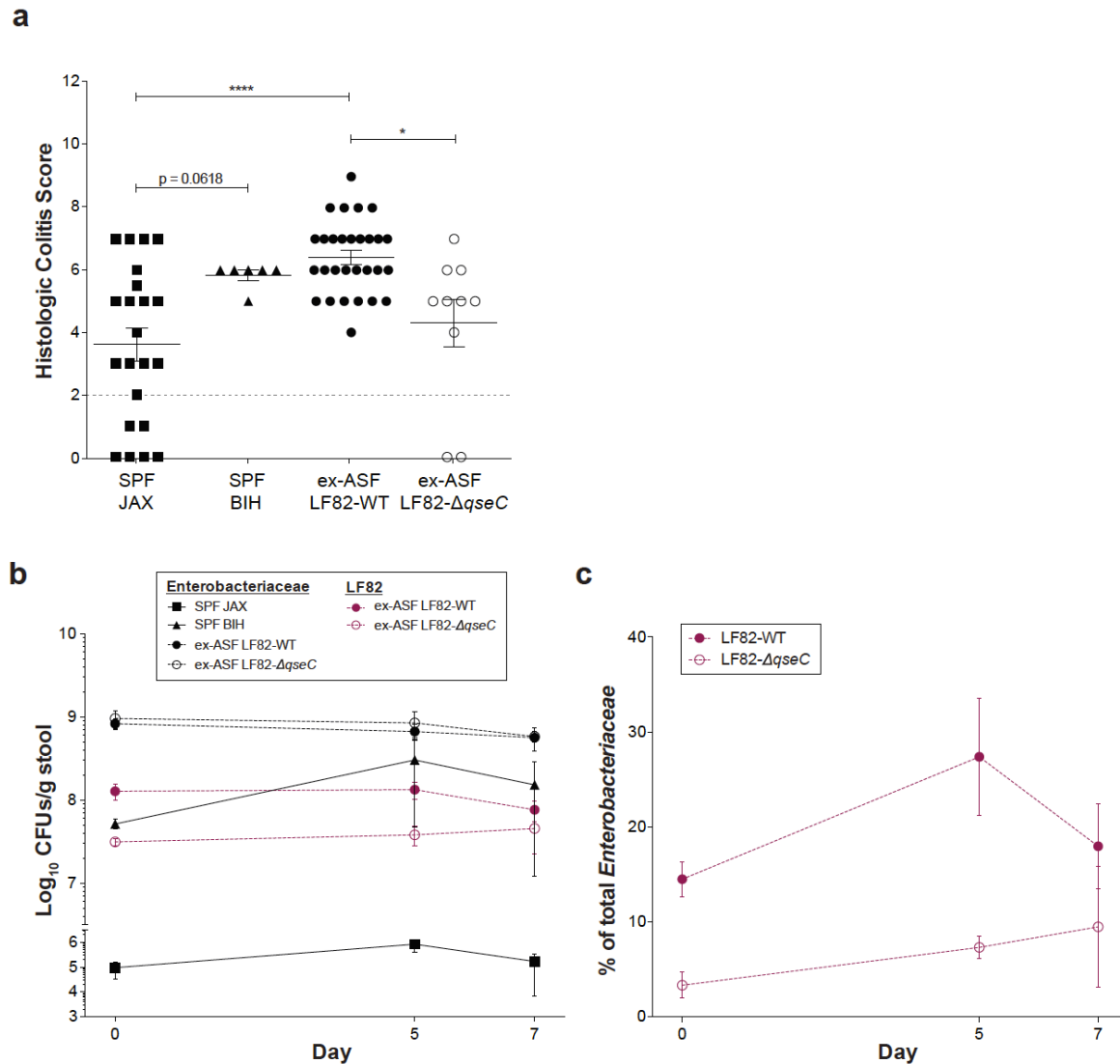


Figure 4.5. Effects of DSS-induced inflammation on the host and on LF82 and *Enterobacteriaceae* levels in mice harboring microbiotas of differing complexity. (a) DSS interventions in BALB/c WT mice: Jackson Laboratories (JAX, n = 22), bred in-house (BIH, n = 6; excluding 2 mice that died before intervention day 7), ex-ASF-LF82-WT (n= 29), and ex-ASF-LF82- Δ qseC (n = 10). Colonic inflammation was chemically-induced by adding 3% (wt/vol) DSS to the drinking water on days 0-5. Symbols represent individual mice. Error bars indicate mean \pm SEM. Colitis scores >2 indicate active disease and scores ≤ 2 remission. One-way ANOVA with Tukey's multiple comparison test: * $P < 0.05$ and **** $P < 0.0001$. (b) Stool was collected on days 0, 5, and 7. Stool serial dilutions were plated onto MacConkey agar \pm Amp/Eryth and grown overnight at 37°C to enumerate total *Enterobacteriaceae* and LF82. The number of Amp^R-Eryth^R LF82 colonies were counted and converted to CFU/gram stool based on wet weight. Symbols represent mean \pm SEM. (c) Calculated percentage of LF82 within the total *Enterobacteriaceae* populations based on measurements in b.

Examining LF82 and *Enterobacteriaceae* abundances in ex-ASF LF82-WT and LF82- $\Delta qseC$ mice at baseline revealed that additional *Enterobacteriaceae* species were acquired from the environment, as these mice had $14.5 \pm 1.8\%$ and $3.3 \pm 1.4\%$ LF82, respectively (**Figure 4.5c**). Colony PCR with primers for the 16S rRNA gene and subsequent alignment of Sanger sequences confirmed presence of *Enterobacter*, *Klebsiella*, *Proteus*, and other *Escherichia* species. However, despite acquiring a more complex community of *Enterobacteriaceae*, ex-ASF-LF82-WT mice had >4-fold more LF82 than ex-ASF-LF82- $\Delta qseC$ mice at the start of the intervention (**Figure 4.5b-c**), mirroring what was observed by 16S rRNA gene surveys (**Figure 4.4b**). Thus, QseC may confer a fitness advantage for LF82 when competing for the same niche as other *Enterobacteriaceae*.

Further analysis of LF82 abundance throughout the DSS-intervention revealed that LF82-WT expanded and represented a greater proportion of the total *Enterobacteriaceae* population compared to the LF82- $\Delta qseC$ mutant, with levels on day 5 reaching $27.4 \pm 6.2\%$ and $7.3 \pm 1.2\%$, respectively (**Figure 4.5c**). These results show that, in the context of inflammation, QseC may play a critical role in mediating the persistence, expansion, and virulence of LF82.

Inactivating *qseC* affects LF82 growth kinetics

As a master regulator of virulence, QseC has been demonstrated to affect many aspects of bacterial metabolism. Previous gene expression analysis comparing WT versus $\Delta qseC$ strains of uropathogenic *E. coli* (UPEC) using an *E. coli*-specific microarray revealed that deletion of *qseC* results in misregulation of nucleotide, amino acids, and carbon metabolism¹⁷. Observing that LF82 was better at persisting in a low complexity microbiota (**Figure 4.4**) and an inflamed gut (**Figure 4.5**), we wanted to assess basic growth dynamics of LF82 *in vitro* to confirm whether loss of *qseC* attenuates virulence, in part, through disrupting metabolism. To determine whether absence of *qseC* affects the growth kinetics of LF82, we grew WT and mutant LF82 strains in LB broth

overnight under aerobic and anaerobic conditions. The growth rate for LF82- $\Delta qseC$ was not significantly different from the LF82-WT or LF82- $\Delta qseC::qseC$ under aerobic conditions; however, LF82- $\Delta qseC$ growth was abrogated under anaerobic conditions (Figure 4.6a-b). Thus, absence of *qseC* appears to alter the metabolism and growth potential of LF82 under anaerobic conditions, which may further influence its ability to colonize and persist *in vivo*.

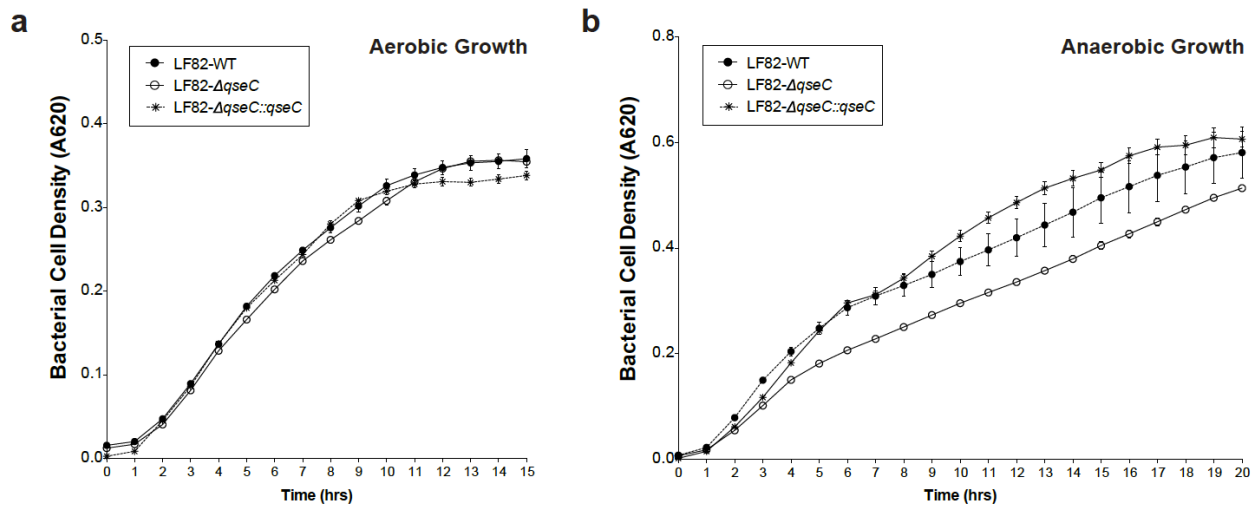


Figure 4.6. Comparing LF82 growth curves under aerobic and anaerobic conditions. Cultures were grown in LB broth for 4 hrs at 37°C with agitation, back diluted to an OD₆₀₀ of 0.01, and transferred to a 96-well plate for overnight growth at 37°C in an automated plate reader. Absorbance at 620 nm was recorded every 30 min (hourly time points plotted). Symbols represent data from two independent experiments with 6 replicates each. (a) Aerobic growth for 15 hrs. (b) Anaerobic growth for 20 hrs.

DISCUSSION

E. coli species have been implicated in the pathogenesis of IBD given their abnormal abundance in mucosal lesions of Crohn's disease patients and their pathogenic properties *in vitro* and *in vivo*⁴⁰. The prototype AIEC strain LF82 is capable of adhering to and invading host cells through the induction of virulence genes for flagellar proteins and type-1 pili proteins¹¹. As a master regulator of virulence, QseC plays a crucial role in promoting the virulence of EHEC, EPEC, and other pathogenic *E. coli* strains⁴¹, but little is known about its regulatory function in

AIEC. The goal of this study was to genetically manipulate QseC and assess whether it regulates LF82 virulence *in vitro* and *in vivo*.

We constructed isogenic deletion (LF82- Δ qseC) and complementation (LF82- Δ qseC::*qseC*) mutants using the λ -Red recombination system^{42,43}. *In vitro* assays aimed at phenotypically and functionally characterizing WT and mutant LF82 strains showed that LF82- Δ qseC had downregulated expression of virulence genes for flagellar assembly and motility by RT-qPCR (**Figure 4.1**), absence of flagellar surface proteins by TEM (**Figure 4.2**), and reduced swimming motility by agar-based methods (**Figure 4.3**). We also demonstrated that defects in flagellar expression and function could be rescued with *qseC* complementation (**Figure 4.1-4.3**). These experiments confirmed that QseC mediates LF82 virulence by activating flagellar protein production, organization, and motility.

Host-microbiota communication is increasingly recognized as an important aspect of both symbiosis and pathogenesis. Integral to the microbiota's surveillance and collective decision-making process are two-component quorum sensing systems. In the case of QseC, presence of microbiota-generated hormone-like compounds (autoinducer-3) or host stress signals (NE or EPI) can initiate a virulence program with detrimental consequences for the host^{18,44}. This prompted us to examine whether NE induces QseC-mediated LF82 virulence *in vitro*. We found that LF82-WT, and not LF82- Δ qseC, exhibited a dose-dependent increase in swimming motility (**Figure 4.3b**) and enhanced expression of genes for NE-related TCSs and flagellar proteins (**Supplementary Figure 4.3**), indicating that QseC functions as an adrenergic receptor in LF82 and mediates NE-induced virulence. In addition, we observed that QseEF, an alternative NE-sensing TCS, was also regulated by QseC activation, as *qseE* expression was reduced in LF82- Δ qseC and levels did not change in the presence of NE (**Figure 4.1** and **Supplementary Figure 4.3**). These findings align

with other reports of QseC being upstream of QseEF²⁴ and establish that NE-induced virulence in LF82 is primarily regulated by QseC.

Shifting focus to LF82's virulence within a host, we established an *in vivo* system for monitoring the effects of *qseC* on LF82 colonization and persistence using ex-germ-free-ASF mice. Absence of Proteobacteria in the ASF microbiota enabled colonization of LF82. Furthermore, 16S rRNA gene surveys and CFU comparisons between mucosal and luminal samples revealed that LF82 and total *Enterobacteriaceae* were more enriched in LF82-WT compared to LF82- $\Delta qseC$ in ex-ASF mice (**Figure 4.4b, Supplementary Figure 4.5**). These results suggest that LF82-WT may have a fitness advantage compared to LF82- $\Delta qseC$ allowing it to colonize and persist at higher levels throughout the intestinal tract.

From the 16S rRNA gene sequencing analysis, additional insights were gleaned that are relevant to the underlying microbial dysbiosis associated with IBD. We observed that microbiotas of LF82-WT mice had less within-sample diversity and were more analogous to the ASF input community compared to microbiotas of LF82- $\Delta qseC$ mice (**Figure 4.4c**). Because LF82 is unable to stably colonize conventional mice under SPF conditions³¹, these data show that LF82 can successfully colonize a host harboring a low complexity microbiota and may even promote the maintenance of a less diverse state in order to ensure its survival. IBD, especially Crohn's disease, is consistently characterized by reduced microbial diversity and expansions in opportunistic bacteria, such as *Enterobacteriaceae*¹. Whether the loss in diversity associated with dysbiosis is a cause or consequence of chronic intestinal inflammation remains elusive. But perhaps certain bacteria, like AIEC, are involved throughout the disease continuum contributing both to the initiation and progression of disease by promoting and sustaining dysbiosis and altered host-microbiota interactions. Evidence that LF82 can preserve a specific microbiota phenotype was observed, as breeding pairs of LF82-inoculated ex-ASF mice had similar microbial community

structures, both in terms of composition and diversity, as their litters (**Figure 4.4**), demonstrating that features of an LF82-associated microbiota may be transmissible. Given the genetic foundation of most complex immune-mediated disorders, such as IBD, increased risk of disease between family members may be augmented by the transmissibility of the microbiome.

We next investigated whether QseC-mediated virulence influences LF82's ability to potentiate intestinal inflammation in the context of DSS-induced colonic injury. To determine if differences in disease severity between ex-ASF LF82-WT and LF82- $\Delta qseC$ mice were related to microbiota complexity and diversity, we included additional non-infected controls from different facilities. We observed that experimental colitis was more severe in BIH than JAX mice (**Figure 4.5a**), which harbor high and low complexity microbiotas, respectively. Monitoring abundance of *Enterobacteriaceae* in these mice revealed that BIH and JAX mice had dramatically different levels of *Enterobacteriaceae* throughout the DSS intervention, with levels being significantly higher in BIH mice (**Figure 4.5b**). In the presence of inflammatory stimuli, *Enterobacteriaceae* burden may be linked to worse disease outcomes regardless of microbiota complexity. Significantly higher histologic colitis scores were also found in ex-ASF-LF82-WT mice compared to JAX and ex-ASF-LF82- $\Delta qseC$ mice (**Figure 4.5a**). This indicates that LF82's inflammatory potential and ability to exacerbate colitis may be regulated by QseC. One way of more definitively correlating LF82 virulence with enhanced inflammation could be by quantifying TLR5 in colons of ex-ASF LF82-WT and LF82- $\Delta qseC$ mice to demonstrate that QseC-induced flagellar protein expression in fact drives enhanced innate immune response pathways via signaling through its cognate pattern-recognition receptor. Furthermore, experiments in *TLR5*^{-/-} mice exposed to LF82-WT and LF82- $\Delta qseC$ could also validate whether LF82 flagellar-mediated virulence is QseC-dependent, as has been shown for *fliC* mutants in this model⁴⁵.

A caveat to our *in vivo* studies is the use of an ASF model community. Although many metabolic and immune defects are restored in gnotobiotic-ASF animals, they still display a phenotype closer to germ-free animals than to colonized animals in some models⁴⁶. Despite sharing morphological and functional features of conventional mice, ASF and other simplified microbial consortia may not possess the full metabolic potential of a complex microbiome. Studies have demonstrated that gnotobiotic-ASF mice are deficient in microbial enzymes required for the inactivation of pancreatic proteases⁴⁷, suggesting that these mice could potentially lack other important microbial functions for the host. Thus, the sustained colonization observed in our experiments with ex-ASF mice may be a byproduct of residual physiological abnormalities present in these mice. This is especially relevant in the context of IBD where many genetic susceptibility loci identified in patients versus healthy controls are in genes influencing host innate immune responses to microbes, including proteins for bacterial recognition, intracellular handling of pathogens, and immune regulation^{48,49}. As a result, any insufficiencies in immunological development or function in ASF-associated mice could result in a partial or oversimplified view of LF82-host interactions. Intriguingly, newer progeny of ex-ASF mice maintained in SPF conditions have reduced or unculturable levels of either LF82-WT or LF82- Δ *qseC* (data not shown). This could be a consequence of other *Enterobacteriaceae* outcompeting LF82, restoration of immune defects in earlier generations of ex-ASF mice from breeding under SPF conditions, or possibly from genetic or epigenetic modifications to LF82. Evidence for the importance of a host-specific microbiota to gut immune maturation has been established⁵⁰. Absence of the human CEACAM6 receptor in mice and the presence of a different anatomical reservoir for LF82 in the cecum versus the ileum in humans, point to LF82 likely having different interactions with the host and other microbes. One way to address whether LF82 has modified its genome is to sequence ex-ASF mouse adapted strains and the parent strain.

Given that LF82 is far more adapted to colonize the intestines of humans rather than mice, transgenic mice expressing human CEACAM6 may be a useful model for studying LF82-host interactions. However, his model requires inducing microbial dysbiosis with antibiotics and subsequent colonic injury with DSS, which does not fully recapitulate the complex events involved in the pathogenesis of human IBD. Nonetheless, it still offers a system for exploring LF82 dynamics and is an important next step for assessing the virulence potential of WT versus mutant LF82 strains. As all *in vivo* experiments involved comparisons between LF82-WT and LF82- Δ qseC, further studies with LF82- Δ qseC::*qseC* are required to confirm the role of QseC in modulating the microbiota and mediating virulence in homeostasis and inflammation.

Finally, the mechanism for reduced virulence in *qseC* mutants, may in part, be due to constitutive expression of QseB (**Figure 4.1, Supplementary Figure 4.3**). Enhanced expression of QseB may cause metabolic perturbations leading to dysregulated virulence gene expression¹⁷. *In vitro* assays to measure the growth kinetics of WT and mutant LF82 strains revealed that LF82- Δ qseC had growth defects under anaerobic but not aerobic conditions (**Figure 4.6**), providing additional support for QseC as a regulator of metabolism. Studies of oxygen tension throughout the intestines show a decrease from the proximal small intestine to the distal colon⁵¹. This could potentially explain why there was a reservoir for LF82 in more aerobic locations like the cecum versus the distal colon and why LF82- Δ qseC was less adept at colonizing and persisting *in vivo*. Because QseC virulence and metabolism are tightly linked to microbial fitness it will be difficult to disentangle these functions; however, the coupling of these metabolic processes offers an advantage from a therapeutic perspective. If QseC can be inhibited, it would not only block virulence and potentially mitigate the potentiation of inflammation, but also reduce the metabolic fitness of LF82 (and other QseC-dependent bacteria) making them less able to survive. Whether the interference with specific aspects of microbial metabolism will result in drug

resistance is unknown, but to date, there are few reports of resistance developing from antivirulence approaches⁵².

In summary, our *in vitro* and *in vivo* results point to QseC being an important regulator of LF82 virulence and modulator of the microbiota and host-microbiota homeostasis. New insights into the virulence potential of LF82 have been gleaned and further investigation into perturbing its function is warranted, potentially through inhibition of QseC with antivirulence inhibitors, such as LED209.

MATERIALS AND METHODS

Bacterial strains, plasmids, and growth conditions

Ampicillin-erythromycin-resistant AIEC strain LF82 was a generous gift from the Darfeuille-Michaud Lab⁸. Luria-Bertani (LB) broth and LB agar (1.5% [wt/vol] Bacto agar) (both Difco) were used for strain maintenance and cloning. When appropriate the following antibiotics were used: 100 µg/ml ampicillin (Amp), 20 µg/ml chloramphenicol (Cm), 20 µg/ml erythromycin (Eryth), 100 µg/ml hygromycin B (Hyg), 50 µg/ml kanamycin (Kan), and 100 µg/ml spectinomycin (Spect). Bacterial growth was measured as optical density at 600 nm (OD₆₀₀) and all experiments were performed under aerobic conditions unless indicated otherwise. Plasmid DNA was isolated using the Qiagen Miniprep or Midiprep kits following the manufacturer's instructions. Strains and plasmids used in this study are listed in **Supplementary Table 4.1**. Primers are listed in **Supplementary Table 4.2**.

Construction of *E. coli* LF82 mutant strains

Generating LF82-ΔqseC deletion mutant. Isogenic mutants were generated with PCR products using the method originally described by Datsenko and Wanner⁴² with modifications for

pathogenic *E. coli*⁵³. Briefly, we replaced the *qseC* chromosomal sequence in LF82 with a selectable resistance gene generated by PCR. This resistance gene was flanked by short flippase recognition target (FRT) sites to facilitate flip recombinase (FLP)-mediated excision. For the *qseC* deletion mutant, this PCR product was generated using 80 base pair (bp) primers with homology to regions adjacent to *qseC* (based on the LF82 genome²²) and the pKD4 plasmid harboring the Kan resistance gene as template. PCR of the pKD4 plasmid was conducted with primers *qseC_80bp_up-F* and *qseC_80bp_dwn-R* and the 50 µl reaction mix contained: 1X AccuPrime Pfx reaction mix, 300 nM each of forward and reverse primers, 0.4 µl (1U) AccuPrime Pfx DNA polymerase (Invitrogen), and 50 ng of pKD4 template. PCR cycling consisted of: an initial denaturation step at 94°C for 2 min; followed by 30 cycles of denaturation at 94°C for 30 sec, annealing at 50°C for 30 sec, and extension at 68°C for 2 min; and a final extension at 68°C for 5 min. PCR fragments were gel purified with the QIAquick Gel Extraction Kit (Qiagen) and underwent two rounds of DpnI (NEB) restriction digests (0.2U/ µl in 1X CutSmart Buffer) at 37°C for 1 hr each and then a final heat inactivation at 80°C for 20 min. Fragments were purified with the QIAquick PCR Purification Kit (Qiagen) and desalted by drop dialysis (Millipore). In parallel, LF82 was transformed with the pTKred plasmid (see Generating electrocompetent LF82 strains), which encodes λ-Red enzymes synthesized under the control of an IPTG (isopropyl-β-D-1-thiogalacto-pyranoside)-inducible promoter. This plasmid was maintained at 30°C with 100 µg/ml Spect and λ-Red expression was induced with 1 mM IPTG (Invitrogen). After bacteria were transformed with the Wanner PCR product, isogenic Kan^R mutants were selected on LB agar containing 50 µg/ml Kan. Gene replacement by the Kan^R cassette in mutants was confirmed by colony PCR using ChoiceTaq DNA polymerase (Denville) according to manufacturer's instructions. LF82-Δ*qseC*::*kan* was transformed with the pCP20 plasmid harboring the FLP enzyme. This plasmid was maintained at 30°C with 10 µg/ml Cm. After bacteria were transformed

with pCP20, isogenic mutants were confirmed to be Cm^S-Kan^S by plating and colony PCR (see **Supplementary Figure 4.1** for ‘PCR confirmation of *qseC* deletion and replacement in LF82 mutant strains’).

Generating LF82- Δ *qseC*::*qseC* complementation mutant. For the *qseC* complementation mutant, the LF82 Δ *qseC*::*kan*/pTKred was transformed with a 5.1-kb PCR fragment from the plasmid pMGR3 generated by Gibson cloning. The pDONR221 plasmid (Invitrogen) with *Apal* and *EcoRV* (NEB) restriction endonuclease sites served as the vector backbone. The pTKIP plasmid harboring the Hyg resistance gene flanked by FRT sites served as the selectable resistance gene to screen for chromosomal integration. PCR products were generated using: 1) primers flanking regions adjacent to the *qseBC* operon and 2) primers for amplifying a 1-kb region downstream of *qseBC*. PCR products were generated with the Q5 High-Fidelity DNA polymerase (NEB) using the LF82 parent strain as template and primer sequences were generated by the Gibson Assembly software (see **Supplementary Figure 4.2** for ‘Gibson plasmid design for *qseC* complementation’). DNA fragments were prepared with 18 bp homology. Gibson assembly reaction contained 2-3 fold molar excess of insert fragments for 100 ng of vector backbone in a total volume of 25 μ l. The reaction was incubated in a thermocycler at 50°C for 60 min. The product was directly transformed into competent *E. coli* DH5 α derivative (NEB) and remaining aliquot was stored at -20°C. Hyg^R colonies were selected and isolated plasmids were screened for correct size and sequence. The pMGR3 plasmid underwent restriction digests with *Apal*-*EcoRV* to generate a 5.1 kb linear fragment. λ -Red expression was induced in LF82 Δ *qseC*::*kan*/pTKred with 1 mM IPTG and bacteria were transformed with the 5.1 kb fragment. Isogenic Hyg^R mutants were selected on low-salt LB agar (0.5% yeast, 1% tryptone, 0.5% NaCl, and 1.5% agar) containing 100 μ g/ml Hyg. LF82- Δ *qseC*::*kan* was transformed with the pCP20 plasmid harboring the FLP enzyme. After bacteria were transformed with pCP20, isogenic mutants were confirmed to be Cm^S-Hyg^S by

plating and colony PCR (see **Supplementary Figure 4.1** for ‘PCR confirmation of *qseC* deletion and replacement in LF82 mutant strains’).

Generating electrocompetent LF82 strains. Electrocompetent LF82 cells were generated using a previously published protocol⁵⁴. Briefly, a single fresh colony was placed into 5 ml of KOB-25 (2% tryptone, 0.5% yeast extract, and 25 g/L potassium acetate [KOAc], 0.05 mM magnesium chloride, 0.05 mM magnesium sulfate (all Sigma)) shaken overnight at 37°C. Overnight cultures were back-diluted 1:100 into 250 ml pre-warmed KOB-35 (same for KOB-25 but with 35 g/L KOAc) and shaken at 37°C until an OD₆₀₀ of 0.6. Cultures were chilled on ice for 1 hr with occasional stirring and then centrifuged at 1,000 *g* for 10 min at 4°C. Pellets were resuspended in 125 ml ice-cold 1.0 mM Hepes (Cellgro) and centrifuged at 3,500 *g* for 10 min at 4°C. Cells were washed with 120 ml ice-cold water and centrifuged at 3,500 *g* for 10 min at 4°C. Cells were washed a second time with 25 ml ice-cold 10% glycerol (Sigma) and centrifuged at 3,500 *g* for 10 min at 4°C. Supernatant were discarded and cells were resuspended in residual 10% glycerol. Cell suspensions were diluted to an OD₆₀₀ of 150-250 using 10% glycerol, aliquoted, and stored at -80°C.

Gene expression analysis

Bacterial RNA isolation. Cultures were grown in LB broth overnight at 37°C without agitation, back diluted to an OD₆₀₀ of 0.02, and grown for 6 hrs in LB broth (or acidified LB broth [pH 6] and LB broth supplemented with 5 µM NE [Sigma]) at 37°C without agitation. Cultures were treated with RNAprotect bacterial reagent (Qiagen) to stabilize and preserve RNA. Total RNA was extracted from bacterial pellets and underwent rigorous DNase treatments prior to cDNA synthesis and RT-qPCR. See extended protocol in **Supplementary Methods**.

RT-qPCR for virulence genes. cDNA was synthesized using the iScript cDNA Synthesis Kit (Bio-Rad) and RT-qPCR was performed using the KAPA SYBR FAST Universal qPCR kits (Kapa

Biosystems). All reactions were performed in duplicate. Genes were normalized to *rpoA*. Fold change was analyzed using the $2^{-\Delta\Delta C_t}$ method⁵⁵, $\Delta\Delta C_t = (C_{t,target\ gene} - C_{t,rpoA})_{experimental} - (C_{t,target} - C_{t,rpoA})_{reference}$. Error is calculated as the fractional standard deviation (SD), fractional SD = (standard deviation)/(mean value) for samples from each treatment group.

TEM analysis

Single colonies were selected from freshly streaked LB agar plates incubated at 37°C overnight and grown in 4 ml LB broth overnight at 37°C without agitation. Cells were applied to carbon-formvar gold grids and were washed with sterile PBS. Negative staining was performed with 1% uranyl formate (pH 4) for 30 sec. Grids were washed twice with sterile water, blotted, and visualized using a JOEL 1200 EX TEM. Representative micrographs were taken at a magnification of 12,000x.

Plate-based motility assays

0.3% LB agar plates were prepared and where indicated contained 50-500 μ M NE (Sigma) or equivalent amounts of acidified to normalize pH to 6. Single colonies were selected from freshly streaked LB agar plates incubated at 37°C overnight and grown in 4 ml LB broth overnight at 37°C without agitation. Overnight cultures were adjusted to an OD₆₀₀ of 1.0. Plates were inoculated with 3 μ l of culture and incubated at 37°C for 8 or 16 hrs. The diameters of the motility halos were measured and compared to assess differences in motility between strains.

Animal husbandry

SPF BALB/c WT mice were housed in the Harvard T.H. Chan School of Public Health barrier facility. BALB/c gnotobiotic mice harboring the ASF consortia were bred and maintained under

sterile conditions in gnotobiotic isolators at Children's Hospital Boston. ASF strains – *Clostridium* sp. (ASF356), *Lactobacillus* sp. (ASF360), *Lactobacillus murinus* (ASF361), *Mucispirillum schaedleri* (ASF457), *Eubacterium plexicaudatum* (ASF492), *Firmicutes* bacterium (ASF500), *Clostridium* sp. (ASF502), and *Parabacteroides* sp. (ASF519) – were obtained from Iowa State University⁵⁶. Both Ex-gnotobiotic-ASF mice and SPF BALB/c mice from Jackson Laboratories were maintained using prudent husbandry practices to minimize microbial transfer from other mouse lines in the colony. Animal experiments were approved and conducted in accordance with Harvard Medical School Standing Committee on Animals and National Institutes of Health guidelines.

Infection with LF82

Single colonies were selected from freshly streaked LB agar plates and grown in 4 ml LB broth overnight at 37°C without agitation. Cultures were harvested by centrifugation at 4,000 *g* for 10 min. The supernatants were discarded and the bacterial pellets were resuspended in LB broth (Cellgro) to 10⁹ CFUs/ml. 6-week old ex-gnotobiotic-ASF mice were orally challenged with 10⁸ CFUs on two consecutive days.

Enumerating LF82 and *Enterobacteriaceae* in stool and harvested tissues

At indicated time points stool, luminal content, or mucosal tissue were collected from individual mice and serially diluted 10-fold using sterile PBS onto MacConkey agar (Difco) without antibiotics for *Enterobacteriaceae* culturable counts and MacConkey agar with 100 µg/ml Amp and 20 µg/ml Eryth for LF82 culturable counts. Plates were grown at 37°C overnight and colonies were counted on plates with bacterial densities of 25-300 CFU. Log₁₀ CFU/g was calculated based on the initial sample wet weight.

16S rRNA gene surveys of gut-associated microbial communities

DNA isolation from cecum and stool. Stool (pre- and post-intervention) was collected and homogenized in RNAlater (Ambion), held at 4°C overnight, and stored at -80°C before processing. Nucleic acids were extracted using a phenol-chloroform bead-beating procedure followed by DNA/RNA separation and purification using the Qiagen AllPrep DNA/RNA mini kit (Qiagen). DNA was quantified using a NanoPhotometer Pearl (Denville). DNA was stored at -20°C. See **Supplementary Methods** for the extended protocol.

16S rRNA gene amplification and high-throughput sequencing. Extracted DNA underwent 16S rRNA gene amplification by PCR using primers that target the V4 hypervariable region and incorporate Illumina adapters and a sample barcode sequence. Primers sequences: 515-F (5'-GTGCCAGCMGCCGCGGTAA-3') and 806-R (5'-GGACTACHVGGGTWTCTAAT-3'). Each reaction mixture of 25 µl contained: 10 µl of diluted template (1:50), 10 µl of HotMasterMix with the HotMaster Taq DNA Polymerase (5 Prime), and 5 µl of primer mix (2 µM of each primer). Thermocycling conditions consisted of an initial denaturation step at 94°C for 3 min, followed by 30 cycles of denaturation at 94°C for 45 sec, annealing at 50 °C for 60 sec, extension at 72°C for 5 min, and a final extension at 72°C for 10 min. Amplicons were quantified using the Quant-iT DNA HS assay kit (Life Technologies), pooled in equimolar concentrations, and size selected to 375-425 bp on the Pippin Prep (Sage Sciences) to reduce non-specific amplification products from host DNA. Final library size and DNA were quantified using the Quant-iT assay. Paired-end sequencing for 150 bp reads was performed on the Illumina MiSeq platform (v2) according to the manufacturer's specifications with addition of 15% PhiX.

Sequence processing and analysis. Overlapping paired-end reads were stitched together (approximately 97 bp overlap) and processed with the pick_closed_reference_otus.py pipeline in QIIME (v1.6.0)³⁵. This pipeline takes raw reads as input and generates an operational taxonomic

unit (OTU) table as output. Taxonomy was assigned using the Greengenes predefined reference set (vGG_13_5). A mean sequence depth of 98,437 reads/sample was obtained. OTUs with less than 2 reads in less than 2 samples were excluded from downstream analysis. Further microbial community analysis for within- and between-sample diversity was performed with QIIME.

DSS Interventions

Mice underwent a 7-day intervention starting on postnatal day 35 ± 5 , with 3% (wt/vol) DSS (Affymetrix) added to the drinking water from experimental day 0 through 5. Body weight, body condition, and stool consistency were measured frequently throughout the intervention to monitor disease activity. Tissues were resected for histological analysis and for enumerating LF82 and *Enterobacteriaceae* levels.

Histology

Upon sacrifice, colons were resected, fixed in 4% paraformaldehyde (Sigma), and embedded in paraffin. Sections were H&E-stained and evaluated in a blinded fashion for epithelial hyperplasia (0–3), epithelial injury (0–3), polymorphonuclear infiltration (0–3), and mononuclear infiltration (0–3), these indices were summed to generate the histologic colitis score⁵⁷.

Plate-based growth assays

Single colonies were selected from freshly streaked LB agar plates incubated at 37°C overnight and grown in 3 ml LB broth for 4 hrs at 37°C with agitation. Optical density was measured and cultures were back diluted in to an OD₆₀₀ of 0.01 in either LB broth or pre-reduced LB broth for aerobic and anaerobic growth, respectively. Culture of each strain were transferred in replicates of six to a 96-well plate for overnight growth at 37°C in an automated plate reader – either located

on a bench top (aerobic measurements) or housed in an anaerobic isolator (anaerobic measurements)(Coy Laboratory Products). Absorbance at 620 nm was recorded every 30 min and included a 5 sec vortex step before each reading.

Statistical analysis

All statistical tests for significance were performed in Prism v6.0h for Mac OS X (GraphPad Software). All averages are mean \pm standard error of the mean (SEM) except for fold change calculations where averages are mean \pm fractional standard deviation (SD).

REFERENCES

1. Kamada, N., Chen, G. Y., Inohara, N. & Nuñez, G. Control of pathogens and pathobionts by the gut microbiota. *Nat. Immunol.* **14**, 685–690 (2013).
2. Clements, A., Young, J. C., Constantinou, N. & Frankel, G. Infection strategies of enteric pathogenic *Escherichia coli*. *Gut Microbes* **3**, 71–87 (2012).
3. Neut, C. *et al.* Changes in the bacterial flora of the neoterminal ileum after ileocolonic resection for Crohn's disease. *Am J Gastroenterol* **97**, 939–946 (2002).
4. Swidsinski, A. *et al.* Mucosal flora in inflammatory bowel disease. *Gastroenterology* **122**, 44–54 (2002).
5. Gjaffer, M. H., Holdsworth, C. D. & Duerden, B. I. Virulence properties of *Escherichia coli* strains isolated from patients with inflammatory bowel disease. *Gut* **33**, 646–650 (1992).
6. Darfeuille-Michaud, A. *et al.* High prevalence of adherent-invasive *Escherichia coli* associated with ileal mucosa in Crohn's disease. *Gastroenterology* **127**, 412–421 (2004).
7. Gevers, D. *et al.* The treatment-naïve microbiome in new-onset Crohn's disease. *Cell Host and Microbe* **15**, 382–392 (2014).
8. Darfeuille-Michaud, A. *et al.* Presence of adherent *Escherichia coli* strains in ileal mucosa of patients with Crohn's disease. *Gastroenterology* **115**, 1405–1413 (1998).
9. Boudeau, J., Glasser, A. L., Masseret, E., Joly, B. & Darfeuille-Michaud, A. Invasive ability of an *Escherichia coli* strain isolated from the ileal mucosa of a patient with Crohn's disease. *Infect. Immun.* **67**, 4499–4509 (1999).
10. Glasser, A. L. *et al.* Adherent invasive *Escherichia coli* strains from patients with Crohn's disease survive and replicate within macrophages without inducing host cell death. *Infect. Immun.* **69**, 5529–5537 (2001).
11. Barnich, N., Boudeau, J., Claret, L. & Darfeuille-Michaud, A. Regulatory and functional co-operation

- of flagella and type 1 pili in adhesive and invasive abilities of AIEC strain LF82 isolated from a patient with Crohn's disease. *Mol. Microbiol.* **48**, 781–794 (2003).
12. Carvalho, F. A. *et al.* Crohn's disease-associated Escherichia coli LF82 aggravates colitis in injured mouse colon via signaling by flagellin. *Inflamm. Bowel Dis.* **14**, 1051–1060 (2008).
 13. Barnich, N. *et al.* CEACAM6 acts as a receptor for adherent-invasive E. coli, supporting ileal mucosa colonization in Crohn disease. *J. Clin. Invest.* **117**, 1566–1574 (2007).
 14. Chan, C. H. F. & Stanners, C. P. Novel mouse model for carcinoembryonic antigen-based therapy. *Mol. Ther.* **9**, 775–785 (2004).
 15. Carvalho, F. A. *et al.* Crohn's disease adherent-invasive Escherichia coli colonize and induce strong gut inflammation in transgenic mice expressing human CEACAM. *J. Exp. Med.* **206**, 2179–2189 (2009).
 16. Sperandio, V., Torres, A. G. & Kaper, J. B. Quorum sensing Escherichia coli regulators B and C (QseBC): a novel two-component regulatory system involved in the regulation of flagella and motility by quorum sensing in E. coli. *Mol. Microbiol.* **43**, 809–821 (2002).
 17. Hadjifrangiskou, M. *et al.* A central metabolic circuit controlled by QseC in pathogenic Escherichia coli. *Mol. Microbiol.* **80**, 1516–1529 (2011).
 18. Sperandio, V., Torres, A. G., Jarvis, B., Nataro, J. P. & Kaper, J. B. Bacteria-host communication: the language of hormones. *Proceedings of the National Academy of Sciences* **100**, 8951–8956 (2003).
 19. Rasko, D. A. *et al.* Targeting QseC signaling and virulence for antibiotic development. *Science* **321**, 1078–1080 (2008).
 20. Curtis, M. M. *et al.* QseC inhibitors as an antivirulence approach for Gram-negative pathogens. *MBio* **5**, e02165 (2014).
 21. Yang, Q., Anh, N. D. Q., Bossier, P. & Defoirdt, T. Norepinephrine and dopamine increase motility, biofilm formation, and virulence of Vibrio harveyi. *Front Microbiol* **5**, 584 (2014).
 22. Miquel, S. *et al.* Complete genome sequence of Crohn's disease-associated adherent-invasive E. coli strain LF82. *PLoS ONE* **5**, e12714 (2010).
 23. Kostakioti, M., Hadjifrangiskou, M., Pinkner, J. S. & Hultgren, S. J. QseC-mediated dephosphorylation of QseB is required for expression of genes associated with virulence in uropathogenic Escherichia coli. *Mol. Microbiol.* **73**, 1020–1031 (2009).
 24. Reading, N. C. *et al.* A novel two-component signaling system that activates transcription of an enterohemorrhagic Escherichia coli effector involved in remodeling of host actin. *J. Bacteriol.* **189**, 2468–2476 (2007).
 25. Müller, D. *et al.* Comparative analysis of the locus of enterocyte effacement and its flanking regions. *Infect. Immun.* **77**, 3501–3513 (2009).
 26. Sperandio, V., Torres, A. G., Jarvis, B., Nataro, J. P. & Kaper, J. B. Bacteria-host communication: the language of hormones. *Proceedings of the National Academy of Sciences* **100**, 8951–8956 (2003).
 27. Asano, Y. *et al.* Critical role of gut microbiota in the production of biologically active, free catecholamines in the gut lumen of mice. *Am. J. Physiol. Gastrointest. Liver Physiol.* **303**, G1288–95 (2012).
 28. Minamino, T., Imae, Y., Oosawa, F., Kobayashi, Y. & Oosawa, K. Effect of intracellular pH on

- rotational speed of bacterial flagellar motors. *J. Bacteriol.* **185**, 1190–1194 (2003).
29. Chang, K.-C., Cheng, S.-J., Chen, Y.-C., Huang, H.-R. & Liou, J.-W. Nanoscopic analysis on pH induced morphological changes of flagella in *Escherichia coli*. *J Microbiol Immunol Infect* **46**, 405–412 (2013).
 30. Reisch, C. R. & Prather, K. L. J. The no-SCAR (Scarless Cas9 Assisted Recombineering) system for genome editing in *Escherichia coli*. *Sci Rep* **5**, 15096 (2015).
 31. Chassaing, B., Koren, O., Carvalho, F. A., Ley, R. E. & Gewirtz, A. T. AIEC pathobiont instigates chronic colitis in susceptible hosts by altering microbiota composition. *Gut* **63**, 1069–1080 (2014).
 32. Schaedler, R. W., DUBS, R. & Costello, R. Association of germfree mice with bacteria isolated from normal mice. *J. Exp. Med.* **122**, 77–82 (1965).
 33. Wymore Brand, M. *et al.* The Altered Schaedler Flora: Continued Applications of a Defined Murine Microbial Community. *ILAR J* **56**, 169–178 (2015).
 34. Kostic, A. D., Xavier, R. J. & Gevers, D. The microbiome in inflammatory bowel disease: current status and the future ahead. *Gastroenterology* **146**, 1489–1499 (2014).
 35. Caporaso, J. G. *et al.* QIIME allows analysis of high-throughput community sequencing data. *Nat. Methods* **7**, 335–336 (2010).
 36. Yasuda, K. *et al.* Biogeography of the intestinal mucosal and luminal microbiome in the rhesus macaque. *Cell Host and Microbe* **17**, 385–391 (2015).
 37. Ericsson, A. C. *et al.* Effects of vendor and genetic background on the composition of the fecal microbiota of inbred mice. *PLoS ONE* **10**, e0116704 (2015).
 38. Howitt, M. R. *et al.* Tuft cells, taste-chemosensory cells, orchestrate parasite type 2 immunity in the gut. *Science* **351**, 1329–1333 (2016).
 39. Mukhopadhyay, I., Hansen, R., El-Omar, E. M. & Hold, G. L. IBD-what role do Proteobacteria play? *Nat Rev Gastroenterol Hepatol* **9**, 219–230 (2012).
 40. Rolhion, N. & Darfeuille-Michaud, A. Adherent-invasive *Escherichia coli* in inflammatory bowel disease. *Inflamm. Bowel Dis.* **13**, 1277–1283 (2007).
 41. Cameron, E. A. & Sperandio, V. Frenemies: Signaling and Nutritional Integration in Pathogen-Microbiota-Host Interactions. *Cell Host and Microbe* **18**, 275–284 (2015).
 42. Datsenko, K. A. & Wanner, B. L. One-step inactivation of chromosomal genes in *Escherichia coli* K-12 using PCR products. *Proc. Natl. Acad. Sci. U.S.A.* **97**, 6640–6645 (2000).
 43. Kuhlman, T. E. & Cox, E. C. Site-specific chromosomal integration of large synthetic constructs. *Nucleic Acids Res.* **38**, e92–e92 (2010).
 44. Sandrini, S., Aldriwesh, M., Alruways, M. & Freestone, P. Microbial endocrinology: host-bacteria communication within the gut microbiome. *J. Endocrinol.* **225**, R21–34 (2015).
 45. Carvalho, F. A. *et al.* Transient inability to manage proteobacteria promotes chronic gut inflammation in TLR5-deficient mice. *Cell Host and Microbe* **12**, 139–152 (2012).
 46. Macpherson, A. J. & McCoy, K. D. Standardised animal models of host microbial mutualism. *Mucosal Immunol* **8**, 476–486 (2015).

47. Norin, E. & Midtvedt, T. Intestinal microflora functions in laboratory mice claimed to harbor a 'normal' intestinal microflora. Is the SPF concept running out of date? *Anaerobe* **16**, 311–313 (2010).
48. Khor, B., Gardet, A. & Xavier, R. J. Genetics and pathogenesis of inflammatory bowel disease. *Nature* **474**, 307–317 (2011).
49. Jostins, L. *et al.* Host-microbe interactions have shaped the genetic architecture of inflammatory bowel disease. *Nature* **491**, 119–124 (2012).
50. Chung, H. *et al.* Gut immune maturation depends on colonization with a host-specific microbiota. *Cell* **149**, 1578–1593 (2012).
51. Donaldson, G. P., Lee, S. M. & Mazmanian, S. K. Gut biogeography of the bacterial microbiota. *Nat. Rev. Microbiol.* **14**, 20–32 (2016).
52. Rasko, D. A. & Sperandio, V. Anti-virulence strategies to combat bacteria-mediated disease. *Nat Rev Drug Discov* **9**, 117–128 (2010).
53. Murphy, K. C. & Campellone, K. G. Lambda Red-mediated recombinogenic engineering of enterohemorrhagic and enteropathogenic *E. coli*. *BMC Mol. Biol.* **4**, 11 (2003).
54. Shi, X. *et al.* Enhancing *Escherichia coli* electrotransformation competency by invoking physiological adaptations to stress and modifying membrane integrity. *Anal. Biochem.* **320**, 152–155 (2003).
55. Livak, K. J. & Schmittgen, T. D. Analysis of relative gene expression data using real-time quantitative PCR and the $2^{-\Delta\Delta C(T)}$ Method. *Methods* **25**, 402–408 (2001).
56. Wannemuehler, M. J., Overstreet, A.-M., Ward, D. V. & Phillips, G. J. Draft genome sequences of the altered schaedler flora, a defined bacterial community from gnotobiotic mice. *Genome Announc* **2**, e00287–14–e00287–14 (2014).
57. Garrett, W. S. *et al.* Communicable ulcerative colitis induced by T-bet deficiency in the innate immune system. *Cell* **131**, 33–45 (2007).

CHAPTER 5

Conclusion

SUMMARY OF FINDINGS

Inflammatory bowel disease (IBD) is a relapsing-remitting and chronic inflammatory disorder influenced by genetic and environmental factors¹. Evidence from animal models and humans consistently implicate microbial dysbiosis and dysregulated host-microbiota interactions in the pathogenesis of IBD²⁻⁴. While advances in tools and technology have enabled an in-depth characterization of the gut microbiome and expanded our understanding of host-microbiota mutualism^{5,6}, it remains unclear whether dysbiosis is a cause or consequence of disease. Here, we explored the gut microbiome in mouse models of experimental colitis and evaluated the contribution of specific microbial clades and pathways in potentiating mucosal inflammation with the goal of identifying novel microbiome-targeted interventions for disease management.

First, we described a computational toolkit for interrogating the gut microbiome using 16S ribosomal RNA (rRNA) gene surveys and whole metagenome shotgun sequencing. Using this computational workflow, we characterized the effects of diverse treatment modalities on host disease status and the gut microbiome in the *T-bet*^{-/-}*RAG2*^{-/-} mouse model of experimental colitis. This analysis revealed that gut microbiomes with persistent colitis had enrichments in *Enterobacteriaceae* and an increased capacity for bacterial pathogenesis, including pathways involved in benzoate metabolism, two-component systems (TCSs), and cell motility. Intriguingly, these pathways are part of a shared bacterial signaling axis found in many Gram-negative pathogens, including *Enterobacteriaceae*. Specifically, the bacterial quorum sensor QseC is part of the QseBC TCS that senses microbiota-generated metabolites (autoinducer-3) and host-derived stress molecules (norepinephrine and epinephrine) and responds by activating a signaling cascade that directly induces expression of virulence genes, including flagellar proteins^{7,8}.

Based on evidence of a QseC inhibitor (LED209) blocking the virulence and persistence of Gram-negative *Enterobacteriaceae* pathogens *in vivo* and in animal infections models^{9,10}, we next

investigated whether LED209 could reduce disease severity in three genetically distinct models of experimental colitis. We observed an attenuation of disease in both TRUC and dextran sodium sulfate (DSS)-exposed mice, and a modest benefit in *Il-10*^{-/-} mice. Intriguingly, LED209's ability to ameliorate disease in *Il-10*^{-/-} and DSS-exposed mice appeared to be dependent on blocking the expansion of *Enterobacteriaceae*, as mice with active colitis, on average, had higher *Enterobacteriaceae* abundances compared to mice in remission. In contrast, the disease status of TRUC mice was not *Enterobacteriaceae*-dependent, as 90% of mice in remission had increases in *Enterobacteriaceae* following LED209 treatment. Experiments in mouse models of experimental colitis suggest an underlying role for QseC virulence in disease pathogenesis. However, more research is needed to understand what features, host or microbiota, are driving differences between LED209 responders and non-responders. One approach for analyzing difference between the microbial communities of these mice is sequencing banked microbial DNA and RNA and identifying whether compositional or functional differences exist.

After observing an attenuation of colitis with biochemical inhibition of QseC, we wanted to confirm the relevance of this approach by genetically inactivating *qseC* in a clinically-relevant pathogen. Adherent-invasive *Escherichia coli* (AIEC) strain LF82 was isolated from a mucosal lesion of a CD patient¹¹ and its virulence is dependent on flagellar and type-1 pili proteins¹²⁻¹⁴, which are downstream of QseC. Given the essential function of flagellar proteins in LF82 virulence and a role for flagella proteins in exacerbating experimental colitis, we hypothesized that targeting QseC may reduce LF82's virulence potential. We generated *qseC* deletion (LF82- $\Delta qseC$) and complementation (LF82- $\Delta qseC::qseC$) mutants and examined phenotypic and functional differences between wild-type and mutant LF82 strains. We observed that LF82- $\Delta qseC$ had downregulated expression of virulence genes for flagellar proteins and defects in flagellar assembly and motility, which were rescued with complementation. Moreover, LF82- $\Delta qseC$ was

not responsive to norepinephrine-induced virulence. Modeling LF82 dynamics using a simplified microbial community *in vivo* revealed that QseC was required for LF82 persistence, which may also be dependent on its ability to maintain a state of low microbial diversity (a characteristic feature shared among IBD microbiomes¹⁵). In the context of DSS-induced colonic injury, the parent LF82 strain was able to expand to a greater extent and exacerbate disease compared to LF82- $\Delta qseC$. These results indicate that QseC is an important regulator of virulence in LF82 and that absence of this sensor leads to reduced fitness. While LF82 is unable to colonize the gut of a healthy host¹⁶, we demonstrate that it can colonize a host with a low complexity microbiota. Intestinal epithelial cells in the ileum of humans express a receptor for LF82, CEACAM6¹⁷. Transgenic mice expressing human CEACAM6 have been useful tools for understanding mechanisms of LF82-host interactions¹⁸. Testing the virulence of LF82 versus LF82- $\Delta qseC$ in this model will be an important next step as well as measuring the effects of LED209 in mice harboring an LF82-associated microbiota.

Collectively, through a large metagenomic study of the gut microbiome in experimental colitis we discovered that host stress molecules may be associated with increased *Enterobacteriaceae* growth and virulence in experimental colitis. We demonstrated that perturbing the *Enterobacteriaceae* adrenergic receptors, QseC, with a biochemical inhibitor can attenuate experimental colitis and genetically inactivating *qseC* in a pathogenic, IBD-associated *E. coli* strain can reduce its virulence *in vitro* and abrogate its ability to persist in a low complexity microbiota *in vivo*. These results provide insights into the use of an antivirulence approach for targeting not only pathogens rather a much larger collection of colitogenic bacteria.

NEW PERSPECTIVES

Host-microbiota mutualism at the intestinal mucosal interface requires tight regulation of inflammatory and regulatory immune responses^{19,20}. Accumulating evidence indicates that, in concert with the microbiota, the gut regulates communication between the epithelium and the immune and nervous systems to coordinate digestive, endocrine, and immune functions essential for maintaining intestinal homeostasis and proper signaling through the gut-brain-axis²¹. This bidirectional crosstalk between the nervous system and the mucosal immune system allows modulation of immune responses via the detection of circulating cytokines and direct input from sensory fibers and enteric neurons. Dysregulated host-microbe interactions and imbalances in sympathetic and parasympathetic tone are increasingly being associated with both gastrointestinal disorders, including IBD and irritable bowel syndrome (IBS), and central nervous system disorders, such as Parkinson's disease and autism spectrum disorder^{21,22}. Furthermore, IBD and IBS are common co-morbidities in stress-related disorders, including depression and anxiety²³. These observations suggest that inflammatory stimuli, including microbes and microbial antigens, may activate the enteric nervous system and induce the release of immunomodulatory mediators, such as catecholamines. In turn, catecholamines may modulate mucosal immune responses and influence the growth and virulence potential of opportunistic bacteria in the gut, and may potentially even reprogram gut-brain-axis signaling.

Efforts outlined in this thesis have attempted to define gut microbiome dysbiosis and dysfunction in IBD and understand the contribution of specific microbes and microbial functions in potentiating the pathogenesis of IBD. This discovery-driven approach prompted exploration of a strategy for modulating a catecholamine-mediated quorum-sensing pathway exploited by colitis-associated bacteria with the goal of re-establishing intestinal immune homeostasis. Further

research is needed to examine host-microbe interactions and the role of catecholamines in the gut and how to modulate the microbiome to prevent and treat disease.

REFERENCES

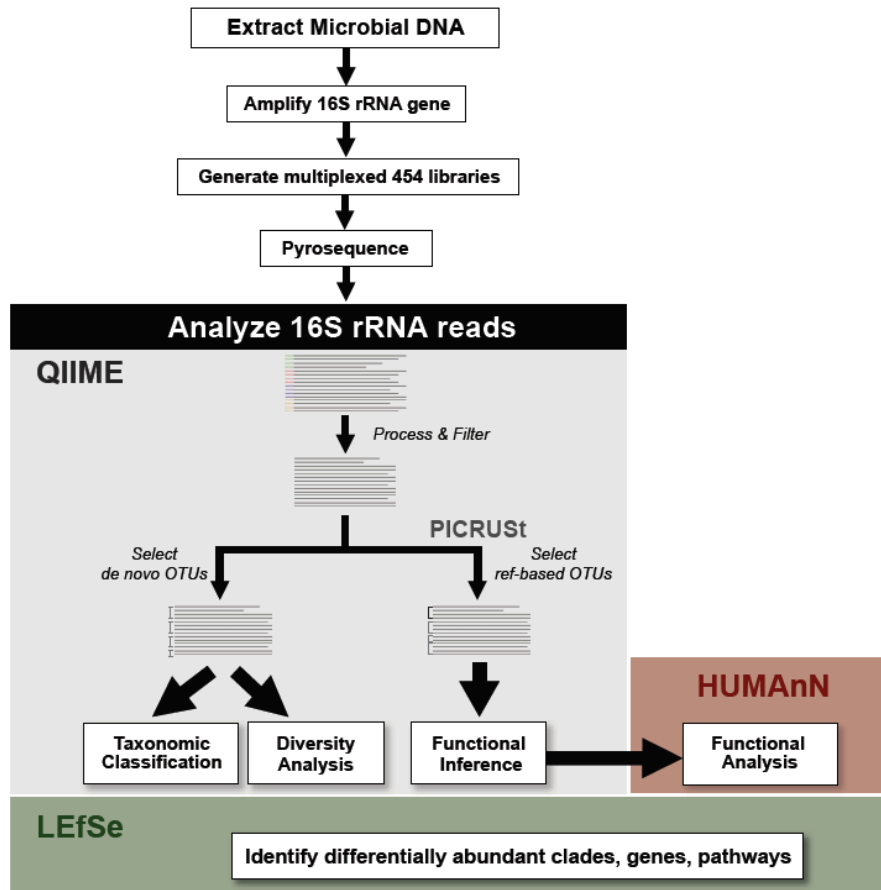
1. Ananthakrishnan, A. N. Epidemiology and risk factors for IBD. *Nat Rev Gastroenterol Hepatol* **12**, 205–217 (2015).
2. Frank, D. N. *et al.* Disease phenotype and genotype are associated with shifts in intestinal-associated microbiota in inflammatory bowel diseases. *Inflamm. Bowel Dis.* **17**, 179–184 (2011).
3. Morgan, X. C. *et al.* Dysfunction of the intestinal microbiome in inflammatory bowel disease and treatment. *Genome Biol.* **13**, R79 (2012).
4. Gevers, D. *et al.* The treatment-naïve microbiome in new-onset Crohn's disease. *Cell Host and Microbe* **15**, 382–392 (2014).
5. Qin, J. *et al.* A human gut microbial gene catalogue established by metagenomic sequencing. *Nature* **464**, 59–65 (2010).
6. Human Microbiome Project Consortium. Structure, function and diversity of the healthy human microbiome. *Nature* **486**, 207–214 (2012).
7. Sperandio, V., Torres, A. G. & Kaper, J. B. Quorum sensing Escherichia coli regulators B and C (QseBC): a novel two-component regulatory system involved in the regulation of flagella and motility by quorum sensing in E. coli. *Mol. Microbiol.* **43**, 809–821 (2002).
8. Clarke, M. B. & Sperandio, V. Transcriptional regulation of flhDC by QseBC and sigma (FliA) in enterohaemorrhagic Escherichia coli. *Mol. Microbiol.* **57**, 1734–1749 (2005).
9. Rasko, D. A. *et al.* Targeting QseC signaling and virulence for antibiotic development. *Science* **321**, 1078–1080 (2008).
10. Curtis, M. M. *et al.* QseC inhibitors as an antivirulence approach for Gram-negative pathogens. *MBio* **5**, e02165 (2014).
11. Darfeuille-Michaud, A. *et al.* Presence of adherent Escherichia coli strains in ileal mucosa of patients with Crohn's disease. *Gastroenterology* **115**, 1405–1413 (1998).
12. Boudeau, J., Barnich, N. & Darfeuille-Michaud, A. Type 1 pili-mediated adherence of Escherichia coli strain LF82 isolated from Crohn's disease is involved in bacterial invasion of intestinal epithelial cells. *Mol. Microbiol.* **39**, 1272–1284 (2001).
13. Barnich, N., Boudeau, J., Claret, L. & Darfeuille-Michaud, A. Regulatory and functional co-operation of flagella and type 1 pili in adhesive and invasive abilities of AIEC strain LF82 isolated from a patient with Crohn's disease. *Mol. Microbiol.* **48**, 781–794 (2003).
14. Carvalho, F. A. *et al.* Crohn's disease-associated Escherichia coli LF82 aggravates colitis in injured mouse colon via signaling by flagellin. *Inflamm. Bowel Dis.* **14**, 1051–1060 (2008).
15. Kostic, A. D., Xavier, R. J. & Gevers, D. The microbiome in inflammatory bowel disease: current status

and the future ahead. *Gastroenterology* **146**, 1489–1499 (2014).

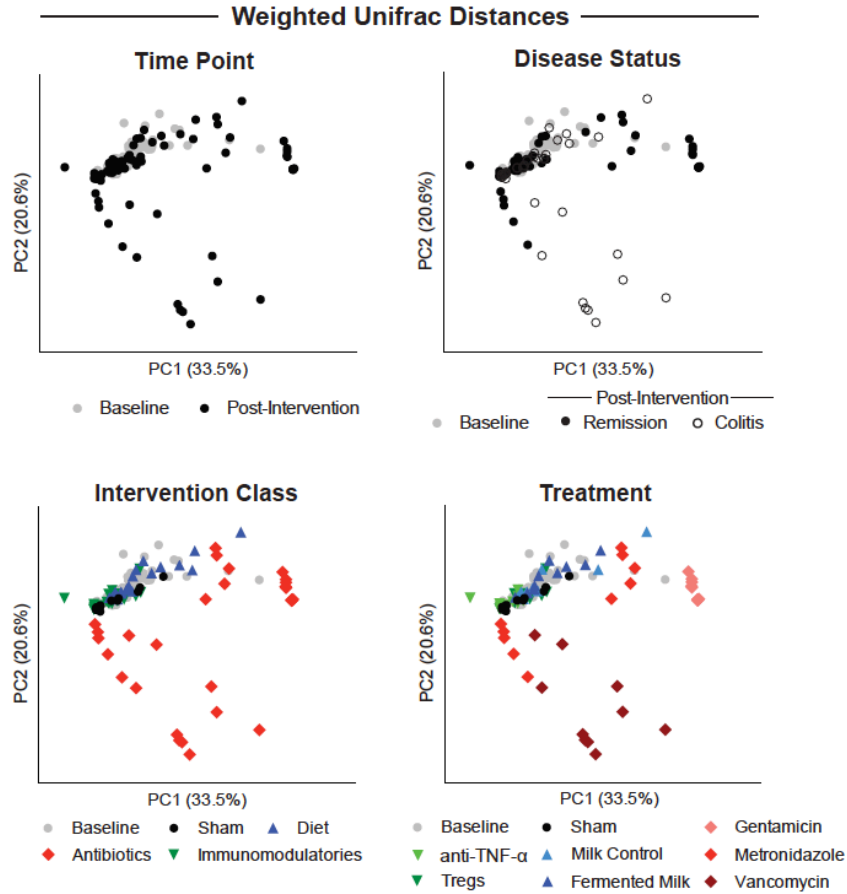
16. Chassaing, B., Koren, O., Carvalho, F. A., Ley, R. E. & Gewirtz, A. T. AIEC pathobiont instigates chronic colitis in susceptible hosts by altering microbiota composition. *Gut* **63**, 1069–1080 (2014).
17. Barnich, N. *et al.* CEACAM6 acts as a receptor for adherent-invasive E. coli, supporting ileal mucosa colonization in Crohn disease. *J. Clin. Invest.* **117**, 1566–1574 (2007).
18. Carvalho, F. A. *et al.* Crohn's disease adherent-invasive Escherichia coli colonize and induce strong gut inflammation in transgenic mice expressing human CEACAM. *J. Exp. Med.* **206**, 2179–2189 (2009).
19. Bäckhed, F., Ley, R. E., Sonnenburg, J. L., Peterson, D. A. & Gordon, J. I. Host-bacterial mutualism in the human intestine. *Science* **307**, 1915–1920 (2005).
20. Littman, D. R. & Pamer, E. G. Role of the commensal microbiota in normal and pathogenic host immune responses. *Cell Host and Microbe* **10**, 311–323 (2011).
21. Mayer, E. A., Tillisch, K. & Gupta, A. Gut/brain axis and the microbiota. *J. Clin. Invest.* **125**, 926–938 (2015).
22. Di Giovangiulio, M. *et al.* The Neuromodulation of the Intestinal Immune System and Its Relevance in Inflammatory Bowel Disease. *Front Immunol* **6**, 590 (2015).
23. Graff, L. A., Walker, J. R. & Bernstein, C. N. Depression and anxiety in inflammatory bowel disease: a review of comorbidity and management. *Inflamm. Bowel Dis.* **15**, 1105–1118 (2009).

APPENDIX A

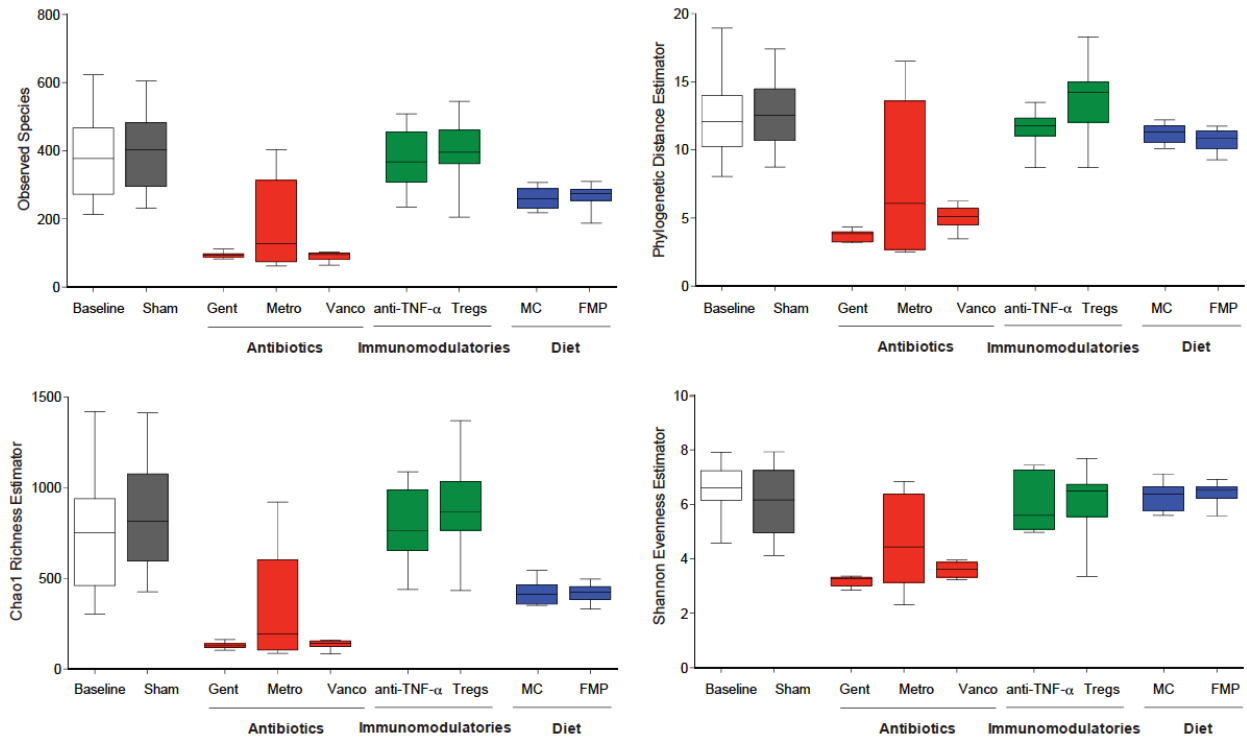
Supplementary Materials



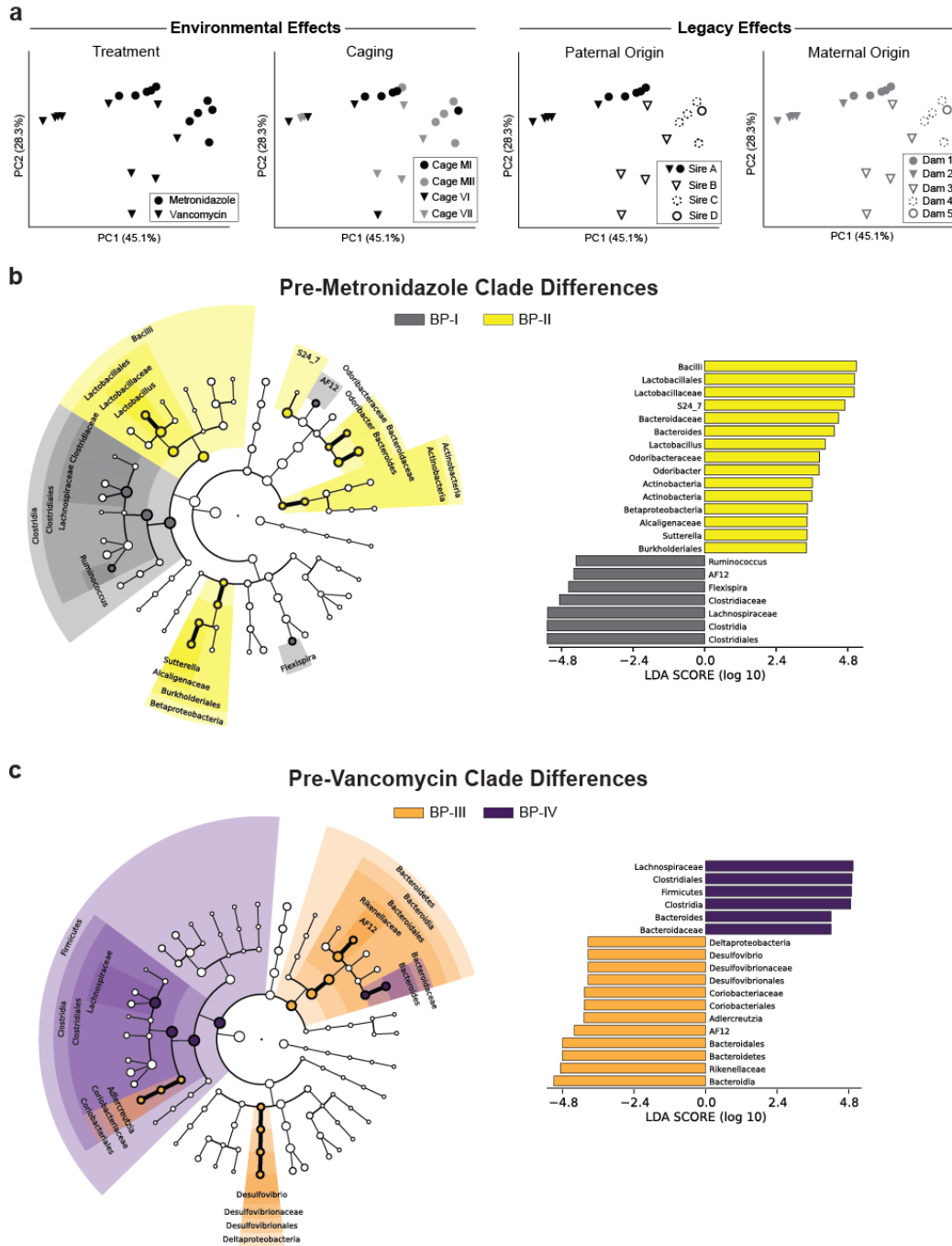
Supplementary Figure 2.1. 16S rRNA analysis pipeline for investigating the influence of perturbations on gut-associated microbial communities. Computational analysis pipeline used to characterize 16S rRNA gene sequences of gut-associated microbial communities. See *Materials and Methods* for computational tool details used in this study. QIIME, Quantitative Insights Into Microbial Ecology; PICRUSt, Phylogenetic Investigation of Communities by Reconstruction of Unobserved States; HUMANn, The HMP Unified Metabolic Analysis Network; LEfSe, Linear Discriminant Analysis with Effect Size.



Supplementary Figure 2.2. PCoA of weighted Unifrac distances of gut microbial communities. PCoA plots of the weighted UniFrac distances of gut microbial communities from stool collected at baseline (pre-intervention) and upon treatment completion (post-intervention). The first two PCs from the PCoA are plotted. Symbols represent data from individual mice, color-coded by the indicated metadata.



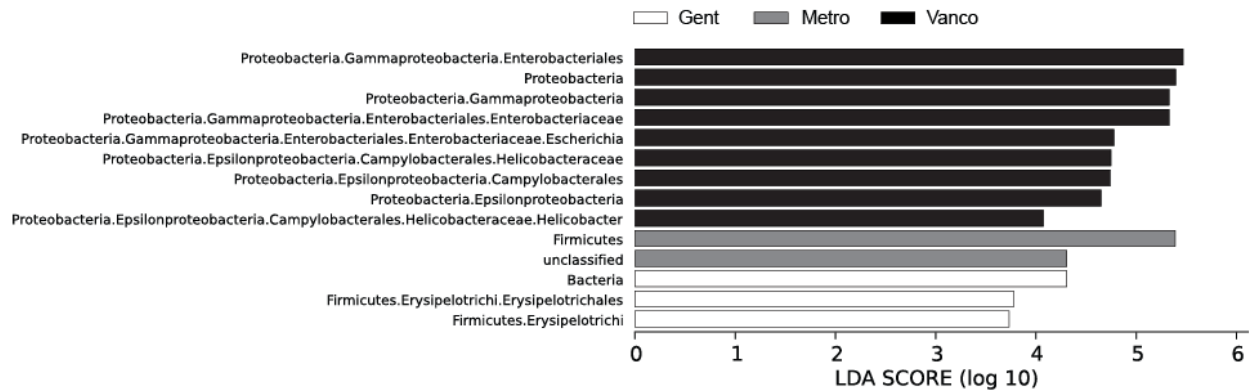
Supplementary Figure 2.3. 16S rRNA gene surveys of gut microbiome diversity following treatment exposure. Within-sample alpha diversity analysis of observed species based on Faith's phylogenetic diversity (PD), Chao1 (richness), and Shannon Index (evenness) measurements of stool samples collected at baseline ($n = 70$) and upon intervention completion ($n = 12$ for sham; $n = 10$ for all other treatment groups). Sham, untreated, handling control; Gent, gentamicin; Metro, metronidazole; Vanco, vancomycin; MC, non-fermented milk control; FMP, fermented milk product; Diet, dietary intervention with FMP or MC in addition to *ad libitum* chow. Each boxplot represents the mean \pm minimum/maximum for samples within each group.



Supplementary Figure 2.4. PCoA and LEfSe analyses to assess the influence of early-life exposures on antibiotic-driven microbial clade responses. (a) PCoA plots of the weighted UniFrac distances of gut microbial communities from stool collected upon completion of treatment with metronidazole ($n = 10$) or vancomycin ($n = 10$). The first two PCs from the PCoA are plotted. Symbols represent data from individual mice, color-coded by the indicated metadata. For caging, M, metronidazole-treated and V, vancomycin-treated. (b) Cladogram and corresponding histogram of the LDA scores for differentially abundant microbial clades in stool from progeny of the breeding pairs (BP) indicated in Figure 2.3c prior to metronidazole treatment. (c) Cladogram and corresponding histogram of the LDA scores for differentially abundant microbial clades in stool from progeny of the breeding pairs indicated in Figure 2.3c prior to vancomycin treatment. For cladograms, white circles delineate non-significant clades.

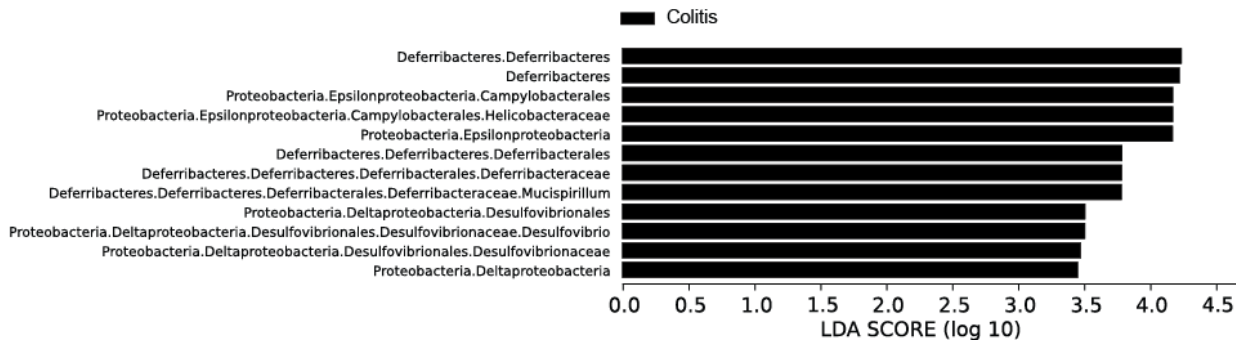
a

Differential Clade Responses with Antibiotic Treatment (Gent vs. Metro vs. Vanco)



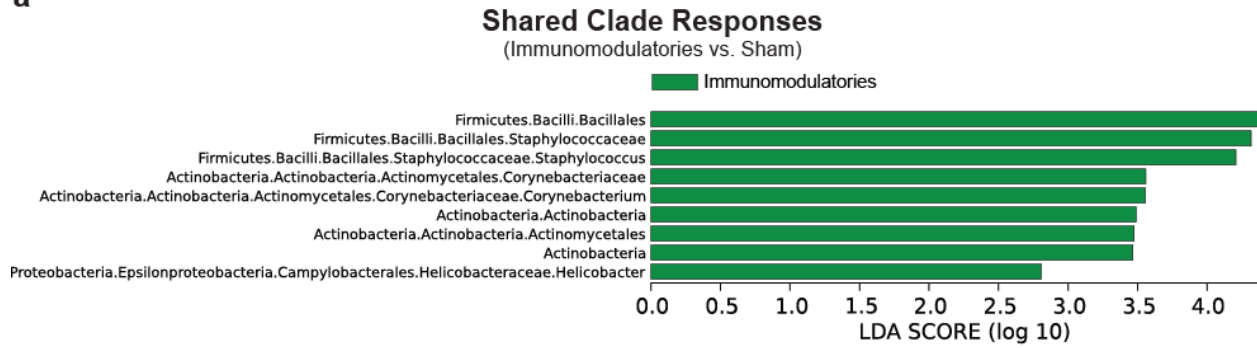
b

Clade Responses Associated with Active Colitis (Colitis [Vanco / Sham] vs. Remission [Gent / Metro])

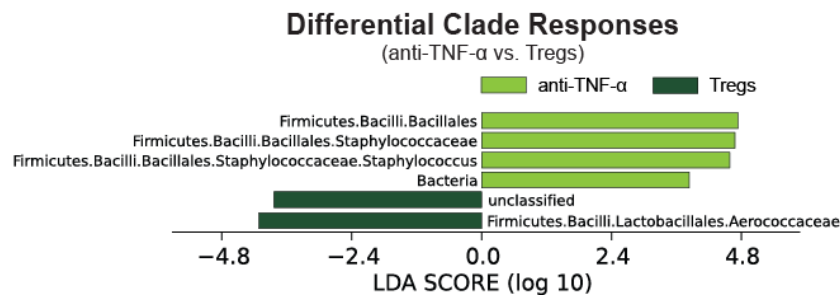


Supplementary Figure 2.5. LEfSe rank plots of differentially abundant microbial clades in gut microbiomes associated with active colitis versus remission following antibiotic treatment. (a) LDA scores for differentially abundant microbial clades in stool from mice treated with gentamicin (gent; $n = 10$), metronidazole (metro; $n = 10$) or vancomycin (vanco; $n = 10$) using an all-against-all multiclass comparison. (b) LDA scores for differentially abundant microbial clades in stool from mice in remission that received gentamicin or metronidazole ($n = 20$) and mice with active colitis that were untreated (sham) or received vancomycin ($n = 22$).

a

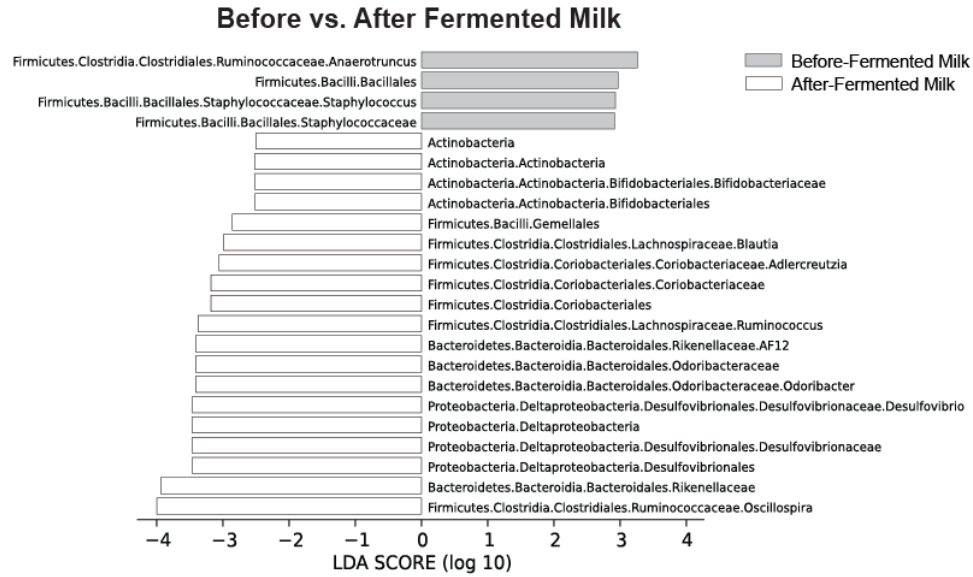


b

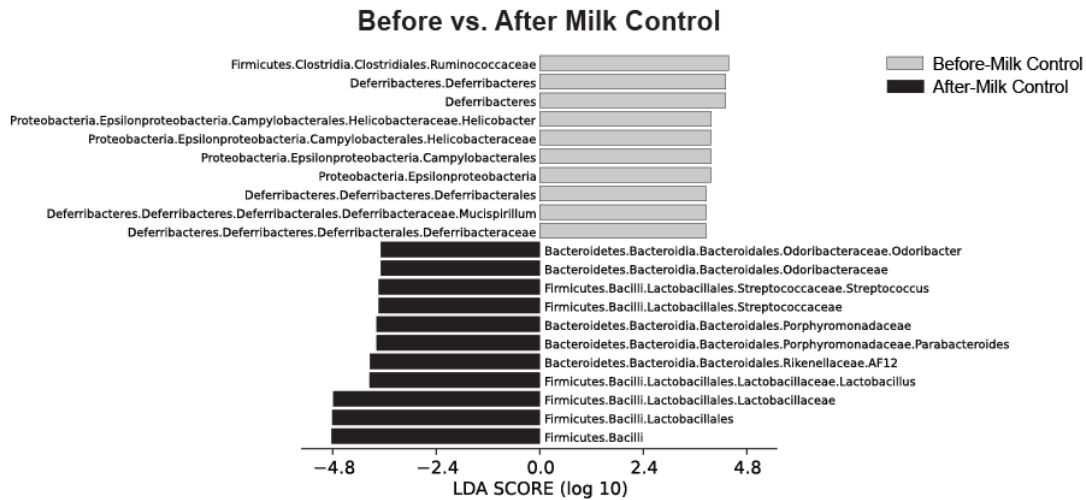


Supplementary Figure 2.6. LEfSe rank plots of differentially abundant microbial clades in gut microbiomes exposed to immunomodulatories. LDA scores for differentially abundant microbial clades in stool from: **(a)** immunomodulatory-treated (anti-TNF- α or T_{Reg}; $n = 20$) versus sham (untreated; $n = 12$) mice, and **(b)** anti-TNF- α ($n = 10$) versus T_{Reg} ($n = 10$) treated mice.

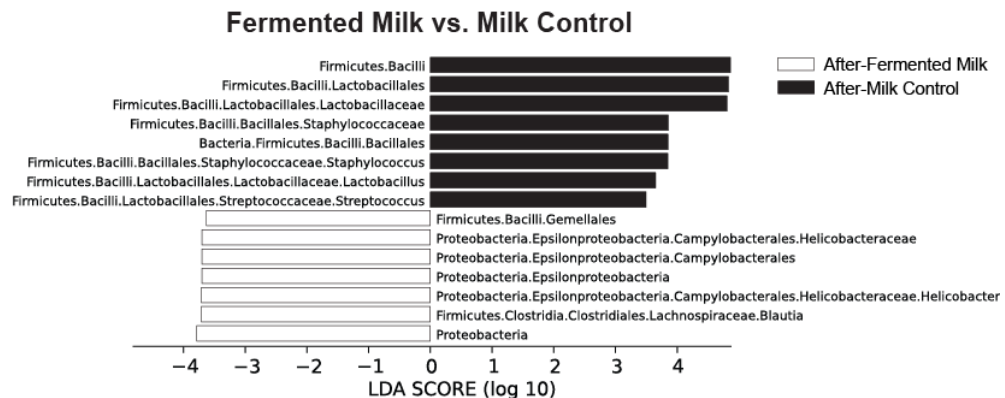
a



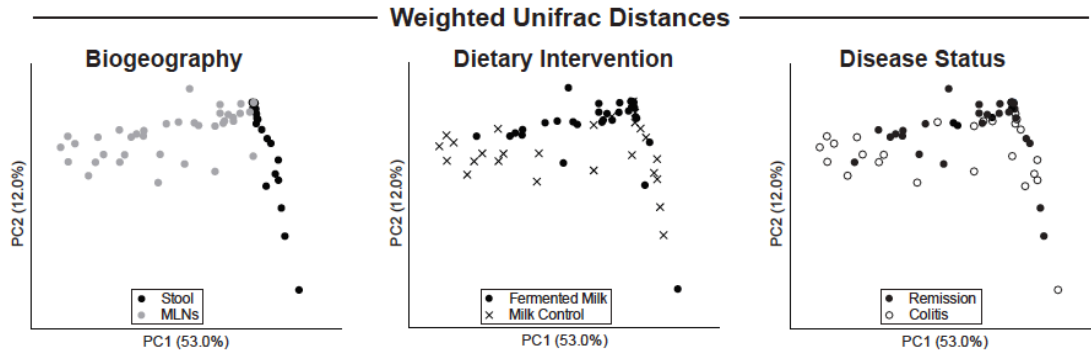
b



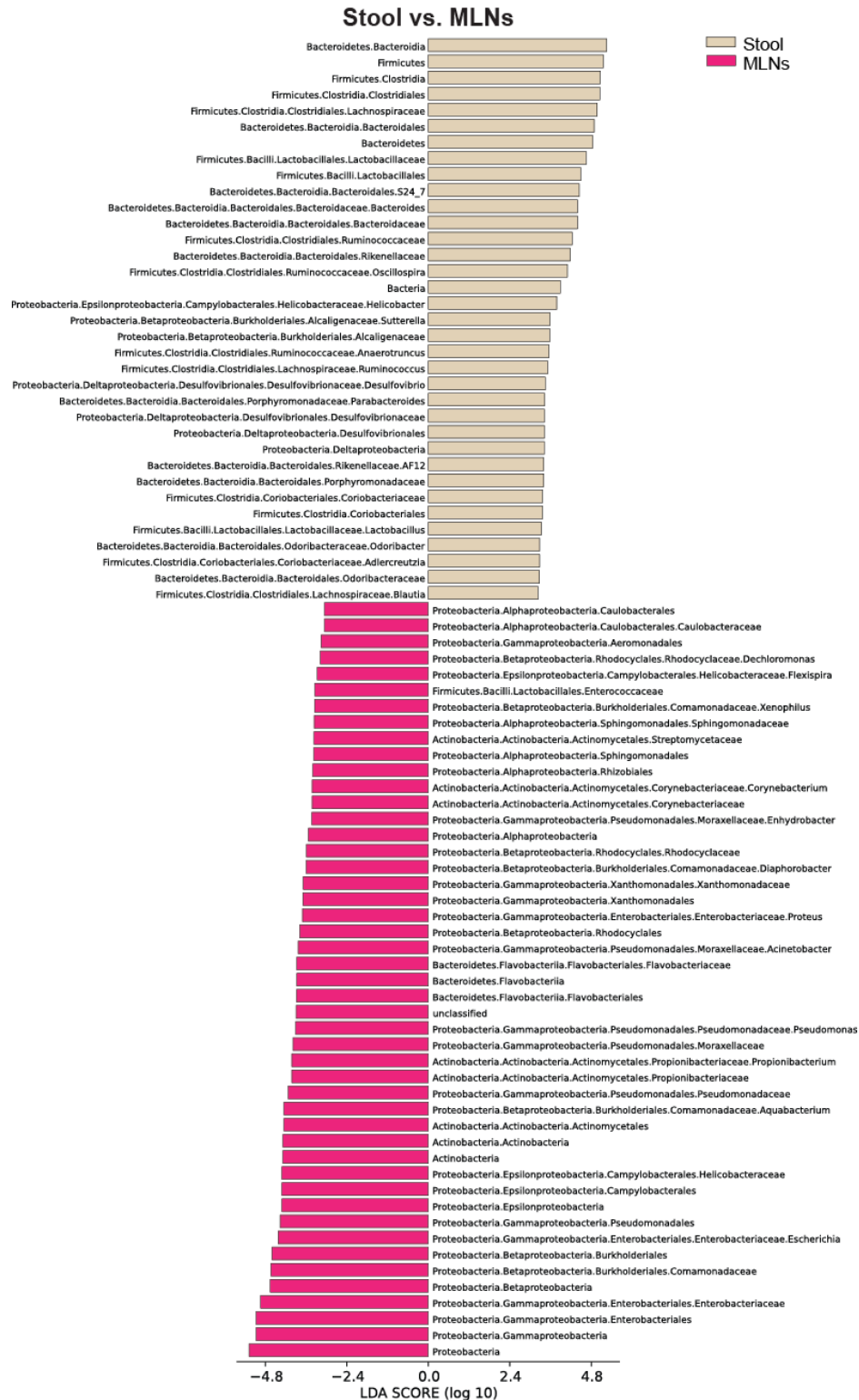
c



Supplementary Figure 2.7. LEfSe rank plots of differentially abundant microbial clades in gut microbiomes following a daily dietary intervention. LDA scores for differentially abundant microbial clades in stool from mice: (a) before and after administration of a FMP ($n = 10$); (b) before and after administration of a MC ($n = 10$); and (c) after administration of a FMP ($n = 10$) versus a MC ($n = 10$).

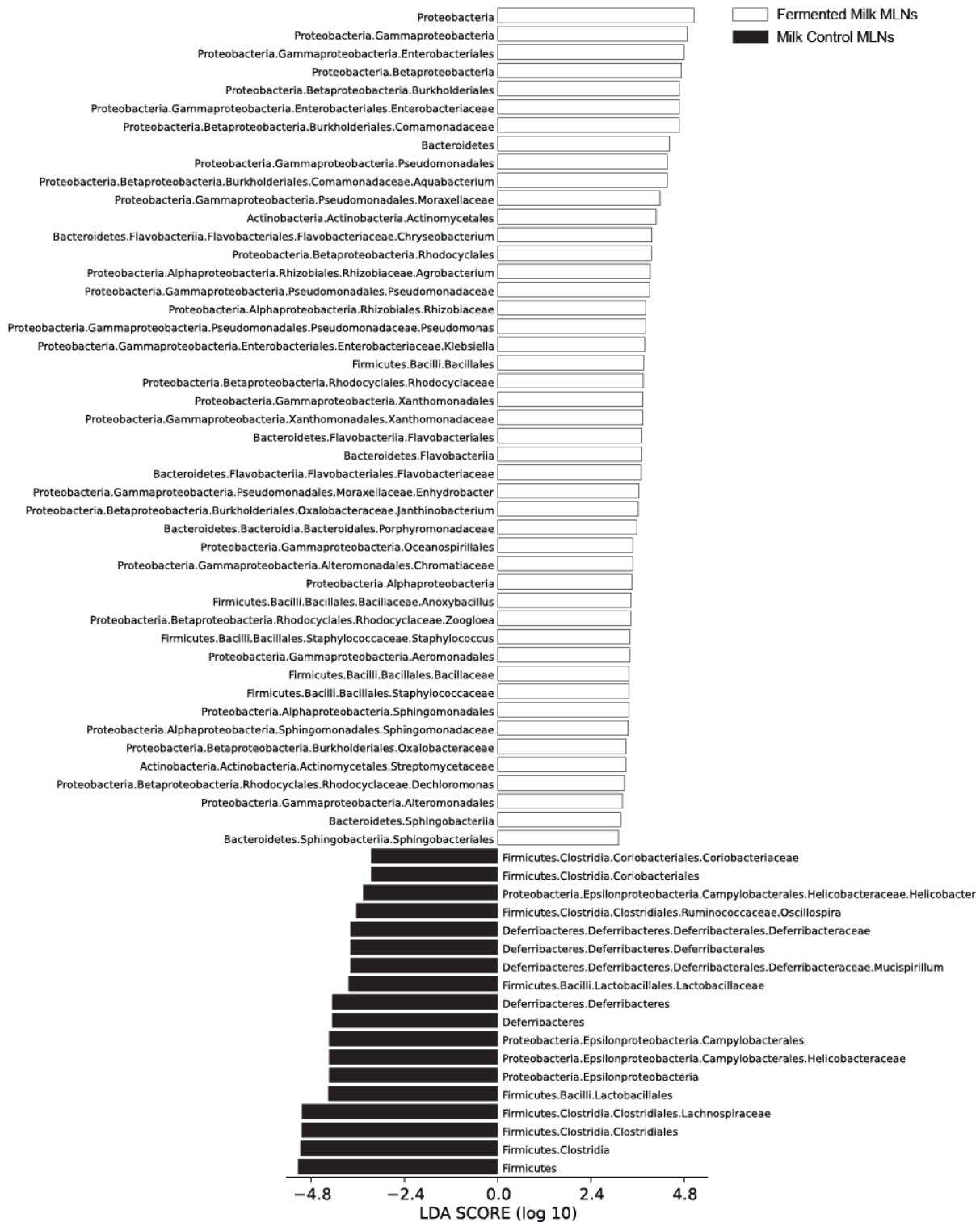


Supplementary Figure 2.8. PCoA of weighted Unifrac distances of stool and MLN microbial communities of mice administered a daily dietary intervention. PCoA plots of the weighted UniFrac distances of microbial communities from stool and MLNs collected upon completion of a dietary intervention with a FMP or MC. The first two PCs from the PCoA are plotted. Symbols represent stool (FMP, $n = 10$; MC, $n = 10$) or pooled MLNs (FMP, $n = 21$; MC, $n = 16$; 5 MLNs per mouse) samples from individual mice, color-coded by the indicated metadata.



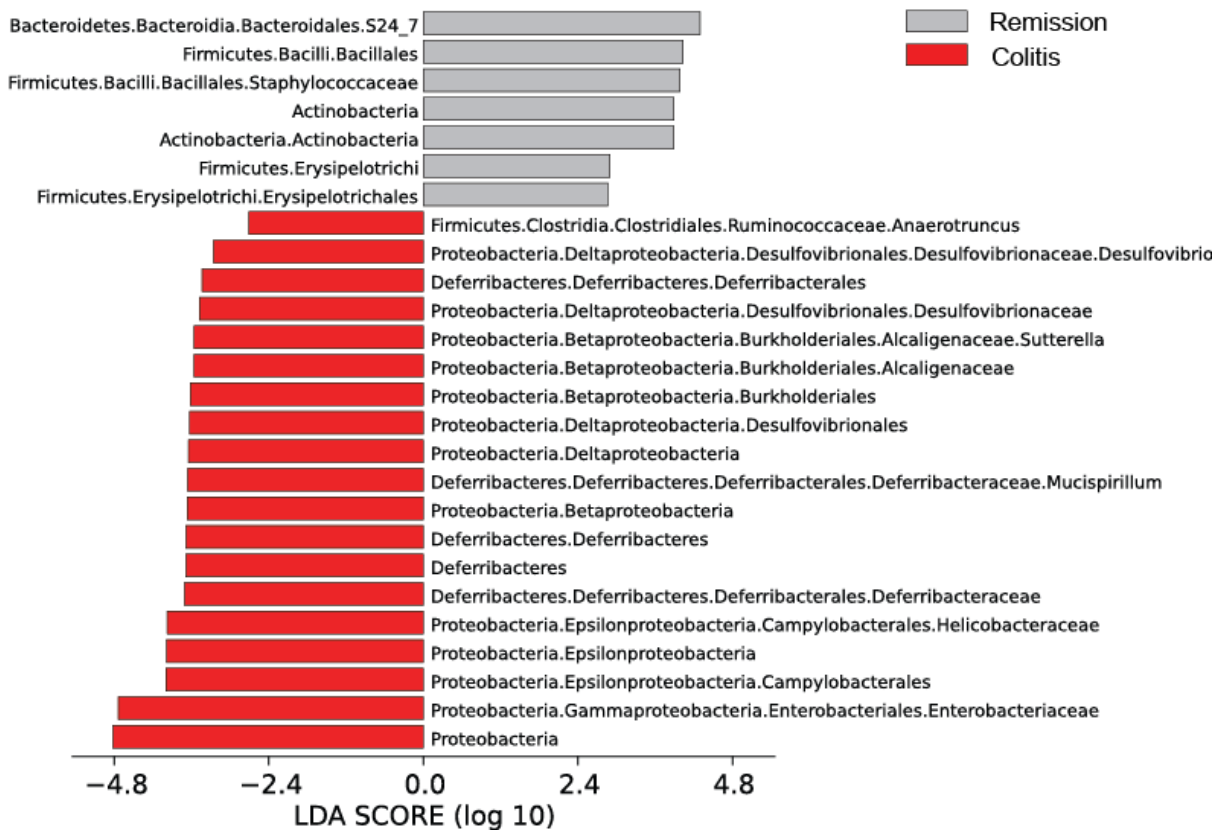
Supplementary Figure 2.9. LEfSe rank plot of differentially abundant microbial clades between stool and MLN microbial communities of mice receiving a daily dietary intervention. LDA scores for differentially abundant microbial clades in stool ($n = 20$) versus MLNs ($n = 37$ mice; 5 MLNs per mouse) of mice receiving either a FMP or MC.

Fermented Milk MLNs vs. Milk Control MLNs



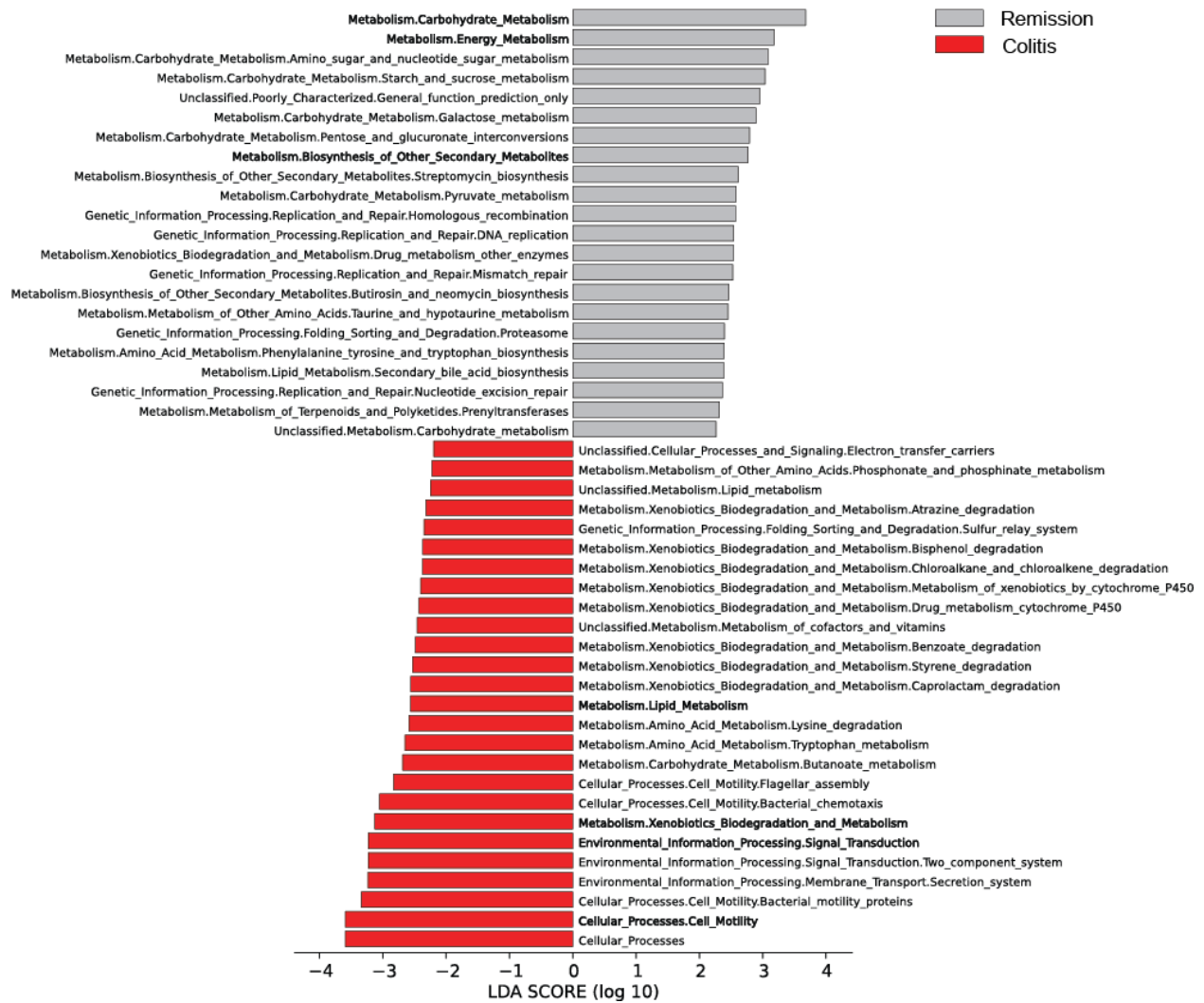
Supplementary Figure 2.10. LefSe rank plot of differentially abundant microbial clades between MLN microbial communities of mice receiving a daily dietary intervention. LDA scores for differentially abundant microbial clades in MLNs from mice (5 MLNs per mouse) receiving a FMP ($n = 21$) versus MC ($n = 16$).

Microbial Clades in Active Colitis vs. Remission

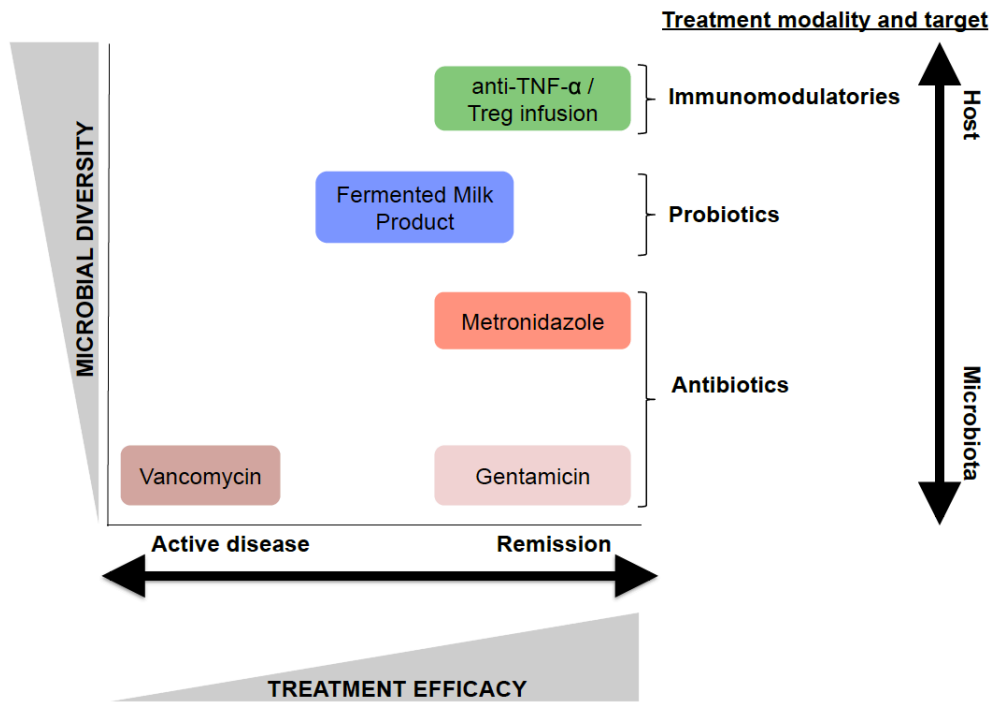


Supplementary Figure 2.11. LEfSe rank plot of differentially abundant microbial clades in gut microbiomes associated with active colitis and treatment-induced remission. LDA scores for differentially abundant microbial clades in stool from mice with active colitis ($n = 31$) versus remission ($n = 51$) upon intervention completion.

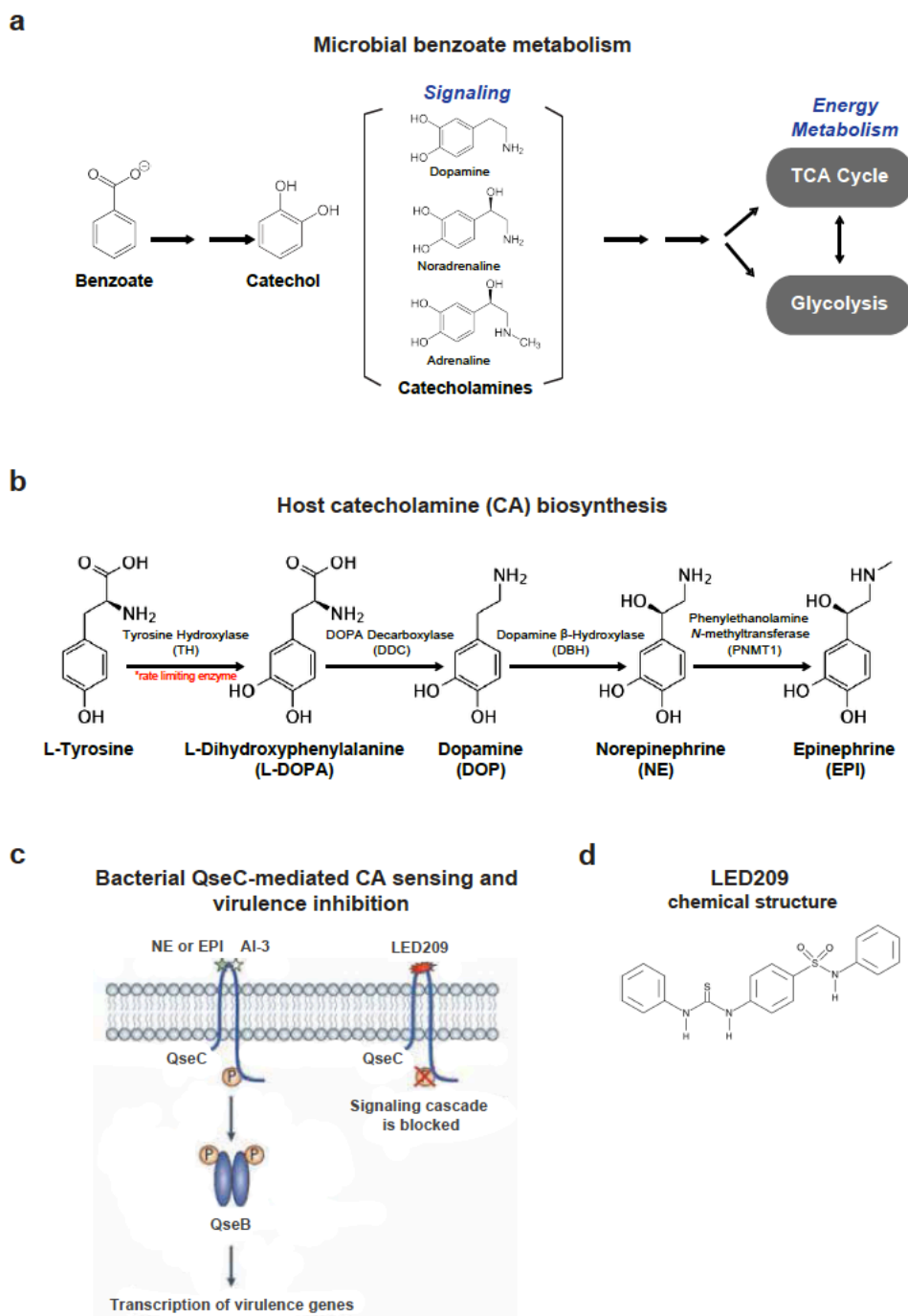
Microbial Functions in Active Colitis vs. Remission



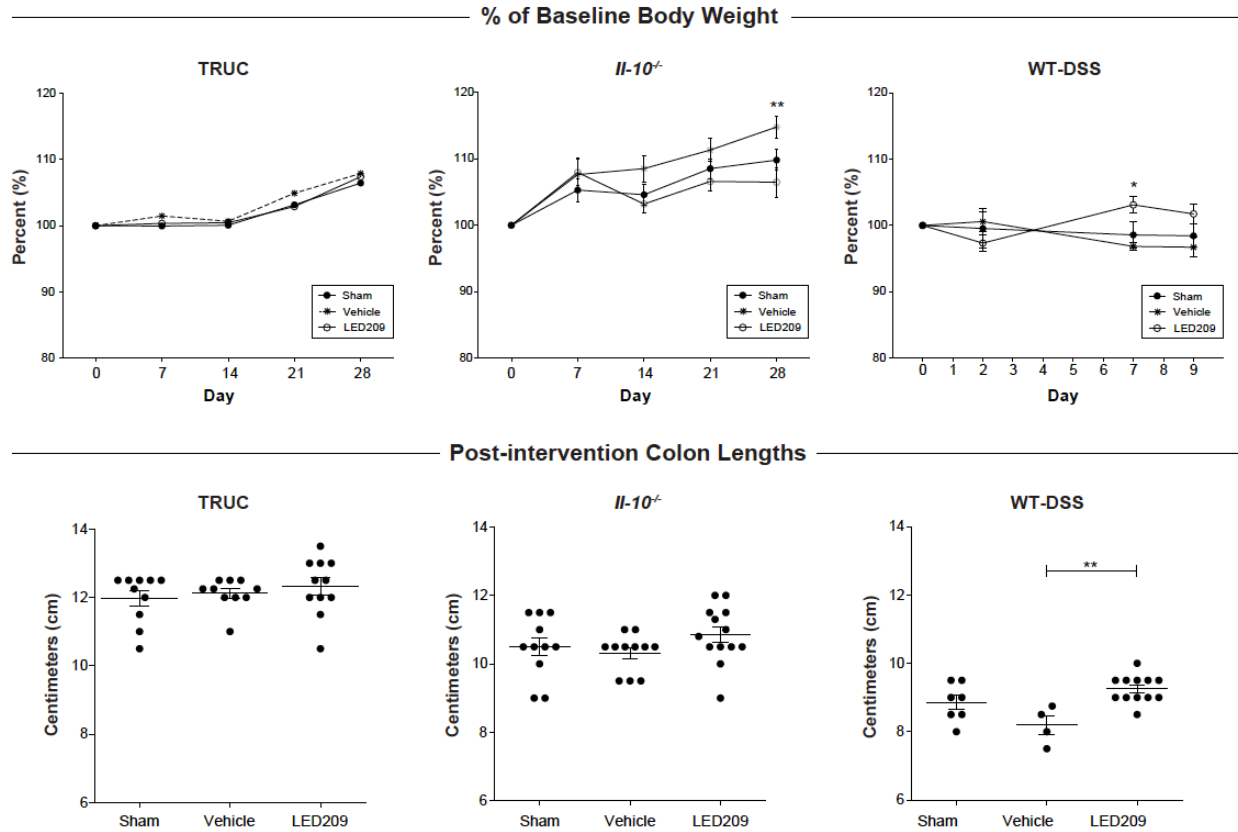
Supplementary Figure 2.12. LEfSe rank plot of differentially abundant microbial genes in gut microbiomes associated with active colitis and treatment-induced remission. LDA scores for differentially abundant PICRUSt predicted microbial genes (specified as KEGG Orthology groups), pathways, and classified functional categories (bold) defined by the KEGG BRITE hierarchy in stool from mice with active colitis ($n = 31$) versus remission ($n = 51$) upon intervention completion.



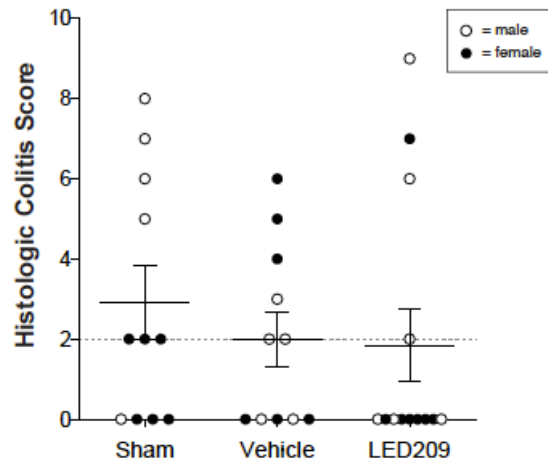
Supplementary Figure 2.13. Model summarizing the effects of treatment interventions in the TRUC model of experimental colitis. Immunomodulators (anti-TNF- α and T_{Regs}), antibiotics (gentamicin, metronidazole, and vancomycin) and a dietary intervention with a fermented milk product, which target diverse aspects of the host-gut microbiota continuum, differentially modified TRUC colitis and perturbed gut microbiota diversity to varying extents.



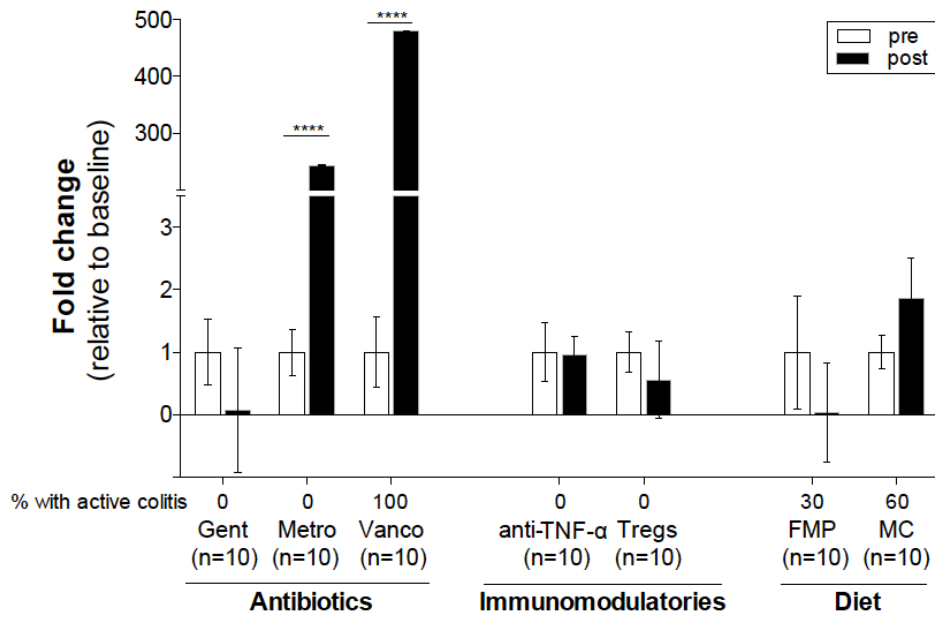
Supplementary Figure 3.1. Microbial benzoate metabolism, host CA biosynthesis, and bacterial QseC-mediated CA sensing and virulence inhibition. Compounds and/or enzymes involved in: (a) microbial benzoate metabolism and (b) host CA biosynthesis. (c) CA-mediated bacterial virulence is induced by QseBC two-component system activation. QseC detection of microbiota-derived autoinducer-3 (AI-3) or host-derived CAs initiates a signaling cascade leading to the upregulation of virulence genes. This signaling cascade can be blocked by the QseC inhibitor LED209. (d) Chemical structure of LED209 [*N*-phenyl-4-(3-phenylthioureido)benzenesulfonamide].



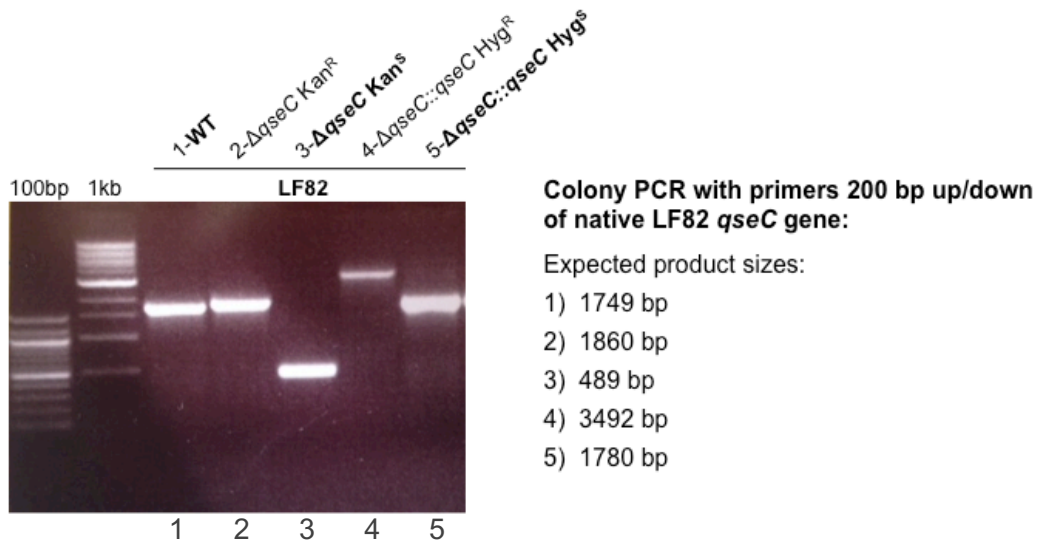
Supplementary Figure 3.2. Changes in baseline body weight and post-intervention colon lengths for an LED209 intervention in three mouse models of experimental colitis. Top panel: Symbols represent mean \pm SEM for each treatment group, color-coded by indicated metadata. Two-way analysis of variance (ANOVA) with Tukey's multiple comparison test: * $P < 0.05$ and ** $P < 0.01$. Significance for *Il-10^{-/-}* and WT-DSS was observed between LED209 and vehicle-control groups on the indicated intervention day. Bottom panel: Symbols represent individual mice. Error bars indicate mean \pm SEM. One-way ANOVA with Tukey's multiple comparison test: ** $P < 0.01$.



Supplementary Figure 3.3. Gender differences in disease severity in *Il-10*^{-/-} mice following an LED209 intervention. Histologic colitis scores. Symbols represent data from individual mice, color-coded by the indicated metadata. Error bars indicate mean ± SEM. Colitis scores >2 indicate active colitis and scores ≤2 remission.



Supplementary Figure 3.4. Shifts in *Enterobacteriaceae* abundance in gut microbiomes of TRUC mice following treatment with antibiotics, immunomodulators, or a dietary intervention. *Enterobacteriaceae* relative abundance based on 16S rRNA gene survey data described in Chapter 2. For each treatment group, the number of mice and the percentage of mice with active colitis (colitis scores >2) are indicated. Fold change was calculated relative to baseline for each treatment group. Error bars indicate mean \pm fractional SD. Two-way ANOVA with Sidak's multiple comparison test to compare pre- and post-intervention *Enterobacteriaceae* levels within each treatment group: **** $P < 0.0001$. Gent, gentamicin; Metro, metronidazole; Vanco, vancomycin; anti-TNF- α , neutralizing antibodies to TNF- α ; T_{Regs}, T-regulatory cell infusion; FMP, fermented-milk product; MC, mild control product.

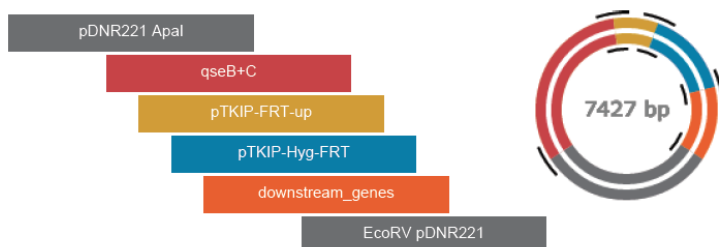


Supplementary Figure 4.1. Confirmation of *qseC* deletion and replacement in the LF82 genome. PCR with *qseC_ver_200bp_up-For* and *qseC_ver_200bp_dwn-Rev* to assess proper fragment lengths using primers flanking native *qseC* in LF82. PCR was performed on bacterial cells from colonies of indicated strains. Expected product sizes for each lane are listed.

Vector Digestion

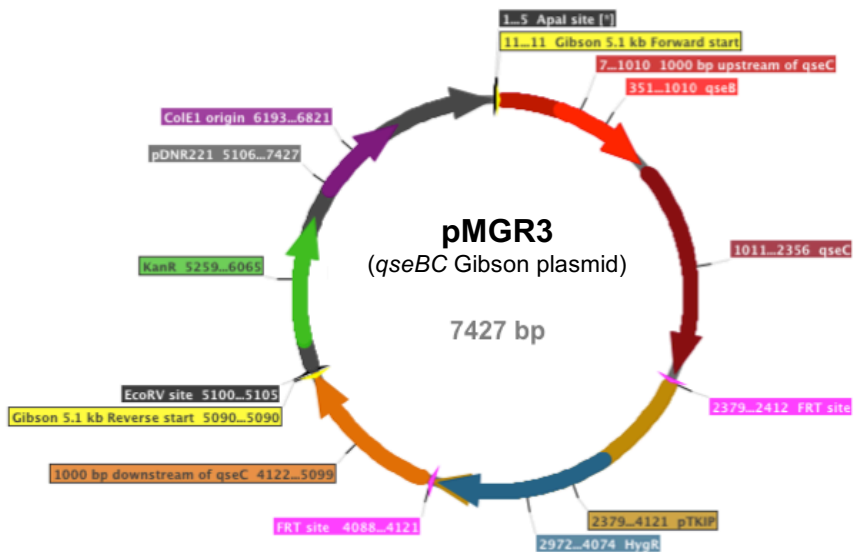
Vector backbone digested with Apal and EcoRV

Fragment Arrangement

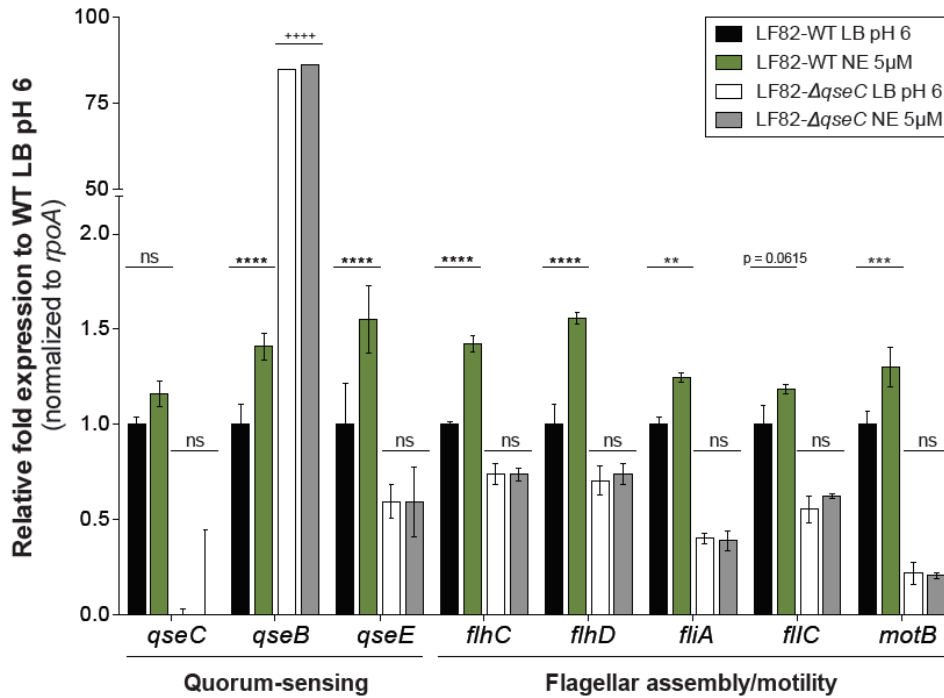


Required Primers

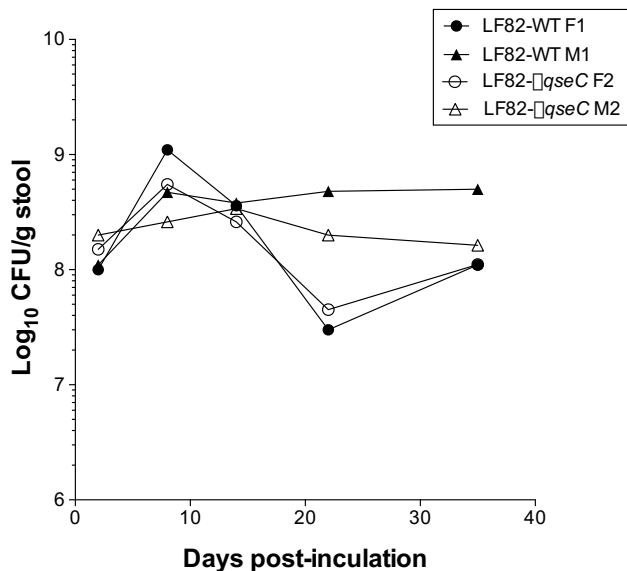
Overlaps	Oligo (Uppercase = gene-specific primer)	Anneals	F/R	3' Tm	3' Ta *	6-Frame
pDNR221	cagtcttaagctcgggcccCGCGCAGGGTTACCCAGG	qseB+C	Fwd	70.0°C	68.7°C	view
pTKIP-FRT-up	aggaacttcACGGCTTCATAGACAGAGAAGTTAC	qseB+C	Rev	65.7°C	68.7°C	view
qseB+C	gagagccgtGAAGTTCCTATTCTCTAGAAAGTATAGGAAC	pTKIP-FRT-up	Fwd	62.0°C	65.0°C	view
pTKIP-Hyg-FRT	caggtcgaaAGGCCCGGAGATGAGGAA	pTKIP-FRT-up	Rev	66.2°C	65.0°C	view
pTKIP-FRT-up	tcggggcctTTCGACCTGCAGCCTGTT	pTKIP-Hyg-FRT	Fwd	64.8°C	65.0°C	view
downstream_genes	gtcgttttaGAAGTTCCTATACTTTCTAGAGAATAGGAAC	pTKIP-Hyg-FRT	Rev	62.0°C	65.0°C	view
pTKIP-Hyg-FRT	aggaacttcTAAACGACTCTCATAGACTTTAC	downstream_genes	Fwd	57.2°C	58.4°C	view
pDNR221	cgactcactataggggatatcAGGAAAAATGATTCGCG	downstream_genes	Rev	55.4°C	58.4°C	view



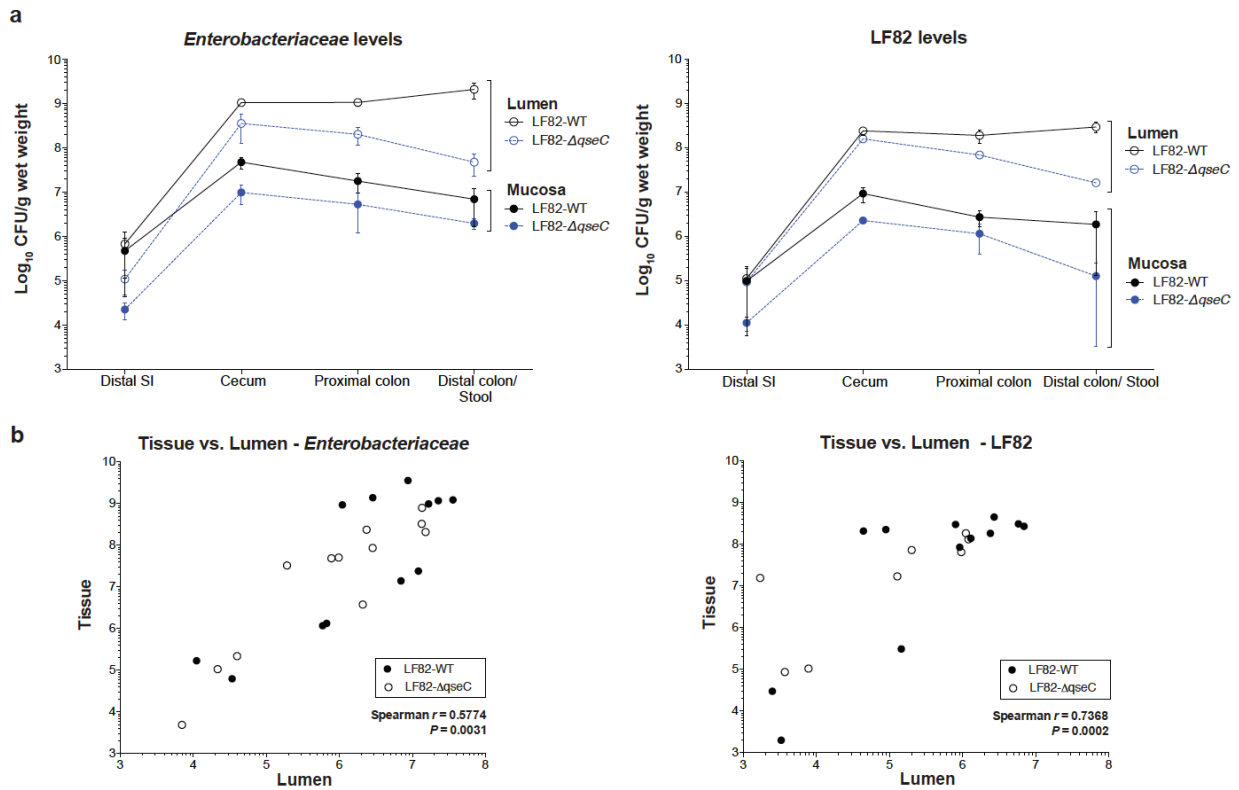
Supplementary Figure 4.2. Gibson plasmid for *qseC* complementation. Details of the primer sequences and recommended PCR conditions for generating a Gibson plasmid containing: Apal-EcoRV restriction digested vector from pDONR221 plasmid, Hyg resistance cassette flanked by FRT sites for selectable recombination marker from pTKIP plasmid, and *qseBC* sequence and 1000 bp downstream sequence for targeted replacement into the LF82 genome. Genes are organized to allow the Hyg cassette to be centered between the *qseBC* sequence and the 1000 bp downstream sequence. Once the pMGR3 was successfully assembled and propagated in competent *E. coli* DH5 α , the plasmid was isolated and digested with Apal-EcoRV to generate a 5.1 kb linear fragment that was transformed into LF82- Δ *qseC*::*kan*/pTKRed for replacement of Kan cassette for the 5.1 kb fragment conferring Hyg resistance.



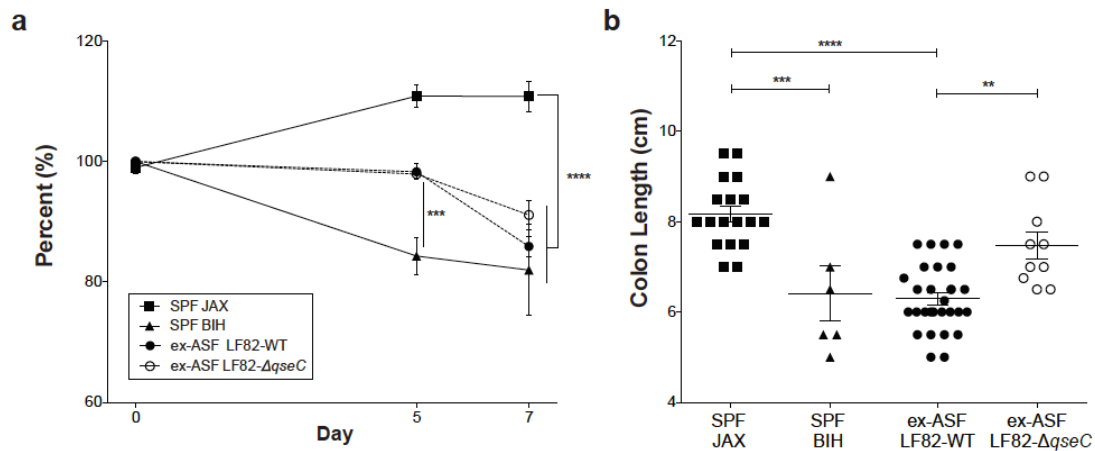
Supplementary Figure 4.3. Effects of *qseC* inactivation on NE-induced expression of LF82 virulence genes. RT-qPCR analysis of QseC-regulated virulence genes in WT and $\Delta qseC$ strains. Cultures were grown overnight at 37°C in either acidified LB broth (pH 6) or LB supplemented with 5 μ M NE, back diluted to an OD_{600} of 0.02, and grown for 6 hrs at 37°C without agitation. Total RNA was extracted from bacterial pellets and underwent rigorous DNase treatments and cDNA synthesis prior to RT-qPCR. Genes were normalized to *rpoA* and fold change was calculated relative to WT grown in LB pH 6 using the $2^{-\Delta\Delta Ct}$ method. Bars represent data from 2 independent experiments. Error bars indicate mean \pm fractional SD. Two-way ANOVA with Sidak's multiple comparison test to compare expression between media conditions (LB pH 6 versus 5 μ M NE) for each strain (WT versus $\Delta qseC$) for each primer set: ** $P < 0.01$, *** $P < 0.001$, **** $P < 0.0001$.



Supplementary Figure 4.4. Culturable counts of LF82 in stool from LF82-inoculated ex-ASF mice. One week after transfer from a GF isolator to a conventional, SPF facility, ex-gnotobiotic-GF mice were inoculated with 10^8 colony-forming units (CFUs) of LF82-WT or LF82- Δ qseC (day 0). Stool samples were collected at various time points following the initial inoculation and serially diluted onto MacConkey agar plates supplemented with 100 μ g per ml ampicillin (Amp) and 20 μ g per ml erythromycin (Eryth). The number of Amp^R-Eryth^R LF82 colonies were counted and converted to CFU per gram stool based on wet weight. Symbols represent individual female (F) or male (M) mice. On day 25, breeding pairs were set up between F1-M1 and F2-M2, which may explain the shifts in LF82 levels between day 22 and 35.



Supplementary Figure 4.5. Biogeography experiments to determine LF82 niche-specificity in the intestinal tract. Biogeography experiments involved paired mucosal tissue and luminal context samples from 4 intestinal sites: distal small intestine (SI), cecum, proximal colon, and distal colon. All samples (mucosal, luminal, stool) were weighted, diluted 1:10 in ice-cold PBS, homogenized, and serially diluted before plating on MacConkey agar \pm Amp-Eryth. CFU = colony forming units.



Supplementary Figure 4.6. Changes in baseline body weight and post-intervention colon lengths for DSS-exposed mice. (a) Symbols represent mean \pm SEM for each group, color-coded by indicated metadata. Two-way ANOVA with Tukey's multiple comparison test: *** $P < 0.001$ and **** $P < 0.0001$. (b) Symbols represent individual mice. Error bars indicate mean \pm SEM. One-way ANOVA with Tukey's multiple comparison test: ** $P < 0.01$, *** $P < 0.001$, and **** $P < 0.0001$. JAX, Jackson mice; BIH, mice bred-in-house; ex-ASF, ex-gnotobiotic-ASF mice colonized with either LF-WT or LF82- $\Delta qseC$.

Supplementary Table 2.1. Summary of pyrosequenced samples. This table details the number of mice in each experimental group, the post-intervention histologic colitis scores, the number of mice with active colitis versus remission upon treatment completion, and the average number of quality-filtered 16S rRNA gene sequences and binned OTUs (selected at 97% sequence identity) for samples in each pre- or post-intervention group. Colitis scores >2 indicate active colitis and scores ≤2 remission. Values represent mean ± SEM.

Treatment	Control			Antibiotics						Immunomodulators						Dietary Interventions					
	Sham (n = 10)	Gentamicin (n = 10)		Metronidazole (n = 10)		Vancomycin (n = 10)		Anti-TNF- α (n = 10)		T-Regulatory cells (n = 10)		Milk Control (n = 10)		Fermented Milk (n = 10)							
Time Point	Post	Pre	Post	Pre	Post	Pre	Post	Pre	Post	Pre	Post	Pre	Post	Pre	Post						
Colitis Score	6.0 ± 0.43		0.0 ± 0.0		0.1 ± 0.32		5.3 ± 0.67		0.4 ± 0.52		0.5 ± 0.56		1.7 ± 1.77		3.4 ± 1.65						
Disease Status	Colitis (n = 12)		Remission (n = 10)		Remission (n = 10)		Colitis (n = 10)		Remission (n = 10)		Remission (n = 10)		Remission (n = 4) Colitis (n = 6)		Remission (n = 7) Colitis (n = 3)						
Sequences	6,172 ± 5,338	7,801 ± 6,157	7,974 ± 4,333	7,968 ± 2,424	7,672 ± 2,842	4,282 ± 4,509	8,735 ± 2,407	10,754 ± 3,944	8,276 ± 6,050	5,771 ± 1,998	8,700 ± 3,864	4,194 ± 1,353	3,874 ± 1,450	3,913 ± 1,196							
OTUs	732 ± 395	702 ± 336	138 ± 20	912 ± 236	363 ± 325	633 ± 292	156 ± 30	1,120 ± 214	814 ± 374	787 ± 139	939 ± 306	369 ± 78	357 ± 56	362 ± 53	365 ± 78						

Supplementary Table 2.2. Summary of PICRUSt analysis of post-intervention samples. Number and percentage of quality-filtered 16S rRNA gene sequences that mapped to Greengenes reference OTUs at 97% sequence identity, the resulting number of binned reference-based OTUs, the calculated weighted Nearest Sequenced Taxon Index (NSTI) score representing the metagenome prediction accuracy (lower values indicate a more accurate prediction), and the number of inferred genes (specified by KEGG Orthology groups) for stool samples from each post-intervention group. Values represent mean \pm SEM.

Treatment	Control			Antibiotics			Immunomodulators			Dietary Interventions		
	Sham (n = 10)	Gentamicin (n = 10)	Metronidazole (n = 10)	Vancomycin (n = 10)	Anti-TNF- α (n = 10)	T-Regulatory cells (n = 10)	Milk Control (n = 10)	Fermented Milk (n = 10)				
Mapped Sequences (% Total)	5,084 \pm 1,344 (80.6 \pm 2.2)	6,896 \pm 1,207 (86.0 \pm 0.7)	6,661 \pm 733 (86.8 \pm 2.4)	8,106 \pm 718 (92.7 \pm 1.4)	7,022 \pm 1,639 (84.9 \pm 1.2)	7,175 \pm 1,055 (82.0 \pm 1.6)	3,954 \pm 355 (96.3 \pm 0.5)	3,707 \pm 365 (94.5 \pm 0.8)				
Reference-based OTUs	197 \pm 19	46 \pm 3	85 \pm 15	43 \pm 5	221 \pm 22	227 \pm 18	196 \pm 9	193 \pm 10				
Weighted NSTI	0.115 \pm 0.004	0.071 \pm 0.006	0.091 \pm 0.011	0.047 \pm 0.002	0.109 \pm 0.007	0.115 \pm 0.004	0.131 \pm 0.003	0.139 \pm 0.006				
KOs	2,634,000 \pm 641,717	2,047,000 \pm 361,900	1,953,000 \pm 242,140	3,243,000 \pm 437,144	3,479,000 \pm 873,417	3,300,000 \pm 534,338	2,065,000 \pm 272,946	2,218,000 \pm 273,132				

Supplementary Table 4.1. Bacterial strains and plasmids used in this study.

Strain or Plasmid		Relevant Characteristics ^a		Source or Reference
<i>E. coli</i> Strains				
LF82	Wild-type adherent-invasive <i>E. coli</i> LF82 isolated from a mucosal lesion of a Crohn's disease patient.	Amp ^R , Eryth ^R		Darfeuille, M. <i>et al.</i> <i>Gastroenterology</i> 115 , (1998)
LF82-Δ <i>qseC</i>	LF82 isogenic mutant with <i>qseC</i> gene deleted			This work
LF82-Δ <i>qseC</i> :: <i>kan</i>	LF82 isogenic mutant with <i>qseC</i> gene deleted, Kan ^R			This work
LF82-Δ <i>qseC</i> :: <i>qseC</i>	LF82-Δ <i>qseC</i> :: <i>kan</i> with WT LF82 <i>qseC</i> gene introduced back into its native genome location			This work
DH5α derivative	Chemically-competent <i>E. coli</i> for Gibson cloning			NEB
Plasmids				
pCP20	Contains FLP recombinase for excising DNA flanked by FRT sites, Amp ^R , Cm ^R , temperature-sensitive			Datsenko, K.A. & Wanner, B.L. <i>PNAS</i> 97 , (2000)
pDONR221	Cloning vector with Kan cassette flanked by Apal and EcoRV sites, Amp ^R , Kan ^R			Invitrogen
pKD4	Cloning vector with Kan cassette flanked by FRT sites, Kan ^R			Datsenko, K.A. & Wanner, B.L. <i>PNAS</i> 97 , (2000)
pTKIP	Cloning vector with Hyg cassette flanked by FRT sites, Amp ^R , Hyg ^R			Kuhlman, T. E. & Cox, E. C. <i>Nucleic Acid Res.</i> 38 , (2010)
pTKred	Contains λ-Red enzymes under IPTG-inducible promoter, Spect ^R , temperature-sensitive			Kuhlman, T. E. & Cox, E. C. <i>Nucleic Acid Res.</i> 38 , (2010)

^aAmp, ampicillin; Cm, chloramphenicol; Eryth, erythromycin; Kan, kanamycin; Hyg, hygromycin; Spect, spectinomycin; IPTG, isopropyl β-D-1-thiogalactopyranoside.

Supplementary Table 4.2. Primers used in this study.

Primer ^a	Oligonucleotide Sequence (5'-to-3')	Reference
Generating isogenic deletion mutant		
LF82_ qseC_80_up-For	GCAAACCTCGGACGTGATTTTATTTCGTACCGTTTCATGGTATTGGCTACACATTAGGTGAGAAATGAAAAGTGTAGGC TGGAGCTGCTTC	This work
LF82_ qseC_80_dwn-Rev	GGGGACGGTTTATATATTTTGGCTATTAGTAAAGTCTATGAGAGTCGTTTTAACGGCTCTCATAGACAGAGAAAGCATA TGAATATCTCTCCTTAG	This work
Verifying qseC gene removal or replacement		
Kan_ver-For	ACCTGCCCATTCGACCACCAAG	This work
Kan_ver-Rev	GGAGAACTGCGTGCAATCCAT	
qseC_ver_200bp_up-For	AAGAAATTTGCCCTGCTGGAATTAC	This work
qseC_ver_200bp_dwn-Rev	CAGCATTTTTCTCTCTGACACCAC	
qseC-ver_internal-For	ACCCAACGCTTAGTCTGCGA	This work
qseC-ver_internal-Rev	GCTTACCTTCGGCTCAAATCC	
RT-qPCR		
flhC-For	AACTGGCTTGTGTAATGGCGTCG	Reiss, R.J. & Mobley, H. L. T. <i>J. Biol. Chem.</i> 286 , (2011).
flhC-Rev	TCAACAAAACCGCACCAATGTCCAG	
flhD-i-For	TCCGCTATGTTCTGCTCGGCATA	Reiss, R.J. & Mobley, H. L. T. <i>J. Biol. Chem.</i> 286 , (2011).
flhD-i-Rev	ACCAGTTGATGGTTTCTGCCAGC	
fliA-For	CGCCGTGCTCTTCGGGCC	Barnich, N. <i>et al.</i> <i>Infect. Immun.</i> 72 , (2004).
fliA-Rev	CGTGCACGCAACGGCGG	
fliC-For	TGGTGTGCAACTGCTAACGC	Barnich, N. <i>et al.</i> <i>Infect. Immun.</i> 72 , (2004).
fliC-Rev	TTATCGGCATATTTTGGCGTAGC	
motB-For (mod)	TGAAAGCCCAATCCCGGTG	Barnich, N. <i>et al.</i> <i>Infect. Immun.</i> 72 , (2004).
motB-Rev	CTTAAGCGCATCGTTGCCCGC	
qseB-For	CGGTGATCCTGGATTTAACCTT	Kendall, M.M. <i>et al.</i> <i>MBio</i> 3 , (2012)
qseB-For	GCTGACCTTTTCTCGCCATT	
qseC-For	AATGGGAATACCGTGAAGACAT	Kendall, M.M. <i>et al.</i> <i>MBio</i> 3 , (2012)
qseC-Rev	CCAGCCACGGGATCAATTG	

Supplementary Table 4.2. (Continued).

qseE-For	ACAATCCCTGGCAATGCTTAA	Kendall, M.M. <i>et al.</i> <i>MBio</i> 3, (2012)
qseE-Rev	GAAGCCACCAGCGAAAAAGG	
rpoA-For	GCGCTCATCTTCTTCCGAAT	Kendall, M.M. <i>et al.</i> <i>MBio</i> 3, (2012)
rpoA-Rev	CGCGGTCGTGGTTATGTG	

^aFor, forward primer; Rev, reverse primer; mod, modified from original sequence.

APPENDIX B

Supplementary Methods

DNA/RNA Co-Isolation from Bacterial Cultures and Stool

Protocol Development

This extraction protocol combines immediate stabilization and preservation of RNA followed by phenol-chloroform extraction and mechanical bead beating prior to DNA/RNA co-isolation.

Materials (in order of use)

RNAprotect Bacteria Reagent (Qiagen; cat. #76506) or RNAlater (Ambion; cat #7024)

Glass Beads, 0.1 mm diameter (BioSpec Products; cat. #11079101)

2 ml sterile vials and caps, 100 count (BioSpec Products; cat. #10831)

Tris, 1 M (Ambion; cat. #AM9855G)

EDTA, 0.5 M (Ambion; cat. #AM9260G)

10% SDS (Ambion; cat. #AM9822)

TE-Saturated Phenol (Sigma; cat. #77607)

Phenol:Chloroform:Isoamyl Alcohol (Sigma; cat. #77617)

Sodium Acetate (3 M [pH 5.2]) (Ambion; cat. #AM9740)

Isopropanol (Sigma; cat. #59304)

PBS (Cellgro; cat. #21040)

AllPrep DNA/RNA Mini Kit (Qiagen; cat. #80204)

β -Mercaptoethanol (β -ME) (Sigma; cat. #63689)

RNase-Free DNase Set (Qiagen; cat; #79254)

TURBO DNA-free Kit (Ambion; cat; #AM1907)

RNAeasy MinElute Kit (Qiagen; cat. #74204)

iScript cDNA Synthesis Kit (BIO-RAD; cat. #170-8891)

SYBR FAST UNIVERSAL qPCR (Kapa Biosystems; cat#KK4600)

Other: 96-100% Ethanol, RNase-free water

Instruments

Bead beater (BioSpec Products; cat. #693)

Vortex

Centrifuge

Water baths at 37°C and 70°C

Important points before starting

- Perform all steps of 'Mechanical Lysis' at 4°C and all subsequent steps at room temperature (RT), unless otherwise indicated.
- Prepare Tris-EDTA-SDS (TE-SDS) Buffer: 200 mM Tris, 80 mM EDTA, 1.68% SDS, pH 8.0
- Pre-weigh 0.3 g of 0.1 mm glass beads in sterile 1.5 ml tubes.
- Prepare fresh 70% and 80% ethanol and store on ice.
- β -ME must be added to Buffer RLT Plus before use. Making a working aliquot in a sterile falcon tube by adding 10 μ l β -ME per 1 ml Buffer RLT Plus.
- Recommendation: For stool, collect maximum of 2-3 pellets/mouse per 1.5 ml sterile tube.
- Note: The maximum capacity of the Qiagen AllPrep column is 100 μ g DNA/RNA.

Bacterial Culture Preparation

1. Transfer 1.5 ml bacterial culture to a 15 ml Falcon tube containing 2 volume (vol) RNAprotect. Immediately vortex for 5 sec and incubate at RT for 10 min.
2. During incubation, measure optical density at 600 nm (OD_{600}) of bacterial culture to determine the number of bacterial cell/ml.
3. Centrifuge at 4,500 *g* for 10 min at RT to pellet cells.
4. Pour off supernatant, dab residual media on paper towel, and invert tubes for 10 sec to air-dry. Note: A pellet may not be visible after centrifugation. This may be result from an interaction between the cells and the stabilization reagent that causes a change in the optical density of cells. The procedure is not affected.
5. Snap freeze bacterial cell pellets in liquid nitrogen (LN_2) and store at $-80^{\circ}C$ (up to 4 wks). Proceed to step 6.

Stool Preparation

For samples stored in RNAlater.

1. Thaw briefly and
2. Vortex sample thoroughly.
3. Centrifuge at 10,000 *g* for 5 min at $4^{\circ}C$.
4. Discard supernatant.
5. Add 1 ml of ice-cold PBS and vortex to mix. Centrifuge at 10,000 *g* for 5 min at $4^{\circ}C$ and discard supernatant. Proceed to step 6.

For samples flash frozen proceed immediately to step 6.

Mechanical Lysis

6. Add 300 μ l of TE-SDS and 500 μ l TE-saturated phenol to each sample. Vortex 20-30 sec to mix.
7. Transfer entire volume to a 2 ml screw cap vial.
8. Add 0.3 g of pre-measured 0.1 mm glass beads to each sample tube.
9. Place 2 ml sample vials in bead beater for 2 min on "homogenize" setting.
10. Remove tubes from the bead beater and centrifuge at 12,000 *g* for 5 min at $4^{\circ}C$ to pellet debris.
11. Transfer the supernatant from bead tube into a sterile 1.5 ml tube.
12. Add 1 vol phenol:chloroform:isoamyl alcohol (~ 280 μ l) and shake vigorously to mix.
13. Centrifuge at 12,000 *g* for 5 min at $4^{\circ}C$.
14. Transfer the aqueous phase (~ 250 μ l) into a sterile 1.5 ml tube.
15. Add 1 vol chloroform (~ 250 μ l) and shake vigorously to mix.

16. Centrifuge at 12,000 *g* for 5 min at 4°C.
17. Transfer the aqueous phase (~200 µl) into a sterile 1.5 ml tube.
18. Add 1/10 vol of 3 M sodium acetate and 1 vol isopropanol. Invert to mix.
19. Centrifuge at 12,000 *g* for 5 min at 4°C. Pipette off supernatant.
20. Add 500 µl of ice-cold 70% ethanol and vortex gently until pellet dislodges.
21. Centrifuge at 12,000 *g* for 5 min at 4°C.
22. Pipette off ethanol and air dry pellet for 10 min on ice.
23. Resuspend pellet in 50-100 µl RNase-free water.
24. Dissolve pellet on ice for 15-30 min. Intermittently pipette to ensure pellet is fully resuspended.
25. Quantify DNA/RNA using a spectrophotometer under the DNA setting.

Separation of DNA/RNA with AllPrep Mini Kit

26. **Add 600 µl of RLT Plus supplemented with β-ME** to a 50 µl aliquot of ≤50-100 µg of each sample from step 23. Mix well by vortexing for 10 sec. Proceed to step 28 or store isolated DNA/RNA mix in RLT Plus at -80°C.
Note: Using >50 µg of DNA/RNA can lead to DNA contaminating the RNA portion. Transferring ≤50 µg is recommended. Bring all 50-100 µg aliquots up to 50 µl using RNase-free water.
27. If using a frozen aliquot, **incubate at 37°C for 5 min** to thaw sample and to dissolve any precipitated salts.
28. **Transfer** the homogenized lysate (650 µl) to the **AllPrep DNA spin column** placed in a 2 ml collection tube (supplied). **Centrifuge** at 10,000 *g* for 1 min.
29. **Place** the AllPrep DNA spin column in a **new 2 ml collection tube** (supplied). **Centrifuge** at 10,000 *g* for 1 min and **store** at 4°C for later DNA purification. **Use the flow-through for RNA purification.**
Note: Do not freeze the AllPrep DNA spin column or store it at RT or at 4°C for long periods.

Total RNA Purification with AllPrep RNeasy columns

30. **Add 1 volume RT 70% ethanol** (650 µl) to the flow through from step 29, and mix well by pipetting up/down. Do not centrifuge. Proceed immediately to next step.
Note: Precipitates may be visible after addition of ethanol. This does not affect the procedure.
31. **Transfer up to 700 µl** of the sample, including any precipitate that may have formed, to an **RNeasy spin column** placed in a 2 ml collection tube (supplied). **Centrifuge** at 10,000 *g* for 1 min. Discard the flow-through. Reuse the collection tube in the next step.
Note: If the sample volume exceeds 700 µl, centrifuge successive aliquots in the same RNeasy spin column. Discard the flow-through after each centrifugation. [This step requires 2 spins.]
32. **Add 350 µl Buffer RW1** to the RNeasy spin column. **Centrifuge** at 10,000 *g* for 1 min to wash the spin column membrane. Discard the flow-through. Reuse the collection tube in next step.

33. **Add 80 µl DNase mix [10 µl DNaseI stock solution + 70 µl RDD buffer]** directly to the RNeasy spin column membrane and incubate at RT for 15 min.
Note: To prepare DNaseI stock, dissolve the lyophilized pellet in 550 µl of provided RNase-free water. Use a needle and syringe to inject the water. Invert vial to mix – DO NOT VORTEX. For long-term storage, divide the stock solution into single-use aliquots and store at -20°C for up to 9 mo. Thawed aliquots can be stored at 4°C for up to 6 wks.
34. **Add 500 µl Buffer RWI** to the RNeasy spin column. **Incubate** at RT for 5 min. **Centrifuge** at 10,000 *g* for 1 min to wash the spin column. Discard the flow-through. Reuse the collection tube in next step.
35. **Add 500 µl Buffer RPE** to the RNeasy spin column. **Centrifuge** at 10,000 for 1 min to wash the spin column membrane. Discard the flow-through. Reuse the collection tube in next step.
36. **Add another 500 µl Buffer RPE** to the RNeasy spin column. **Centrifuge** at 10,000 *g* for 2 min to wash the spin column membrane. Discard the flow-through and collection tube.
37. **Place** the RNeasy spin column in a **new 2 ml collection tube** (supplied). **Centrifuge** at 14,000 *g* for 1 min.
Note: Perform this step to eliminate any possible carryover of Buffer RPE.
38. **Place** the RNeasy spin column in a **capless 1.5 ml tube** (user supplied). **Add 45 µl RNase-free water** directly to the spin column membrane. **Incubate** at RT for 1 min. **Centrifuge** at 10,000 *g* for 1 min to elute the RNA. Store column and collection tube on ice.
39. **Add another 45 µl RNase-free water** directly to spin column membrane. **Incubate** on ice for 1 min. **Centrifuge** at 10,000 *g* for 1 min to elute the RNA.
40. **Transfer** the combined RNA eluates (~90 µl total) **to a sterile 1.5 ml collection tube**
41. **Quantify RNA** using a spectrophotometer and ensure all RNA samples are <20 µg in total.

Secondary DNase Treatment with TURBO DNA-free Kit

42. **Transfer** up to 10 µg (1x) or 20 µg (2x) of RNA to a 0.5 ml tube. Bring volume up to 88 µl (1x) or 86 µl (2x) using RNase-free water. **Add 10 µl DNA-free buffer** and **2.5 µl rDNase** to each sample.
43. **Incubate** in a 37°C water bath for 30 min. For 2x reactions, **add an additional 2.5 µl rDNase** and **incubate** in a 37°C water bath for an additional 30 min.
44. **Add 20 µl DNase Inactivation Reagent** and mix well by flicking tube. **Incubate** at RT for 4-5 min while flicking continuously. **Centrifuge** at <10,000 *g* for 2 min.
45. **Transfer** RNA supernatant (avoiding any beads; ~95 µl) to a sterile 1.5 ml tube.

RNA Cleanup with RNeasy MinElute Kit (optional)

46. **Add 350 µl of Buffer RLT** to RNA from step 45 and mix well by pipetting up/down.
47. **Add 250 µl of 100% ethanol** to the diluted RNA and mix well by pipetting up/down. Proceed immediately to next step.

48. **Transfer** the sample (700 μ l) to an **RNeasy MinElute spin column** placed in a 2 ml collection tube (supplied). **Centrifuge** at 10,000 *g* for 1 min. Discard the flow-through. Reuse the collection tube in next step.
49. **Add 500 μ l Buffer RPE** to the RNeasy MinElute spin column. **Centrifuge** at 10,000 *g* for 1 min to wash the spin column membrane. Discard the flow-through. Reuse the collection tube in next step.
50. **Add 500 μ l 80% ethanol** to the RNeasy MinElute spin column. **Centrifuge** at 10,000 *g* for 2 min to wash the spin column membrane. Discard the flow-through. Reuse the collection tube in next step.
51. **Cut off RNeasy MinElute spin column cap** with scissors. **Centrifuge** at 14,000 *g* for 5 min.
52. **Place** the RNeasy spin column in a **capless 1.5 ml tube** (user supplied). **Add 18 μ l RNase-free water** directly to the spin column membrane. **Incubate** at RT for 1 min. **Centrifuge** at 14,000 *g* for 1 min to elute the RNA.
53. **Add another 18 μ l RNase-free water** directly to the spin column membrane. **Incubate** on ice for 1 min. **Centrifuge** at 14,000 *g* for 1 min to elute the RNA.
54. **Transfer** the RNA eluate (~30 μ l total) **to a sterile 1.5 ml collection tube**.
55. **Quantify RNA** using the Qubit Quant-IT RNA HS assay.
56. **Store RNA at -80°C**.

Note: Converting RNA to cDNA on the same day of isolation is recommended.

Optional QC: Perform PCR with 16S rRNA gene to confirm efficient DNase treatment.

Total DNA Purification with AllPrep DNA columns

57. **Incubate** 1.5 ml tube aliquots of **EB** (supplied) in **70°C** water bath before proceeding to step 58.
58. **Add 500 μ l Buffer AW1** to the AllPrep DNA spin column from step 29 (stored at 4°C). **Incubate** at RT for 2 min. **Centrifuge** at 10,000 *g* for 1 min to wash the spin column membrane. Discard the flow through. Reuse the spin column in next step.
Note: Buffer AW1 is supplied as a concentrate. Ensure that ethanol is added to Buffer AW1 before use.
59. **Add 500 μ l Buffer AW2** to the AllPrep DNA spin column. **Incubate** at RT for 5 min. **Centrifuge** at 14,000 *g* for 2 min to wash the spin column membrane.
Note: Buffer AW2 is supplied as a concentrate. Ensure that ethanol is added to Buffer AW2 before use. The long centrifugation dries the spin column membrane, ensuring that no ethanol is carried over during DNA elution. Residual ethanol may interfere with downstream reactions.
60. **Place** the AllPrep DNA spin column in a **new capless 1.5 ml collection tube** (user supplied). **Add 32 μ l pre-warmed EB** directly to the spin column membrane. **Incubate** at RT for 10 min. **Centrifuge** at 10,000 *g* for 1 min to elute the DNA.
61. **Add another 32 μ l pre-warmed EB** directly to the spin column membrane. **Incubate** at RT for 5 min. **Centrifuge** at 10,000 *g* for 1 min to elute the DNA.
62. **Transfer** the combined DNA eluates (~60 μ l total) **to a sterile 1.5 ml collection tube**.

63. **Quantify DNA** using a spectrophotometer or Quant-iT DNA HS assay.
64. **Store DNA at -20°C.**

cDNA synthesis

1. Prepare a cDNA synthesis master mix:

<u>Ingredient</u>	<u>Per 20 µl reaction (µl)</u>	<u>Per 40 µl reaction (µl)</u>	<u>Per 60 µl reaction (µl)</u>
5x Buffer	4	8	12
RT enzyme	1	2	3
Total	5	10	15

2. For + RT: Add 1, 2, or 3 µg of RNA (in 15, 30, or 45 µl water) to 5, 10, or 15 µl of master mix in 200-µl PCR strip tubes.
3. For - RT: Add 250 ng of RNA dissolved in 25 µl of water to 200-µl PCR strip tubes
4. Mix by gentle flicking and briefly spin.
5. Thermocycling conditions: 5 min at 25°C, 30 min at 42°C, 5 min at 85°C, 4°C hold].
6. Add 80, 120, or 240 µl water to bring total volume of + RT reactions up to 100, 200, or 300 µl (10 ng/µl final concentration). Pipette up/down to mix.
Note: Diluted cDNA may be stored short-term at -20°C.

RT-qPCR

1. Perform duplicate or triplicate reactions per gene, per cDNA sample.
2. Prepare a qPCR master mix.

<u>Ingredient</u>	<u>Per 20 µl reaction</u>	<u>Per 25 µl reaction</u>
10 uM F primer	0.4 (0.2 uM final)	0.5 (0.2 uM final)
10 uM R primer	0.4 (0.2 uM final)	0.5 (0.2 uM final)
2X SYBR green	10	12.5
water	5.2	6.5
Total	16	20

3. Set-up 2-STEP program on the RT-qPCR machine and prepare the qPCR plate.
4. Add 16 or 20 µl master mix to desired wells using a multichannel pipette.
5. Transfer 4 or 5 µl of diluted cDNA to desired wells for 20 and 25 µl reactions, respectively.
6. Cap plate and vortex gently to mix.
7. Centrifuge briefly.
8. Thermocycling conditions: 3 min at 95°C then 40 cycles of 3 sec at 95°C and 20 sec at 60°C. Thermal dissociation curve recommended: 1 min at 95°C, 20 sec at 60°C, and 30 sec at 95°C.
Optional QC: Save plate and check for single amplicon bands by gel electrophoresis.

APPENDIX III

Additional Data

Michelle G. Rooks¹, Matthew J. Lavoie^{2,3}, Monia Michaud¹, Carey Ann Gallini¹, Jonathan N. Glickman³, and Wendy S. Garrett^{1,3,5}.

¹Harvard T.H. Chan School of Public Health, Boston, MA, USA

²Brigham and Women's Hospital, Boston, MA, USA

³Harvard Medical School, Boston, MA, USA

⁴Broad Institute of MIT and Harvard, Cambridge, MA, USA

⁵Dana-Farber Cancer Institute, Boston, MA USA

Author Contributions:

M.G.R. and W.S.G. conceived and designed the study. All experiments were performed by M.G.R., with the following exceptions. M.J.L. assisted with brain microdissections. M.M. offered technical assistance and advice on protocols. C.A.G. helped with animal husbandry. J.N.G. performed blinded histological assessment.

Characterizing host colonic catecholamine metabolism

BACKGROUND

Host stress molecules, including the catecholamines (CAs) dopamine (DOP), norepinephrine (NE), and epinephrine (EPI), are well-established neurotransmitters and hormones produced by the central nervous system (CNS) and the enteric nervous system (ENS). Within the gastrointestinal tract, local CAs regulate key functions such as motility, secretion, and immune responses¹. These host stress molecules are detectable in the luminal contents and adjacent tissues of the intestine, including the ileum, cecum, and colon². However, which cells are responsible for colonic CA production in health and disease is not well described. Thus, we sought to identify and characterize colonic CA-synthesizing cell populations and to understand host regulation of CA metabolism in homeostasis.

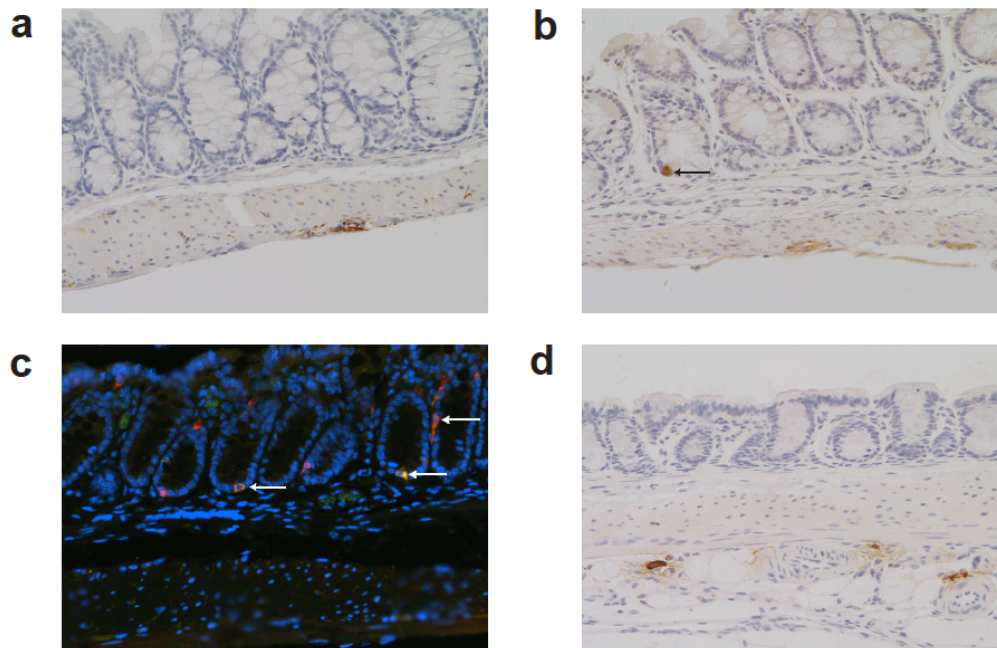
RESULTS

Localization of colonic CA synthesizing enzymes using indirect immunostaining and microscopy

Immunohistochemistry (IHC) and immunofluorescence (IF) were performed on colon sections from wild-type (WT) mice using antibodies against CA-biosynthetic enzymes, including tyrosine hydroxylase (TH) and dopamine β -hydroxylase (DBH). TH is the rate limiting enzyme that converts L-tyrosine into L-3,4-dihydroxyphenylalanine (L-DOPA) and DBH is the downstream enzyme that converts DOP into NE¹, the most abundant CA in intestinal tissues¹. We observed TH and DBH expression in the ganglia and nerve fibers of the ENS (**Appendix Figure C.1a-b**). DBH is also expressed by a distinct subset of epithelial cells (**Appendix Figure C1.b**), which were confirmed by sequential dual-labeling IF to be neuroendocrine cells via co-localization of DBH with the enteroendocrine marker chromogranin A (CgA) (**Appendix Figure**

C.1c). These observations indicate that epithelial cells positive for DBH and CgA are likely enterochromaffin cells with enteroendocrine and neuroendocrine function distinct from the ENS.

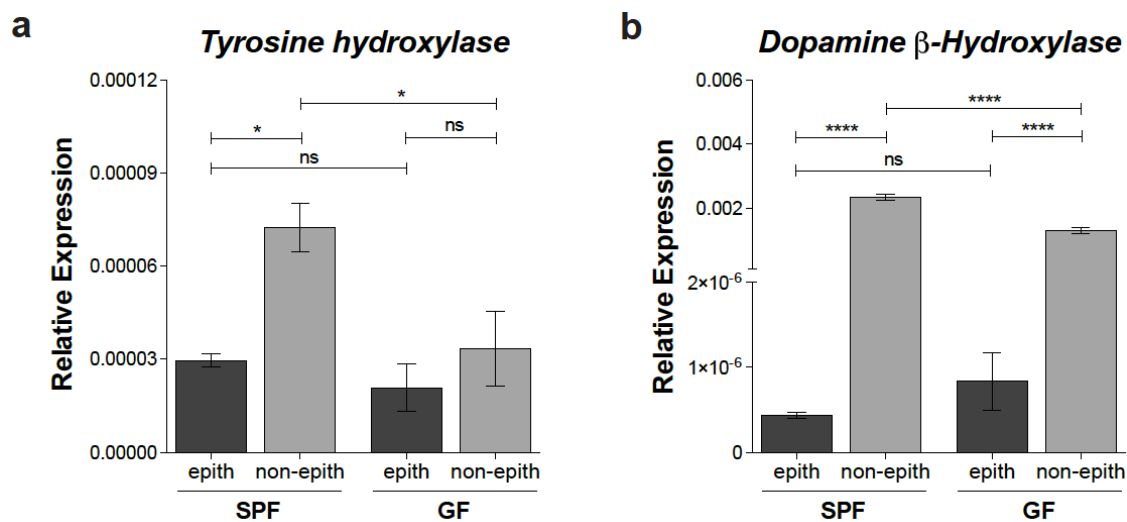
Tight regulation of host CA biosynthesis and degradation are required to maintain colonic CA levels. Polymorphisms in the catechol-O-methyltransferase gene (COMT), a CA catabolic enzyme, have been observed in irritable bowel syndrome³ and other disorders associated with dysbiosis and dysregulated gut-brain-axis signaling^{4,5}. Recent evidence also suggests that inflammatory stimuli can lead to decreased COMT expression in a nuclear factor-kappa B (NF- κ B)-dependent manner⁶. Thus, COMT expression was evaluated by IHC in homeostasis. COMT expression was substantially less abundant than TH or DBH and was predominantly localized to the ENS of the distal colon (**Appendix Figure C.1d**). Collectively, we demonstrated that the ENS and specific epithelial cell subsets are capable of CA metabolism using indirect immunostaining and microscopy.



Appendix Figure C.1. Catecholamine metabolic enzyme expression in colons. Representative images of colons of wild-type mice stained with antibodies against: (a) tyrosine hydroxylase, (b) dopamine β -hydroxylase, (c) dopamine β -hydroxylase (green) and chromogranin A (red) with DAPI [4',6-diamidino-2-phenylindole (blue)], and (d) catechol-O-methyltransferase. Arrows indicate DBH⁺ epithelial cells in (b) and double positive DBH⁺CgA⁺ epithelial cells in (c). All images acquired at a magnification of 20X.

CA biosynthesis in epithelial versus non-epithelial cell compartments

Immune cells can also produce CAs, including regulatory T cells, cytotoxic T cells, as well as other lymphocytes and mononuclear cells, as measured by high-performance liquid chromatography with electrochemical detection (HPLC-ED) and flow cytometry⁷⁻¹¹. To understand the contribution of epithelial cells versus other colonic cell populations, we partitioned colons of specified pathogen-free (SPF) WT mice into epithelial and non-epithelial cell fractions and measured CA biosynthetic gene expression by real-time quantitative PCR (RT-qPCR). Gene expression analysis revealed that *Th* and *Dbh* dominate the non-epithelial cell compartment (**Appendix Figure C.2a-b**), which includes immune cells of the lamina propria. Applying the same procedure to germ-free (GF) WT mice demonstrated a similar trend in gene expression between epithelial and non-epithelial fractions for DBH but no significant difference between fractions for TH (**Appendix Figure C.2a-b**). Compared to SPF mice, both *Th* and *Dbh* levels were only significantly reduced in the non-epithelial cell compartment of GF mice (**Appendix Figure C.2b**). These findings point to non-epithelial cells as key contributors to the CA economy of the colon and further support that CA levels may be gut microbiota-dependent³.



Appendix Figure C.2. Catecholamine biosynthetic gene expression of colonic cell subsets.

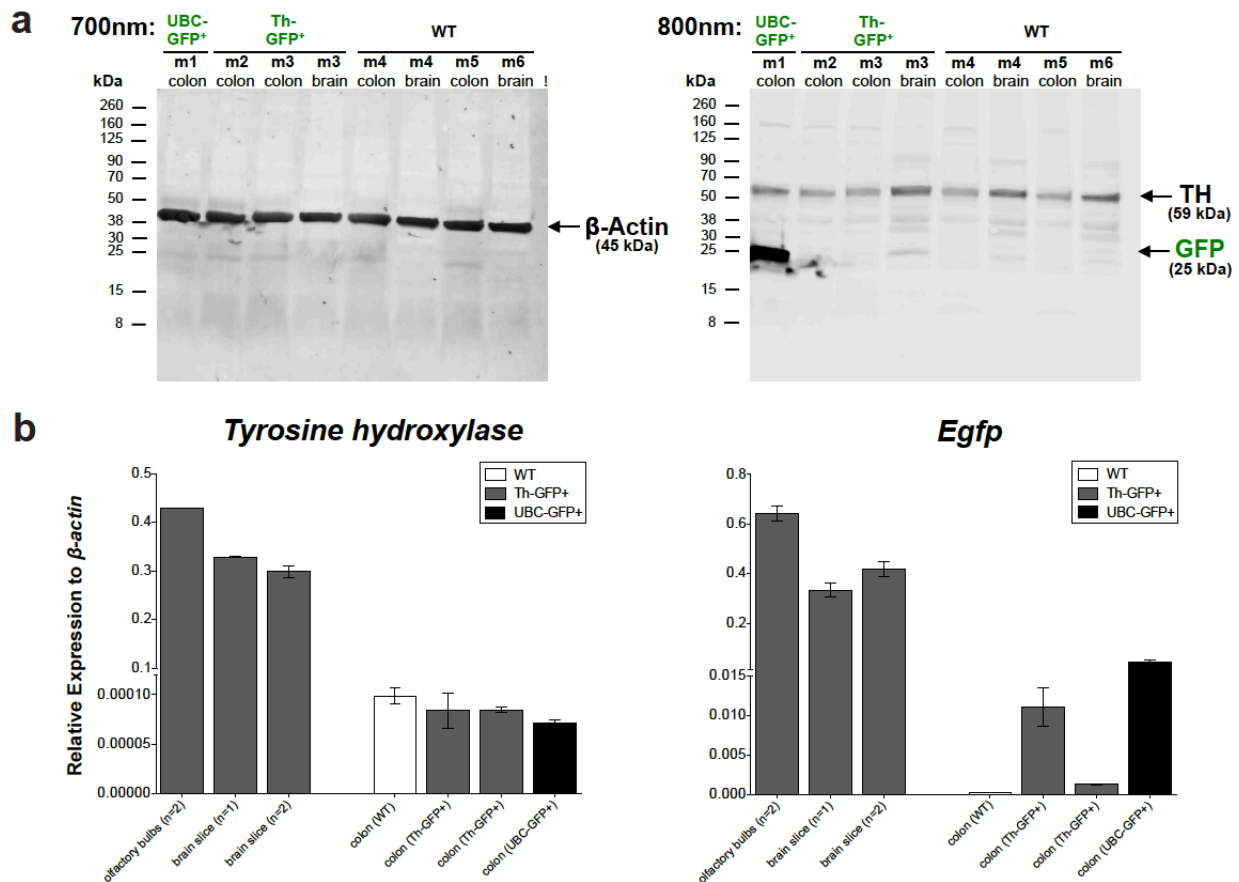
Appendix Figure C.2. (Continued). Relative expression of tyrosine hydroxylase (a) and dopamine β -hydroxylase (b) in epithelial (epith) and non-epithelial (non-epith) cell fractions of colons from specified pathogen-free (SPF) and germ-free (GF) mice. Gene expression was normalized to three reference genes: *β -actin*, *Hprt1*, and *Gapdh*. Error bars indicate mean \pm SEM. One-way analysis of variance (ANOVA) with Sidak's multiple comparison test to compare expression of epithelial and non-epithelial cells within SPF or GF groups and between epithelial or non-epithelial cells between SPF and GF groups: * $P < 0.05$, **** $P < 0.0001$; ns, not significant.

Use of GFP reporter mice to facilitate TH expression analysis of immune cell populations

We next wanted to map the expression of TH in specific colonic immune cell populations. We acquired Tg(Th-EGFP)₂₁₋₃₁Koba (Th-GFP) mice, which express GFP under the control of the *Th* promoter¹². However, efforts to map GFP expression in whole tissues and isolated immune cells were largely unsuccessful. GFP expression in frozen tissue sections – processed with and without anti-GFP antibodies – was detected in specific regions of the brain by IHC and IF, but was undetectable in intestinal tissues even with tyramide-mediated signal amplification (data not shown). Tissue lysates from brains and colons of Th-GFP and WT littermate controls were also probed for TH and GFP by western blot. Despite TH expression across tissue types, with higher levels in brains than colons, only a weak GFP signal was observed in brain lysates of Th-GFP mice (**Appendix Figure C.3a**). GFP expression was also absent in splenic immune cells when measured by flow cytometry (data not shown).

To obtain positive control tissue for measuring *Gfp* expression by RT-qPCR, brain micro-dissections were performed on Th-GFP mice to isolate dopaminergic-rich regions [olfactory bulbs, substantia nigra pars compacta (SNc), and ventral tegmental area (VTA)]. While colons of WT control and Th-GFP mice expressed *Th* to the same extent, *Gfp* levels were not significantly different between mice (**Appendix Figure C.3b**). For western blot, flow cytometry, and RT-qPCR analyses, Tg(UBC-GFP)₃₀Scha/J reporter mice were used as a positive GFP control. These mice express GFP under the direction of the human ubiquitin C (UBC) promoter, which enables tracking of differentiated immune cells across tissues.

Taken together, these observations suggest that, in homeostasis, *Th*-driven GFP expression may be restricted to brain-specific dopaminergic neurons in Th-GFP mice. To follow-up, Th-GFP and WT control mice were treated with dextran sodium sulfate (DSS) to induce colonic injury and examined whether mucosal inflammation could trigger GFP expression. In DSS-exposed mice, colons lacked GFP expression by IHC and splenic monocytes had undetectable GFP expression by flow cytometry and RT-qPCR (data not shown). Based on these findings, we ruled out the utility of this model for analyzing TH expression in colonic immune cell populations in health and active disease.



Appendix Figure C.3. TH expression analysis of colons and brains of GFP reporter mice. (a) Western blot for β -actin (loading control) and tyrosine hydroxylase (TH) and green fluorescent protein (GFP) in whole colons or brains of Tg(UBC-GFP), Tg(Th-GFP), and WT control mice. Each lane contains 50- μ g protein of the indicated tissue from an individual mouse. (b) Relative expression of tyrosine hydroxylase and enhanced GFP (*Egfp*) in brain and colon tissues of indicated mice. Gene expression was normalized to β -actin. Error bars indicate mean \pm SEM.

CONCLUSION

The ability of colonic epithelial and immune cells to synthesize CAs strengthens the role of CAs in the crosstalk between the epithelium and the immune and nervous systems. Understanding dopaminergic and adrenergic pathways in these cells may provide insight into modulating immune responses and maintaining intestinal homeostasis. Whether CA synthesis occurs in all immune cells or in specific immune cell subsets and what conditions drive CA production is still unknown. As many questions remain unanswered, additional tools, techniques, and genetically-engineered animal models are needed to specifically profile CA production within the colon in health and disease states.

MATERIALS AND METHODS

Animal husbandry

All SPF mice [BALB/c WT, C57BL/6-Tg(Th-GFP), and C57BL/6-Tg(UBC-GFP)] were housed in the Harvard T.H. Chan School of Public Health barrier facility. GF BALB/c mice were bred and maintained under sterile conditions in GF isolators at Children's Hospital Boston. Animal experiments were approved and conducted in accordance with Harvard Medical School Standing Committee on Animals and National Institutes of Health guidelines.

DSS interventions

Mice underwent a 7-day intervention starting on postnatal day 35 ± 5 , with 3% (wt/vol) DSS (Affymetrix) added to the drinking water from experimental day 0 through 5. Body weight, body condition, and stool consistency were measured frequently throughout the intervention to monitor disease activity.

Histology

Upon sacrifice, tissues were resected, fixed in 4% paraformaldehyde (Sigma), and embedded in paraffin. Colon sections were H&E-stained and evaluated in a blinded fashion for epithelial hyperplasia (0–3), epithelial injury (0–3), polymorphonuclear infiltration (0–3), and mononuclear infiltration (0–3), these indices were summed to generate the histologic colitis score¹³.

Indirect immunostaining and microscopy

Immunohistochemistry. Paraffin blocks were cut into 5 µm sections and were initially deparaffinized and rehydrated. Endogenous peroxidases were quenched with 3% H₂O₂ in methanol (both Sigma) for 20 min. Head-mediated antigen retrieval was performed in 1X Citrate Buffer, pH 6 (Dako) diluted in sterile water for 10 min at 95°C. Afterwards, slides were washed in 1X TBS (0.1 M Tris, 0.15 M NaCl, pH 7.6) with 0.05% Tween-20 (TBS-T) (all Sigma) and blocked for 1 hr at room temperature (RT) in 1X PBS (Cellgro) containing 1% bovine serum albumin (BSA, Jackson ImmunoResearch), 10% donkey serum (Jackson ImmunoResearch), and 0.4% Triton X-100 (Sigma). Primary antibodies were incubated overnight at 4°C, sections were washed in TBS-T, and secondary antibodies were applied for 1 hr at RT. Antibodies included: rabbit anti-TH (1:100, ab75875, Abcam), rabbit anti-DBH (1:800 for, ab43868, Abcam), rabbit anti-COMT (1:100, ab126618, Abcam), rabbit anti-GFP (1:250, ab183735, Abcam), and donkey anti-rabbit-HRP (1:500, Jackson ImmunoResearch). Antibodies were diluted in 0.5% TNB Blocking Buffer (Perkin-Elmer). Antibodies were visualized with DAB (Dako) and counterstained with hematoxylin.

Immunofluorescence. Paraffin blocks were cut into 5 µm sections and were initially deparaffinized and rehydrated. Head-mediated antigen retrieval was performed in 1X Citrate Buffer, pH 6 (Dako) for 20 min at 95°C. Slides were then washed in 1X PBS with 0.3% Triton x-100 (PBS-T) and blocked for 1 hr at RT in PBS-T containing 3% BSA and 10% donkey serum. Rabbit

anti-CgA (1:100, ab15160, Abcam) was incubated overnight at 4°C, sections were washed in PBS-T, and donkey anti-rabbit-IgG-594 (1:250, 406405, Biolegend) was applied for 1 hr at RT in the dark. Slides were washed again in PBS-T and blocked again for 1 hr at RT in PBS-T containing 3% BSA and 10% donkey serum. Anti-rabbit DBH (1:300 for, ab43868, Abcam) was incubated overnight at 4°C, sections were washed in PBS-T, and donkey anti-rabbit-IgG-488 (1:250, 406404, Biolegend) was applied for 1 hr at room temperature in the dark. All antibodies were diluted in 0.5% TNB Blocking Buffer (Perkin-Elmer). DNA was labeled with DAPI (0.5 µg/ml).

Visualization. Images were captured with Nikon eclipse Ni-U microscope and processed with NIS-elements software.

RNA isolation and RT-qPCR analysis

Tissue collection and processing. Whole colons or brains were resected, flash frozen in liquid nitrogen, and stored at -80°C. To generate epithelial and non-epithelial cell fractions, colons were resected and flushed with ice-cold 1X PBS to remove luminal contents. Colons were opened longitudinally and gently agitated in PBS with 2% FBS (Cellgro), 5 mM HEPES (Cellgro), 1 mM DTT (Sigma) for 10 min at 4°C. Colons were then transferred into pre-warmed PBS with 5 mM EDTA (Amresco) and rotated at 37°C for 15 minutes followed by vigorous shaking to remove epithelial cells. This was repeated and epithelial cells from both fractions were combined, passed through a 40-µm filter, and washed with PBS. Non-epithelial fractions were also washed with 1X PBS. Fractions were flash frozen in liquid nitrogen and stored at -80°C.

RNA isolation. Whole tissue and non-epithelial cell fractions were homogenized in 1-2 ml Qiazol using a TissueRuptor (both Qiagen) at high-speed for 30 sec. Epithelial cells were homogenized in 2 ml Qiazol using a 5 ml syringe with a 22.5G needle. Homogenized lysates were transferred to pre-spun phase lock gel tubes (5 Prime) (1 ml/tube) and incubated at RT for 5 min.

200 µl chloroform (Sigma) was added to lysates, shaken vigorously for 15 sec, and incubated another 3 min at RT. After centrifugation at 12,000 *g* for 10 min at 4°C, aqueous phases were transferred to sterile tubes. To precipitate RNA, 500 µl of isopropanol (Sigma) was added and samples were incubated for 10 min at RT prior to undergoing centrifugation at 12,000 *g* for 10 min at 4°C. Supernatants were discarded, pellets were washed in 1 ml 70% ethanol, and resuspended in sterile water. DNase treatments (Ambion) were performed and RNA was quantified using a NanoPhotometer Pearl (Denville). Purified RNA was stored at -80°C.

Lithium chloride extraction of RNA from DSS-treated mice. *In vivo* DSS treatment can completely inhibit the activity of polymerases and therefore affect qPCR amplification and analysis of extracted RNA from exposed tissues¹⁴. To remove residual DSS, extracted RNA from DSS-exposed mice was purified using a lithium chloride (LiCl)-based method published for RNA¹⁴ prior to undergoing DNase treatment. RNA was incubated with 0.1 volume of 8M LiCl (Cellgro) diluted in RNase-free water (Ambion) at -20°C for 30 min and then centrifuged at 14,000 *g* for 30 min at 4°C. RNA pellets were resuspended in 200 µl of water. The 30-min incubation with LiCl, the centrifugation, and the pellet resuspension were repeated for a second round. RNA was precipitated at -20°C for 30 min in 200 µl 3M sodium acetate pH 5.2 (Ambion) and 400 µl 100% ethanol. RNA was centrifuged for 30 min at 4°C. RNA pellets were washed with 500 µl 70% ethanol, centrifuged for 10 min at 4°C, resuspended in water, and stored at -80°C.

RT-qPCR for relative gene expression. cDNA was synthesized using the iScript cDNA Synthesis Kit (Bio-Rad) and RT-qPCR was performed using the KAPA SYBR FAST Universal qPCR kits (Kapa Biosystems). Genes were normalized to the following reference genes: *β-actin*, *Gapdh*, and *Hprt1*. Relative expression was analyzed using the $2^{-\Delta C_t}$ method, $\Delta C_t = C_{t, \text{target gene}} - C_{t, \text{reference genes}}$ and $C_{t, \text{reference genes}} = (C_{t, \text{actin}} * C_{t, \text{Gapdh}} * C_{t, \text{Hprt1}})^{1/3}$. The following primers were used: *β-actin*-For (5'-TACCACCATGTACCCAGGCA-3') and *β-actin*-Rev (5'-CTCAGGAGGAGCAATGATCTTGAT-3'); *Gapdh*-

For (5'-GGCATGGACTGTGGTCATGA-3') and Gapdh-Rev (5'-TTCACCACCATGGAGAAGGC-3'); Hprt1-For (5'-GACCGTCCCGTCATGC-3') and Hprt1-Rev (5'-TCATAACCTGGTTCATCATCGC-3'); Th-For (5'-TGCACACAGTACATCCGTCATGC-3') and Th-Rev (5'-GCAAATGTGCGGTCAGCCAACA-3')¹⁵; Dbh-For (5'-GAGACTGCCTTTGTGTTGACCG-3') and Dbh-Rev (5'-CGAGCACAGTAACCACCTTCCT-3')¹⁵; Egfp-For (5'-CCTACGGCGTGCAGTGCTTCAGC-3') and Egfp-Rev (5'-CGGCGAGCTGCACGCTGCGTCCTC-3'). All qPCR reactions were performed in duplicate and involved an annealing step at 60°C for 20 sec. A melting curve was produced to verify single PCR product amplification.

Western blot analysis

Brain and colons were resected and washed in PBS containing cComplete ULTRA and PhosSTOP inhibitor tablets (Sigma) diluted 1 tablet per 10 ml. Tissues were flash frozen in liquid nitrogen and stored at -80°C. Total proteins were extracted via homogenization in 100 mg/ml T-PER (Thermo Scientific) using a TissueRuptor (Qiagen) set to medium-speed for 30-60 sec. Homogenized samples were incubated on ice for 30 min and centrifuged at 10,000 *g* for 10 min at 4°C to pellet cells and tissue debris. Supernatants were collected and centrifuged again at 10,000 *g* for 10 min at 4°C. Supernatant were collected, aliquoted, and stored at -80°C. Total protein was measured using the Pierce BCA Protein Assay (Thermo Scientific) following manufacturer's instructions. Thawed frozen lysates were diluted to 1.3 mg/ml in 4x Laemmli Sample Buffer (Bio-Rad). Sample were denatured at 95-100°C for 10 min and centrifuged at 14,000 *g* for 5 min at RT. 40 µl (50 µg) of each sample and 10 µl Chameleon Duo Protein Ladder (LI-COR) were loaded on a 4-20% Mini-PROTEAN Precast Protein Gel (Bio-Rad). Samples were run with 1X SDS/Tris/Glycine Running Buffer (BioRad) diluted in sterile water at 80-100V for 1-1.5 hrs. Transfer to an activated PVDF membrane was performed with 1X Novex Tris-Glycine Transfer Buffer (Thermo Scientific) diluted in 20% methanol (Sigma) at 22V for 2 hrs on ice. Afterwards, membranes were blocked

using a 1:1 mixture of Blocking Buffer (LI-COR) and 1X PBS for 2hrs with rocking at RT. Membranes were incubated with primary antibodies diluted in 1:1 Blocking Buffer overnight with rocking at 4°C. Primary antibodies included: rabbit anti-TH (59 kDa, 1:500, ab75875, Abcam), rabbit anti-GFP (25 kDa, 1:2000, ab6556, Abam), and mouse anti- β -actin (45 kDa, 1:1000, 8H10D10, Cell Signaling). Membranes were washed 3 x 5 min in 0.05% TBS-T at RT and incubated with secondary antibodies for 2 hrs with rocking at RT in the dark. Secondary antibodies included: donkey anti-rabbit 800CW (1:10,000) and goat anti-mouse 680LT (1:20,000) (both LI-COR). Membranes were washed in 0.05% TBS-T followed by PBS. Membranes were visualized with a LI-COR Odyssey Scanner at 700 and 800 nm and processed with Image Studio software.

Flow cytometry analysis

Spleen were excised and mashed over a 70- μ m filter. Red blood cells were lysed with an ammonium chloride solution (StemCell Technologies). Cells were filtered through a 40- μ m cell strainer. The resulting single cell suspension was resuspended in staining buffer (1X PBS containing 1% FBS and/or 1 mM EDTA) at 4°C. Live/dead cells were stained with a fixable yellow dead cell kit (Thermo Scientific) and Fc blocked with anti-CD16/CD32 (clone 93, Biolegend) for 10 min at 4°C. For surface marker staining, cells were incubated with the following antibodies or corresponding isotype controls from BioLegend: CD45 (clone 30-F11), CD11b (M1/70), CD11c (N418), Gr-1 (RB6-8C5), CD3 ϵ (145-2C11), CD4 (RM4-5), and CD8 (53-6.7). Stained cells were acquired using an LSRII flow cytometer (BD) and analyzed with FlowJo software.

Statistical analysis

All statistical tests for significance were performed in Prism v6.0h for Mac OS X (GraphPad Software). All averages are mean \pm standard error of the mean (SEM).

REFERENCES

1. Lomax, A. E., Sharkey, K. A. & Furness, J. B. The participation of the sympathetic innervation of the gastrointestinal tract in disease states. *Neurogastroenterol. Motil.* **22**, 7–18 (2010).
2. Asano, Y. *et al.* Critical role of gut microbiota in the production of biologically active, free catecholamines in the gut lumen of mice. *Am. J. Physiol. Gastrointest. Liver Physiol.* **303**, G1288–95 (2012).
3. Karling, P. *et al.* The relationship between the val158met catechol-O-methyltransferase (COMT) polymorphism and irritable bowel syndrome. *PLoS ONE* **6**, e18035 (2011).
4. Behari, M. & Singhal, K. K. Cell based therapies in Parkinson's Disease. *Ann Neurosci* **18**, 76–83 (2011).
5. Serretti, A. & Olgiati, P. Catechol-o-methyltransferase and Alzheimer's disease: a review of biological and genetic findings. *CNS Neurol Disord Drug Targets* **11**, 299–305 (2012).
6. Hartung, J. E. *et al.* Nuclear factor-kappa B regulates pain and COMT expression in a rodent model of inflammation. *Brain Behav. Immun.* **50**, 196–202 (2015).
7. Cosentino, M. *et al.* Human CD4+CD25+ regulatory T cells selectively express tyrosine hydroxylase and contain endogenous catecholamines subserving an autocrine/paracrine inhibitory functional loop. *Blood* **109**, 632–642 (2007).
8. Bai, A., Lu, N., Guo, Y., Chen, J. & Liu, Z. Modulation of inflammatory response via α 2-adrenoceptor blockade in acute murine colitis. *Clinical & Experimental Immunology* **156**, 353–362 (2009).
9. Nguyen, K. D. *et al.* Alternatively activated macrophages produce catecholamines to sustain adaptive thermogenesis. *Nature* **480**, 104–108 (2011).
10. Musso, N. R., Brenci, S., Setti, M., Indiveri, F. & Lotti, G. Catecholamine content and in vitro catecholamine synthesis in peripheral human lymphocytes. *The Journal of Clinical Endocrinology & Metabolism* **81**, 3553–3557 (2013).
11. Mignini, F. *et al.* T-cell subpopulations express a different pattern of dopaminergic markers in intra- and extra-thymic compartments. *J Biol Regul Homeost Agents* **27**, 463–475 (2013).
12. Matsushita, N. *et al.* Dynamics of tyrosine hydroxylase promoter activity during midbrain dopaminergic neuron development. *Journal of Neurochemistry* **82**, 295–304 (2002).
13. Garrett, W. S. *et al.* Communicable ulcerative colitis induced by T-bet deficiency in the innate immune system. *Cell* **131**, 33–45 (2007).
14. Viennois, E., Chen, F., Laroui, H., Baker, M. T. & Merlin, D. Dextran sodium sulfate inhibits the activities of both polymerase and reverse transcriptase: lithium chloride purification, a rapid and efficient technique to purify RNA. *BMC Res Notes* **6**, 360 (2013).
15. Lehmann, M. *et al.* Evidence for a critical role of catecholamines for cardiomyocyte lineage commitment in murine embryonic stem cells. *PLoS ONE* **8**, e70913 (2013).